

AS
SL

ASTROPHYSICS AND
SPACE SCIENCE LIBRARY

ASTRONOMY-INSPIRED ATOMIC AND MOLECULAR PHYSICS

A.R.P. RAU



KLUWER ACADEMIC PUBLISHERS

ASTRONOMY-INSPIRED ATOMIC AND MOLECULAR PHYSICS

ASTROPHYSICS AND SPACE SCIENCE LIBRARY

VOLUME 271

EDITORIAL BOARD

Chairman

W. B. BURTON, *National Radio Astronomy Observatory, Charlottesville, Virginia, U.S.A.*
burton@starband.net;
University of Leiden, The Netherlands
burton@strw.leidenuniv.nl

Executive Committee

J. M. E. KUIJPERS, *Faculty of Science, Nijmegen, The Netherlands*
E. P. J. VAN DEN HEUVEL, *Astronomical Institute, University of Amsterdam,
The Netherlands*
H. VAN DER LAAN, *Astronomical Institute, University of Utrecht,
The Netherlands*

MEMBERS

I. APPENZELLER, *Landessternwarte Heidelberg-Königstuhl, Germany*
J. N. BAHCALL, *The Institute for Advanced Study, Princeton, U.S.A.*
F. BERTOLA, *Università di Padova, Italy*
J. P. CASSINELLI, *University of Wisconsin, Madison, U.S.A.*
C. J. CESARSKY, *Centre d'Etudes de Saclay, Gif-sur-Yvette Cedex, France*
O. ENGVOLD, *Institute of Theoretical Astrophysics, University of Oslo, Norway*
R. McCRAY, *University of Colorado, JILA, Boulder, U.S.A.*
P. G. MURDIN, *Institute of Astronomy, Cambridge, U.K.*
F. PACINI, *Istituto Astronomia Arcetri, Firenze, Italy*
V. RADHAKRISHNAN, *Raman Research Institute, Bangalore, India*
K. SATO, *School of Science, The University of Tokyo, Japan*
F. H. SHU, *University of California, Berkeley, U.S.A.*
B. V. SOMOV, *Astronomical Institute, Moscow State University, Russia*
R. A. SUNYAEV, *Space Research Institute, Moscow, Russia*
Y. TANAKA, *Institute of Space & Astronautical Science, Kanagawa, Japan*
S. TREMAINE, *CITA, Princeton University, U.S.A.*
N. O. WEISS, *University of Cambridge, U.K.*

ASTRONOMY-INSPIRED ATOMIC AND MOLECULAR PHYSICS

by

A.R.P. RAU

*Department of Physics and Astronomy,
Louisiana State University, Baton Rouge, U.S.A.*

KLUWER ACADEMIC PUBLISHERS

NEW YORK, BOSTON, DORDRECHT, LONDON, MOSCOW

eBook ISBN: 0-306-47820-X
Print ISBN: 1-4020-0467-2

©2003 Kluwer Academic Publishers
New York, Boston, Dordrecht, London, Moscow

Print ©2002 Kluwer Academic Publishers
Dordrecht

All rights reserved

No part of this eBook may be reproduced or transmitted in any form or by any means, electronic, mechanical, recording, or otherwise, without written consent from the Publisher

Created in the United States of America

Visit Kluwer Online at: <http://kluweronline.com>
and Kluwer's eBookstore at: <http://ebooks.kluweronline.com>

Contents

Preface	ix
1. ATOMIC STRUCTURE	1
1 Beginnings	1
2 The Hydrogen Atom	3
2.1 Eigenstates in the spherical representation	3
2.2 High symmetry of the hydrogen atom, separation in parabolic coordinates	6
3 The Two-electron Atom	8
3.1 The ground state of helium	9
3.2 Excited states	12
3.3 Configuration interaction	16
4 Heavier Atoms	17
4.1 Configurations and states	17
4.2 Simple screening pictures	20
4.3 The Thomas-Fermi self-consistent field model	22
4.4 Exact treatments: Hartree-Fock and configuration interaction	28
5 Line Spectra and Their Uses	30
5.1 Atomic spectra in astronomy	30
5.2 Doppler shifts of spectral lines	34
Problems	37
2. COUPLING OF ATOMS TO RADIATION	41
1 Introduction	41
2 Photoabsorption and Photoemission	42
2.1 The Oscillator strength	43

2.2	Alternative forms of the dipole matrix element	46
2.3	Selection rules	49
2.4	Moments and sum rules	53
3	Charged-particle Collisions	55
3.1	The Generalized Oscillator strength	55
3.2	Total cross-section	59
4	The Negative Ion of Hydrogen	60
4.1	The ground state of H^-	61
4.2	Photodetachment of H^-	63
4.3	Radiative capture	64
	Problems	66
3.	ATOMS IN WEAK, STATIC FIELDS	69
1	Introduction	69
2	External Electric and Magnetic Fields	70
2.1	Coupling to external fields	70
2.2	Time-independent perturbation theory	71
2.3	The Stark effect	76
2.4	The Zeeman effect	78
3	Internal Perturbations in an Atom	82
3.1	Relativistic mass correction	82
3.2	Spin-orbit coupling	83
3.3	Other corrections	84
	Problems	85
4.	ATOMS IN STRONG MAGNETIC FIELDS	87
1	Introduction	87
1.1	Free electrons in a magnetic field	88
2	Excited States in a Magnetic Field	91
2.1	Basic Hamiltonian and spectrum	91
2.2	Degenerate perturbation theory in an n -manifold	97
2.3	Large-scale numerical calculations	106
2.4	Quasi-classical JWKB analysis	110
2.5	Rydberg diamagnetism in other atoms	114
3	Strong Field Effects on Low-lying States	114
3.1	Introduction	114
3.2	Hydrogen in an ultrastrong magnetic field	115

3.3	Complex atoms in ultrastrong fields	122
3.4	Complex atoms in very strong, but not ultrastrong, fields	126
4	Strong Magnetic Fields in Astronomy	131
	Problems	133
5.	ELECTRON CORRELATIONS	135
1	Introduction	135
2	Electron Correlations	136
2.1	Qualitative picture	136
2.2	The spectrum of He and H^-	137
2.3	Experimental observation	141
3	Hyperspherical Coordinates	142
3.1	Coulomb potential and hyperspherical harmonics in six dimensions	149
3.2	Adiabatic hyperspherical method	151
3.3	Description of resonances	156
3.4	High-lying doubly-excited states and double ionization	161
4	Dielectronic Recombination	164
	Problems	167
6.	DIATOMIC MOLECULES	169
1	Introduction	169
2	Structure of Diatomic Molecules	170
2.1	Basic mechanism and nomenclature of covalent bonds	170
2.2	Molecular orbitals and states of simple diatomic molecules	173
2.3	The Born-Oppenheimer approximation	176
2.4	Rotations and vibrations of the internuclear axis	179
2.5	Anharmonicities and rotation-vibration coupling	182
2.6	Parity of molecular states	184
2.7	Effect of nuclear spin	185
3	Molecular Spectra	187
3.1	Rotational spectra	187
3.2	Vibrational spectra	189
3.3	Raman spectra	192
3.4	Electronic spectra	193

3.5	External field effects on molecular spectra	199
3.6	Collisional processes	199
4	Astrophysical Applications	200
	Problems	205
7.	POLYATOMIC MOLECULES	207
1	Introduction	207
2	Structure and Spectra of Polyatomic Molecules	207
2.1	Born-Oppenheimer approximation and electronic structure	207
2.2	Rotation of polyatomic molecules and spectra	211
2.3	Vibrations of polyatomic molecules	215
2.4	Degeneracies and rovibronic couplings	221
3	Astrophysical Applications	224
	Problems	227
	References	229
	Index	233

Preface

This book deals with topics in atomic and molecular structure and dynamics that are important to astronomy. Indeed, the topics selected are of central interest to the field of astronomy, many having been initiated by the needs of understanding worlds other than ours. Except for some lunar surface material returned by the Apollo missions, and material naturally delivered to us by cosmic rays, comets, and meteors, our only access to the other worlds of our astronomical Universe is through our observations of electromagnetic radiation from them. (Very recently, neutrinos from the Sun and supernovae have also been studied, and there are hopes for observations of gravitational waves in the next decades.)

Overwhelmingly, therefore, our knowledge of the astronomical world is derived from the emission, absorption, and scattering of electromagnetic radiation from atoms and molecules. We “touch” and discern the material content of these distant objects only through such absorptions and emissions. As a result, there is a strong coupling between the subjects of astronomy and atomic and molecular physics. Indeed, a major theme for this book is that at several times, both in the beginnings of these subjects and continuing today, atomic and molecular problems have been directly stimulated, even initiated, by the needs of astronomy. In turn, of course, they have proved vital to astronomy. It seemed appropriate, therefore, to compile a primer on atomic and molecular physics within this context of astronomy. The focus is on the basic physics of atoms and molecules with a sample of their astronomical applications. This book is designed as a possible textbook for a course in atomic physics for students in astronomy programs, either at the senior undergraduate or first-year graduate school level in U.S. universities, or their equivalents. The only preparation presumed is of knowledge of quantum physics at the level of a one semester- or year-long undergraduate course. Each

chapter ends with problems suited for homework assignments. They are of two types, some to work out derivations only sketched in the text, and others to illustrate applications of results.

Chapter 1 considers the early beginnings of a modern, scientific study of the astronomical Universe, when spectra from the Sun and other stars provided the first handle on the nature of matter on them. The development of quantum physics in the first three decades of the twentieth century went hand in hand with the understanding of atomic structure and of the coupling of atoms to the electromagnetic field. This chapter will consider energy levels, particularly discrete, in hydrogen as well as in heavier atoms and positive ions, and techniques for calculating them and of the transitions between them that correspond to spectral observations. Such transition energies, and their Doppler shifts, already provide vital information both on individual objects and the large scale structure of the Universe. Chapter 2 turns to intensities and polarizations of spectra, important for the study of stellar atmospheres, introducing also loosely bound atomic systems such as negative ions which have a major role. External field effects on spectra, particularly of magnetic fields, are the subject of Chapter 3, illuminating both the almost ubiquitous occurrence of these fields in the Universe and the role of their study in developing general mathematical techniques of perturbation analysis which transcend atomic physics to cover all physics. Chapter 4 considers more recent studies of very strong fields, associated with magnetic white dwarfs and neutron stars, and the impetus they provide to understanding atoms under very strong perturbations that can even alter their basic structure. The role of electron correlations, already important in ground state properties of negative ions, but central to multiple excitations of atoms, is taken up in Chapter 5, inspired by the astronomically important phenomenon of dielectronic recombination for the capture of electrons by positive ions. This chapter also considers the effect of electric and magnetic fields on this phenomenon, of importance both in the laboratory and in astrophysical plasmas. Chapter 6 deals with molecular structure and spectra, particularly of simple diatomic molecules, which serve to introduce the basic elements of molecular physics. The final Chapter 7 extends to larger molecules and to the variety of molecular interactions that have been studied in recent years for interstellar clouds and for the early stages of stellar formation. This chapter also deals with maser emission seen from a variety of astrophysical objects.

References have been placed within square brackets in the text and listed in order at the end of the book. These references are not intended to assign credit, and original contributions are not always cited. Rather, they have been used as pointers to the literature for specific items or

for more detailed consultation and, therefore, are heavily weighted to review articles and textbooks. Most of our knowledge and understanding come from such sources and this is an appropriate place to indicate my indebtedness. Much of the quantum mechanics I have learnt is from L. D. Landau and E. M. Lifshitz, *Quantum Mechanics: Non-relativistic theory* (Pergamon, Oxford, 1977). I have learnt most of what I know of molecular physics from two books: J. I. Steinfeld, *An Introduction to Molecular Spectra* (M.I.T. Press, Cambridge, MA, 1974), and I. N. Levine, *Molecular Spectroscopy* (John Wiley, New York, 1975). This is reflected in Chapters 6 and 7.

I also owe immensely to my many teachers, starting with my high school science teacher, the late Mr. G. C. Gupta of Dehra Dun, India. The selection of topics in this book reflect for the most part areas that have been of research interest to me over the years. Most of what I have learnt about atomic physics and research I owe to the late Professor Ugo Fano of The University of Chicago and Professor Larry Spruch of New York University. Their influence pervades the content and style throughout this book. Regular visits to, and discussions with colleagues at the Raman Research Institute (Bangalore, India) have contributed to my interests in astronomy-related matters. Indeed, the initial suggestion to write this book came from Professor V. Radhakrishnan of this institute.

The writing of this book was done during a period of sabbatical leave from Louisiana State University. I am grateful for its support and to my hosts and their institutions: Professors Jürgen Hinze and Farhad Faisal (University of Bielefeld, Germany) and Professor Stephen Buckman (Australian National University). I also acknowledge support from the Alexander von Humboldt Stiftung. For the typing of the manuscript, I am grateful to Ms. Ophelia Dudley and Ms. Monika Lee, and for the figures to Ms. Luz Barona and Mr. Enrique Hurtado, all of Louisiana State University.

Chapter 1

ATOMIC STRUCTURE

1. Beginnings

Although the scientific study of astronomy dates back to the work of Galileo and Newton, the nature of astronomical bodies remained unknown till the middle of the nineteenth century. The same year 1859, which saw other major advances such as Karl Marx's "*A Critique of Political Economy*," Maxwell's discussion of the velocity distribution in the kinetic theory of gases, and Charles Darwin's "*On the Origin of Species*" is a significant date for astrophysics. Gustav Kirchhoff made the connection between the lines seen by Fraunhofer in the spectrum of the Sun with his own laboratory "flame spectroscopic" observations of absorption spectra to conclude that matter on the Sun is made of the same stuff as matter here on Earth. This was an important step, particularly away from historical beliefs that the heavens are composed of a fifth element, called quintessence. (This word is now again being attached by some cosmologists to a certain kind of conjectured unseen matter in the Universe.) This supposedly unique and perfect element, from which the word quintessential is derived, was thought to be different from the four (earth, air, water, and fire) that make up our Earth.

The recognition that stars and other objects in the Universe are constituted of the same elements and atoms as in the laboratory opened the doors to modern astronomy and to the study of the material constituency of the heavens. As Helmholtz put it, "It had in fact most extraordinary consequences of the most palpable kind, and has become of the highest importance for all branches of natural science. It has excited the admiration and stimulated the fancy of men as hardly any other discovery has done, because it has permitted an insight into worlds that

seemed forever veiled to us.” (F. Cajori: *A History of Physics* (MacMillan, N.Y., 1899), p. 160). Spectroscopy gave a handle on these distant worlds that were not in direct reach. Already, in his first observations, Kirchhoff made a model for Fraunhofer’s dark lines as due to light from extremely hot deeper layers passing through a cooler atmosphere, giving absorption lines at the same corresponding positions where he observed emission lines from sodium and potassium in his flames. He also noted the absence of lithium.

The study of spectra in German and other European laboratories in the second half of the nineteenth century, inspired in large part by astronomy, paved also the way to fundamental advances in quantum physics and the understanding of atomic structure. On the one hand, continuous emission spectra, such as of a black body, led to Planck’s revolutionary replacement of the Rayleigh-Jeans and Wien’s distributions by his quantum distribution as a better fit to the laboratory data of his colleagues like Lummer and Pringsheim. Planck, a student of Kirchhoff, was following his teacher who, also in 1859, had established the theorems of radiation absorption and emission. On the other hand, line spectra seen in emission and absorption to be characteristic of the different elements were organized into simple series by Angstrom, Rydberg and others, setting the stage for Balmer’s crucial analysis of them which in turn set the stage for Bohr and the development of quantum physics. It is interesting that the Bunsen burner played an important role in making it possible to observe such emission spectra. The first public laboratory (Magnus had an earlier private laboratory in Berlin) devoted specifically to physics was established in 1846 at the University of Heidelberg in Germany for Bunsen and Kirchhoff; laboratories for chemistry existed before at Giessen since 1824, and also at the Rennselaer Polytechnic Institute (1824) and in Scotland (1831).

Balmer, himself not a spectroscopist but rather a Swiss high school (Gymnasium) teacher, observed (1885) purely empirically that line spectra in a series such as in Angstrom’s study of hydrogen conformed to a simple expression, their frequencies being given by

$$\nu_{kn} = \text{Ry} \left(\frac{1}{k^2} - \frac{1}{n^2} \right), \quad (1.1)$$

with $k = 2, n = 3, 4, 5, \dots$. The constant Ry, named since for Rydberg, has the value $109,737 \text{ cm}^{-1}$ ($\approx 13.605 \text{ eV} \approx 3.2898 \times 10^{15} \text{ Hz}$) and is today one of the most precisely measured fundamental constants of nature [1]: $R_\infty = 109,737.315\,685\,16(84) \text{ cm}^{-1}$ and the $1s-2s$ frequency in hydrogen is $2,466,061,413,187,103 (46) \text{ Hz}$.

Theoretical understanding of the Balmer formula (1.1), and specifically of the role of the integers contained in it, emerged in part from Bohr's (1913) model of the hydrogen atom as consisting of quantized orbits of the electron around the nucleus with specific integral values of the angular momentum in units of \hbar , and later fully through the quantum mechanics of Heisenberg and Schrödinger. Bound states of this three-dimensional system are characterized by three quantum numbers, n, ℓ , and m , with $n = 1, 2, 3, \dots$ the principal quantum number, $\ell = 0, 1, 2, \dots, (n - 1)$, or s, p, d, f, \dots , denoting the orbital angular momentum $\ell\hbar$, and $m = 0, \pm 1, \dots, \pm\ell$ the azimuthal (or magnetic) projection of angular momentum on a quantization axis, usually referred to as the z -axis. The energy of such a stationary bound state depends only on n ,

$$E_n = -Ry/n^2, \quad (1.2)$$

with $Ry = (\mu e^4/2\hbar^2) = (e^2/2a_0)$, $a_0 \equiv \hbar^2/\mu e^2$ the Bohr radius (≈ 0.053 nm ≈ 0.53 Å), and μ the reduced mass of the electron. Throughout, we take $(-e)$ to be the charge of an electron, with $e = 4.8 \times 10^{-10}$ esu. "Atomic units (a.u.)" set $e = \hbar = \mu = 1$.

The n^2 states differing in ℓ and m but sharing the same n value are "degenerate" in energy. Transitions between stationary states of different principal quantum numbers correspond to the specific energies emitted as electromagnetic radiation as in (1.1), each k providing a series. Each series terminates at a highest frequency value known as the band edge. The "Balmer series", with $k = 2$, lying as it does in an accessible visible region of the spectrum ($H_\alpha = 656.3$, $H_\beta = 486.1$, $H_\gamma = 434.0$, $H_\delta = 410.2, \dots$ nm), was naturally the first observed. Others of prominence in astronomy are $k = 3$ (Paschen, observed in 1908) and $k = 4$ (Brackett) in the infrared, and $k = 1$ (Lyman: $Ly_\alpha = 121.6$, $Ly_\beta = 102.6, \dots$ nm) in the ultraviolet range.

2. The Hydrogen Atom

2.1 Eigenstates in the spherical representation

The energies in (1.2), together with a continuous spectrum, $0 \leq E < \infty$, are the eigenvalues of the time-independent Schrödinger equation,

$$H|n\ell m\rangle = E_n|n\ell m\rangle, \quad (1.3)$$

with the one-electron Hamiltonian

$$H = \frac{\mathbf{p}^2}{2\mu} - \frac{Ze^2}{r} = -\frac{\hbar^2}{2\mu} \nabla^2 - \frac{Ze^2}{r}. \quad (1.4)$$

Here μ is the reduced mass of (electron+nucleus): $\mu = mM(m+M)^{-1}$, and $E_n = -Z^2 \text{Ry}/n^2$, where we have generalized (1.2) to an arbitrary charge Z for the nucleus which proves convenient for handling other hydrogen-like positive ions and atoms heavier than hydrogen. The spherical symmetry of the Coulomb potential is reflected in the labels used in (1.3), the operators of orbital angular momentum L^2 and projection L_z forming, together with H , a complete set of mutually commuting operators. Together with (1.3), we also have

$$\begin{aligned} L^2|n\ell m\rangle &= \ell(\ell+1)\hbar^2|n\ell m\rangle, \\ L_z|n\ell m\rangle &= m\hbar|n\ell m\rangle. \end{aligned} \quad (1.5)$$

All three operators being even under space reflection, $\mathbf{r} \rightarrow -\mathbf{r}$, the states $|n\ell m\rangle$ are also eigenstates of parity. With three being the maximal set for characterizing a three-dimensional system, parity is not an independent fourth label. Indeed, the parity eigenvalue is $(-1)^\ell$.

The corresponding eigenfunctions or wave functions in the coordinate representation,

$$\psi(\mathbf{r}) \equiv \langle \mathbf{r} | n\ell m \rangle, \quad (1.6)$$

are factorized in the coordinates $\mathbf{r} = (r, \theta, \varphi)$ as

$$\psi(\mathbf{r}) = R_{n\ell}(r) Y_\ell^m(\theta, \varphi), \quad (1.7)$$

where $Y_\ell^m(\theta, \varphi)$ are the standard spherical harmonics (themselves factorized in their θ and φ dependence) and $R_{n\ell}(r)$ the radial wave functions, solutions of the radial equation

$$\left[-\frac{\hbar^2}{2\mu} \left(\frac{d^2}{dr^2} + \frac{2}{r} \frac{d}{dr} \right) + \frac{\hbar^2 \ell(\ell+1)}{2\mu r^2} - \frac{Ze^2}{r} \right] R_{n\ell}(r) = E_n R_{n\ell}(r). \quad (1.8)$$

The radial functions are composed of three factors apart from a normalization constant $N_{n\ell}$,

$$R_{n\ell}(r) = N_{n\ell} (Zr/a_0)^\ell p_{n-\ell-1}(Zr/a_0) \exp(-Zr/na_0), \quad (1.9)$$

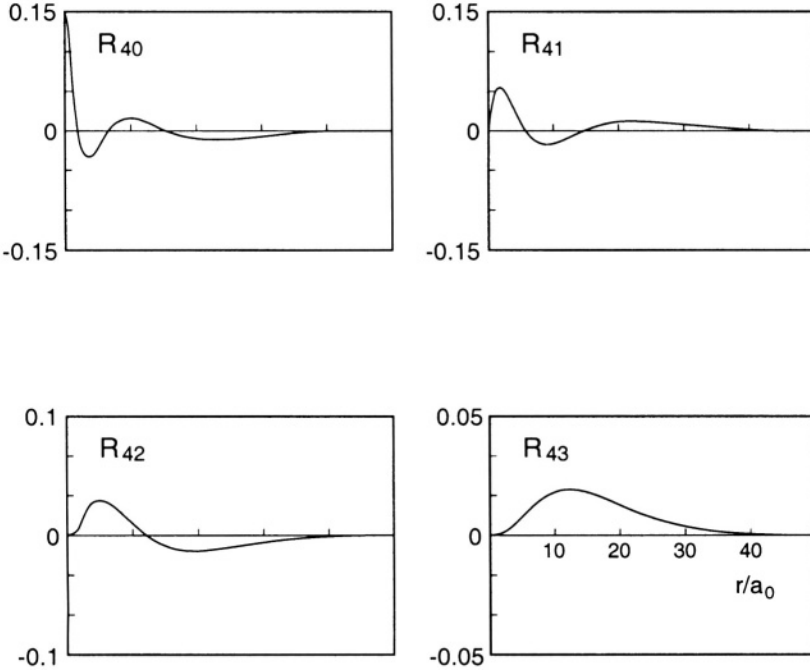


Figure 1.1. Radial wave functions of the hydrogen atom, $n = 4$, $\ell = 0 - 3$, from S. Brandt and H. D. Dahmen, *The Picture Book of Quantum Mechanics* (John Wiley, New York, 1985), with permission of John Wiley and Sons, Inc.

reflecting, respectively, behavior near the origin, at intermediate r , and at asymptotic distances. The intermediate factor is a polynomial in r with $n_r \equiv n - \ell - 1$ nodes, where n_r is the “radial quantum number”. Fig. 1.1 provides a representative sketch. For the corresponding functions in the continuous spectrum, n in (1.9) is replaced by iZ/ka_0 , where the wave number k is defined in the usual manner as $E \equiv \hbar^2 k^2 / 2\mu$, and the factor $p_{n-\ell-1}$ is no longer a polynomial, but a confluent hypergeometric function, ${}_2F_1\left(\frac{iZ}{ka_0} - \ell - 1, 2\ell + 1, 2ikr\right)$.

Useful scaling relations that follow from these solutions are that radial distances in an $|nlm\rangle$ state scale as n^2/Z , energies as Z^2/n^2 , and the amplitude of the $\ell = 0$ function at the origin (all $\ell \neq 0$ functions vanishing there), N_{n0} , as $(Z/na_0)^{3/2}$. The velocity of the electron is given by $(Zc/137n)$. Some of the most useful expectation values of r^s in such states, for s an integer, are

$$\begin{aligned}
\langle 1/r \rangle &= Z/n^2 a_0, \\
\langle r \rangle &= \frac{n^2 a_0}{2Z} \left[3 - \ell(\ell + 1)/n^2 \right], \\
\langle r^2 \rangle &= \frac{n^4 a_0^2}{2Z^2} \left[5 - 3\ell(\ell + 1)/n^2 + 1/n^2 \right], \\
\langle 1/r^2 \rangle &= (Z^2/a_0^2) \left[n^3(\ell + \frac{1}{2}) \right]^{-1}, \\
\langle 1/r^3 \rangle &= (Z/a_0)^3 \left[n^3 \ell(\ell + \frac{1}{2})(\ell + 1) \right]^{-1}. \quad (1.10)
\end{aligned}$$

The first of these reflects the virial relation for a Coulomb potential, $\langle -Ze^2/r \rangle = -2E_n$, the second enters in the study of electric field (“Stark”) effects (Section 3.2.3), the third in the study of diamagnetic effects on atoms (Section 4.2), and the last two in the evaluation of relativistic corrections (Sections 3.3.1 and 3.3.2).

2.2 High symmetry of the hydrogen atom, separation in parabolic coordinates

Degeneracy of stationary states is always a pointer to symmetries of the Hamiltonian. The evident spherical symmetry of (1.4) means, of course, that no direction in space is distinguished and all states differing only in their m quantum numbers have the same energy. This is also evident in (1.8) in that m does not occur in the radial eigenvalue problem. In general, however, the energy eigenvalues of this equation may have been expected to depend on both n and ℓ . That they do not depend on ℓ is unique to a few spherical symmetric potentials such as the Coulomb and isotropic harmonic oscillator ($V(r) \propto r^2$). The special status of these potentials was already known in classical and celestial mechanics, even as far back as Laplace’s elaborations on Newtonian mechanics for gravitationally bound systems.

In quantum physics, the degeneracy implies the existence of other operators that also commute with the Hamiltonian, and of other coordinate systems in which the Schrödinger equation separates. The operator is the one associated with a vector investigated by Laplace, and now called the Laplace-Runge-Lenz vector in the context of the hydrogen atom,

$$\mathbf{A} = \left(-2E/\mu e^4 \right)^{-\frac{1}{2}} \left[\left(2\mu e^2 \right)^{-1} (\mathbf{L} \times \mathbf{p} - \mathbf{p} \times \mathbf{L}) + \mathbf{r}/r \right]. \quad (1.11)$$

In classical mechanics, this vector has magnitude equal to the eccentricity of the Kepler orbit and points in the direction of the semi-major

axis from the force center. Further, \mathbf{L} and \mathbf{A} are orthogonal: $\mathbf{L}\cdot\mathbf{A} = 0$. Together with H and L_z, A_z forms a triad of mutually commuting operators, an alternative to the $\{H, L^2, L_z\}$ set considered above. The Hamiltonian can be written as $H = -(\mu e^4/2\hbar^2)(\mathbf{L}^2 + \mathbf{A}^2 + 1)^{-1}$.

Correspondingly, therefore, an alternative set of eigenstates $|n_1 n_2 m\rangle$ also describes the hydrogen atom:

$$\begin{aligned} H|n_1 n_2 m\rangle &= -(Z^2 R_y/n^2)|n_1 n_2 m\rangle, \\ L_z|n_1 n_2 m\rangle &= m\hbar|n_1 n_2 m\rangle, \\ A_z|n_1 n_2 m\rangle &= (n_1 - n_2)\hbar|n_1 n_2 m\rangle, \\ n &= n_1 + n_2 + |m| + 1. \end{aligned} \quad (1.12)$$

Unlike \mathbf{L} , an axial vector, \mathbf{A} is polar so that A_z is odd under parity. Therefore, unlike the states $|n\ell m\rangle$, these $|n_1 n_2 m\rangle$ states do not have well-defined parity but are “mixed”. The z -direction is, therefore, distinguished for them which makes this set natural for describing problems in which a direction in space is singled out, as when an electric field is applied to the hydrogen atom (Section 3.2.3).

The corresponding coordinates in which the Schrödinger equation separates are the parabolic coordinates which single out such a z -direction in their very definition: $\xi = r + z$, $\eta = r - z$, and φ . We have now, instead of (1.7),

$$\psi(\mathbf{r}) = N \left(\frac{Z^2 \xi \eta}{n^2 a_0^2} \right)^{\frac{|m|}{2}} f_{n_1} \left(\frac{Z\xi}{na_0} \right) f_{n_2} \left(\frac{Z\eta}{na_0} \right) e^{-Z(\xi+\eta)/2na_0} e^{im\varphi}, \quad (1.13)$$

where f_{n_1} and f_{n_2} are polynomials with n_1 and n_2 nodes, respectively.

The spherical and the parabolic descriptions provide alternative bases for describing the states of the hydrogen atom. As in any such situation of alternative bases at the same energy for a quantum system, a unitary transformation links the two sets. Its realization is most immediate from the linear combinations of the two vectors \mathbf{L} and \mathbf{A} ,

$$j_1 = \frac{1}{2}(\mathbf{L} + \mathbf{A}), \quad j_2 = \frac{1}{2}(\mathbf{L} - \mathbf{A}). \quad (1.14)$$

In terms of them, the parabolic description stems from the set $\{H, j_{1z}, j_{2z}\}$ whereas the spherical is given by $\{H, \mathbf{j}_1 + \mathbf{j}_2, j_{1z} + j_{2z}\}$. It can also be shown through commutators of their components, that \mathbf{j}_1 and \mathbf{j}_2 behave like two independent angular momenta, each of magnitude $\frac{1}{2}(n-1)$,

so that the unitary transformation coincides with that of adding two angular momenta: $\mathbf{j}_1 + \mathbf{j}_2 = \mathbf{L}$,

$$\begin{aligned} |n_1 n_2 m\rangle &= \sum_{\ell} |n\ell m\rangle \langle n\ell m | n_1 n_2 m\rangle, \\ |n\ell m\rangle &= \sum_{n_1} |n_1 n_2 m\rangle \langle n_1 n_2 m | n\ell m\rangle, \end{aligned} \quad (1.15)$$

the brackets being, therefore, the Clebsch-Gordan (or Wigner) coefficients of such an addition. With m being common to both representations, states of the same n and m that differ only in one quantum number, ℓ or n_1 (or n_2), are superposed in transforming from one representation to the other.

In particular, for $n = 2$ and $m = 0$, the parabolic states are

$$\begin{aligned} |100\rangle &= [|2s0\rangle + |2p0\rangle]/\sqrt{2} \\ |010\rangle &= [|2s0\rangle - |2p0\rangle]/\sqrt{2}. \end{aligned} \quad (1.16)$$

In coordinate space, the first of these involves $(r + z) = \xi$, the second $(r - z) = \eta$, so that the wave functions are concentrated at positive and negative z , respectively. Such plots of spherical and parabolic functions or probability densities as in Fig. 1.2, or elsewhere [2] for higher n , are instructive in visualizing the nature of these states. Note finally that the existence of two vector operators, \mathbf{L} and \mathbf{A} , both of whom commute with H , signifies that this Coulomb Hamiltonian is invariant not only with respect to rotations in the familiar three-dimensional space of coordinates but also with respect to rotations in a four-dimensional space wherein six independent rotations (or planes) are possible. For this reason, the Coulomb problem is said to have the higher symmetry of the orthogonal group in four-dimensions, O_4 , not just, under O_3 which, of course, it shares with any spherically-symmetric potential. The four dimensions can be interpreted as those of momentum space, with the momentum \mathbf{p} and energy constituting the four coordinates, and the Schrödinger equation for the hydrogen atom in momentum space separating in spherical polar coordinates.

3. The Two-electron Atom

In going beyond hydrogen to other atoms, an additional quantum principle becomes important. Identical particles in quantum physics have to be described by wave functions that are totally antisymmetric (symmetric) under the interchange of any pair of them if they are fermions (bosons), that is, if their intrinsic spins are half-odd integers

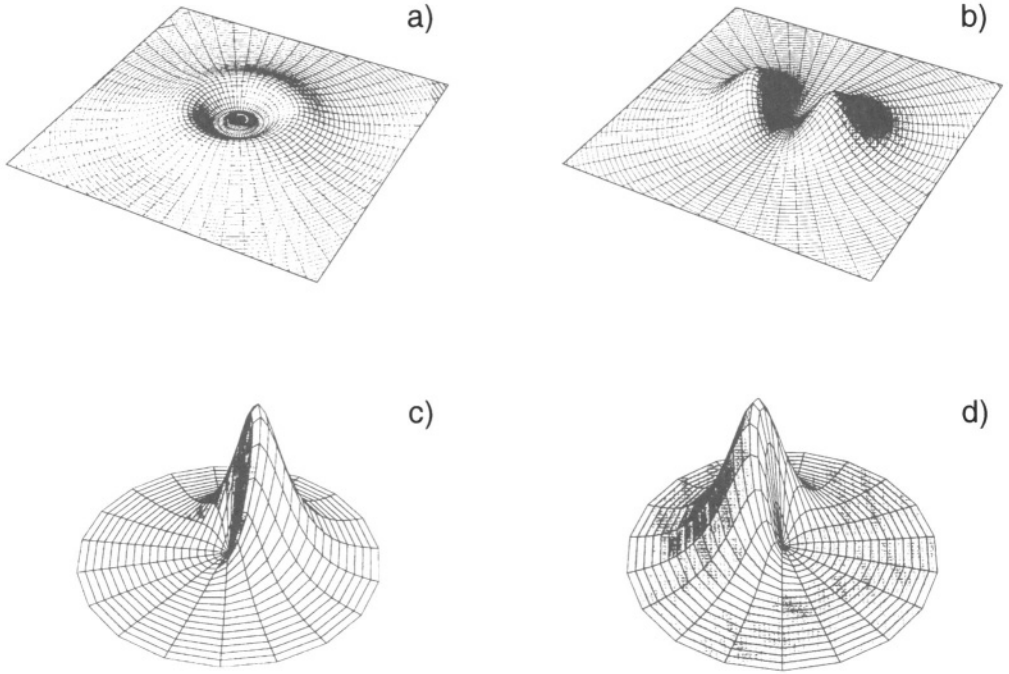


Figure 1.2. Probability distribution of $n = 2$ states of the hydrogen atom: (a) $2s$, (b) $2p$, and parabolic states (c) $n_1 = 0, n_2 = 1$, (d) $n_1 = 1, n_2 = 0$, courtesy of Roger Wendell and Phay Jo Ho.

(integers). For the electrons in an atom, this “Pauli exclusion principle” about antisymmetric functions acts as a constraint on the states that successive electrons can occupy. Elsewhere, for systems with a large number of electrons, this same constraint, acting almost like a dynamical force, the “electron degeneracy pressure”, underlies basic characteristics of conduction in metals and semi-conductors, and the structure and stability of white dwarf stars.

3.1 The ground state of helium

The two-electron atom, helium, illustrates the effect of the Pauli principle. Interestingly, this element named for Helios, the Sun, was first identified in solar spectra in 1868 by Pierre Janssen and Joseph Lockyer, 27 years before its observation on Earth. In its ground state, both

electrons can occupy the lowest hydrogenic “orbital”, $1s$, thereby being symmetric under exchange of their spatial coordinates \mathbf{r}_1 and \mathbf{r}_2 , if and only if they are antisymmetric under the interchange of their spin labels. This occurs in only one way, the total spin function being a “singlet” with $\frac{1}{2} + \frac{1}{2} = 0$, denoted in an obvious notation by $(|\uparrow\downarrow\rangle - |\downarrow\uparrow\rangle)/\sqrt{2}$.

The spatial wave function, symmetric under interchange, can be written in a variety of ways. No exact solution is known, the Hamiltonian

$$H(\mathbf{r}_1, \mathbf{r}_2) = \frac{\mathbf{p}_1^2}{2\mu} + \frac{\mathbf{p}_2^2}{2\mu} - \frac{Ze^2}{r_1} - \frac{Ze^2}{r_2} + \frac{e^2}{r_{12}}, \quad (1.17)$$

with $r_{12} = |\mathbf{r}_1 - \mathbf{r}_2|$, being not separable in any coordinate system. We have again left the nuclear charge Z unspecified so that these considerations apply equally to helium and all its isoelectronic two-electron family.

Were the last electron-electron repulsion term in (1.17) to be absent, the exact ground state wave function would be simply the product of two hydrogenic functions in \mathbf{r}_1 and \mathbf{r}_2 . Since the inter-electron repulsion in atoms is generally weaker than the attractive electron-nucleus terms (roughly 10% as will be seen below and in Section 1.4.3), this serves as a clue to one line of approach for the ground and low-lying states of helium. The ground state, in particular, yields immediately to the “Rayleigh-Ritz” variational principle which is based on the fact that this is the state of lowest energy. Therefore, any normalized two-electron “trial function”, $\psi_t(\mathbf{r}_1, \mathbf{r}_2)$, will give an energy expectation value, $\langle\psi_t|H|\psi_t\rangle$, that will necessarily lie above the exact ground state energy. Further, the difference will be second order in the “error”, the amount by which ψ_t differs from the exact ground state wave function. The strategy then is to pick a trial function with open constants, evaluate the energy expectation value, and then vary the resulting energy with respect to those open parameters to achieve a minimum value. In this manner, the best possible function within that class of trial functions is obtained as an approximation to the exact ground state.

The simplest choice, a product of two hydrogenic $1s$ functions with an effective charge Z_{eff} as a variational parameter,

$$\psi_t(\mathbf{r}_1, \mathbf{r}_2) = N \exp[-Z_{\text{eff}}(r_1 + r_2)/a_0], \quad (1.18)$$

is already instructive. N is a normalization constant, determined in terms of Z_{eff} so as to satisfy $\iint \psi_t^2 d\mathbf{r}_1 d\mathbf{r}_2 = 1$. Upon evaluating the expectation value of H in (1.17) with such a function, elementary integrations lead to

$$E = \left(Z_{\text{eff}}^2 - 2Z Z_{\text{eff}} + \frac{5}{8} Z_{\text{eff}} \right) (e^2/a_0), \quad (1.19)$$

the three terms being, respectively, the kinetic, electron-nucleus, and electron-electron energies. This expression reaches a minimum at $Z_{\text{eff}} = Z - \frac{5}{16}$, with value

$$E_{\text{min}} = - \left(Z - \frac{5}{16} \right)^2 (e^2/a_0) \approx -5.70 \text{ Ry for } Z = 2. \quad (1.20)$$

This compares favorably (lying above, as expected) with the “exact” [3] non-relativistic helium ground state energy of -5.8074487540682391966 . The effective charge seen by each electron is smaller than the nuclear charge Z by $\frac{5}{16}$ which can be interpreted as the partial screening of the nuclear field provided by the other electron. The corresponding wave function in (1.18) is, therefore, a reasonable first approximation although, as usual in such variational applications, it will fare poorer, containing “first-order errors” when used for any other physical quantity than the energy for which it has been variationally tailored.

Indeed, with particles 1 and 2 completely independent, the wave function in (1.18) is grossly deficient in one regard because it contains no correlation at all between the two electrons. As will become important in Section 2.4.1, this is a particular failing for describing helium’s isoelectronic partner, the negative ion H^- (with $Z = 1$), where such electronic correlation is already crucially important in the ground state. As can be seen from (1.20) with $Z = 1$, the obtained E_{min} is less negative than -1 Ry , which is the energy of $\text{H}(1s) + \text{electron}$ at infinity, so that we cannot even conclude that a bound negative ion exists.

Further terms with more variational parameters can be included in (1.18). In particular, an explicit dependence on r_{12} introduces electron “correlations”. Such trial wave functions,

$$\psi_t = N \exp[-Z_{\text{eff}}(r_1 + r_2)] \Sigma_{abc} C_{abc} r_1^a r_2^b r_{12}^c, \quad (1.21)$$

with as many as a thousand parameters C have been used by Hylleraas, Pekeris, Kinoshita, and others to get the “essentially exact” ground state for He with the numerical value for the energy quoted below (1.20). These calculations are carried out to many more figures than experimentally available results on the helium atom which include, of course, relativistic contributions. This is because one of the purposes of the very accurate non-relativistic computations is to assess these additional relativistic terms, including quantum electrodynamic corrections, and

test our theoretical ability to calculate them. Along with the cited ground state energy of -5.81 Ry, these calculations provide expectation values for other quantities. Thus $\langle 1/r_1 \rangle = 1.69 a_0^{-1}$ which means that the electron-nucleus terms in (1.17) provide -13.5 Ry; the kinetic energy terms, by virtue of the virial theorem, give $+5.81$ Ry, so that the electron-electron repulsion gives 1.88 Ry. Note that this is approximately $(-1/7)$ of the electron-nucleus energy (see Section 1.4.3). Also, one finds $\langle \cos \theta_{12} \rangle \approx -0.065$ for the angle θ_{12} between the two electrons, reflecting a slight angular correlation that tends to keep the electrons apart.

3.2 Excited states

Turning next to excited states in helium, the lowest of these has one electron placed in the first excited hydrogenic orbitals $2s$ or $2p$. In hydrogen, these states are degenerate but no longer so in helium, that degeneracy which is characteristic of the pure Coulomb attraction invalidated by the electron-electron repulsion term. With the two electrons distinguished now in the n quantum number ($n = 1$ and 2), the Pauli principle no longer restricts to a single state. Both singlet and triplet combinations of the spins of the two electrons are allowed, unlike in the ground state where the triplet was forbidden. The principle is still in operation, however, in requiring overall antisymmetry of the wave function under interchange of the two electrons. Since singlet (triplet) is antisymmetric (symmetric) under interchange of spin labels, it must go with the multiplicative spatial wave function which is symmetric (antisymmetric) under the interchange $\mathbf{r}_1 \leftrightarrow \mathbf{r}_2$. Therefore, we have

$$\begin{aligned} \psi(2^1S) &= \frac{1}{\sqrt{2}}[1s(\mathbf{r}_1)2s(\mathbf{r}_2) + 1s(\mathbf{r}_2)2s(\mathbf{r}_1)](|\uparrow\downarrow\rangle - |\downarrow\uparrow\rangle)/\sqrt{2}, \\ \psi(2^3S) &= \frac{1}{\sqrt{2}}[1s(\mathbf{r}_1)2s(\mathbf{r}_2) - 1s(\mathbf{r}_2)2s(\mathbf{r}_1)] \begin{cases} |\uparrow\uparrow\rangle \\ \frac{1}{\sqrt{2}}(|\uparrow\downarrow\rangle + |\downarrow\uparrow\rangle) \\ |\downarrow\downarrow\rangle \end{cases} \quad (1.22) \end{aligned}$$

and a similar set for the 2^1P and 2^3P states. We have used here a standard spectroscopic notation for multi-electron states, the total spin S and total orbital angular momentum L of the electrons denoted as $2^{S+1}L$. The 2 in front is used in helium for describing the n quantum number of the outer electron in such singly-excited states.

In evaluating the expectation value of H in (1.17) with the wave functions (1.22), the spins play no further role, the non-relativistic Hamiltonian containing no spin dependence (spin-orbit and such weak relativistic

corrections to H are handled through perturbation theory – see Section 3.3). With the individual orbitals assumed orthonormalized, we have

$$\begin{aligned} \langle H \rangle &= E_{1s} + E_{2s} + e^2 \iint \frac{|1s(\mathbf{r}_1)|^2 |2s(\mathbf{r}_2)|^2}{r_{12}} d\mathbf{r}_1 d\mathbf{r}_2 \\ &\pm e^2 \iint 1s^*(\mathbf{r}_1) 2s^*(\mathbf{r}_2) \frac{1}{r_{12}} 1s(\mathbf{r}_2) 2s(\mathbf{r}_1) d\mathbf{r}_1 d\mathbf{r}_2, \quad (1.23) \end{aligned}$$

where E_{1s} (and also E_{2s}) is a “one-electron energy”, $\langle 1s | \frac{\mathbf{p}^2}{2\mu} - \frac{Ze^2}{r} | 1s \rangle$. The electron-electron interaction gives rise to a pair of “two-electron” terms, respectively referred to as “direct” and “exchange”, the latter carrying the \pm signs of singlet/triplet contained in (1.22). The direct term, common to both, has an obvious classical interpretation as the electrostatic repulsion of the two charge densities of $1s$ and $2s$ and is clearly positive. The exchange term, arising from the Pauli principle, depends explicitly on the wave functions of the orbitals and is of purely quantum character, having no classical counterpart (although Section 1.4.3 will give an approximate description in terms of densities). The orbitals $1s$ and $2s$ being purely real, the complex conjugates in (1.22) are redundant but have been retained so as to be applicable to other orbitals $n\ell m$ that may carry complex elements through their φ dependence.

Although originating in spin and the attendant Pauli principle, the exchange term depends on non-relativistic elements alone, namely, on the wave functions involved. Through a Fourier identity,

$$\frac{1}{r_{12}} = \frac{1}{2\pi^2} \int e^{i\mathbf{k}\cdot(\mathbf{r}_1-\mathbf{r}_2)} d\mathbf{k}/k^2, \quad (1.24)$$

the integral itself in the exchange contribution is non-negative (the integrand is explicitly so, involving a product of a function and its complex conjugate and other squared factors). Thereby it follows that triplet states lie lower in energy than their singlet counterparts, as shown in Fig. 1.3. This same argument is at the heart of the fundamental mechanism for ferromagnetism called the “Heisenberg exchange interaction”, as a result of which a state of aligned spins lies lower in energy. Note that whereas one-electron terms are of the order of 1 Ry, exchange splittings are about an order of magnitude smaller.

Higher, singly-excited states in He, $n^{1,3}L$, can be treated in a similar fashion, with an $n\ell$, $\ell = L$, in place of the $2s$ orbital in (1.22). For each (S, L) , these will form a “Rydberg” series in n converging finally, as $n \rightarrow \infty$, to the single ionization limit of $\text{He}^+(1s)$ which, being hydrogenic with $Z = 2$, lies at -4 Ry. Such a series of singly-excited states is

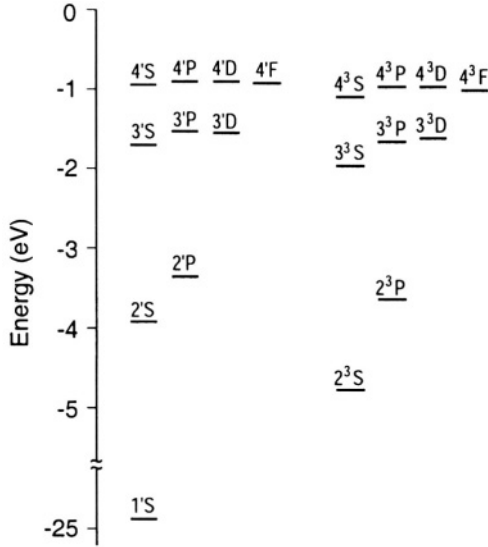


Figure 1.3. Singly-excited states of helium: singlet (parahelium) and triplet (orthohelium).

similar to the Bohr spectrum for hydrogen in that the outer electron, particularly with increasing n , sees a core of charge $Z = 1$, but with one important difference. Their energies below the -4 Ry of the $\text{He}^+(1s)$ state fit the modified expression,

$$-Ry/(n - \mu_\ell)^2, \quad (1.25)$$

rather than the Bohr (1.2), with μ_ℓ a positive constant between 0 and 1. Fitting spectroscopic data in He to this formula gives, for instance, $\mu_0 \approx 0.14$, $\mu_1 \approx -0.012$. These constants μ_ℓ are called quantum defects (correspondingly, $n^* \equiv n - \mu_\ell$ is an “effective quantum number”) and represent the somewhat stronger binding the outer electron experiences than in the hydrogen atom due to its excursions into and within the orbit of the inner $1s$ electron where it sees a stronger nuclear attraction. As expected from the first factor in the radial functions in (1.9), the higher the ℓ the lower is the probability for being in the small- r core region and, therefore, the smaller the quantum defect μ_ℓ . In most atoms, for orbitals with $\ell > 3$, μ_ℓ is essentially zero. In Li, we have $\mu_0 = 0.4$, $\mu_1 = 0.05$, and $\mu_2 = 0.002$.

Although the quantal origins of the quantum defect were recognized later, an expression such as (1.25) was used much earlier as a purely empirical organization of spectral levels in atoms other than hydrogen, so that this formula is often referred to as the Bohr-Rydberg formula for atomic energy levels. The differing roles of n and μ_ℓ are significant. The dominant variation, from one level n to the next, is controlled by the $1/n^2$ form characteristic of the Coulomb field which the outer electron sees over most of its motion at larger r . The μ_ℓ , which are only very weakly dependent on energy or n (indeed, sensibly constant once past the first few initial values of n), reflect dependences on the small- r region where strong potentials prevail so that changes in the asymptotic (or total) energy are dwarfed into insignificance. Since these considerations apply not only in helium but in any many-electron atom for singly-excited states where one electron moves out further and further from the rest of the core, the Bohr-Rydberg expression and its interpretation in terms of the differing roles of n and μ_ℓ apply to all atoms.

These differing roles of large- r and small- r regions form the basis of a powerful method of analysis called quantum defect theory. Not restricted to Coulomb fields alone, any combination of a long and short range potential, the former common to many systems whereas the latter may be specific to each system, can be analyzed analogously. The long range part is sensitive to small changes in energy and is best treated analytically, whereas the short range has stronger potentials so that the scale of variation is set by larger energies. Numerical handling of each specific system can then be confined to the short range and carried out over a coarse grid [4].

Finally, with reference to Fig. 1.3, all the singlet levels (which include the ground state) constitute a separate family from the triplets, because operators that do not explicitly involve coupling of spin and orbit cannot connect a state of one group to any state of the other, singlets and triplets being orthogonal. The non-relativistic Hamiltonian itself in (1.17), couplings of the electrons to the electromagnetic field which are involved in photoabsorption and emission, etc., fail to connect the two families so that they behave almost like two different species, called orthohelium ($S = 1$) and parahelium ($S = 0$). This feature remains true in other light atoms as well besides helium, also in molecules (see Section 6.2.7). Only in heavier atoms, where the relativistic corrections become more important and the attendant spin-orbit interactions that couple S and L become appreciable, are such “inter-combination” transitions between states of different S seen, the notable example being the spectrum of Hg, its familiar blue lines arising from $^3P \rightarrow ^1S$.

3.3 Configuration interaction

The two-electron Hamiltonian in (1.17) being non-separable in \mathbf{r}_1 and \mathbf{r}_2 , the corresponding one-particle quantum numbers, $n_1\ell_1m_1$ and $n_2\ell_2m_2$, do not have exact validity. Thus, descriptions of the ground state as $(1s)^2$ or an excited state as $(1s)(n\ell)$ are, necessarily, approximate. Of course, again as a result of the weakness of the electron-electron potential that is responsible for the non-separability when compared with other terms in the Hamiltonian, the approximation of using such “single configurations” for describing atomic states is quite good and reasonable as a starting point. Nevertheless, in principle, the only exactly conserved quantities and, therefore, good quantum numbers are those like parity, S , and L , which belong to the combined two-electron system and whose operators commute with H . In principle, any state of helium, of say 1S symmetry, is a linear combination of the various independent-particle configurations compatible with this symmetry: $1s^2$; $1s2s$, $1s3s, \dots 1sns \dots$; $2s^2$, $2s3s, \dots 2sns, \dots$; $2p^2 \dots 2pnp, \dots$; \dots . The set includes not only the bound configurations n but also the corresponding ones in the continuum because it is only such a full set of all product hydrogenic orbitals that provides a complete basis for writing the two particle wave function $\psi(^1S)$. Note also the inclusions of configurations in which neither electron is in $n = 1$. These are called “doubly-excited” configurations.

This picture provides an alternative view and, at the same time, an alternative calculational procedure for the states of the helium atom. Going under the name of the “configuration interaction (CI) method”, one writes $\psi_t(\mathbf{r}_1, \mathbf{r}_2)$ as a superposition of some finite number of configurations, the coefficients of superposition and even possibly of parameters in the individual orbitals left as open variational parameters. Upon evaluating $\langle \psi_t | H | \psi_t \rangle$ with such a choice, the variational principle can again be exploited to determine the ground state by minimizing the energy with respect to the variational parameters. The final result will be a superposition with dominant $(1s)^2$ but some mix of other configurations as an approximation to the exact (and unknown) helium ground state two-electron wave function. In this approach, it is the admix of other configurations that describes correlations between the electrons. Thus, so long as no $\ell \neq 0$ configurations are in the mix, there is no angular correlation between the two electrons, with the directions \hat{r}_1 and \hat{r}_2 totally uncorrelated. It is the occurrence of $\ell \neq 0$ (though, of course, with $\ell_1 = \ell_2$ to maintain the overall $L = 0$) configurations that leads to a non-trivial dependence on $\hat{r}_1 \cdot \hat{r}_2 = \cos \theta_{12}$, that is, on the angle between the two radius vectors. It is only by superposing different ℓ values that any structure in the conjugate variable θ_{12} can be realized. Similarly,

the superposition of different n_1 and n_2 configurations leads to radial correlation between the relative distances r_1 and r_2 of the two electrons from the nucleus.

The configuration interaction approach also has the merit of providing simultaneously excited states of the same (S, L) symmetry along with the ground state. Thus, if N such configurations are chosen and the coefficients of their superposition varied, this is tantamount to setting up an $N \times N$ energy-matrix formed out of matrix elements of H between them. The N eigenvalues of this matrix provide upper bounds successively on the energies of the lowest N states of that (S, L) symmetry. This is a matrix version of the Rayleigh-Ritz variational principle to which is sometimes attached other names such as Hylleraas, Undheim, and MacDonald. Thus, within the 1S space, the lowest eigenvalues will always lie above the exact ground state, the next higher one above 2^1S , etc. As additional variational parameters in the one-electron orbitals or additional configurations are added, the variational principle guarantees continued improvement in each of the bounds. Of course, the lower eigenvalues provide a better description of the corresponding states than the higher ones which may be very poor, sometimes lying far above the exact energy of the state they purport to describe.

4. Heavier Atoms

4.1 Configurations and states

The methods of the previous section for helium extend readily to other many-electron atoms and ions. We will consider successively more sophisticated treatments, starting with the simplest semi-empirical ones. The first step in describing the ground or low-lying states is to select the dominant configuration and determine the total quantum numbers of the angular momenta of the electrons. The Pauli principle provides the starting point for determining the configuration. Since each electron has to be distinguished in at least one of the four labels, n , ℓ , m , and m_s ($= \uparrow$ or \downarrow) for its spin projection, successive filling of the lowest orbitals determines the filled shells, $(1s)^2$, $(2s)^2$, $(2p)^6$, etc.

For the higher orbitals with $\ell \geq 2$, an empirical rule due to Madelung, that the shells fill according to the value of $(n + \ell)$ and that, for the same $n + \ell$, the higher ℓ is occupied first, needs to be applied. This departure from the “hydrogenic ordering” is made plausible by the feature seen, for instance, in (1.10), that electrons in such states have smaller radial extent and lie below the “surface” of the atom. This is first manifest in the transition elements where, once $1s, 2s, 2p, 3s$, and $3p$ shells are filled, with 18 electrons in the noble gas Ar, the next two electrons fill $4s$ rather

than $3d$ ($n + \ell = 4$ vs 5). The dominant ground state configuration of Ca(20) is, therefore, $1s^2 2s^2 p^6 3s^2 p^6 4s^2$. After this, the $3d$ is occupied and then the $4p$ (same $n + \ell = 5$, the d taking precedence). The $3d$ shell being “subsurface”, the entire set of transition elements from Sc(21) through Cu(29) share the common chemistry of the outer $4s$ electron and occupy a single position in The Periodic Table. There are slight “glitches”, again because of another feature, that a completely closed or even half-closed (thus d^{10} or d^5) shell is more strongly bound. As a result, instead of the $3d^9 4s^2$, the $3d^{10} 4s$ may be more favored, similarly $3d^5 4s$ rather than $3d^4 4s^2$. This also means that such close, competing configurations may be strongly mixed in the ground and low-lying states of such atoms. The same features occur later in The Periodic Table for the $4d$ or $5d$ and the f shells, all having this “sub-surface” quality as seen, for instance, in the values of $\langle r \rangle$ and $\langle r^2 \rangle$ in (1.10).

With the configuration decided, the spectroscopic state follows by angular momentum addition, together with the Pauli principle. Any filled shell can occur in only one unique way, each electron allotted to one each of the available (n, ℓ, m, m_s) . That there is only one state means $S = 0$ and $L = 0$, namely, 1S . Thus, as far as angular momenta are concerned, a filled shell has the same quantum numbers as vacuum. As elsewhere in field theories or in semi-conductor energy bands, a useful corollary is to regard an “almost-filled” configuration as “holes” in the vacuum which again, for angular momentum considerations, can be handled as spin- $\frac{1}{2}$ particles. In this manner, the overall S and L quantum numbers follow from all the partially filled shells in the configuration.

An example of the first row in The Periodic Table beyond helium will illustrate the essentials. Li has the configuration $1s^2 2s$ in the ground state, that one last electron giving the labels 2S . Next, Be is $1s^2 2s^2$ and, with both shells filled, is 1S . The next electron in B goes into $2p$ to give $1s^2 2s^2 p$ 2P . The carbon atom has the configuration $1s^2 2s^2 p^2$. There are now two p electrons (apart from closed shells) whose angular momenta have to be added. First, the rules for such addition alone allow $S = 0, 1$ and $L = 0, 1, 2$. But, the two electrons being identical in n and ℓ , the Pauli principle constrains the possibilities just as in the discussion for helium in Section 1.3. As before, the singlet (triplet) being antisymmetric (symmetric) in interchange of spin coordinates, it has to accompany symmetry (antisymmetry) under spatial interchange. For the case of two particles, and only for two, this is determined by whether L is even (odd). Thus, the only allowed states are 3P , 1S , and 1D , the other combinations of 1P , 3S , and 3D being forbidden for a pair of identical fermions. A check is provided by the total number of states which is $(3 \times 3) + (1 \times 1) + (1 \times 5) = 15$, exactly the number of antisym-

metric elements, the binomial coefficient $\binom{6}{2}$, for a p configuration with its basic $2(2\ell+1) = 6$ states. Two non-identical p electrons, as in an excited configuration $1s^2 2s^2 p^3 p$ of carbon, would have all $6^2 = 36$ states, but the antisymmetry requirement of the Pauli principle cuts the number by more than half when the two p electrons have the same n . A simple statement of this rule for a pair ℓ^2 of spin- $\frac{1}{2}$ particles is that $S + L$ must be even, whatever the ℓ .

The next question of which of the three states lies lowest in energy, and is thereby the ground state of the carbon atom, is determined by the so-called Hund's rules. The first of these three rules says that, for the same reasons discussed in Section 1.3 for the exchange energy in helium, the highest allowed S is the most bound. Thus 3P gives the labels for carbon's ground state. In this example, there is no need to go further but, when several alternative L values share the highest S , Hund's second rule points to the largest L for the strongest binding. Finally, Hund's third rule fixes the total angular momentum J obtained from $\mathbf{S} + \mathbf{L} = \mathbf{J}$. Thus, of the three J values (together called a "term") in carbon's 3P , the lowest J , namely zero, has the lowest energy. Spin-orbit interactions (Section 3.3.2) cause "fine-structure" splittings, raising slightly the $J = 1$ and 2 states. For later purposes below, this rule is exactly reversed in the case of holes rather than electrons, when the highest J constitutes the ground state. The gain in binding energy with S also lies behind the earlier observation that half-filled shell configurations are favored over neighbouring configurations.

The next atom, nitrogen, has a third p electron, its ground state configuration being $1s^2 2s^2 p^3$. The three p electrons determine the state labels. The addition of three spins allows $S = \frac{1}{2}$ (in two ways) and $\frac{3}{2}$. Of these, by Hund's first rule, the $\frac{3}{2}$ or quartet will have the lowest energy. Simple addition of orbital angular momenta, $\mathbf{1} + \mathbf{1} + \mathbf{1}$, gives rise to many possibilities for L so that it is more convenient now to consider the Pauli principle first, and in the following version. Since $S = \frac{3}{2}$ has as one state all three spins aligned, whether $\uparrow\uparrow\uparrow$ or $\downarrow\downarrow\downarrow$, this means the three electrons share a common n, ℓ , and m_s . They have perforce to be distinguished in the fourth label m by having each in $m = 1, 0$, and -1 , the three allowed values for p -electrons. This can be accomplished in only one way so that the total L must be zero. Therefore, nitrogen's ground state is ${}^4S_{\frac{3}{2}}$, the J subscript uniquely fixed in this case as $\frac{3}{2}$. The total number of antisymmetric configurations for three p electrons is $\binom{6}{3} = 20$. Besides the four-fold degenerate ${}^4S_{\frac{3}{2}}$ ground state, the others are the

six-fold 2P and the ten-fold 2D . These are low-lying excitations of the ground configuration's multiplet structure.

Oxygen follows, with configuration $1s^22s^2p^4$. Here, the view of it as two p -holes in a filled p -shell reduces the problem to the one already discussed for carbon with 3P as the ground state. Hund's third rule, now applicable for this case of holes, fixes the ground state as 3P_2 . The next atom, fluorine $1s^22s^2p^5$, has one p -hole so that ${}^2P_{3/2}$ is its ground state. The row ends with neon and a filled p -shell, $1s^22s^2p^6 {}^1S_0$.

Finally, a fourth label besides $\{S, L, J\}$ is also included in specifying the spectroscopic state, the total parity of the system which is also a good quantum number, the parity operator commuting with the atomic Hamiltonian. Being a multiplicative quantum number, this is simply the product of the parities $(-1)^\ell$ of each electron; in particular, only the unfilled shells contribute and, for the above examples of the first row, we have

$$\text{Li}({}^2S_{\frac{1}{2}}^e), \text{Be}({}^1S_0^e), \text{B}({}^2P_{\frac{1}{2}}^o), \text{C}({}^3P_0^e), \text{N}({}^4S_{\frac{3}{2}}^o), \text{O}({}^3P_2^e), \text{F}({}^2P_{\frac{3}{2}}^o).$$

The parity label, e(ven) or o(dd), is an independent fourth label, having nothing to do with the coupling of angular momenta to give $\{S, L, J\}$ but fixed entirely by the configuration itself. Because the parity of a single electron's wave function is given by ℓ , a common misconception is to carry this over to many-electron states but, as seen in the above list, any particular L can have either even or odd parity.

The labels L and S are meaningful in light atoms and at low excitation when relativistic effects such as spin-orbit coupling (Section 3.3.2) are weak. The coupling of all electronic orbital angular momenta to L , and spins to S , is referred to as LS-coupling or Russell-Saunders coupling. It arose from the work of the Harvard astronomer Henry Norton Russell and his spectroscopy colleague Saunders; Russell's name is also attached to the famous Hertzsprung-Russell diagram of stellar luminosities and temperatures.

4.2 Simple screening pictures

With the configuration and state specified, the simplest description of the energy and wave function of an atom's ground state is given by a product of the orbital functions, with hydrogenic wave functions (1.7) and (1.9) serving as the first choice. The influence of the other electrons can be accounted for by an average screening they provide. As in the picture provided by (1.18) for helium, each $1s$ electron can be regarded as reducing the nuclear charge Z by approximately 0.3 for the other. A set of empirical rules of this kind, called Slater screening

constants, have been developed for each orbital. With shells arranged in the sequence $1s; 2sp; 3sp; 3d; 4sp; 4d; 4f; 5sp; 5d; \dots$, these rules are that for any of these shells, the amount of screening due to each of the other electrons is [5]

0.35 if in same shell except 0.3 for $1s$, 0.85 for each s and p of n less by 1 and 1 for more inner $n's$, 1 from all inner orbits for all d and f .
(1.26)

The above values are fixed by a classical electrostatic picture, that electronic charge distribution interior to any electron of interest provides an “inner screening” tantamount to that charge residing at the center, that is, at the nucleus. Likewise, all the exterior orbitals provide an “outer screening” which is a constant potential V_0 (there being no electrostatic force inside a shell of charge). In the Schrödinger equation, this just shifts the energy without affecting the wave function. The other aspect of core penetration by an outer electron, as discussed in Section 1.3.2, can also be incorporated by replacing n in the radial wave function for any $n\ell$ by an “effective quantum number” $n^* = n - \mu_\ell$. Once again, one simple empirical set of numbers is $n^* = 1, 2, 3, 3.7, 4$ and 4.2 for $n = 1, 2, \dots, 6$.

Together, such a model of screening (inner and outer) and core penetration leads to a description of the energy for any orbital $n\ell$,

$$\varepsilon_{n\ell} = -\frac{Z_{\text{eff}}^2 \text{Ry}}{n^{*2}} + V_0 \quad , \quad (1.27)$$

and a corresponding wave function which, for example, in B would be $1s \uparrow(1) 1s \downarrow(2) 2s \uparrow(3) 2s \downarrow(4) 2p \uparrow(5)$, again with each factor involving its own Z_{eff} and n^* . Although a relatively simple approximation based on classical physics and ignoring antisymmetrization and attendant exchange effects, such a screening model is a fairly good initial description of any atom.

Antisymmetrization is the next quantum feature that can be built in. Beyond two electrons, the factorization into orbital and spin wave functions as in (1.22) no longer holds but these expressions point to the required extension. By specifying both orbital and spin labels for each orbital, each of the four terms in (1.22) can be cast in the form of 2×2 determinants. Thus, the singlet state in (1.22) can be written as

$$\frac{1}{\sqrt{2}} \left[\frac{1}{\sqrt{2}} \begin{vmatrix} 1s \uparrow(1) & 1s \uparrow(2) \\ 2s \downarrow(1) & 2s \downarrow(2) \end{vmatrix} - \frac{1}{\sqrt{2}} \begin{vmatrix} 1s \downarrow(1) & 1s \downarrow(2) \\ 2s \uparrow(1) & 2s \uparrow(2) \end{vmatrix} \right], \quad (1.28)$$

where the 1 and 2 within parentheses stand for the combined orbital and spin coordinates of the two electrons. The middle member of the triplet state in (1.22) differs from (1.28) only in a change in sign from minus to plus, while the other two members of the triplet have a single determinant. This structure points to a convenient rendering of antisymmetrization through so-called “Slater determinants”. For the example above of boron, we have a 5×5 determinant,

$$\frac{1}{\sqrt{5!}} \begin{vmatrix} 1s \uparrow (1) & 1s \uparrow (2) & 1s \uparrow (3) & 1s \uparrow (4) & 1s \uparrow (5) \\ 1s \downarrow (1) & 1s \downarrow (2) & 1s \downarrow (3) & 1s \downarrow (4) & 1s \downarrow (5) \\ 2s \uparrow (1) & 2s \uparrow (2) & 2s \uparrow (3) & 2s \uparrow (4) & 2s \uparrow (5) \\ 2s \downarrow (1) & 2s \downarrow (2) & 2s \downarrow (3) & 2s \downarrow (4) & 2s \downarrow (5) \\ 2p \uparrow (1) & 2p \uparrow (2) & 2p \uparrow (3) & 2p \uparrow (4) & 2p \uparrow (5) \end{vmatrix}. \quad (1.29)$$

The factor in front is for normalization, each individual orbital assumed normalized. Evaluating $\langle \psi | H | \psi \rangle$ with such determinantal wave functions leads naturally to the exchange terms. The determinantal form naturally and explicitly exhibits alternative renderings of the Pauli principle. Thus, if the same orbital occurs more than once, such a determinant vanishes by virtue of having two identical rows. Also, interchange of the coordinates of any two electrons means interchanging two columns which leads to a change in sign of the wave function.

4.3 **The Thomas-Fermi self-consistent field model**

A universal model for atoms, due to Thomas and Fermi, pre-dates the Schrödinger equation and stands separate from developments in terms of wave functions, but is worth considering for a variety of reasons [6]. First, it provides a simple picture in terms of a single equation and potential capable of describing any atom, together with reasonably accurate scaling relations of atomic properties as a function of Z . Although it does not have shell structure, it provides a good accounting across The Periodic Table when averaged over shell structure. And, in more recent times, it has been proved to be mathematically exact as an asymptotic theory when $Z \rightarrow \infty$ (admittedly, an academic limit for a non-relativistic atomic description). And, most importantly, the model is the natural precursor of “density functional” calculations that are now widespread in atomic, molecular, and condensed matter calculations in physics and in quantum chemistry. It shares with density functional theories the virtue that instead of a $3N$ -coordinate complex wave function for an N -electron atom, it deals with a 3-dimensional real electron density

distribution. Indeed, this provides the computational and conceptual attraction that has led to the widespread use of the density functional method [7].

As we saw with the helium Hamiltonian (1.17), the kinetic energy and the exchange part of the electron-electron interaction are the ones that require wave functions explicitly in their evaluation, while the electron-nucleus and direct electron-electron energies require only a one-electron charge or number density. This is true for any atom, so that these latter pieces can be written immediately as

$$-Ze^2 \int \frac{\rho(\mathbf{r}) d\mathbf{r}}{r} + \frac{e^2}{2} \iint \frac{\rho(\mathbf{r}_1) \rho(\mathbf{r}_2) d\mathbf{r}_1 d\mathbf{r}_2}{r_{12}}, \quad (1.30)$$

with $\rho(\mathbf{r})$ the one-electron number density, normalized according to

$$\int \rho(\mathbf{r}) d\mathbf{r} = N, \quad (1.31)$$

N being the number of electrons. We will let N be a new parameter, possibly different from Z , so as to handle positive ions and neutral atoms equally.

Setting aside for a moment the exchange part of the electron-electron interaction as generally an order of magnitude smaller than the other terms, the question that remains, and which was addressed by Thomas and Fermi, is how to write the kinetic energy as a functional of $\rho(\mathbf{r})$ [6]. The clue is to consider the electrons in an atom as constituting a free electron gas. For a uniform electron gas, the density ρ can be related to the Fermi momentum p_F by a straightforward argument of quantum physics, that every element of phase space volume of size h^3 can accommodate only two electrons (more generally, any fermions of spin- $\frac{1}{2}$) with spins \uparrow and \downarrow . Therefore, we have

$$\rho = 2 \frac{4\pi}{3} \frac{p_F^3}{h^3} = p_F^3 / \pi^2 \hbar^3. \quad (1.32)$$

This relationship is now applied locally, at any point \mathbf{r} in the atom, to provide a connection between the local density $\rho(\mathbf{r})$ and the Fermi momentum $p_F(\mathbf{r})$ that represents the highest momentum state occupied. Next, an average “kinetic energy density” at any \mathbf{r} is taken as

$$t(\mathbf{r}) = \langle \mathbf{p}^2 / 2\mu \rangle = \frac{2 \int (\mathbf{p}^2 / 2\mu) d\mathbf{p}}{2 \int d\mathbf{p}} = \frac{3}{5} \frac{p_F^2(\mathbf{r})}{2\mu}, \quad (1.33)$$

and thus related through (1.32) to the local density,

$$t(\mathbf{r}) = (3/10\mu) \left(3\pi^2\hbar^3\rho(\mathbf{r})\right)^{2/3}. \quad (1.34)$$

The total kinetic energy $T = \int t(\mathbf{r})\rho(\mathbf{r})d\mathbf{r}$ is then given by

$$T = (3/10\mu) (3\pi^2\hbar^3)^{2/3} \int \rho^{5/3}(\mathbf{r})d\mathbf{r}. \quad (1.35)$$

The above key relationship permits one to write the energy of an atom as a functional of $\rho(\mathbf{r})$, that is as a function of $\rho(\mathbf{r})$ which is itself a function of \mathbf{r} :

$$E = K \int \rho^{5/3}(\mathbf{r})d\mathbf{r} - Ze^2 \int d\mathbf{r} \rho(\mathbf{r})/r + \frac{e^2}{2} \iint d\mathbf{r}_1 d\mathbf{r}_2 \rho(\mathbf{r}_1)\rho(\mathbf{r}_2)/r_{12}, \quad (1.36)$$

with $K = (3/10)(3\pi^2)^{2/3}(\hbar^2/\mu)$ dependent on fundamental constants alone. The index 5/3, called the non-relativistic adiabatic index, is according to the above derivation $(1+ 2/\text{dimension})$, dependent only on the dimensionality of space. It occurs elsewhere in physics; specifically, just the above term in (1.35), together with its counterpart for a relativistically degenerate electron gas which has an index 4/3, is responsible for holding a white dwarf stable against gravitational collapse till the ‘‘Chandrasekhar limiting mass’’ is exceeded [8].

With the ground state energy in (1.36) a functional of $\rho(\mathbf{r})$, the best density follows from the variational principle $\delta E/\delta\rho = 0$,

$$(5K/3)\rho^{2/3}(\mathbf{r}) - (Ze^2/r) + e^2 \int d\mathbf{r}' \rho(\mathbf{r}')/|\mathbf{r} - \mathbf{r}'| = \lambda, \quad (1.37)$$

the λ a Lagrange constant to reflect the constraint (1.31). It is called the chemical potential and vanishes for a neutral atom. The second and third terms represent, of course, the electrostatic potential at a point \mathbf{r} due to the nucleus and the electronic charge distribution. Using Poisson’s equation, operating by ∇^2 on (1.37) converts it into an equivalent differential equation,

$$\nabla^2 \rho^{2/3}(\mathbf{r}) = (12\pi/5K) \rho(\mathbf{r}). \quad (1.38)$$

Eqs. (1.37) and (1.38) constitute alternative forms of the Thomas-Fermi equation. Note they are nonlinear. The latter, in particular, can be solved once and for all as a universal $\rho(\mathbf{r})$ that describes any

atom or positive ion. Fig. 1.4 gives the corresponding “universal atomic potential” $\phi(x)$ provided by the Thomas-Fermi model, defined through

$$\frac{5K}{3} \rho^{2/3} - \lambda = -V(r) = \frac{Z}{r} \phi(r), \quad (1.39)$$

with x a dimensionless distance, $r = \frac{x}{2} \left(\frac{3\pi}{4}\right)^{2/3} Z^{-1/3}$.

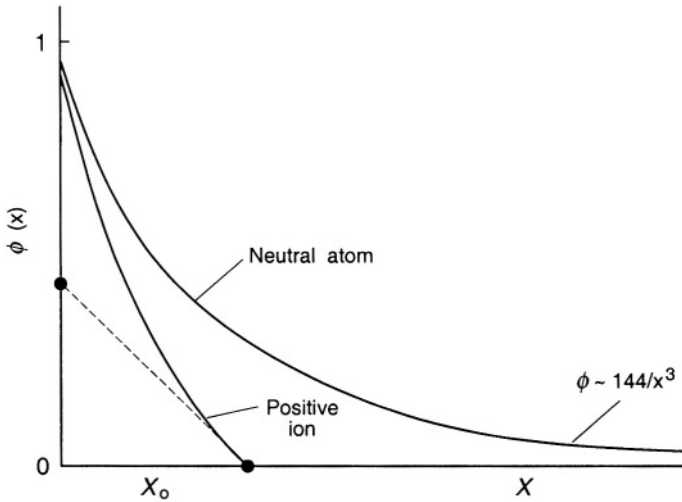


Figure 1.4. Atomic potential (1.39) in the Thomas-Fermi model.

The energy E in (1.36) in the Thomas-Fermi model for a Z -electron atom is given by $-1.537 Z^{7/3}$ Ry. The characteristic scaling with Z follows straightforwardly from (1.31) and (1.36), together with a corresponding relation that distances scale as $(0.885 a_0) Z^{-1/3}$. As shown in Fig. 1.5 for a comparison with experimental data, although the model does not contain local variations reflecting shell structure, the result in (1.39) is a fairly good approximation across The Periodic Table. Of course, since it rests on the concept of a local electron density, regions of the atom such as $r \rightarrow 0$ or $r \rightarrow \infty$ where there are too few electrons for a density to be meaningful cannot be expected to be adequately described. It has been proved that this result, both in the $7/3$ power and in the numerical coefficient in front in E , is asymptotically exact for the real non-relativistic quantum-mechanical Hamiltonian for a Z -electron atom [6]. For these reasons, and for the simple scaling results it provides for many atomic properties, the Thomas-Fermi model remains useful even

in these days of more sophisticated quantum-mechanical treatments. It is also a consequence of the model that the electron-electron term in (1.36) turns out to be $-1/7$ of the electron-nucleus energy, as observed earlier (Section 1.3.1) for helium.

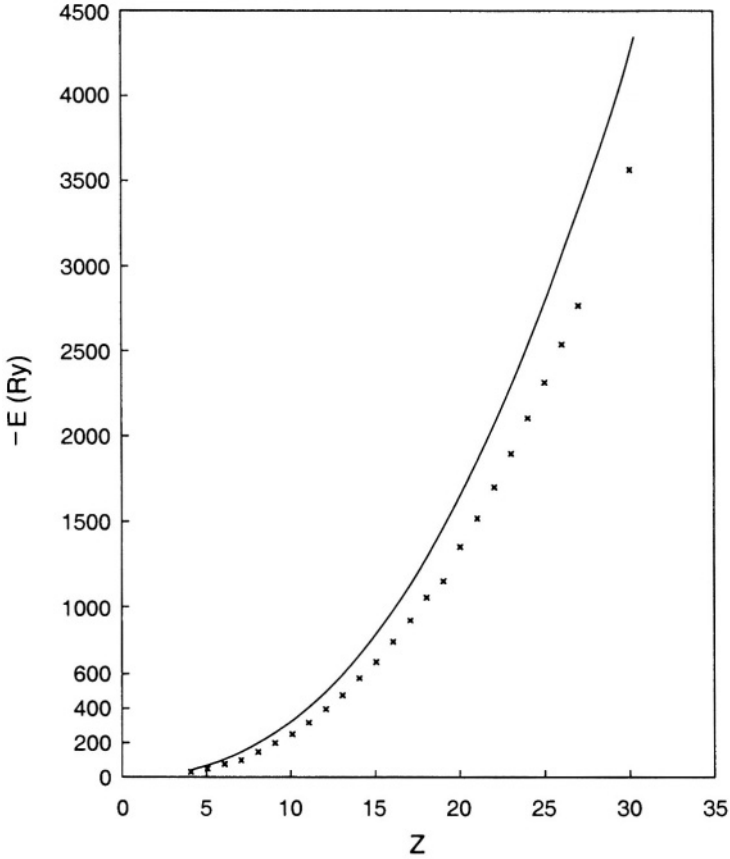


Figure 1.5. Total ground state energy of atoms. Solid line is from the Thomas-Fermi model, crosses from experimental data and indistinguishable from the three-parameter fit given in the text.

The characteristic Z -scalings above have their origins in a simple model one can construct based only on the Bohr expression (1.2) and the Pauli principle's restriction of $2n^2$ electrons for each shell. For simplicity, if we consider a Z -electron atom with all shells from $n = 1$ to some n_{\max} filled, and ignore completely the electron-electron interaction, the energy is easily written down,

$$E = -Z^2 \sum_{n=1}^{n_{\max}} 2n^2 \left(\text{Ry}/n^2 \right) = - \left(2Z^2 n_{\max} \right) \text{Ry}. \quad (1.40)$$

At the same time,

$$\sum_{n=1}^{n_{\max}} 2n^2 = Z, \quad (1.41)$$

which for large Z and n_{\max} can be approximated by an integral to give $n_{\max} = (3Z/2)^{1/3}$. This gives in (1.40) the result $E \propto -Z^{7/3}$. Further, it shows that the expansion parameter for further correction terms beyond the leading $Z^{7/3}$ is $Z^{-1/3}$. Indeed, an expression of the form $E = a Z^{7/3} + bZ^2 + cZ^{5/3}$ gives a very good fit to the entire set of data in Fig. 1.5.

The exchange part of the electron-electron energy which is intrinsically quantum in nature can also be approximated by an expression in terms of the density $\rho(\mathbf{r})$. An algebraic expression can be derived based on using plane waves to describe the electron gas, as one expects from the assumption of a uniform density, but here we give a plausibility argument which contains the essential physics. Exchange, associated with the Pauli *exclusion* principle, arises from the fact that once an electron is present at some point \mathbf{r} , another identical one with the same spin projection is excluded. Therefore, each electron can be considered to dig a ‘‘Fermi’’ hole in the background density which can be modeled as a sphere of radius r_F such that $(4\pi/3)r_F^3\rho = 1$. The absence of negative charge in this sphere can be achieved by superposing a positive charge distribution uniformly over the sphere to cancel the electronic ρ . As a result, the electron at the center gains an attractive energy of interaction with this positive charge of $-e^2(9\pi\rho/2)^{1/3}$. The total exchange energy is, therefore,

$$E_{\text{exch}} = -e^2(9\pi/2)^{1/3} \int \rho^{4/3}(\mathbf{r}) d\mathbf{r}. \quad (1.42)$$

Such a term, also a functional in density, can be readily incorporated into (1.36) and gives what is called the Thomas-Fermi-Dirac model. From the scaling relations noted earlier, it follows that $E_{\text{exch}} \propto Z^{5/3}$, the exchange energy being relatively of lower order than the three terms in (1.36), all with a $Z^{7/3}$ dependence.

Modern density-functional theories for many electron systems, whether in atoms, in quantum chemistry, or in condensed matter, employ much more sophisticated functional dependences on $\rho(\mathbf{r})$ than those in (1.36) and (1.42) for the kinetic and exchange energies. A theorem due to Kohn and Hohenberg proves the existence of an energy functional that is exact for the quantum-mechanical system without specifying the form of

that functional. Undoubtedly, it will have some very complicated *non-local* dependence on $\rho(\mathbf{r})$ but all calculational schemes, starting with the work of Kohn and Sham, seek increasingly better *local* density functionals to provide successively better approximations to the exact ground state energy [7].

4.4 Exact treatments: Hartree-Fock and configuration interaction

Although, already as in the case of helium, an exact closed form solution of a many-electron Hamiltonian is not possible, schemes are available that are, in principle, capable of reaching iteratively any desired accuracy. One method is the immediate generalization of Section 1.3.3's configuration interaction method for helium. Thus, a properly antisymmetrized determinantal wave function as in (1.29) is constructed for each of the dominant configurations that may be expected to describe the low-lying spectrum of an atom, the orbitals themselves of suitable form with open variational parameters. The Hamiltonian matrix between these configurations is solved for its lowest eigenvalues, and the variational parameters determined so as to get the lowest energy value possible. Corresponding superpositions of the configuration wave functions will then describe the ground and lowest lying excited states of the atom for any $^{2S+1}L_J$ symmetry.

An alternative approach, which gives a set of integro-differential equations to be solved for the orbitals, is called the Hartree-Fock method. Again, several Slater determinants can be used for higher accuracy but, to illustrate the method, consider again one such as in (1.29) for boron. When $\langle H \rangle$ for the atomic Hamiltonian is evaluated with such a function, the expression for the energy consists of one-electron and two-electron "direct" and "exchange" energies just as in the example in (1.23). At this stage, regarding the N orbital functions ϕ_i for the N -electron atom/ion as unknown, formal variation of E with respect to each of them is set equal to zero to give a set of coupled equations for the N orbitals. These equations have the form

$$\left\{ -\frac{\hbar^2}{2\mu} \nabla^2 - e^2 \sum_{j \neq i} \int d\mathbf{r}' \frac{|\phi_j(\mathbf{r}')|^2}{|\mathbf{r} - \mathbf{r}'|} \right\} \phi_i(\mathbf{r}) \pm e^2 \sum_{j \neq i} \int d\mathbf{r}' \frac{\phi_j^*(\mathbf{r}') \phi_i(\mathbf{r}')}{|\mathbf{r} - \mathbf{r}'|} \phi_j(\mathbf{r}) = \varepsilon_i \phi_i(\mathbf{r}), \quad (1.43)$$

with $i = 1, 2, \dots, N$. Besides the one-electron kinetic, electron-nucleus, and direct electron-electron energies, the exchange interaction couples the set of equations for $\{\phi_i\}$, making them integro-differential.

In principle, any approach to solving such coupled integro-differential equations may be used but, most often, the practical one is to convert it again to a variational scheme by assuming appropriate forms for the orbitals and varying open parameters so as to achieve a minimum energy. Such a procedure constitutes a self-consistent-field (SCF) method, each electron moving in the field of the nucleus and of all the others. The orbitals are obtained through a self-consistent solution, with the field determining and being in turn determined by the orbital functions. Multi-configuration Hartree-Fock (MCHF) or multi-configuration SCF, or relativistic counterparts such as multi-configuration Dirac-Fock (MCDF, using the Dirac Hamiltonian in place of the Schrödinger) are among the most accurate techniques for atomic structure and properties [9].

The exchange term in (1.43) both couples the equations for different ϕ_i and makes the equations non-local (the value of ϕ_i at \mathbf{r} depending on ϕ_i at all \mathbf{r}'). A variant that replaces this term by a simpler, local, uncoupled term, even if approximate, has therefore enormous attraction and is called the Hartree-Fock-Slater method. In one such scheme, an approximation as in (1.42) based on the density, $\rho(\mathbf{r}) = \sum_i |\phi_i(\mathbf{r})|^2$, is used. With such a system, for every atom across The Periodic Table, a simple potential $V(r)$, corresponding orbital energies ε_i , and functions ϕ_i have been tabulated [10]. Fig. 1.6 gives a sketch of $V(r, Z)$, providing at a glance much information on the self-consistent potential seen by an electron in any atom at various distances from the nucleus [11].

This is a slightly more complicated, but also a better, approximation than the Thomas-Fermi potential in Fig. 1.4. In particular, shell structure is clearly reflected in the potential surface itself, including variations seen as sub-surface d and f shells fill, as discussed in Section 1.4.1. Also for large r , at the edge of the atom which plays the dominant role in ordinary chemistry, abrupt drops in the potential occur at the noble gases, reflecting their stronger binding and chemical inertness compared to the alkali atoms that lie next. On the other hand, somewhat more in the interior of the atom at intermediate- r , similar drops occur for instance in Cu, Ag, or Au, reflecting the inertness of these noble metals in their metallic state.

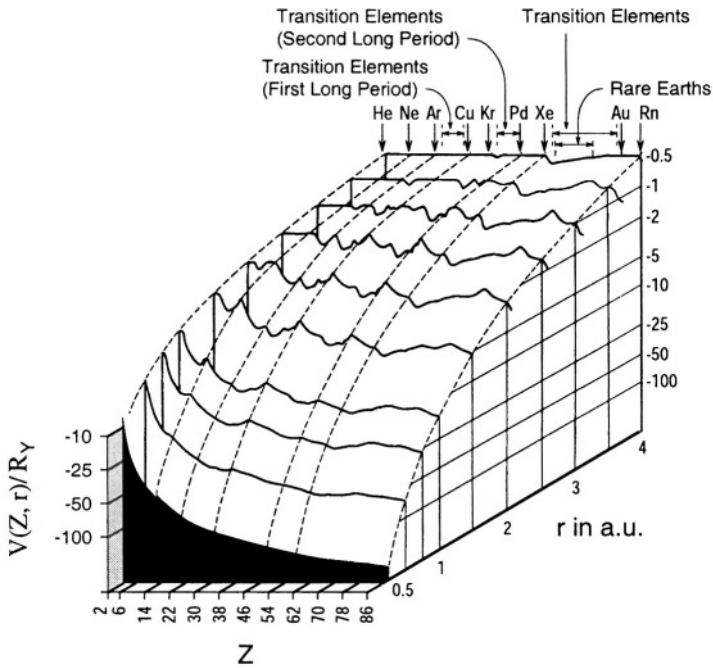


Figure 1.6. Atomic potential as a function of distance r from the nucleus for all neutral atoms across The Periodic Table. From [11], with data from [10].

5. Line Spectra and Their Uses

5.1 Atomic spectra in astronomy

The previous sections have detailed the calculation of the ground and low-lying bound states of atoms and positive ions to varying levels of accuracy through methods of varying sophistication. Transitions between these levels, whether in absorption or emission, give rise to observed line spectra. Since they are unique to each atom and to specific states, they convey a wealth of information on the systems with which they are associated. The first formation of atoms, according to The Big Bang model of the origin of our Universe, occurred roughly 300,000 years after that primordial explosion, when the Universe had cooled sufficiently to about 3000 K to permit nuclei and electrons to combine. This so-called “recombination era” separates the epoch in which the Universe was opaque because of scattering of photons by the free electrons abundantly present from the one when these electrons were mostly locked up

in bound atomic states making the Universe transparent to light. This is as far back as we can “see”.

The various series in hydrogen, Lyman, Balmer, and Paschen, have already been discussed in Section 1.2.1. Similar sequences are characteristic of He^+ , except that all frequencies are quadrupled or wavelengths reduced by a factor of 4 because $Z = 2$. (The slight difference in reduced mass alters this ratio to 4.0016). In neutral He (He I in astronomical terminology whereas He^+ is He II), as in Fig. 1.3, the main transition from the ground 1^1S to 2^1P is at a photon energy of 21.2 eV or wavelength 58.4 nm, a far ultraviolet line. The 164.1 nm $n = 2 \rightarrow n = 3$ He II line has been seen by the IUE (International Ultraviolet Explorer) satellite, along with other ultraviolet lines, such as 124.3 nm from N V $2s^2S_{1/2} \rightarrow 2P$ and 133.5 nm from C II $2s^2 \rightarrow 2sp^2$. The helium abundance is a key parameter of cosmological theories, and observation of $3D \rightarrow 3P$ transitions at 447.1 and 587.6 nm and the $3^1D \rightarrow 2^1P$ at 667.8 nm provides such data.

Extensive tables on all atoms and for various stages of ionization, as derived either by calculation or laboratory measurement, provide the line spectra for other elements and are central to the analysis of the observed spectrum of any object. Besides identifying the species involved, the presence of a characteristic line also provides information on the local conditions such as the temperature of the medium. A bright emission line signifies a tenuous gas at a sufficient temperature for the excited state involved to be sufficiently populated. A dark, absorption line similarly denotes an intervening gas containing that element which is being excited by background illumination. The crucial result from thermodynamics and statistical mechanics for a stage of either excitation or ionization is the Boltzmann population factor, $\exp(-E/kT)$. Thus, for instance, the relative amount of atoms that have lost r electrons or $(r+1)$, as given by the Boltzmann-Saha ionization formula is

$$\frac{N(r+1)}{N(r)} \propto T^{3/2} \frac{g_{r+1}}{g_r} e^{-\text{I.P.}/kT}, \quad (1.44)$$

where the g 's are degeneracy factors and the $T^{3/2}$ and other constant factors in front come from phase space. The controlling exponential factor here involves the ionization potential (I.P.) to remove the $(r+1)$ -th electron. Excitation and ionization energies, and how they compare with the local temperature, therefore determine what spectral lines are observed. Recall that $10^4 \text{ K} \approx 1 \text{ eV}$ and, as a rule of thumb, that appreciable population of a state can be expected when the Boltzmann exponent drops below 10.

The very classification of stars according to spectral types O, B, A, F, G, K, M, N, etc., follows from this. These are arranged in decreasing order of their surface temperatures. In the hottest, stars of type O with temperatures of about 50,000 K, any hydrogen is completely ionized so that no emission lines from it are seen, only lines of ionized He, O, and N. Stars of type B with 15,000 K show lines of neutral He, whereas lines of H are at their maximum in A stars (9000 K). Because the first excitation in H at 10.2 eV is comparatively high, in cooler stars like F (7600 K), H lines decline but those from metals like Ca^+ (I.P. of Ca \approx 6.1 eV), with lower ionization and excitation energies, get more prominent. Such lines of Ca^+ are at their maximum and very prominent in G stars like our Sun (6000 K). This tendency of increased metal lines continues with cooler temperatures, along with the appearance of bands due to molecules, like cyanogen in K stars and TiO in M stars, which have even lower excitation energies (Section 6.2.1).

The two competing trends, sufficient temperature to excite but not so high as to ionize completely the species, is nicely illustrated by the example of excited Mg^+ , prominent in Sirius at 448.1 nm. The excitation here starts being appreciable only around 6000 K, rises and peaks at 10,000 K after which it declines as all the Mg^+ is further ionized.

In solar spectra, in the chromosphere which is considerably hotter than the surface or photosphere (5000 K), lines of He, Ne, Si, C, Mg^+ , Ne^+ and Sj^+ , along with strong Lyman lines of H, indicate temperatures of 10^5 K. The corona is even hotter (perhaps due to acoustic and magnet hydrodynamic heating), approximately 10^{6-7} K, with the result that H and He are completely stripped and not seen, whereas Fe, Ni, and Ca up to even 9–12 times ionized are displayed in its spectrum. Such high temperatures and stages of ionization were so unexpected that for a time the 530.3 nm Fe^{12+} green line was even attributed to a new element dubbed coronium! The transition region from chromosphere to corona is only about 100 km thick and rich in ultraviolet and x-ray lines. X-ray surveys also show lines from highly ionized C, O, and Fe in a local hot bubble around the solar system.

Other astronomical objects besides stars are also of interest. Thus, in the spectra of swift meteors, lines of H and Ca^+ are prominent and examples are known with Fe, Mn, Si, Al, Mg, and Na. The frictional temperatures generated on these objects by their atmospheric entry also leads to lines of nitrogen and oxygen from the heated air. Ariel and OSO8 satellites have seen iron x-ray lines at 6.9 keV, the Ly_α transition in Fe^{25+} . This suggests temperatures in excess of 10^7 K for gas between galaxies in clusters and that the iron abundance is substantially the same as solar. Other low density plasmas are diffuse nebulae (10^{3-4} K,

10^{2-4} cm^{-3}), the ionized region of the interstellar medium near hot stars (10^{4-5} K) with all hydrogen ionized by the wavelengths shorter than 91.2 nm, and planetary nebulae (10^{4-5} cm^{-3}) formed by mass ejection from stars with masses less than $4 M_{\odot}$ and ionized by the star's radiation.

Spectra from light elements and the light they throw on their relative abundances play an important role in cosmological models. The resonance doublet of Li at 670.7 nm is easily accessible but even in cool stars, lithium's low ionization potential means it is mostly present as Li^+ (Li II). Its resonant line is at 19.9 nm. The resonant line of Be at 234.86 nm is also inaccessible to ground-based telescopes. B and B^+ also have resonant lines in the ultraviolet, at 249.77 and 136.25 nm. The former has been observed in rocket observations to give the solar abundance of boron whereas Hubble Space Telescope observations of interstellar gas provide information on the interstellar medium ($\text{B}/\text{H} \approx 6 \times 10^{-10}$). Spectra of Ba, Fe, and Eu play an important role in understanding the so-called s- and r- processes in stars for the nucleosynthesis of heavy elements through slow and rapid neutron capture, respectively. Thorium is formed only in the r-process and the 401.9 nm of Th II is a key for cosmochronology in estimating the age of a galaxy. Simultaneous observation of near-ultraviolet spectral lines from Th II and ^{238}U II in old stars have recently provided an age of $(12 \pm 3) \times 10^9$ yrs for the Universe.

Transitions in an entirely different region of the spectrum, at much longer wavelengths than the above in the visible and near-visible regions, are also seen. Thus an atomic transition involving two neighbouring n values with $n \approx 100$ gives rise to "radio-recombination lines", the corresponding wavelength of $\approx 5 \text{ cm}$, or a few GHz in frequency, lying in the radio region. The $n = 109 \rightarrow 108$ line of H at 5009 MHz is seen in many nebular spectra and has been used for mapping H II regions. Transitions $n + m \rightarrow n$ correspond to frequencies $\nu \approx 6.58 \text{ m} (100/n)^3 \text{ GHz}$ and are labeled α, β, \dots for $m = 1, 2, \dots$. Transitions around $n \approx 40$ lie in the mm-wavelength and those around $n \approx 300$ in the meter wavelength range. Today's radio telescopes cover the entire range. At such high n , it does not matter much which atom is involved, the difference between (1.2) and (1.25) being small but, of course, in the astronomical context, these lines are generally from H, the most commonly occurring element. And, spectroscopic precision allows distinguishing 109_{α} from H, He, or C, all having been seen in Orion.

The n^2 scaling of the radius of such orbits necessarily implies that these lines arise in regions of very low density so that the average separation between atoms exceeds their individual size (in a nebula of 10^4 cm^{-3} , the ratio of these two lengths for $n \approx 100$ is about 1000), permitting them to exist without being destroyed by collisions as they would

be in the laboratory. Even n values larger than 600 have been recorded, the 26.131 MHz transition from the supernova remnant in Cass A being possibly 631_{α} in C. The intensities and widths of the observed lines provide information on the temperature, density, and local motions of the sources, whether H II regions, planetary nebulae, or the ionized gas in galactic nuclei.

The radio region and H are again involved in what is perhaps one of the most important lines of astronomy, the 21 cm line that is central to radioastronomy. The transition involved is not electronic but indeed is from regions of such low temperatures (as, for example, interstellar and inter-galactic) that all H atoms are in their ground state $1s^2S_{\frac{1}{2}}$. But, the spin $J = \frac{1}{2}$, in combination with the spin- $\frac{1}{2}$ of the proton (therefore, very different in hydrogen and deuterium), leads to a pair of hyperfine levels, with $F = 1$ and 0, with a separation of 1420 MHz or the corresponding 21 cm in wavelength.

5.2 Doppler shifts of spectral lines

In combination with the well-known shift in frequencies of emission or absorption when a source is in relative motion with respect to the observer, atomic spectral lines provide even further and vital astronomical information. For our purposes, the Doppler shifts are very simply rendered as $\Delta\lambda/\lambda = v/c$, the velocities with which most astronomical objects move being generally much smaller than the speed of light. Shifts of 0.1 nm out of 400 nm correspond to velocities of 75 km/s. Spectroscopic precision that permits very small $\Delta\lambda/\lambda$ to be measured makes these Doppler shifts very useful in astronomy. As a first application, the same solar spectral lines are seen to be shifted in different amounts depending on whether the telescope is focused on the eastern or western edges of the solar disk. This is a direct indication of the Sun's rotation, the edge approaching us having lines shifted to the violet and at the other edge to the red. In this manner, we determine a 25-day rotation period at the Sun's equator, increasing towards polar latitudes, evidence of differential rotation. A similar application to two objects orbiting one another serves to identify binary stars and their orbits and, even when not resolved, the effects of an extrasolar planet's tug on its parent star. More subtly, natural acoustic modes of oscillation of the Sun that are driven by turbulent convection in the outer layers are manifest as oscillations of the visible surface layers and observed through Doppler shifts. A whole field of helioseismology that has developed is now being extended to more distant stars.

Disks of most other stars are not resolved but the Doppler shift gives evidence of their radial velocities with respect to us. Typical such velocities are a few ten km/s. Radial velocities of stars in galaxies are a vital marker of the mass distribution, Kepler's laws providing an immediate estimate of the mass interior to that radius where the velocity is measured. Much of the evidence for the amount of matter in the Universe, and the related speculations about "missing mass", rest on these measurements.

Doppler shifts are also seen from planets. Thus, the infrared spectrum of H_3^+ at $3.953 \mu\text{m}$ is prominent near Jupiter's poles in both northern and southern aurora, together with Doppler shifts that indicate fast-moving local winds. The motion of large interstellar clouds also shows up through Doppler shifts, as also oscillations and pulsations of certain sources. Thus, for instance, in a nova outburst, dark lines displaced towards the violet are seen during the initial brightening, indicating absorption in gases approaching us. Once maximum brightness is reached, broad undisplaced emission lines are seen as the expanding shell become transparent allowing emission from all parts to come through. With some from parts approaching and some from others receding from us, the blend of both red and blue shifted lines shows up as a broad line, centered at the undisplaced wavelength. Different layers cause different shifts, the inner ones with higher velocities catching up with the outer ones ejected earlier. As the nova's brightness decreases, the broad emission lines become stronger and sets of absorption lines appear, each displaced more and more to the violet; Doppler velocities as large as 3000 km/s are seen.

One particular application of pulsations as seen through Doppler shifts plays a crucial role in astronomy for measuring distances. The group of "Cepheid variables" show oscillations with periodicities that correlate with their luminosities. The nature of the physical processes involved in the oscillating emission from these objects is clearly the reason for this correlation but the fact of its existence for this class of stars proves extremely important. From the observation of the period, the physical models provide their intrinsic luminosity which can be combined with their observed luminosity to provide a distance to these objects. Serving thus as "standard candles", Cepheids in various galaxies provide the basic step in the astronomical distance scale, once we go past nearby objects whose parallax can be measured to give a direct geometrical distance. Evidence for the "Hubble flow" in our Universe is derived in this way [12].

Red-shifts due to this flow, out to even larger distances, are also measured through spectra. Spectacular examples are provided by quasars,

the first ones discovered having $\Delta\lambda/\lambda \approx 0.37$ and 0.16 . This ratio is known as the z parameter. The red-shifts $\Delta\lambda$ may even exceed the unshifted λ so that the Lyman series in H may appear in the visible. Indeed, it was astonishing at the time of the first identification of quasars that there could be such large red-shifts and, by implication from the Hubble flow, that these must be extremely distant objects. A quasi-stellar object (QSO) with $z = 2.8094$ shifts Ly_α from 121.567 to 463.103 nm and one with $z = 2.8102$ shifts Ly_β from 102.572 to 390.829 nm. The largest values of z observed are about 6 for galaxies and even larger for quasars. Note in this connection that the recombination era (Section 1.5.1) corresponds to $z \approx 1000$.

Both emission and absorption lines are seen from QSOs, and of various species: Ly_α , C II, Si II, Fe II, N V, O VI, etc. Velocities range from 10 km s^{-1} to thousands of km s^{-1} . Certain objects display a very large number of Lyman absorption lines towards shorter wavelengths of the Ly_α emission line. Referred to as “the Ly_α forest”, these speak to intervening gas clouds of varying velocities. Roughly half the QSOs, mostly those with emission $z \approx 2.7$, have absorption Lyman discontinuities within $13,000 \text{ km s}^{-1}$ of the emission Lyman limit.

These discontinuities in H and its D isotope have a crucial role in determining the primordial deuterium abundance of the Universe, a key parameter of cosmological theories. Deuterium is a very sensitive measure of the baryon density, has indeed been called a “baryometer” because its abundance drops sharply with increasing baryon density. It is also fragile and always destroyed in stars so that it is best measured in clouds where star formation has not yet occurred. High red-shift ($z \approx 2.5$) Ly_α clouds towards distant QSOs are, therefore, prime candidates for determining deuterium abundance, Fig. 1.7 providing an example, and giving values $\text{D}/\text{H} \approx 2.9 - 4 \times 10^{-5}$ [13]. Much higher spectral resolution is possible with 21 cm studies and several QSOs have been so measured. Typical neutral hydrogen column densities of Ly_α forest regions are 10^{14} cm^{-2} and sizes of the emission regions are larger than 10^{19} cm . An upper limit to cloud size, that they be stable against gravitational collapse, is about 10^{23} cm . Cloud temperatures are around 10^4 K . VLBI (Very Long Baseline Interferometry) 21 cm measurements of 3C286 give a cloud size of 250 pc. Very large Doppler shifts, $z \approx 4$, are also seen in the 21 cm transition which is then observed by meter-wave telescopes.

Excitation of fine-structure levels is increasingly becoming a temperature indicator of the early Universe. Thus, the 3P ground state of carbon’s fine structure level of $J = 2$ lies 38.9 K above the $J = 1$ level which itself lies 23.6 K above the $J = 0$. Absorption from dense, neutral, highly shielded gas clouds in front of a quasar with $z = 2.337$ have been

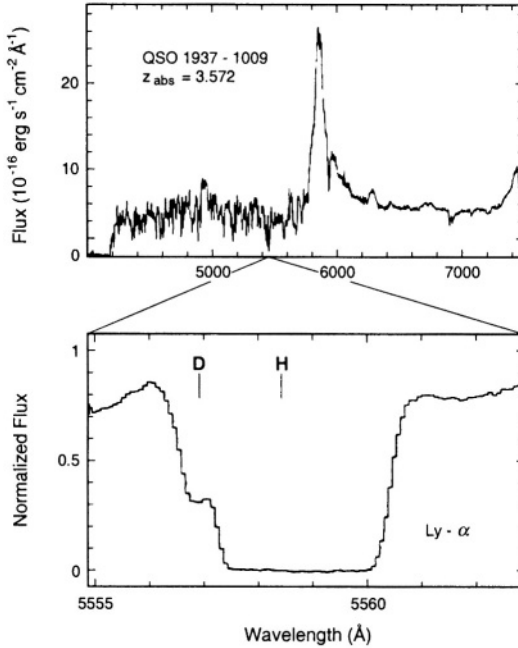


Figure 1.7. Optical spectrum of a quasar with high red-shift, showing a “Lyman- α forest” of absorption lines between 420 nm and 580 nm, as well as prominent emission lines at higher wavelengths. Higher resolution spectrum in the lower panel showing absorption lines from both hydrogen and deuterium from the same gas translate to a primordial D/H ratio of $3.3 \pm 0.3 \times 10^{-5}$. From [13], with permission of author and Elsevier Science.

used recently to estimate the temperature of the cosmic background radiation at that epoch. Given today’s value of 2.7 K for this temperature, the expectation of $2.7(1+z) \approx 9.1$ K is compatible with the observations.

Problems

- 1.1 Compute the wavelengths of the first four lines and the band edge for the Paschen and Brackett series in the hydrogen atom.
- 1.2 A muon ($m_{\mu} = 207 m_e$) binds to a proton to form muonic-hydrogen. What is the binding energy of the ground state? What is the wavelength of the resonance transition?
- 1.3 Calculate the expectation value of the operator z for the two $n = 2$ parabolic states of hydrogen in (1.16).

- 1.4** In analogy to (1.16), but for $n = 3$, construct the parabolic states of hydrogen with $m = 0$ in terms of the spherical states. Thereby, set up the transformation matrix in (1.15) for this case and verify that it is unitary.
- 1.5** Carry out the explicit integrations involved to arrive at (1.19).
- 1.6** Consider the “Bethe trial function” given by (1.18) with an additional factor $(1 + cr_{12})$. Use the Rayleigh-Ritz variational principle with such a trial function, Z_{eff} and c the variational parameters, to get a variational estimate of the ground state energy of the He isoelectronic sequence. Note particularly the numerical values for $\text{H}^-(Z = 1)$ and $\text{He}(Z = 2)$. Integrals are conveniently carried out in terms of $s = r_1 + r_2$, $t = r_1 - r_2$, and $u = r_{12}$ as $2\pi^2 \int_0^\infty ds \int_0^s du \int_0^u dt u (s^2 - t^2)$.
- 1.7** Carry out the procedure sketched in the text to establish (1.23).
- 1.8** A section of tables of energy levels [14] in helium reads as follows for $^1S^e$ and $^1P^o$ states measured in cm^{-1} above the ground state.

<i>State</i>	cm^{-1}	<i>State</i>	cm^{-1}	<i>State</i>	cm^{-1}
1s2s	166271.7	1s5s	193657.8	1s8s	196529.0
1s2p	171129.1	1s5p	193936.8	1s8p	196595.6
1s3s	184859.1	1s6s	195109.2	1s9s	196907.1
1s3p	186203.6	1s6p	195269.2	1s9p	196954.0
1s4s	190934.5	1s7s	195973.2	1s10s	197176.4
1s4p	191487.0	1s7p	196073.4	1s10p	197210.4

From this data, extract the quantum defects μ_0 and μ_1 in (1.25).

- 1.9** For the two-particle Hamiltonian, use the Rayleigh-Ritz principle with a trial $\psi_t(\mathbf{r}_1, \mathbf{r}_2) = \frac{1}{\sqrt{2}} (\phi_1(\mathbf{r}_1)\phi_2(\mathbf{r}_2) + \phi_1(\mathbf{r}_2)\phi_2(\mathbf{r}_1))$, and vary with respect to the functions ϕ_1 and ϕ_2 to get the Hartree-Fock equations defining them.
- 1.10** Use as trial functions for the ground and first excited 1S states of He the hydrogenic form in (1.18) and (1.22) with hydrogenic wave functions and the same Z_{eff} as a variational parameter. Carry out such a two-configuration interaction calculation to get variational estimates for these two states. Compare the improvement for the ground state over using (1.18) alone with the improvement obtained in Problem 6. Contrast also the relative amount of work involved in the two computations.

- 1.11** For ℓ^2 configurations of two electrons, establish explicitly the $L + S = \text{even}$ rule for the states allowed by the Pauli principle.
- 1.12** For two non-identical d -electrons, identify the possible $^{2S+1}L_J$ states.
- 1.13** How many states are allowed for the configurations (i) d^3 and (ii) f^4 ?
- 1.14** Applying the Madelung and Hund's rules, give the ground state configuration and its $^{2S+1}L_J$ labels for the atoms (i) Ni, (ii) Cu, (iii) Zn, and (iv) a superheavy element $Z=110$.
- 1.15** Adapt the phase space derivation in the text to derive the counterpart Thomas-Fermi expression to (1.36) that is valid in a one-dimensional world. Note that the adiabatic index γ takes the value 3.
- 1.16** (i) Use the Thomas-Fermi expressions (1.36) or (1.37) to establish the scaling with Z of the energy and radius of an atom.
(ii) With the results of Problem 15, establish similar scaling relations for "one-dimensional atoms".
- 1.17** Following the procedure sketched in the text, use the expression (1.42) for the exchange energy to derive the Thomas-Fermi-Dirac equation.
- 1.18** Use the 25-day rotational period of the Sun to estimate the spread $\Delta\lambda$ of the Balmer- α line as observed from the opposite limbs of the Equator.
- 1.19** From Fig. 1.7, estimate the red-shift of this object.

Chapter 2

COUPLING OF ATOMS TO RADIATION

1. Introduction

Atomic energy levels are observed through the electromagnetic radiation, emitted or absorbed, when the atom or ion changes from one level to another. Besides the transition energies, which themselves carry a wealth of information as we have seen in Chapter 1, other important astronomical knowledge is contained in the intensities, widths and polarizations of these transitions. We will now take up their study, and of the underlying atomic physics. It is clear already at the outset, even without any further detailed examination, that the structure of atoms controls even how far out telescopes can see in a wavelength range. Thus, the ionization potential of H being 13.6 eV, corresponding to a wavelength 91.2 nm, ultraviolet radiation of λ smaller than this will be absorbed by intervening H between the source and our ultraviolet telescopes (which already have to be in orbit so as to avoid atmospheric absorption). Given an average interstellar density of 1 H atom/cm³, and taking the geometrical cross-section of an atom, approximately 10^{-17} cm², as the continuum absorption cross-section of H (which we will see is a good estimate), the attenuation factor over a distance of 10 pc (≈ 30 ltyr $\approx 3 \times 10^{14}$ km), is 300 which means that any initial intensity will be too feeble for observation here on Earth. Therefore, our observations in the far ultraviolet are limited to distances smaller than this, except in certain directions where the density along the line of sight is much less, $\approx 10^{-3}$ /cm³, in which case we can see out to about 100 pc.

When electromagnetic radiation passes through a medium containing atoms, energy balance governs its transport. Denoting by I_λ the intensity or flux of radiation in a wavelength interval $(\lambda, \lambda + d\lambda)$ pass-

ing through an element of area dA and in a solid angle $d\omega$, the amount of energy E_λ is, correspondingly, $E_\lambda = I_\lambda d\lambda dA d\omega$. If the medium has an absorptivity (or opacity) K_λ , then in a distance ds , an amount of energy $dE_\lambda = K_\lambda E_\lambda ds$ is absorbed. On the other hand, with ε_λ the emissivity, an amount $dE_\lambda = \varepsilon_\lambda d\lambda dA d\omega$ is added so that the classical energy-balance relationship is given by

$$\frac{dI_\lambda}{ds} = -K_\lambda I_\lambda + \varepsilon_\lambda, \quad (2.1)$$

or, alternatively, upon defining $d\tau_\lambda \equiv K_\lambda ds$, we have

$$\frac{dI_\lambda}{d\tau_\lambda} = -I_\lambda + S_\lambda, \quad (2.2)$$

where $S_\lambda \equiv \varepsilon_\lambda/K_\lambda$ is called the source function. These are the radiation transport equations given by Kirchhoff in the mid-nineteenth century. With no incident intensity, a hot gas will emit $I_\lambda = \tau_\lambda S_\lambda$, if $\tau_\lambda \ll 1$ (called ‘‘optically thin’’) whereas if $\tau_\lambda \gg 1$ (optically thick), $I_\lambda = S_\lambda$, independent of K_λ . In complete thermal equilibrium, S_λ is the black-body distribution. With the advent of quantum physics, these quantities such as K_λ and S_λ could be calculated from first principles, the former in terms of atomic structure and the latter in terms of the modes of the electromagnetic field. Most astrophysical settings, e.g. the chromosphere, planetary nebulae, or clouds in interstellar space, are not in thermodynamic equilibrium, so that one needs all the atomic excitation and de-excitation processes to understand radiation transport. When $\varepsilon_\lambda = 0$ in (2.1), the intensity is attenuated according to $I_\lambda(s) = I_\lambda(0) \exp(-K_\lambda s)$, the mean free path of a photon given by $1/K_\lambda$. In stellar interiors, this may be less than 1 mm.

2. Photoabsorption and Photoemission

With considerations similar to those leading to (2.1) and (2.2), if N_i and N_j are the number of atoms in a lower and an upper energy level, respectively, the rate equation can be written as

$$\frac{dN_j}{dt} = -A_{ji} N_j - B_{ji} \rho(\nu) N_j + B_{ij} \rho(\nu) N_i, \quad (2.3)$$

where $\rho(\nu)$ is the energy density of the radiation field (energy per unit volume per unit frequency interval). The first term on the right-hand side represents the spontaneous decay down to i which depletes the number in the level j , and the third term the enhancement in N_j because of

absorption by the atoms in i . The coefficients A and B were introduced by Einstein, along with the middle, non-classical term in (2.3) representing a “stimulated emission” from level j to i due to the radiation present. Through considerations of detailed balance and thermodynamic equilibrium, which requires

$$N_j/N_i = \exp(-h\nu_{ji}/kT), \quad (2.4)$$

Einstein also related the coefficients according to

$$B_{ij} = B_{ji} = (8\pi h\nu_{ji}^3/c^3)^{-1} A_{ji}, \quad (2.5)$$

and $\rho(\nu)$ to the Planck black-body distribution.

The absorption coefficient B_{ij} , with dimensions (length/mass), is conveniently replaced by a dimensionless absorption “oscillator strength”

$$f_{ij} = (\mu/\pi e^2)(h\nu_{ij})B_{ij}. \quad (2.6)$$

The coefficients B , regarded in classical physics as parameters characterizing the coupling of matter to radiation, were given a microscopic grounding with the advent of quantum mechanics. The oscillator strength depends on the transition energy difference between atomic levels i and j through the factor ν_{ij} and, as we will see, on a transition matrix element involving the corresponding wave functions which enters through B_{ij} . At the same time, a closely allied concept from scattering theory, namely a cross-section for photoabsorption or photoemission involving the levels i and j , coincides with the oscillator strength except for simple multiplicative factors. Oscillator strengths for a large number of atoms and ions, along with collisional cross-sections for atoms and ions with each other and with electrons, are key inputs to computing the opacity of stars. As one example, it has been observed that questions in the theory of pulsating stars (Cepheids) can be resolved if heavy element opacities were increased by a factor of two or three over what was believed. This has given rise to a major “Opacity Project” now under way for compiling reliable atomic and molecular data [15].

2.1 The Oscillator strength

Except in modern intense lasers, electric and magnetic field strengths in most electromagnetic waves of interest to physics and astronomy are weak compared to the internal fields in an atom. Recall that for hydrogen in the ground state, the electric field is, approximately, $13.6 \text{ V}/(0.053 \text{ nm})$, and the magnetic field, that due to an electron in a Bohr orbit, is $2I/cr \approx 2e/Tcr \approx (e/\pi r^2)(v/c) \approx 4 \text{ T}$. The coupling to the radiation

field has, therefore, only a slight “perturbative” effect on the atom. Further, in non-relativistic physics, the magnetic field of radiation is far less important than the coupling of its electric field to the electronic charge,

$$U = e\mathcal{E}(\mathbf{r}, t) \cdot \mathbf{r}. \quad (2.7)$$

For many-electron atoms, \mathbf{r} is replaced by $\sum_s \mathbf{r}_s$. The central quantum-mechanical result of such a time-dependent perturbation on a system with a Hamiltonian H_0 is that it causes transitions from an initial state $|i\rangle$ to a final state $|f\rangle$ at a rate (transition probability per unit time) given by the Fermi-Wentzel “golden rule”,

$$P = (2\pi/\hbar)|\langle f|U|i\rangle|^2. \quad (2.8)$$

With the electric field of a standing wave of polarization $\hat{\epsilon}$, frequency ω , and wave vector \mathbf{k} , given by

$$\mathcal{E} = \hat{\epsilon} \mathcal{E}_0 [\exp i(\mathbf{k} \cdot \mathbf{r} - \omega t) + \text{complex conjugate}], \quad (2.9)$$

with $\hat{\epsilon} \cdot \mathbf{k} = 0$ and $\omega = ck$, we have $U = e\mathcal{E}_0 \hat{\epsilon} \cdot \mathbf{r} \exp(i\mathbf{k} \cdot \mathbf{r})$ plus a conjugate term. Dividing P in (2.8) by the incident intensity removes the dependence on \mathcal{E}_0 to give the cross-section for photoionization from the initial state $|i\rangle$ to a final continuum state $|f\rangle$ for the ejected electron as

$$\sigma = (4\pi^2 e^2/3)(\omega/c)|\langle f|\mathbf{r} \exp(i\mathbf{k} \cdot \mathbf{r})|i\rangle \cdot \hat{\epsilon}|^2, \quad (2.10)$$

where the factor (1/3) has been added to average over directions.

Alternatively, one can consider the polarization induced in the atom’s electronic charge distribution by the interaction (2.7). Choosing $\hat{\epsilon}$ as the z -direction, and dropping $\mathbf{k} \cdot \mathbf{r}$ as small (“dipole approximation” to be discussed further below, atomic size being much smaller than the wavelength of the radiation), this perturbative interaction mixes into the initial wavefunction $\psi_i \exp(-iE_i t/\hbar)$ a small superposition of other states:

$$\psi = \psi_i \exp(-iE_i t/\hbar) + \sum_j c_j(t) \psi_j \exp(-iE_j t/\hbar). \quad (2.11)$$

Inserting into the Schrödinger equation

$$i\hbar \frac{\partial \psi}{\partial t} = [H_0 + U \exp(i\omega t) + U \exp(-i\omega t)]\psi, \quad (2.12)$$

and using the orthonormality of the set $\{\psi_i\}$ of eigenstates of H_0 , gives to first order in the coefficients c_j ,

$$\frac{dc_j}{dt} = \frac{ie\mathcal{E}_0}{\hbar} \langle j|z|i\rangle \exp[i(E_j - E_i)t/\hbar] [\exp(i\omega t) + \exp(-i\omega t)], \quad (2.13)$$

Solving for c_j , and from (2.11) evaluating the induced dipole moment $\langle \psi|z|\psi\rangle$, again to first order in \mathcal{E}_0 , gives

$$e\langle \psi|z|\psi\rangle = \frac{2e^2\mathcal{E}_0}{\hbar} \sum_j \omega_{ji} \frac{\langle i|z|j\rangle \langle j|z|i\rangle}{\omega_{ji}^2 - \omega^2 - i\gamma_j\omega} [\exp(i\omega t) + \exp(-i\omega t)], \quad (2.14)$$

with $\omega_{ji} \equiv (E_j - E_i)/\hbar$. A phenomenological damping term in γ_j has been added to describe the decay of excited states j : $E_i - E_j = \hbar(\omega_{ji} - i\gamma_j/2)$. The ratio of the induced dipole moment to the imposed electric field, called the polarizability, is therefore,

$$\alpha(\omega) = \sum_j \frac{(e^2/\mu)f_{ji}}{\omega_{ji}^2 - \omega^2 - i\gamma_j\omega}, \quad (2.15)$$

with f_{ji} defined as

$$f_{ji} = \frac{2\mu\omega_{ji}}{\hbar} |\langle j|z|i\rangle|^2. \quad (2.16)$$

The expression (2.14) for the induced dipole response is of the same form as that of a classical, charged harmonic oscillator with normal mode frequencies ω_{ji} and damping constants γ_j . The numerator in (2.15) denotes a phenomenological strength of the coupling of each normal mode to the driving electric field, so that the (dimensionless) f_{ji} is the ‘‘oscillator strength’’, now given explicitly in this quantum derivation in terms of the transition energy and a squared matrix element of the dipole operator z between the states. Restoring the vector \mathbf{r} and arbitrary polarization direction, and also the $\exp(i\mathbf{k}\cdot\mathbf{r})$ factor, an alternative rendering of (2.16), again with a (1/3) factor introduced for three equivalent directions, is

$$f_{ji} = \frac{2\mu\omega_{ji}}{3\hbar} |\langle j|\mathbf{r} \exp(i\mathbf{k}\cdot\mathbf{r})|i\rangle \cdot \hat{\varepsilon}|^2. \quad (2.17)$$

While (2.17) represents the strength of absorption or emission between two discrete states i and j , it takes the form of the corresponding differential element, $(df/dE)dE$, when one considers photoionization from the initial state i into the continuum of atomic states $(E, E + dE)$ once the photon energy exceeds the ionization potential, $\hbar\omega = E$, $E \geq -E_i$:

$$\frac{df}{dE} = \frac{2\mu E}{3\hbar^2} |\langle f | \mathbf{r} \exp(i\mathbf{k}\cdot\mathbf{r}) | i \rangle \cdot \hat{\boldsymbol{\varepsilon}}|^2 . \quad (2.18)$$

Whereas the discrete oscillator strength in (2.17) is dimensionless, with the corresponding wave functions of discrete states i and j normalized per unit volume, the left-hand side of (2.18) has dimensions of inverse energy, this dimensional element being carried on the right-hand side by the continuum normalization per unit energy of the state $|f\rangle$, so that $\psi_f = \langle \mathbf{r} | f \rangle$ has dimensions of $(\text{energy} \times \text{volume})^{-1/2}$.

Comparing (2.10) and (2.18), the photoionization cross-section and continuum oscillator strength differ only in a multiplicative factor involving fundamental constants,

$$\sigma = (2\pi^2 e^2 \hbar / c\mu)(df/dE) . \quad (2.19)$$

The constant factor has dimensions of $(\text{energy} \times \text{area})$ and the value $8.0672784 \times 10^{-18} \text{ Ry cm}^2 = 1.097618 \times 10^{-16} \text{ eV cm}^2$. The oscillator strength in (2.16) for both discrete and continuum states in the hydrogen atom can be evaluated analytically using the wave functions from chapter 1, with the results shown in Fig. 2.1. By laying out the discrete $f_n = f_{n0}$ for absorption from the ground state in the form of histogram blocks, this figure illustrates the continuity of the oscillator strength distribution across the ionization threshold. On the other hand, monitoring only the ionization continuum as in Fig. 2.2 for helium, the photoionization cross-section shows up as a characteristic “edge”, with an onset at threshold (for photons of wavelength 91.2 nm in H and 50.4 nm in He) and a drop-off towards higher photon energies (shorter wavelengths). Whereas the Lyman edge and Lyman continuum lie in the far ultraviolet, analogous ones from H atoms in $n = 2$ provide the Balmer (λ shorter than 364.8 nm), Paschen ($n = 3$, $\lambda \leq 820.8 \text{ nm}$), and other continua.

2.2 Alternative forms of the dipole matrix element

The expressions for the oscillator strength in the previous section were derived starting with the coupling of the electrons to the electric field as $e\mathcal{E}\cdot\mathbf{r} = e\mathcal{E}z$. However, the actual evaluation of the atomic matrix element in (2.16) can be carried out in a variety of ways with the recognition that with any atomic Hamiltonian H_0 , we have

$$[H_0, z_s] = \left[\left(p_{zs}^2 / 2\mu \right), z_s \right] = (\hbar / \mu i) p_{zs} . \quad (2.20)$$

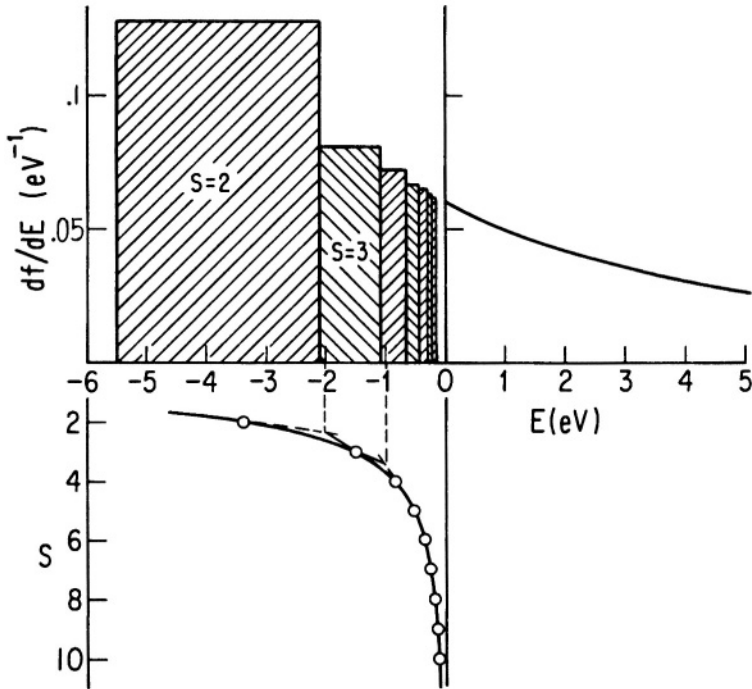


Figure 2.1. Oscillator strengths in hydrogen from the ground state to discrete excited and continuum states. The former are shown as histogram blocks with base determined by tangents to the E_s vs s curve shown in the lower part of the figure. Note the continuity of oscillator strength distribution across the ionization threshold. From U. Fano and J. W. Cooper, *Rev. Mod. Phys.* **40**, 441 (1968).

This is a valid identity even in a many-electron atom, $s = 1, 2, \dots, N$, for the exact Hamiltonian as for example, in (1.17), or in any approximation scheme that involves only local potentials. Only when non-local potentials are involved, as in the Hartree-Fock approximation (1.43) with its exchange terms introducing non-locality, will (2.20) be invalid, such terms being equivalent to momentum-dependent potentials that also will contribute non-zero commutators to the right-hand side of (2.20).

Inserting $\langle j|$ and $|i\rangle$ onto the identity (2.20) from either side gives a relationship

$$(E_j - E_i)\langle j|z|i\rangle = (\hbar/\mu i)\langle j|p_z|i\rangle. \quad (2.21)$$

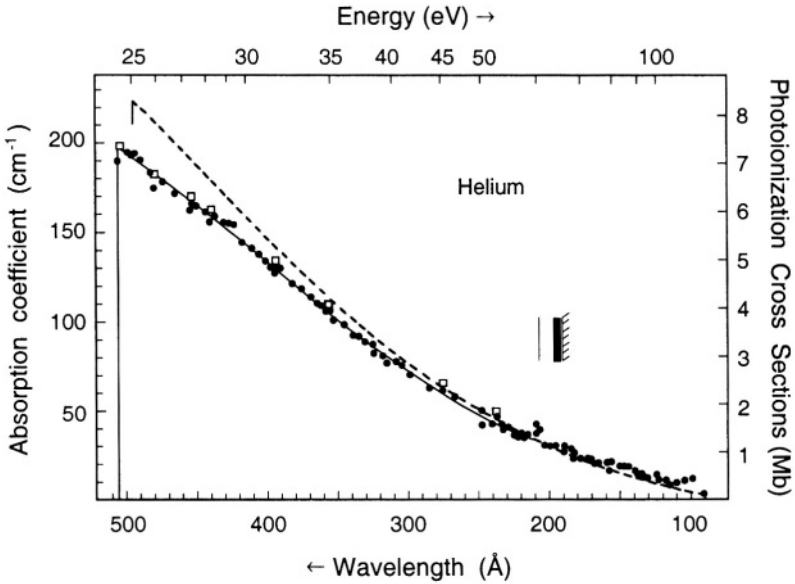


Figure 2.2. Photoionization cross-section from the ground state of helium. From J. A. R. Samson, *Adv. At. Mol. Phys.* **2**, 177 (1966), with permission of author and publisher.

Therefore, (2.16) can be rewritten in terms of a matrix element of p_z as

$$f_{ji} = (2/\mu\hbar\omega_{ji})|\langle j|p_z|i\rangle|^2. \quad (2.22)$$

Because of their form, the alternative matrix elements on the left- and right-hand sides of (2.21) are referred to as “length” and “velocity” forms, respectively. Clearly, the process can be continued through other commutators, thus $[H_0, p_z] = i\hbar(\partial V/\partial z)$, to develop yet other alternatives such as $\langle j|\mu^{-1}\partial V/\partial z|i\rangle$, an “acceleration” form, etc. All these are exactly equivalent as long as one has exact wave functions of H_0 but the equivalence breaks down when only approximate solutions are available. Since, as we have seen in Chapter 1, we are restricted to such approximate solutions for any atom other than hydrogen, the calculated oscillator strengths may differ depending on the form used. With the transitions operators $z, p_z, \partial V/\partial z$, etc. weighting different regimes of the radial distance differently, the length emphasizing larger r while the others emphasize smaller r where velocities and accelerations are larger, one or the other may be preferred if we know where the approximate wave

functions are more reliable. Indeed, these alternative forms were actually introduced into atomic physics in the context of the astrophysical problem of absorption by the negative ion H^- (Section 2.4.2) as a way of assessing the reliability of different approximate trial wave functions for this delicately bound system. Note, however, from the earlier remark that the alternatives coincide so long as local potentials are involved that such an agreement among the different forms is not in itself a guarantee that we are close to an exact description. Generally, with most approximations being based on the energy variational principle, the velocity form which weights the same regions that contribute most to the energy is most reliable, although there are cases when the length form is more accurate.

Among these equivalent forms, the one between length and velocity which allows, as an alternative to (2.17), the expression

$$f_{ji} = (3\mu\hbar\omega_{ji}/2)^{-1} |\langle j | \mathbf{p} \exp(i\mathbf{k}\cdot\mathbf{r}) | i \rangle \cdot \hat{\boldsymbol{\epsilon}}|^2 \quad (2.23)$$

is interesting for another reason. An alternative general procedure for coupling electric charges to an electromagnetic field is by “minimal coupling”, wherein \mathbf{p} in H_0 is replaced by $(\mathbf{p} + e\mathbf{A}/c)$. From the kinetic energy operator, we obtain then the atom-field coupling as $(e/\mu c) \mathbf{p}\cdot\mathbf{A}$. For the electric field in (2.9), the corresponding vector potential is $\mathbf{A} = (c\boldsymbol{\mathcal{E}}/\omega)$ and leads directly to (2.23) as the expression for the oscillator strength.

2.3 Selection rules

Symmetries of the states $|i\rangle$ and $|j\rangle$ and of the operator involved in the transition matrix element in (2.17) or (2.23) constrain transitions between states. As already noted, because of the relative size of atoms and the wavelength of the radiation involved, $\mathbf{k}\cdot\mathbf{r}$ is small compared to unity so that the dominant transitions, usually called “allowed”, arise from the operators \mathbf{r} or \mathbf{p} as in (2.16) and (2.21). More precisely, they should be termed electric-dipole allowed and denoted E1, the unity representing the vector or dipole character. All other transitions are called “forbidden” although, as we will now see, they can also occur in some situations but, arising as they do from the expansion $\exp(i\mathbf{k}\cdot\mathbf{r}) = 1 + i\mathbf{k}\cdot\mathbf{r} + \dots$, are relatively weaker in their intensity by successive powers of $(a_0/\lambda)^2$. For allowed E1 transitions, estimating from (2.16), $f \approx (\mu e^2 a_0 / \hbar^2) \approx 1$, and using (2.5) and (2.6), the Einstein A coefficient for spontaneous emission is, approximately, 10^8 s^{-1} .

For the allowed transitions, since \mathbf{r} and \mathbf{p} are vector operators, the matrix element being a number which should be unchanged under rotations and reflections of coordinates, the product of the states must transform as a vector as well. This means that $|i\rangle$ and $|j\rangle$ must be of opposite parity and that their angular momenta must add to unity:

$$\mathbf{J}_i + \mathbf{1} = \mathbf{J}_j. \quad (2.24)$$

Equivalently, this means $\Delta J_i = |J_i - J_j|$ must be 0 or 1 and both J_i and J_j cannot simultaneously be zero. These provide the “selection rules” for such transitions, which take their name, electric dipole (E1), from the operator $e\mathbf{r}$. The selection rule applies properly to the total angular momentum of the system. But, since the operators involve spatial and not spin variables, in the absence of appreciable spin-orbit coupling (as in smaller atoms), the rule may be regarded as applying to orbital angular momentum alone so that $\mathbf{L}_i + \mathbf{1} = \mathbf{L}_j$, and $S_i = S_j$. Thus, the first absorption from the ground $1s$ state in H (called the “resonance transition”) is to the $2p$ (not $2s$) and in He from $1s^2\ ^1S_0^e$ to $1s2p\ ^1P_1^o$. However, in a heavy atom, this particular form may be violated even while (2.24) remains sacrosanct, the blue line in Hg which arises from $^3P_1^o \rightarrow ^1S_0^e$ providing a standard example, spin-orbit coupling mediating this E1 transition.

Selection rules regarding the M quantum numbers are straightforward, accompanying those for L and J . Thereby $\Delta M = 0$ or ± 1 . These values carry the information on the polarization of the E1 radiation, $\Delta M = 0$ representing linear and ± 1 left/right-circular polarizations. For this purpose, rather than the Cartesian vector \mathbf{r} or \mathbf{p} , one considers the “spherical tensors”, z and $(x \pm iy)/\sqrt{2}$, respectively, which have azimuthal angular dependence 1 and $\exp(\pm i\varphi)$. Together, this set of three transforms like a vector under rotations of the coordinate axes.

For states $|i\rangle$ and $|j\rangle$ that do not conform to (2.24), E1 transitions are ruled out, necessitating consideration of the next term in the expansion of the matrix element in (2.23),

$$\langle j | (\hat{\boldsymbol{\varepsilon}} \cdot \mathbf{p}) (\mathbf{k} \cdot \mathbf{r}) | i \rangle. \quad (2.25)$$

Once again, the overall matrix element having to remain invariant, the product of the states must have the same transformation under rotations and reflections as the operator in between. The parity rule is immediate, that the two states must have the same parity since the operator is even. For the rotational behavior, we need to disentangle operators pertain-

ing to the radiation from those pertaining to the atom which alone are relevant for evaluation between the atomic states $\langle j |$ and $| i \rangle$. Constructing combinations of (2.25) that are symmetric and antisymmetric under interchange of \mathbf{r} and \mathbf{p} ,

$$\frac{1}{2}[(\hat{\varepsilon} \cdot \mathbf{p})(\mathbf{k} \cdot \mathbf{r}) + (\hat{\varepsilon} \cdot \mathbf{r})(\mathbf{k} \cdot \mathbf{p})] + \frac{1}{2}[(\hat{\varepsilon} \cdot \mathbf{p})(\mathbf{k} \cdot \mathbf{r}) - (\hat{\varepsilon} \cdot \mathbf{r})(\mathbf{k} \cdot \mathbf{p})], \quad (2.26)$$

the second term is recognized as $\frac{1}{2}(\hat{\varepsilon} \times \mathbf{k}) \cdot (\mathbf{r} \times \mathbf{p}) = \frac{1}{2}(\hat{\varepsilon} \times \mathbf{k}) \cdot \boldsymbol{\ell}$, with $\boldsymbol{\ell}$ the orbital angular momentum of the electron.

Since $\boldsymbol{\ell}$ also behaves as a vector under rotation, (2.24) again applies as a selection rule; however, as already noted, since $\boldsymbol{\ell}$ is an axial vector, unlike the polar \mathbf{r} or \mathbf{p} , this time the states must not differ in parity. Such transitions are called magnetic dipole (M1) because the operator involved is $e\hbar\boldsymbol{\ell}/2\mu c$, the magnetic moment (of the transition). It couples to the magnetic field, $\hat{\varepsilon} \times \hat{k}$, of the radiation. The $1s2s\ ^3S_1^e$ excited state of He decays in this fashion to the ground $1s2s\ ^1S_0^e$ state. Since a spin change is involved, necessitating a spin-flip that can only come through weak spin-orbit interactions, the decay is very weak and the state “metastable”. Interestingly, when studied in a heavier iso-electronic analog to He, the enhanced spin-orbit couplings dramatically lower the lifetime. Thus the decay rate $1.27 \times 10^{-4} \text{ s}^{-1}$ in He increases, to 2×10^8 in Fe^{24+} , scaling roughly as Z^{10} . Such M1 transitions from He-like Ne^{8+} (NeIX), Mg^{10+} (MgXI), and Fe^{24+} (FeXXV) are seen in the solar spectrum. Relativistic effects are important for such highly stripped ions, also in the calculation of oscillator strengths. The requisite wave functions can be obtained through perturbation theory as in Section 3.3.2.

The $2s$ excited state in H provides an even more dramatic illustration. This $2s\ ^2S_{1/2}^e \rightarrow 1s\ ^2S_{1/2}^e$ transition satisfies the M1 selection rule (2.24) but, in terms of orbital angular momentum alone, is an instance of $L_i = L_j = 0$ which is forbidden. So, a spin interaction is again involved which, as in He, makes it weak but now is further compounded by the fact that the spatial part, which is just the overlap of $2s$ and $1s$ wave functions, vanishes in the non-relativistic description. Only with relativistic solutions of the Dirac equation for the H atom is a very tiny matrix element realized for this transition, making the lifetime of the $2s$ state about two days, thirteen orders or magnitude larger than an allowed rate as, for instance, of its energy-degenerate partner $2p$ state. Indeed, for the $2s$ state, a competing process wins out, namely the next order of coupling beyond (2.7) between atom and electromagnetic field, which is generally weaker in amount by α the fine-structure constant,

involving two interactions with the field. Such “two-photon transitions”, which amount to two E1 steps from $2s$ down to $1s$ through an intermediate virtual state with the emission of two photons that together carry away the 10.2 eV of energy, give a lifetime of (1/7)s to the $2s$ state. As in the case of He, M1 transitions increase rapidly with Z so that for $Z > 45$ in H-like ions, the M1 transition dominates over two-photon decay. The M1 lifetime in U^{91+} is 5×10^{-15} s. In contrast, the two-photon rate of He 2^3S_1 is very small, $4 \times 10^{-9} \text{ s}^{-1}$.

The first term in (2.26) which is symmetric under the \mathbf{r} and \mathbf{p} interchange is also of comparable strength to M1, and also requires the parity of the two states to be the same, but under rotations behaves like a tensor of rank 2. As a result, these transitions are called electric quadrupole (E2) and obey the selection rule

$$\mathbf{J}_i + \mathbf{2} = \mathbf{J}_j. \quad (2.27)$$

Equivalently, ΔJ must now be 0, 1, or 2, and both J_i and J_j cannot simultaneously be 0 or 1/2. In Section 1.4.1, alternative $2S+1L_J$ states of the ground state configuration of oxygen and nitrogen were discussed. Transitions between them, such as $^1D \rightarrow ^3P$ (630 nm) and $^1S \rightarrow ^3P$ (297.2 nm) in O I, and $^2D \rightarrow ^4S$ (520 nm) and $^2P \rightarrow ^4S$ (346.6 nm) in N I are such quadrupolar emission lines seen in auroral light (630 nm forms the “auroral red”), electrons in the upper atmosphere collisionally exciting the upper states. The decay rates are, approximately, 10^{-3} s^{-1} .

Another example, the $12.8 \mu\text{m}$ Ne II $^2P_{1/2} \rightarrow ^2P_{3/2}$ line seen from planetary nebulae, provides the Ne/H ratio in such systems ($\approx 10^{-4}$). Such nebulae are a relatively short-lived phase (10^4 yrs) in a star’s evolution from a red giant to a white dwarf as it ejects shells of matter. Forbidden transitions which are strongly suppressed at higher density such as in laboratory plasmas are often seen in these lower density situations. This is because each excitation is followed by collisional de-excitation at high densities but by emission when densities are low. As a result, in the latter case, the radiation transition probability does not enter, only the excitation rate by collisions with electrons (typical number densities $\approx 10^4 \text{ cm}^{-3}$), so that forbidden lines can be as strong or stronger than the allowed ones. This is also the mechanism for cooling such a low density plasma, collisional excitation being followed by emission of radiation. If there are two excited states, 2 and 3, above the ground state 1, then in the ratio of the $2 \rightarrow 1$ and $3 \rightarrow 1$ intensities, the number density of electrons cancels out and the ratio is proportional to $\exp[(E_2 - E_3)/kT]$. Such ratios are, therefore, good diagnostics of the temperature of such plasmas. Lines in O^{2+} (O III) $1s^2 2s^2 p^2 \ ^1D_2 \rightarrow \ ^3P_2$

(500.7 nm), ${}^1D_2 \rightarrow {}^3P_1$ (495.9 nm), and ${}^1S \rightarrow {}^1D$ (436.3 nm) seen in planetary nebulae provide a good example, ratios of their intensities being very sensitive to the temperature. Interestingly, these narrow emission lines have been observed for over a hundred years and for a time, before they were identified by Bowen (1927) as arising from oxygen ions, were even thought to indicate a new element nebulium!

Each higher term in the expansion of the exponential in (2.23) brings down an additional $(\mathbf{k}\cdot\mathbf{r})$ factor. Upon rearrangement, a pair of electric and magnetic multipoles. M2 and E3, M3 and E4, etc., occur at each higher order in a_0/λ . Selection rules follow in similar manner, each order alternating as far as the parity change is concerned between $|i\rangle$ and $|j\rangle$, and the multipole index n fixing the analog of (2.27) as $\mathbf{J}_i + n = \mathbf{J}_j$.

2.4 Moments and sum rules

The distribution of oscillator strength (we again return to E1 transitions) across the spectrum, as in Fig. 2.1, provides the response of an atom to electromagnetic radiation. Laboratory measurements and calculations of varying degree of accuracy are available for most atoms and ions of interest. As with any distribution, its various moments provide more limited but nevertheless useful information. A few of the lower moments, and associated sum rules, are also interestingly related to other gross physical properties of the atom.

The lowest moment, denoted by S_0 , is simply the area under the curve in Fig. 2.1,

$$S_0 = \int dE \frac{df}{dE}, \quad (2.28)$$

where such integrals will be understood to include sums $\sum f_n$ over the discrete part of the spectrum. The oscillator strength having been defined so as to express how much in proportion the atomic electrons couple to that particular frequency range, clearly the total in (2.28) will represent the total number N of oscillators/electrons available so that we have a “sum rule” named for Thomas, Reiche, and Kuhn,

$$S_0 = N. \quad (2.29)$$

A “quantum-mechanical proof” of this follows from a further commutation step in (2.20), namely,

$$\sum_s [[H_0, z_s], z_s] = \sum_s (1/\mu) (\hbar/i)^2. \quad (2.30)$$

Sandwiching both sides between $\langle i|$ and $|i\rangle$ and inserting a complete set in between through the closure relation $\sum_j |j\rangle\langle j|$ reduces the left-hand side to $(-\hbar^2/\mu)\sum_s \sum_j f_{ji}$ from which (2.29) follows. In the development of quantum mechanics, the reverse procedure, namely that the total integrated oscillator strength must equal the total number of electrons, whatever the microscopic mechanics governing atoms and radiation, played a crucial role in Heisenberg's formulation of the basic commutation relationship between z and p_z .

Next, the moments, $S_{\pm 1} = \int dE E^{\pm 1} (df/dE)$ are especially interesting. For S_1 , using the form (2.22), the factors involving energy or ω_{ji} cancel and the sum over j collapses through closure to give $S_1 = \sum_s \langle i|2p_{zs}^2/\mu|i\rangle$. Through the virial theorem, this moment is simply $(4/3)|E_i|$. For S_{-1} , the form (2.16) similarly reduces to an expectation value in the state i ,

$$S_{-1} = \sum_s (2\mu/\hbar^2) \langle i|z_s^2|i\rangle. \quad (2.31)$$

For a spherically-symmetric state $|i\rangle$, S_{-1} is therefore simply related to the expectation value of r^2 which is also a measure of the diamagnetic susceptibility of the atom (Section 3.2.1). For the ground-state of H, using (1.10) we have $S_{-1} = 2a_0/e^2 = (1/\text{Ry})$. From (2.15), it follows that S_{-2} is simply related through constant factors to the static ($\omega = 0$) electric polarizability of the state $|i\rangle$.

Table 2.1. Moments S_ℓ in atomic units (Rev. Mod. Phys. **40**, 441 (1968)).

r	-2	-1	0	1	2
H	4.5	2	1	2/3	4/3
He	0.346	0.752	2	8.17	121
Ne	0.667	1.95	10	320	1.1×10^5
Ar	2.77	5.3	18	1150	1.16×10^6
Kr	4.18	7.5	36	5300	1.9×10^7
Xe	6.82	10.3	54	1.3×10^4	10^8

In H, as with the oscillator strength itself, all these moments can be evaluated analytically in closed form. In other atoms, with only approximate wave functions available, these moments and their connections to other measurable quantities serve as checks on the wave functions. Table 2.1 gives a sample of results. Among other general features of photoabsorption and photoionization, of the two values $\ell_j = \ell_i \pm 1$ allowed by the E1 selection rules, it turns out that the matrix elements

are an order of magnitude larger for $\ell_i + 1$. This is plausible on the grounds that absorption of energy by the atom should be accompanied by a gain in angular momentum. Although not a selection rule in that there is no underlying symmetry, only an empirical observation of the dynamics, such “propensity rules” are often useful guidelines. Similarly, at high energy in the continuum, df/dE falls off as $E^{-(\ell_i + \frac{7}{2})}$, as follows from matrix elements of hydrogen which all atoms closely approximate in this limit. Note, as a consequence, that for the oscillator strength distribution from the ground state, higher moments beyond S_3 are not defined. Also, because of configuration mixing, the lowest values of ℓ_i compatible with parity, namely 0 or 1, always govern the high energy behavior.

3. Charged-particle Collisions

Although collision of charged particles with atoms differs from the interaction of atoms with electromagnetic radiation (particularly so at low collisional energies), there are close similarities between the two and certain complementary aspects that make it natural to study them in this chapter. When a charged particle passes by an atom with high velocity, its dominant effect is that of the pulse of electromagnetic fields that the atom experiences. The effect is of illuminating the atom with a broad-band electromagnetic spectrum so that the atomic response is described by an analog of the (optical) oscillator strength. There are some differences, notably in the selection rules so that certain transitions not seen in photon impact can be excited by charged particles, but it is this “generalized oscillator strength” that we will study in this section. Encounters between atoms and charged particles, whether ions or electrons, are of course important in a variety of astronomical contexts wherein such a mix. of entities is present. As a result, collisional cross-section data are very important in astrophysics [16].

3.1 The Generalized Oscillator strength

A fast collision also shares with the earlier study of radiation interaction with atoms the feature that it is perturbative, in this instance because of the short time of interaction. The charged projectile may, therefore, be considered to be changed only in its momentum, that is, in its speed and direction of its trajectory, while the atom may be left either in its initial state or, with small probability, excited to a state, either discrete or in the continuum (in which case, an atomic electron is ejected). More sophisticated treatment of the distortion of the projectile is possible but, at this simplest level, it will be treated as a plane

wave both before and after the collision. This constitutes the well-known “Born approximation” of scattering theory.

Representing the incident charged particle of charge ze and reduced mass M with respect to the atom by a plane wave, $(2\pi\hbar)^{-3/2} \exp(i\mathbf{p}_i \cdot \mathbf{r}/\hbar)$, the initial state of the atom by $|i\rangle$, and similarly the projectile’s final state after scattering by $(2\pi\hbar)^{-3/2} \exp(i\mathbf{p}_f \cdot \mathbf{r}/\hbar)$, and the atom’s by $|f\rangle$, energy conservation requires

$$\left(\mathbf{p}_i^2/2M\right) + E_i = \left(\mathbf{p}_f^2/2M\right) + E_f. \quad (2.32)$$

The normalization “per unit \mathbf{p} ” chosen for the plane waves means that the incident flux is $(2\pi\hbar)^{-3} p_i/M$. The differential scattering cross-section for the projectile of final momentum \mathbf{p}_f into a solid angle $d\Omega_f$ is again given by $(2\pi/\hbar)$ times a transition matrix element squared as in (2.8), multiplied by the scattered particle velocity p_f/M to give the scattered flux, and divided by the incident flux:

$$\frac{dr}{d\Omega_f} = \frac{(4\pi^2 M \hbar)^2 p_f}{(2\pi\hbar)^6 p_i} \left| \int \psi_f^*(\{\mathbf{r}_s\}) e^{[i(\mathbf{p}_i - \mathbf{p}_f) \cdot \mathbf{r}/\hbar]} V(\mathbf{r}) \psi_i(\{\mathbf{r}_s\}) d\mathbf{r} \prod_s d\mathbf{r}_s \right|^2. \quad (2.33)$$

The Coulomb interaction of the projectile with the atom is

$$V(\mathbf{r}) = \frac{zZe^2}{r} - \sum_s \frac{ze^2}{|\mathbf{r} - \mathbf{r}_s|}, \quad (2.34)$$

the first term the interaction with the nucleus of the atom (chosen as the origin of coordinates) and the second the projectile-electron interactions, \mathbf{r} and \mathbf{r}_s the corresponding distances from the atomic nucleus to the projectile and the s -th electron, respectively. Carrying out the integration over \mathbf{r} first which gives the Fourier transform of the Coulomb potentials with respect to the “momentum transfer” $\mathbf{k}_{fi} = (\mathbf{p}_f - \mathbf{p}_i)/\hbar$ from projectile to target, we have

$$\frac{d\sigma}{d\Omega_f} = \left(\frac{2Mze^2}{|\mathbf{p}_f - \mathbf{p}_i|^2} \right)^2 \frac{p_f}{p_i} (Z\delta_{if} - F_{fi})^2, \quad (2.35)$$

where we have defined

$$F_{fi} = \left| \sum_s \langle f | \exp(i\mathbf{k}_{fi} \cdot \mathbf{r}_s) | i \rangle \right|^2, \quad (2.36)$$

called a “form factor”. Also elsewhere in physics, such form factors are of importance because they capsule the form of the system’s response.

In (2.34), the projectile-nucleus interaction, which involves no electronic coordinates, is diagonal in the atomic states and can only lead to elastic scattering. Indeed, this term with the squared prefactor in parenthesis is precisely the Rutherford scattering cross-section of a charge ze off another charge Ze . The second term, from projectile-electron interactions, is the only one that can lead to inelastic scattering with excitation of the atom from $|i\rangle$ to $|f\rangle$. Thus the inelasticity is expressed entirely as a factor dependent on projectile alone, namely the Rutherford factor multiplied by p_f/p_i , and a form factor that depends on the atomic response through the single parameter of the momentum transferred to it, and on atomic properties through the wave functions ψ_i and ψ_f .

Although the Rutherford factor is singular, note how the unity in the expansion of the exponential in (2.36) precisely cancels in (2.35) the nuclear term for elastic scattering, rendering that cross-section finite as one would expect for scattering from a neutral atom. For inelastic scattering, the form factor gets no contribution from the unity in the exponential but only from the next terms in its expansion. The first of these and, therefore, the one dominant for small momentum transfer, is precisely the dipole matrix element of optical transitions. Indeed, defining therefore

$$f_{fi}(\mathbf{k}_{fi}) = \frac{2M(E_f - E_i)}{\hbar^2} \left| \frac{F_{fi}}{k_{fi}} \right|^2, \quad (2.37)$$

as a, “generalized oscillator strength”, it reduces precisely to the optical oscillator strength in (2.16) for $\mathbf{k}_{fi} \rightarrow 0$. (See Fig. 2.3). As before, for $|f\rangle$ a discrete state, this generalized oscillator strength is dimensionless whereas when it is a continuum state, normalized per unit energy, the oscillator strength is a differential quantity with dimensions of $(\text{energy})^{-1}$. A sum rule similar to (2.29),

$$\sum_f f_{fi}(\mathbf{k}_{fi}) = Z, \quad (2.38)$$

obtains for the same reason that the total number of oscillators is the number Z of electrons, whatever the value of \mathbf{k}_{fi} .

A given momentum transfer \mathbf{k}_{fi} to the atom does not transfer a fixed energy $(\hbar\mathbf{k}_{fi})^2/2M$ to the atom but varied transitions with energy $E_f - E_i$ are possible, reflecting atomic dynamics. The simple energy-momentum balance is realized only at large momentum transfer, reflected in the generalized oscillator strength peaking at that specific

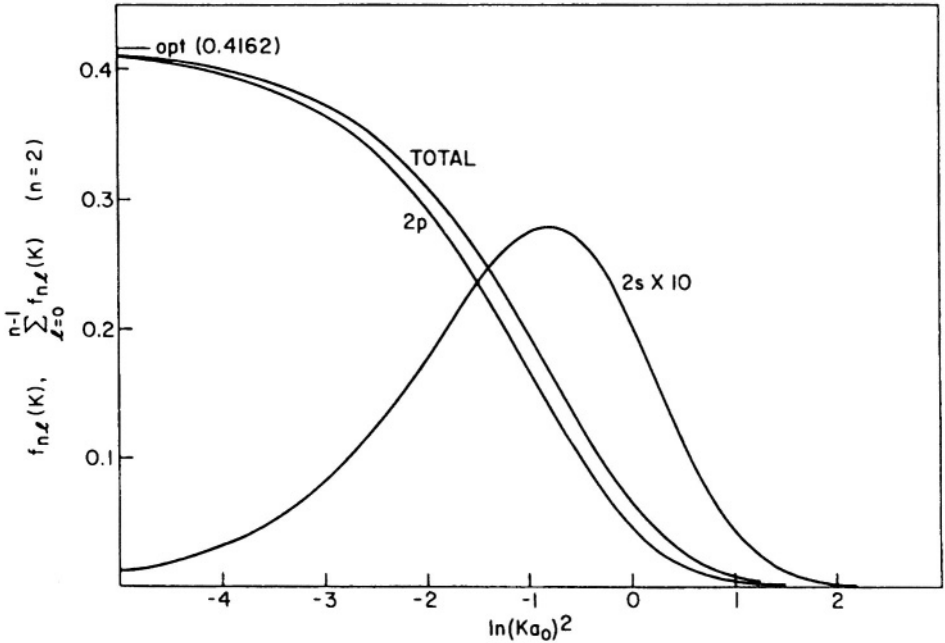


Figure 2.3. Generalized oscillator strength from the ground state to the $n = 2$ levels of hydrogen as a function of momentum transfer $\hbar K$. Note the convergence of the optically allowed $2p$ state to the optical oscillator strength as $K \rightarrow 0$. From [16].

energy E_f . In the opposite limit of low momentum transfer where we have already observed that it reduces to the optical oscillator strength, there are still differences from the absorption of radiation. First, the limit $k_{fi} \rightarrow 0$ is never exactly reached in inelastic scattering because of the need to satisfy (2.32). Also, the selection rules for the operator in (2.36) are different from those for (2.16) so that optically forbidden transitions are excited by charged particle impact. As an example in He, at 35 eV incident energy, the generalized oscillator strengths for $1^1S \rightarrow 2^1P$, 1^1S , 3^1P are in the ratio 1: 0.18: 0.12, whereas the optical oscillator strengths are $1:10^{-6}$ (an E2 transition): 10^{-10} (a spin-flip excitation). The 2^3P excitation, involving a spin-flip, happens only extremely weakly through spin-orbit couplings in photoabsorption whereas under electron or H_2^+ impact, an exchange of spin between the incident and one atomic electron can take place more readily: Fig. 2.4.

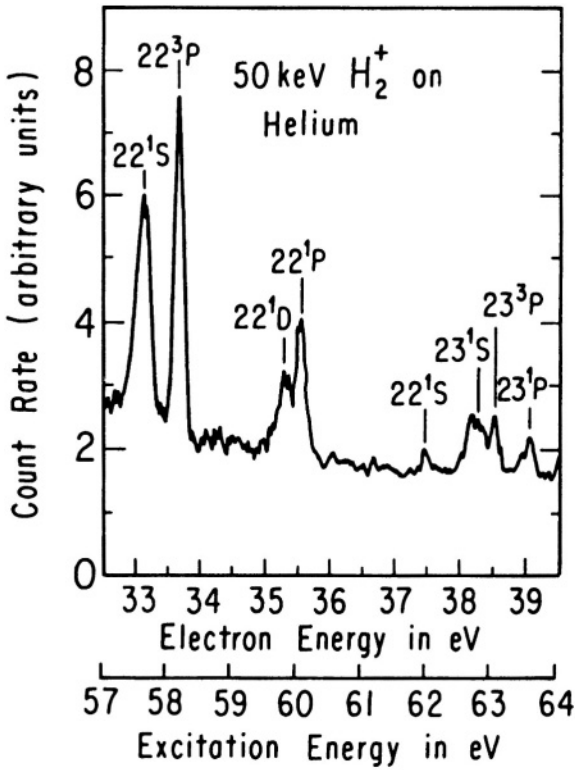


Figure 2.4. Excitation of helium by 50 keV H_2^+ ion impact, showing various doubly-excited states lying about 60 eV above the ground state. From M. E. Rudd, Phys. Rev. Lett. 13, 503 (1964).

3.2 Total cross-section

The total cross-section for exciting the atom from $|i\rangle$ to $|f\rangle$ is given by integrating over the scattering angles of the projectile. In general, when $|i\rangle$ is the ground state, azimuthal symmetry prevails either because the ground state of most atoms is spherically symmetric or, even when not, because atoms are randomly oriented. In such cases, F in (2.36) is a function only of the magnitude and not vector direction of \mathbf{k}_{fi} . Writing $d\Omega_f = \pi \hbar^2 d(k_{fi}^2)/p_i p_f$, and thereby

$$d\sigma_{fi} = \frac{4\pi a_0^2 z^2}{(\hbar v/e^2)^2} \left(\frac{f_{fi}(k_{fi})}{(E_f - E_i)/Ry} \right)^2 d \ln [(k_{fi} a_0)^2], \quad (2.39)$$

where v is the incident velocity of the projectile, the integral is conveniently performed over k_{fi} . Its kinematically allowed limits follow from $(\hbar k_{fi})^2 = p_i^2 + p_f^2 - 2p_i p_f \cos \theta$ and the energy conservation relation (2.32). Here, the behavior of the $k_{fi} \rightarrow 0$ limit proves decisive. For optically allowed transitions, wherein this approaches a constant f_{fi} , the total cross-section σ increases logarithmically with the incident energy of the projectile,

$$\sigma = \frac{4\pi a_0^2 z^2}{(\hbar v/e^2)^2} \frac{\text{Ry}}{E_f - E_i} f_{fi} \ln \left[4C_{fi} \left(\frac{\hbar v}{e^2} \right)^2 \right], \quad (2.40)$$

where C_{fi} is a numerical constant. For optically forbidden transitions, where the middle factor in squared parenthesis in (2.39) vanishes at both small and large k_{fi} , the integral over this variable becomes a constant b_{fi} and we get

$$\sigma = \frac{4\pi a_0^2 z^2}{(\hbar v/e^2)^2} b_{fi}. \quad (2.41)$$

Knowledge of these cross-sections, when coupled with observed excitation or de-excitation rates due to collisions with electrons in planetary nebulae or other low density plasmas, provides the number density of electrons present.

4. The Negative Ion of Hydrogen

Energy from the interior of a star has to be radiatively transferred through the outer layers of stellar atmospheres before we finally observe it. Continuum absorption by atoms and ions in these layers is, therefore, central to our understanding of the opacity of stellar atmospheres [17]. As we have already seen, for H atoms in the ground state or even in $n = 2$, this continuous absorption lies in the ultraviolet. This is also true for most atoms in the ground state, the ionization potentials always exceeding 5 or 6 eV. For positive ions, these energies are even larger. Only for atoms that are more highly excited, of which there are generally fewer, is the visible range of the spectrum involved. Discrete excitation of ground state atoms is similar, the first excitation energies being at least 3–4 eV even if not as large as the 10.2 eV in H. Therefore, for most of the visible spectrum, with photon energies less than 3 eV, atoms and positive ions do not contribute much to stellar opacities and we have to look elsewhere for species that can play a role. It was Wildt who first suggested that the weakly bound negative ion of H would be a significant contributor to stellar opacities for stars such as our Sun.

With both hydrogen and low energy electrons abundantly present in such stellar atmospheres, one would expect H^- to be formed through their attachment. Subsequent photodetachment, the analogous process to photoionization when dealing with negative ions, serves to absorb low energy photons. This possibility spurred the investigation of H^- (and other negative ions) in atomic physics. Studies showed a binding energy (alternatively, “electron affinity” of H) of 0.75 eV and that indeed H^- is the dominant contributor to opacities in A-G stars. Other negative ions, such as C^- with a binding energy of 1.25 eV, also prove important, particularly in H-deficient stars, but given hydrogen’s dominance in the Universe, H^- is the most important negative ion for stellar opacities.

4.1 The ground state of H^-

H^- is a member of the isoelectronic series of He but differs from all others of the sequence in not having a dominant Coulomb attraction by the nucleus for both electrons. The interaction between the electrons is, therefore, more important from the start, even in the ground state. Whereas perturbation and variational methods with simple uncorrelated trial functions such as the one in (1.18) give a reasonably good description of He, they fail even to predict binding for H^- as already noted below (1.20). See also Problem 1.6. The minimum energy in (1.20) for $Z = 1$ lies at $-(121/128)$ Ry which is a poor upper bound considering that placing an electron infinitely far from the hydrogen atom in the ground state already gives -1 Ry. It was, therefore, not possible to conclude that energy is to be gained by attaching an electron to H till a 1929 calculation by Bethe (Problem 1.6) using a 3-parameter wave function of the form in (1.21),

$$\psi_t = [1 + \alpha r_{12} + \beta(r_1 - r_2)^2] \exp[-Z_{\text{eff}}(r_1 + r_2)], \quad (2.42)$$

with explicit electron correlation through the term in r_{12} . Soon after, a 6-parameter function by Hylleraas improved the estimated binding energy and, subsequently, just as in He, elaborate variational calculations with many parameters in (1.21) have provided very accurate values for this binding energy of, approximately, 0.75 eV. High resolution laser photodetachment of H^- has provided the best experimental values of $6082.99 \pm 0.15 \text{ cm}^{-1}$ for the electron affinity of H ($F = 0$, where F is the sum of the electron’s $J = \frac{1}{2}$ and the nuclear spin $\frac{1}{2}$) and $6086.2 \pm 0.6 \text{ cm}^{-1}$ for the deuterium isotope D ($F = \frac{1}{2}$).

An alternative trial function, while not as accurate as (2.42), suffices already to predict binding and is, therefore, instructive. This “Chandrasekhar function” generalizes (1.18) to introduce two different effective

charges, α and β , for the otherwise equivalent electrons. The ground state 1S , being antisymmetric in spin interchange, is required by the Pauli principle to be spatially symmetric so that we take

$$\psi_t = N[\exp(-\alpha r_1 - \beta r_2) + \exp(-\alpha r_2 - \beta r_1)], \quad (2.43)$$

with N a normalization constant. An energy minimum which lies below -1 Ry is attained for $\alpha = 1.039$ and $\beta = 0.283$. Although no explicit inclusion of electronic correlation through dependencies on r_{12} is included, (2.43) is nevertheless correlated by virtue of the Pauli principle. This function has a “radial in-out” correlation, the very different values of α and β having the effect that when one electron is “in” close to the nucleus, the other is kept “out”. Alternatively, that α is larger than the nuclear charge of unity may be interpreted as saying that the presence of the other, “outer”, electron forces the inner one “to see” more of the nuclear attraction than it would were it to be by itself as in the hydrogen atom. At the same time, the outer electron itself acquires a non-zero β , sufficient to bind it as well.

The much more elaborate variational functions also support this fundamental picture which is very important for our understanding of H^- , that radial correlations are crucial, far more so than angular correlations between the electrons, and that the two electrons are on different footings, one very loosely attached at a much larger distance ($\approx 4 - 5 a_0$) than the other. This suggests a useful “one-electron model” for H^- wherein this electron may be regarded as weakly bound in a short-range attractive potential. There are close similarities to other weakly bound quantum systems such as the deuteron in nuclear physics. An extreme model for such systems is to consider an attraction of “zero range” or, indeed, as a delta-function potential well, with a single parameter, the binding energy characterizing the wave function of the outer electron as $\exp(-\kappa_B r)/r$, where $\hbar^2 \kappa_B^2 / 2\mu \approx 0.75$ eV. The complete two-electron wave function can then be written as

$$(\sqrt{2}) (1 + P_{12}) \psi_0(r_1) N \exp(-\kappa_B r_2) / r_2, \quad (2.44)$$

where P_{12} represents exchange of coordinates 1 and 2, ψ_0 is the ground state of H, and N a normalization constant with numerical value 0.31552.

The zero-range model also incorporates another feature of H^- borne out by more elaborate calculation: apart from the bound state $1s^2\ ^1S$, this system has no singly-excited bound spectrum. This is not implausible considering that, even in the ground state, the second electron is barely bound (0.75 eV *vs* hydrogen’s 13.6 eV) but a mathematical proof

has emerged only relatively recently, demonstrating how different H^- is from its higher isoelectronic analogs. But the fact of only one bound state is compatible with the similar fact for an attractive delta-function potential. Careful laser photodetachment studies have also ruled out any singly-excited states, the only excited states of H^- being, therefore, those involving both electrons. Such doubly-excited states, which are unstable against decay through electron emission, will be considered in Section 5.2.2.

4.2 Photodetachment of H^-

With a binding energy of 0.75 eV, any photons of energy larger than that ($\lambda \lesssim 1.6 \mu\text{m}$) can be absorbed in photodetaching H^- . Here, another feature that distinguishes negative ions from neutral atoms or positive ions also proves decisive. Unlike in Figs. 2.1 or 2.2, with photoionization cross-sections starting at a finite value at threshold and then decreasing for higher photon energies, the shape of a photodetachment cross-section is very different, rising from zero at threshold to a maximum and later falling off towards higher energies: Fig. 2.5. In both photoionization of H and photodetachment of H^- , an initial s electron departs as a p -wave because of (electric) dipole selection rules. The low-energy electrons just above threshold experience the angular momentum barrier $\ell(\ell + 1)\hbar^2/2\mu r^2$ which acts to suppress their escape in the case of H^- but not in H because of the overwhelming influence of the attractive Coulomb potential which is of longer range than angular momentum. Photoionization cross-sections are, therefore, both finite and independent of ℓ near threshold whereas photodetachment is suppressed, even more strongly so for larger ℓ . Indeed, the “Wigner threshold law” that $\sigma \propto E^{(\ell+\frac{1}{2})}$, where E is the excess energy above threshold, is an expression of this suppression [18]. The contrast between negative ions and neutral atoms can also be seen below threshold. Unlike in Fig. 2.1 for neutral atoms, there are no discrete line strengths in a negative ion which has no bound excited states.

The shape of the H^- photodetachment cross-section in Fig. 2.5 makes this ion important for opacity in the visible range, the major part of the peak lying in this region of the spectrum. It had long been known that the opacity for many stars with surface temperatures less than 10^4 K increased by about a factor of two from 400 to 900 nm, then decreased to a minimum at 1600 nm, a shape exactly mirrored by H^- ^1S absorption. This species itself accounts, therefore, for the continuum absorption coefficient in the solar atmosphere from 400 to 2500 nm.

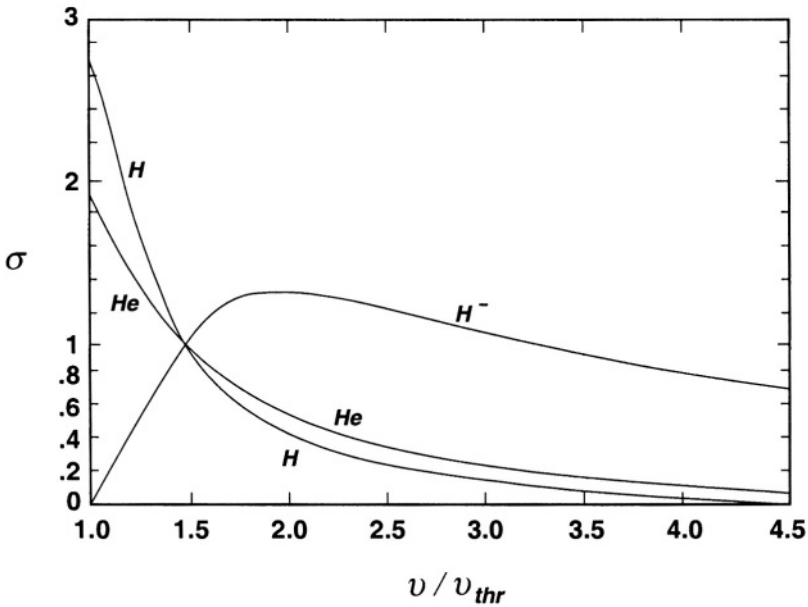


Figure 2.5. Photoionization and photodetachment cross-sections as a function of energy above threshold in units of threshold energy. From H. A. Bethe and E. E. Salpeter, *Quantum Mechanics of One- and Two-Electron Atoms* (Plenum, New York, 1977), with permission from author and publisher.

Fig. 2.6 provides the results both from the simple wave function in (2.44) and more elaborate many-parameter variational solutions [19].

It was in the context of these opacity calculations, and in the realization that different approximate functions of H^- may be inaccurate at larger distances, that the alternative “velocity” and “acceleration” forms to the “length” in (2.16) were developed and introduced into atomic physics, as discussed in Section 2.2.2.

4.3 Radiative capture

The process inverse to photodetachment or photoionization is the capture of electrons by neutral atoms or positive ions with the binding energy released through the photon that is emitted. An immediate estimate shows that such captures occur with low probability because the collision time for an electron of a few eV with an atom is approximately 10^{-15} s which is the time of traversal over the size of an atom. Radiative rates being 10^8 s^{-1} (recall that allowed transitions have lifetimes of 10^{-8}



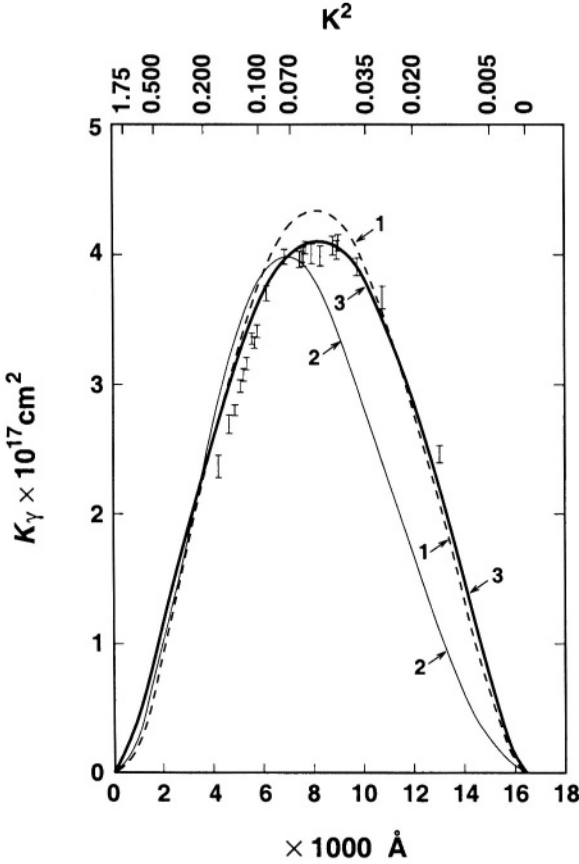


Figure 2.6. Continuous absorption coefficient for the photodetachment of H^- . Results (3) using the simple wave function in (2.44) are contrasted with data from experiment and calculation using 20-parameter numerical wave functions as in (1.21) in the dipole length (1) and dipole velocity (2) forms. From [4] and [19].

s), the probability of radiation during a collision is very small, $\approx 10^{-7}$. The same result can be seen through cross-sections, the two processes of radiative capture and photodetachment being related through detailed balance, differing only in kinematic prefactors but otherwise sharing the same transition matrix elements:

$$g_-(h\nu)^2 \sigma_{\text{photodetachment}} = g_0(\mu v^2)(\mu c^2)\sigma_{\text{capture}}, \quad (2.45)$$

where g_- and g_0 are statistical weights of the negative ion and neutral atom. With the photon energy $h\nu$ comparable to the electron kinetic en-

ergy $\frac{1}{2}\mu v^2$, the difference lies in the $h\nu/\mu c^2$ factor so that, cross-sections for photodetachment being $\approx 10^{-16} \text{ cm}^2$, those for radiative capture are $\approx 10^{-22} \text{ cm}^2$.

Most captures, therefore, take place through the mediation of a third body, such three-body collisional capture dominating for densities exceeding 10^{16} cm^{-3} . Capture of an electron by a positive ion to form an excited Rydberg state, particularly of high principal quantum number n , is also very unlikely. Such an electron being almost free, as is the initial electron in the continuum, the transition is forbidden by the rule that a free electron cannot spontaneously emit or absorb a photon, both energy and momentum balance not being possible because of the photon's zero mass. Such a capture, important in many astronomical contexts, proceeds through doubly-excited states in a process called dielectronic recombination (Section 5.4).

Problems

- 2.1** Compute the oscillator strength for the $1s \rightarrow 2p$ transition in the hydrogen atom, using both the expressions in (2.16) and (2.22). Thus, verify (2.21) explicitly.
- 2.2** The equation of motion determining the dipole moment of a classical normal mode r is

$$\mu \ddot{\mathbf{p}}_r + \mu \gamma_r \dot{\mathbf{p}}_r + \mu \omega_r^2 \mathbf{p}_r = e^2 f_r \hat{\mathcal{E}}_0 e^{-i\omega t},$$

with ω_r and γ_r the frequency and damping constant of the mode. Show that the total induced moment is

$$\mathbf{p} = \sum_r \mathbf{p}_r = \sum \mathbf{p}_{0r} e^{-i\omega t},$$

with

$$\mathbf{p}_{0r} = \frac{e^2 f_r / \mu}{\omega_r^2 - \omega^2 - i\gamma_r \omega} \hat{\mathcal{E}}_0 \equiv \alpha \hat{\mathcal{E}}_0.$$

Therefore, derive an expression for the real and imaginary parts of the dielectric constant $\varepsilon = 1 + 4\pi N\alpha$.

- 2.3** Determine a lower bound on the static dipole polarizability of the ground state of the hydrogen atom, taking into account the main transition to the $2p$ state.

- 2.4 What are the normalization factors for plane waves in three dimensions, using (a) normalization in a box of volume V , (b) normalization per unit momentum, and (c) normalization per unit energy.
- 2.5 Identify the multipole transition for the following in hydrogen: (i) $5f \rightarrow 4d$, (ii) $3d \rightarrow 2p$, (iii) $4f \rightarrow 2p$, (iv) $4d \rightarrow 3d$.
- 2.6 Prove the Thomas-Reiche-Kuhn sum rule (2.29) by the procedure indicated in the text.
- 2.7 Evaluate S_{-1} for the hydrogen atom.
- 2.8 Establish (2.35), following the steps indicated in the text.
- 2.9 Prove the sum rule (2.38) for the generalized oscillator strength.
- 2.10 Using r_1 and r_2 as axes for a two-dimensional plot, construct contours of the normalized Chandrasekhar wave function in (2.43).
- 2.11 The potential seen by an electron incident on a hydrogen atom in its ground state is $-e^2[(1/r) + (1/a_0)] \exp(-2r/a_0)$. Calculate the form factor for elastic scattering in the Born approximation and verify that it depends only the magnitude of the momentum transfer.

Chapter 3

ATOMS IN WEAK, STATIC FIELDS

1. Introduction

Chapter 2 has considered the effect of weak electromagnetic fields on atoms, such time-dependent fields causing transitions between different states. Static, or time-independent, fields, on the other hand, cannot cause transitions but are of interest for their effects on the energy levels and wave functions of atoms. The combined atomic Hamiltonian and coupling to the field are still characterized by stationary states which are, however, different from the stationary states of the atom in the absence of the external field. It is these changes in the structure of the atom that will be the subject of our study in this and the next chapter. We will first consider in this chapter weak fields whose effects are perturbative, leading to small corrections in the energies and wave functions (and, as a result, on other atomic properties). As in the previous chapter, most static fields in laboratory or astronomical contexts are indeed weak relative to the internal electric and magnetic fields in an atom so that the perturbation theory and its applications we study here are widely relevant. More recently, however, very strong external fields (mostly magnetic) have been discovered on some stellar objects which lead to drastic changes in the atomic structure studied in Chapter 1 and this will be the subject of the next chapter.

At the outset, it is clear that atoms experience weak electric and magnetic fields in a variety of situations. The Earth's magnetic field (≈ 1 Gauss), and similar fields on other planets and on the Sun and on other stars (≈ 1 –100 Gauss), and fields pervading interstellar regions in galaxies ($\approx 10^{-5}$ Gauss), have important observable consequences. We hear less of static electric fields, our Universe having free electric charges

but seeming not to have their counterpart magnetic monopoles. With charges free to flow, they “short out” incipient electric fields, never permitting them to build up appreciably whereas no such mechanism constrains the existence of magnetic fields. (Indeed, galactic magnetic fields are used to set limits on the magnetic monopole density.) In local environments, however, the electric fields due to electrons and ions alter the structure of atoms in their neighborhood. We will study perturbations due to both electric and magnetic fields and also “internal” weak fields inside an atom that arise from relativistic and other corrections which we have ignored so far in concentrating on the dominant non-relativistic description of atoms.

2. External Electric and Magnetic Fields

2.1 Coupling to external fields

As in Section 2.2.1 with a time-dependent electric field, the basic interaction of an atom’s electrons with a static, electric field \mathcal{E} is

$$e\mathcal{E}\cdot\mathbf{r} = e\mathcal{E}z. \quad (3.1)$$

Also, as before in Chapter 2, the internal field in an atom being of the order of a few volts over a few nm, even an external field of 10^6 V/cm is weak in comparison. The atomic unit of electric field is $(e/a_0^2) \approx 5.15 \times 10^9$ V/cm. Therefore, we expect the additional interaction to be a small perturbation to the atomic Hamiltonian H_0 . Such a perturbative effect is called the Stark effect.

The option of minimal coupling, with the replacement of \mathbf{p} by $\mathbf{p} + (e\mathbf{A}/c)$, where \mathbf{A} is the vector potential, is not used with a static electric field because \mathbf{A} then is necessarily time-dependent and we want to consider in this chapter stationary states in a time-independent description. However, for a static magnetic field \mathbf{B} , the procedure is indeed through the corresponding vector potential related to \mathbf{A} through $\mathbf{B} = \nabla \times \mathbf{A}$. As usual in such a description, alternative gauge choices for \mathbf{A} are available, all of which lead to the same physics. Some of these other gauges will be considered in Section 4.1.1 for strong magnetic fields but, in this chapter, we make use of $\mathbf{A} = \frac{1}{2} \mathbf{B} \times \mathbf{r}$ which leads to the Hamiltonian

$$H = \sum_s \left(\mathbf{p}_s + \frac{e\mathbf{B} \times \mathbf{r}_s}{2c} \right)^2 / 2\mu + V, \quad (3.2)$$

with V the atomic potential and $s = 1, 2, \dots, N$ for an N -electron atom. The Hamiltonian H differs from the atomic H_0 by the interaction terms

$$H' = \sum_s \frac{e}{2\mu c} \mathbf{B} \cdot (\mathbf{r}_s \times \mathbf{p}_s) + \frac{e^2}{8\mu c^2} (\mathbf{B} \times \mathbf{r}_s)^2 . \quad (3.3)$$

The first term, linear in magnetic field strength, is $-\boldsymbol{\mu} \cdot \mathbf{B}$, where the magnetic moment $\boldsymbol{\mu} = -(e/2\mu c) \sum_s \boldsymbol{\ell}_s = -(e/2\mu c) \mathbf{L}$. This is the paramagnetic or “linear Zeeman” interaction. The quadratic term is the diamagnetic or “quadratic Zeeman” interaction and is proportional to the area of the orbit of the electron. Again, as with electric fields, for most magnetic field strengths of interest in physics and astronomy, except those of the order of 10^5 T or greater, both terms in (3.3) lead to small, perturbative corrections to energy levels and wave functions of stationary states. The atomic unit of magnetic field is $(m^2 e^3 c / \hbar^3) = 2.35 \times 10^5$ T. Further, the diamagnetic term is generally even smaller than the paramagnetic and becomes appreciable only for excited states with high n , the \mathbf{r}^2 scaling as n^4 .

2.2 Time-independent perturbation theory

The Stark and Zeeman effects played a crucial role in the early development of quantum-mechanical perturbation theory by Schrödinger and others, and have since been used throughout all branches of physics. Spectroscopists had observed that spectral lines were broadened or split by externally imposed electric and magnetic fields. An astronomical connection was Zeeman’s observations in 1896 that lines from sunspots were broader than from the rest of the disk. The actual connection of this observation to the magnetic fields of sunspots was made in 1908 by Hale. The linear Zeeman effect also played a crucial role in elucidating the azimuthal quantum number m in quantum physics (hence, also called the magnetic quantum number). The perturbation-theoretic treatment was, of course, not born in quantum mechanics, was already familiar in classical physics and mathematics, but its specific form in the context of quantum-mechanical Hamiltonians and effects on stationary states is due to Schrödinger, who adapted Rayleigh’s classical perturbation theory for this purpose.

The key result is that for every state $|n\rangle$ with energy $E_n^{(0)}$ and wave function $\psi_n^{(0)}$ of the unperturbed Hamiltonian H_0 , there is a corresponding state of $H = H_0 + H'$ which can be expanded in terms of the basis provided by the complete set $(\mathbf{I} = \sum_n |n\rangle \langle n|)$ of states of H_0 :

$$\begin{aligned} E_n &= E_n^{(0)} + E_n^{(1)} + E_n^{(2)} + \dots , \\ \psi_n &= \psi_n^{(0)} + \psi_n^{(1)} + \psi_n^{(2)} + \dots , \end{aligned} \quad (3.4)$$

with the superscripts indicating successively smaller, or higher order, corrections. The order of smallness is in terms of some parameter contained in H' , the field strengths \mathcal{E} and B providing such parameters in our current context. Any $\psi_n^{(r)}$ can be expanded as $\sum_m c_{nm}^{(r)} \psi_m^{(0)}$. Inserting this expansion, along with (3.4) into the Schrödinger equation, $H\psi_n = E_n \psi_n$, multiplying from the left by the unperturbed $\psi_m^{(0)}$, and equating terms of the same order of smallness on both sides of the equation gives an algebraic set which can be solved for $E_n^{(r)}$ and $c_{nm}^{(r)}$. The first couple of terms are familiar,

$$E_n^{(1)} = \langle n | H' | n \rangle, \quad (3.5)$$

$$c_{nm}^{(1)} = \frac{\langle m | H' | n \rangle}{E_n^{(0)} - E_m^{(0)}}, \quad n \neq m, \quad c_{nn}^{(1)} = 0, \quad (3.6)$$

$$E_n^{(2)} = \sum_{m \neq n} \frac{\langle n | H' | n \rangle \langle m | H' | n \rangle}{E_n^{(0)} - E_m^{(0)}}. \quad (3.7)$$

The algebraic set that the Schrödinger equation reduces to gives all $E_n^{(r)}$ and $c_{nm}^{(r)}$, $n \neq m$, the coefficients $c_{nn}^{(r)}$ determined through the supplementary requirement that ψ_n in (3.4) be normalized to unity just as are $\psi_n^{(0)}$ or the states $|n\rangle$.

In the case of degeneracy, when two states of H_0 share the same energy, or even for near-degeneracy, the denominators in (3.6) and (3.7) make such “perturbative corrections” meaningless. In this situation, within this subset of degenerate or near-degenerate states, H' is diagonalized exactly as in a finite-matrix diagonalization, only the states m not part of the subset being treated through the perturbative formulae (3.6) and (3.7).

A useful diagrammatic prescription can be developed for the perturbation series. Representing the interaction H' by a dashed “interaction line” terminating in a cross, and the state $|n\rangle$ of interest by a downward-going line and any other state $|m\rangle$ by an upward-going line, the matrix elements that occur in (3.5) – (3.7) and their counterparts in higher order are all expressible in terms of the four basic ones in Fig. 3.1. In the diagram representing any $E_n^{(r)}$, there will be r such interaction lines, all connected together, a final two closed so as to leave no open lines representing states. Thus, (3.5) is represented by Fig. 3.2, which is essentially the same as in Fig. 3.1 but the two lines- n closed into a loop. Fig. 3.3

represents the second-order energy in (3.7). To connect the diagram into the algebraic expression, we read from bottom to top, building up the expression from right to left by writing the corresponding matrix element from Fig. 3.1 for each interaction encountered. A horizontal slice between each interaction and the next intersects one downward and one upward line and is interpreted as a corresponding $E_n^{(0)} - E_m^{(0)}$ in the denominator. The downward line n is always kept at the extreme left and so these energy denominators always start with $E_n^{(0)}$. A summation over all upward lines m is understood, as also that $m \neq n$. With this set of rules, Fig. 3.3 is translated into (3.7). One more rule enters in describing terms beyond the second order, a sign $(-1)^{h+\ell}$ attached to the algebraic expression, where h is the number of downward lines (stands for “hole” in the terminology of many-body perturbation theory in atomic, condensed matter and nuclear physics where similar diagrams are employed [20]) and ℓ the number of “loops”. Thus for both Figs. 3.2 and 3.3, this sign is positive, there being one downward line- n and one loop.

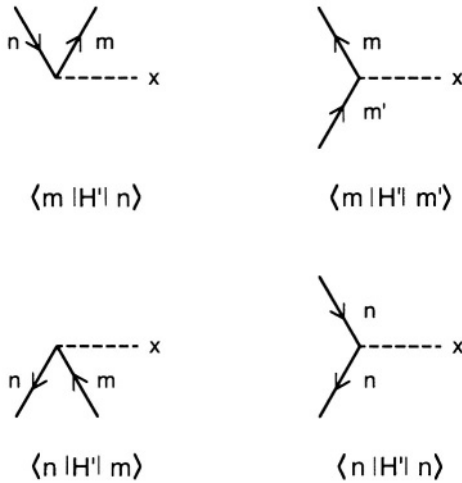


Figure 3.1. Diagrams representing the basic matrix elements in time-independent perturbation theory for a state n , other states denoted by m and m' .

As an application, Fig. 3.4 provides the next, third-order, diagrams. Note there are now two; in general, there are $(r-1)!$ diagrams at the r -th order. Following the above rules, the algebraic rendering of the two diagrams in Fig. 3.4 gives the two terms in the expression for $E_n^{(3)}$,

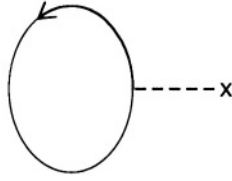


Figure 3.2. Diagram for first-order energy correction in (3.5).

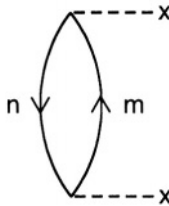


Figure 3.3. Diagram for second-order energy correction in (3.7).

$$\begin{aligned}
 E_n^{(3)} &= \sum_{m \neq n} \sum_{m' \neq n} \frac{\langle n | H' | m' \rangle \langle m' | H' | m \rangle \langle m | H' | n \rangle}{(E_n^{(0)} - E_{m'}^{(0)}) (E_n^{(0)} - E_m^{(0)})} \\
 &- E_n^{(1)} \sum_{m \neq n} \frac{\langle n | H' | m \rangle \langle m | H' | n \rangle}{(E_n^{(0)} - E_m^{(0)})^2}.
 \end{aligned} \tag{3.8}$$

At the r -th order, therefore, we draw r interaction lines stacked vertically and connect them with downward and upward lines in all possible distinct ways to get closed diagrams with a “continuous circulation of the arrows”. An alternative, iterative view is also useful, each order related to the one below by the consideration that an extra interaction line is “inserted” in all possible distinct ways onto the diagrams. Thus, in the passage from Fig. 3.3 for second- to Fig. 3.4 for third-order, there are two places for such an insertion, either on the line- n or the line- m . Clearly, in the next step from Fig. 3.4, one can write the six diagrams of $E_n^{(4)}$ by the three possible insertions on each of the two diagrams.

Most applications of perturbation theory do not go beyond the second order, although the Stark effect has been computed in recent times even

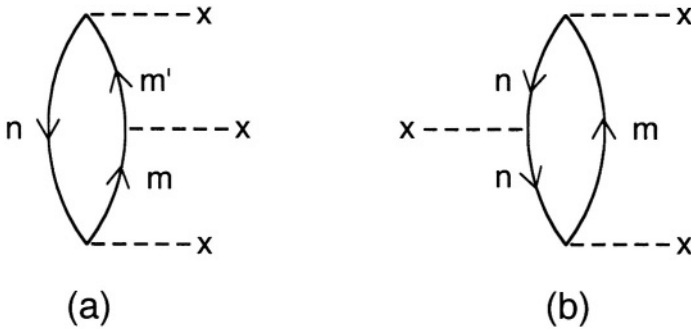


Figure 3.4. Diagram for third-order energy correction, representing the two terms in (3.8).

to orders beyond one hundred [21] and so also the diamagnetic Zeeman effect to very high order (Section 4.3.2). In certain contexts, one also sums to very high order the contribution of a subset of diagrams that are deemed as dominant. An example is provided by the diagrams in Fig. 3.3, Fig. 3.4(a), and higher members of the sequence, each with an additional interaction line inserted always on the upward lines. Furthermore, among this sequence, if one restricts all intermediate m sums in expressions such as the first term in (3.7) to $m = m' = m'' \dots$, which is reasonable for interactions H' whose diagonal matrix elements are much larger than the off-diagonal, then as can be seen from (3.7) and (3.8), successive members of this sequence differ by a multiplicative factor

$$k = \frac{\langle m|H'|m\rangle - \langle n|H'|n\rangle}{E_n^{(0)} - E_m^{(0)}} \quad (3.9)$$

As a result, the infinite sequence of such terms can be summed readily:

$$\sum_{m \neq n} \frac{\langle n|H'|m\rangle \langle m|H'|n\rangle}{(E_n^{(0)} - E_m^{(0)})} \{1 + k + k^2 + \dots\} = \sum_{m \neq n} \frac{\langle n|H'|m\rangle \langle m|H'|n\rangle}{(E_n^{(0)} + E_n^{(1)} - E_m^{(0)} - E_m^{(1)})} \quad (3.10)$$

an expression very similar to (3.7) except for the replacement in the denominator of zeroth-order energies by those corrected to first order. The counterpart of such an approximate summation of the perturbation series to infinite order in many-body perturbation theory goes under the name of the Random Phase Approximation [20] (the off-diagonal elements $\langle m|H'|m'\rangle$ considered vanishingly small by virtue of the random phases of the states, leaving behind only the diagonal entries.)

2.3 The Stark effect

With the perturbation H' as in (3.1), the electric field strength \mathcal{E} serving as the small parameter, the oddness under parity of this operator makes the first-order energy correction in (3.5) vanish for any states of well-defined parity. Since, as we saw in Chapter 1, most atomic states are indeed eigenstates of parity, this means that the first-order or linear Stark effect is generally zero. Only excited states of hydrogen (or very high singly-excited states of any atom), which have degenerate manifolds of states of both odd and even ℓ , and therefore of parity, exhibit the linear Stark effect. The interaction (3.1) has to be diagonalized within this manifold to get energy corrections of first order in \mathcal{E} . Equivalently, the parabolic states of Section 1.2.2 are precisely the products of such a diagonalization and provide the eigenstates of the linear Stark effect. Specifically for $n = 2$, the two states (1.16) which have no well-defined parity provide through (3.5) the first-order correction to the energy

$$E^{(1)} = \pm 3e\mathcal{E}a_0. \quad (3.11)$$

More generally, for any $|n_1 n_2 m\rangle$, the correction is

$$E^{(1)} = \frac{3}{2} e\mathcal{E}n(n_1 - n_2)a_0. \quad (3.12)$$

Comparison with (1.12) shows that it is the value of A_z in the parabolic states that determines the linear Stark correction according to the prescription $z \mapsto \frac{3}{2}n(a_0/\hbar)A_z$.

A linear response to an external electric field being characteristic of an electric dipole $\mathbf{d} (= -e\mathbf{r})$, the energy being correspondingly $-\mathbf{d}\cdot\boldsymbol{\mathcal{E}}$, the linear Stark effect may be alternatively interpreted as the corresponding atomic state having a dipole moment, of value $-3ea_0$ in the case of $\text{H}(n = 2)$. Such a dipole exerts a $1/r^2$ potential for an electron in the vicinity and is responsible for dipole-bound doubly-excited states of the negative ion H^- (Section 5.2.2).

For all other atoms, as also for the ground state of hydrogen, the first-order correction (3.5) vanishes and we have to proceed to the second-order (3.7) to see the first non-trivial response to an external electric

field. This correction being proportional to \mathcal{E}^2 , this response is termed the quadratic Stark effect. The matrix elements involved in (3.7) are of z between the state $|n\rangle$ of interest and other states $|m\rangle$ appearing as intermediate states in the summation. Clearly these are states opposite in parity to that of $|n\rangle$. Indeed, the matrix elements being the same as those in (2.16) which appear in a different context, the same rules single out for the intermediate states $|m\rangle$ only those that satisfy an analogous selection rule to (2.24). For the ground state of hydrogen, these are all the p states with azimuthal quantum number $m = 0$. This still leaves an infinite sum over all $n \geq 2$ in (3.7):

$$\begin{aligned}
 E_0^{(2)} &= -\frac{1}{2} \alpha_D \mathcal{E}^2, \\
 \alpha_D &\equiv 2 \sum_{np} \frac{\langle 0|ez|np\rangle \langle np|ez|0\rangle}{E_n^{(0)} - E_0^{(0)}}.
 \end{aligned}
 \tag{3.13}$$

The above result has been cast in a standard fashion that exhibits immediately that the second-order energy is negative (as always for the ground state for any perturbation), each term in the sum explicitly positive, and that it depends on a single parameter α_D which is evaluated in terms of zeroth-order atomic eigenstates and energies. This parameter, with dimensions of volume, is the static dipole polarizability ((2.15) with $\omega = 0$) of the atom (more precisely, of its ground state). The factors of 2 included in the definition stem from the alternative interpretation as an induced effect, the atom's ground state itself having no permanent electric dipole moment (being spherically symmetric) but the external field \mathcal{E} inducing a polarization of the electron distribution which then couples back to \mathcal{E} (hence, according to Lenz's law, always a negative energy).

Explicit evaluation of α_D still requires an infinite sum even when the matrix elements can be computed analytically, as they can be with hydrogenic eigenstates. Note the "sum" includes integration over the continuum p wave functions. However, with little effort, upper and lower bounds on its value can be set straightforwardly. Thus, since every term is positive, retaining only a few lowest, such as just $n = 2$ say, gives a lower bound to α_D . In hydrogen, a simple calculation (Problem 2.3) gives $\alpha_D > 2.96 a_0^3$. On the other hand, replacing $E_n^{(0)}$ in the denominator of (3.13) by $E_2^{(0)}$ for which the energy denominator has its lowest value gives an upper bound, the numerator and sum then collapsing under closure (for this purpose, the sum has first to be extended from np to all n states of hydrogen which is readily done, all these others having zero matrix elements anyway, before closure over the complete set of states

of hydrogen can be applied) to leave behind a single matrix element $\langle 0|e^2 z^2|0\rangle$. And this number is easily computed, being $(e^2/3)\langle 0|r^2|0\rangle$ because of the ground state's spherical symmetry, and $\langle 0|r^2|0\rangle = 3a_0^2$ from (1.10). Thus $\alpha_D \leq \frac{16}{3}a_0^3$. The exact value of α_D for hydrogen is $\frac{9}{2}a_0^3$, a value that itself can be obtained without too much difficulty by converting the infinite summation into solving instead an inhomogeneous Schrödinger equation.

The calculation of the second-order Stark energy for any other atom besides hydrogen is, of course, more tedious and difficult but the form of the correction is still as in (3.13). As discussed in Chapter 1, atomic states are characterized by other conserved quantum numbers such as S, L, J , and M of angular momentum, and the coefficient α_D will, in general, depend on them. The dependence on M can be anticipated to involve only even powers because of general considerations of time reversal. Under this reversal, the coupling (3.1) to an electric field is unchanged whereas a state of some M is mapped into its analog with $-M$. Such states have, therefore, to remain degenerate in any electric field. This is called the Kramers degeneracy and is removed only by an external magnetic field as we will see in Section 3.2.4; magnetic fields break time-reversal invariance, depending as they do on electric currents which carry a time sense unlike electric charges and fields.

2.4 The Zeeman effect

As exhibited in (3.2), an external magnetic field \mathbf{B} couples both linearly and quadratically to the electrons in an atom. The first has been observed and studied since the days of the earliest spectroscopists like Zeeman, and his name is now attached to both as linear and quadratic Zeeman effects. In terms of the atomic unit of magnetic field, 2.35×10^5 T, even a 1 Tesla field that is otherwise hefty in most laboratory and astrophysical contexts is puny in comparison. As an estimate, for low lying atomic states of radial extent of approximately a_0 and angular momentum \hbar , $(e\hbar B/2\mu c) \approx 5 \times 10^{-5}$ eV and $(e^2 B^2 a_0^2/8\mu c^2) \approx 5 \times 10^{-11}$ eV for a 1 T field. While the former is accessible, the quadratic term lies far out of reach of ordinary spectroscopic precision. However, being quadratic both in B and the radius of the orbit, it grows rapidly when these quantities are larger, becoming very important for highly excited states or in the very high fields of magnetic white dwarf and neutron stars. In such contexts, not only can the quadratic term overwhelm the linear but even cease to being a small perturbation. Such “non-perturbative” effects are of considerable interest and will be the study of Chapter 4 but in this section we restrict ourselves to the linear Zeeman effect.

The perturbative Hamiltonian, $H' = (e/2\mu c) \mathbf{B} \cdot \boldsymbol{\ell}$, involves only the angular momentum of the electron and is independent of the radial aspects or the principal quantum number n . Hence, unlike the quadratic coupling which does depend on radius and n , the linear Zeeman effect is common to all members of a Rydberg series of atomic states. At this point, we need to incorporate also the electron's spin \mathbf{s} , because the magnetic moment due to spin also couples to \mathbf{B} at the same level, indeed as $(e/\mu c) \mathbf{B} \cdot \mathbf{s}$. Spin is intrinsically a relativistic phenomenon, arising first in the description of the electron through the Dirac equation. Other relativistic perturbations due to it, such as spin-orbit coupling, will be considered in Section 3.3 but here we treat only its magnetic moment. A second aspect, also relativistic and naturally incorporated into the Dirac equation, is that spin couples to a magnetic field with an additional factor of 2 relative to orbital angular momenta. In all, the perturbation is

$$H' = (e/2\mu c) \mathbf{B} \cdot (\boldsymbol{\ell} + 2\mathbf{s}) ,$$

or equivalently, in a many-electron atomic state $^{2S+1}L_J$:

$$\begin{aligned} H' &= (e/2\mu c) \mathbf{B} \cdot (\mathbf{L} + 2\mathbf{S}) \\ &= (e/2\mu c) \mathbf{B} \cdot (\mathbf{J} + \mathbf{S}) . \end{aligned} \quad (3.14)$$

Choosing the direction of the magnetic field as the z -axis of quantization, the interaction in (3.14) involves only the azimuthal projections of angular momenta so that the first-order correction to the energy as given by (3.5) is easily evaluated. The choice in (3.14) between the $|M_L M_S\rangle$ or $|M_J\rangle$ representation of the atomic states depends on the relative magnitudes of the linear Zeeman and spin-orbit splitting energies. In light atoms or excited states of heavy atoms, spin-orbit energies are smaller, particularly for reasonable field strengths B , and the $|M_L M_S\rangle$ representation is appropriate. In such situations, the first-order energy correction follows immediately from (3.14):

$$E^{(1)} = (e\hbar B/2\mu c)(M_L + 2M_S). \quad (3.15)$$

This result, sometimes called the Paschen-Back effect, lifts the degeneracy of the manifold of $(2L + 1)(2S + 1)$ states $|M_L M_S\rangle$ which in the absence of the magnetic field have the same energy. Note that even though we are dealing with a degenerate manifold, we do not formally need degenerate perturbation theory but can apply (3.5) to each individual state $|M_L M_S\rangle$ because the first interaction in (3.14) is diagonal in this basis. The degeneracy is not completely lifted; for example, if

$M_S = \pm \frac{1}{2}$, then the states $|M_L - 1, \frac{1}{2}\rangle$ and $|M_L + 1, -\frac{1}{2}\rangle$ have the same perturbed energy (3.15).

In heavier atoms or weaker magnetic fields, if the spin-orbit energy is relatively larger than the magnetic, the appropriate states are characterized by M_J , or more completely by $|LSJM_J\rangle$, and the second of (3.14) is the operator of choice to evaluate (3.5). For this purpose, the operator \mathbf{S} is itself cast first in terms of \mathbf{J} for such a manifold through the identity

$$\mathbf{S} = \left(\mathbf{S} \cdot \mathbf{J} / J^2 \right) \mathbf{J},$$

both $\mathbf{S} \cdot \mathbf{J}$ and J^2 being diagonal in this basis. Indeed, upon squaring $\mathbf{L} = \mathbf{J} - \mathbf{S}$, we have

$$\begin{aligned} \left\langle LSJM_J \left| \frac{\mathbf{S} \cdot \mathbf{J}}{J^2} \right| LSJM_J \right\rangle &= \left\langle LSJM_J \left| \frac{J^2 + S^2 - L^2}{2J^2} \right| LSJM_J \right\rangle \\ &= \frac{J(J+1) + S(S+1) - L(L+1)}{2J(J+1)} \end{aligned} \quad (3.16)$$

so that (3.14) in (3.5) gives the linear Zeeman energy

$$E^{(1)} = (e\hbar B / 2\mu c) g M_J, \quad (3.17)$$

with

$$g = 1 + \frac{J(J+1) + S(S+1) - L(L+1)}{2J(J+1)}. \quad (3.18)$$

The ‘‘Landé g -factor’’ in (3.18) reduces to unity for pure orbital angular momentum ($S = 0, J = L$) and the Dirac value of 2 for pure spin ($L = 0, J = S$), generally taking values in between these two limits. The degeneracy is completely lifted, the $(2J + 1)$ degenerate $^{2S+1}L_J$ states in the absence of B getting individually distinct energies (3.17).

For $J = 1$, $E^{(1)}$ in (3.17) is a triplet of energies as in the first observations by Zeeman. Observation of spectral lines involves, of course, differences in energy of initial and final states, needing consideration of the splitting according to (3.17) of both, together with the electric-dipole selection rules, $\Delta M_J = 0, \pm 1$, as in Section 2.2.3. Fig. 3.5 gives an example. Observed perpendicular to the magnetic field, three spectral lines are seen, all linearly polarized, whereas for observations along the field, the line at the undisplaced energy is missing, the other two symmetrically on either side seen as left and right circularly polarized.

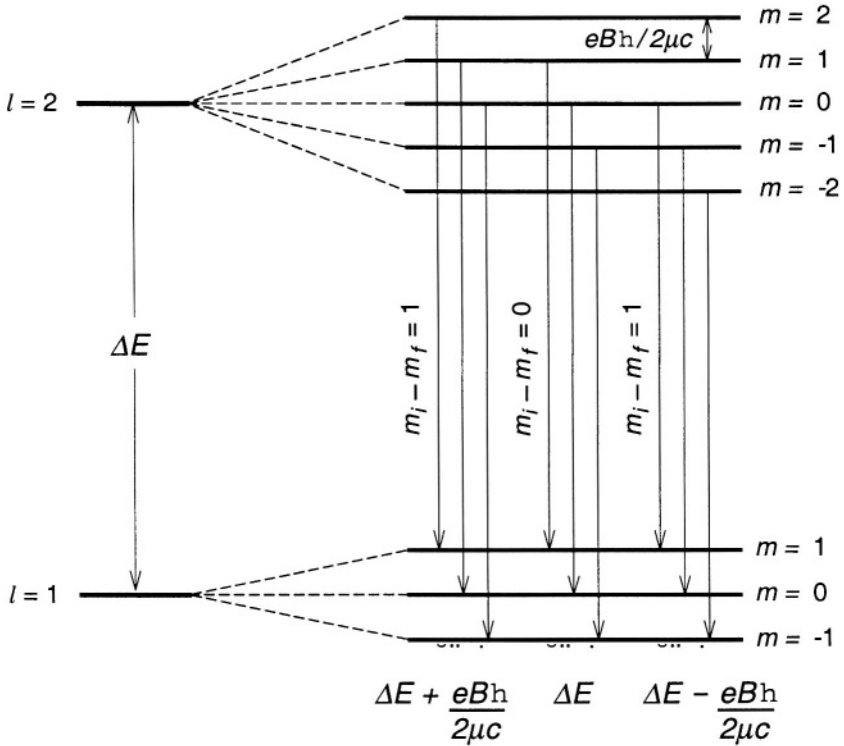


Figure 3.5. Zeeman effect in a $l = 2$ to $l = 1$ transition, showing a “normal” triplet of transition energies. From S. Gasiorowicz, *Quantum Physics* (John Wiley, New York, 1996), with permission of John Wiley and Sons, Inc.

In such a case, where a triplet of lines is seen in a magnetic field, one says we have the normal Zeeman effect, contrasting with the term “anomalous Zeeman effect” when the multiplicity is different. These terms are historical, before azimuthal quantum numbers were used, and are now rightly fading, all unified by the single expression (3.17) and differing only in the values of S, L , and J . Indeed, it was in the understanding of the Zeeman effect that the azimuthal quantum numbers were introduced and their role appreciated in quantum physics. In frequency units (cm^{-1}), the term representing the Zeeman splitting, $(eB/4\pi mc)$, has the value $4.66 \times 10^{-5} (B/\text{Gauss})$ or equivalently $\Delta\lambda = \lambda^2 (4.66 \times 10^{-5} B)$.

Solar magnetic fields in sunspots, and fields on many G, K, and M stars have values typically 1–3 kGauss so that unresolved Zeeman split-

tings are seen as broadening of spectral lines, the Zeeman widths being comparable to widths due to other causes. Often one compares widths of two lines of different Zeeman sensitivities to make this identification, a canonical example being lines of Fe I, the one at 617.33 nm and width 5 nm being sensitive while the one at 624.07 nm and width 4 nm relatively insensitive to the Zeeman perturbation.

3. Internal Perturbations in an Atom

Our treatment so far has been non-relativistic, which is adequate for most purposes of laboratory and astrophysical study of atoms and molecules. However, in this section, we will consider some of the basic relativistic corrections arising from the motion of the electrons. Recall from Section 1.2.1 that the velocity in the first Bohr orbit is $(Z / 137)c$, so that inner shell electrons in a heavy atom may be expected to have appreciable relativistic corrections. However, in so far as these are still small in comparison with the basic non-relativistic energy, perturbation theory applies and we will, in this section, so consider some of the dominant relativistic perturbations of atomic energy levels.

3.1 Relativistic mass correction

The kinetic energy is the obvious place to start, the non-relativistic expression $(\mathbf{p}^2/2\mu)$ being an approximation to the energy-momentum relation of Special Relativity, $(c^2 \mathbf{p}^2 + \mu^2 c^4)^{1/2} - \mu c^2$. Dirac showed the proper way, through spinors, to handle the square-root operator and thereby the complete relativistic treatment of the electron. In this section, however, in the spirit of perturbation theory, we will only view the next term beyond the non-relativistic kinetic energy in the binomial expansion of the square-root, namely,

$$H' = -\mathbf{p}^4/(8\mu^3 c^2). \quad (3.19)$$

Direct evaluation of the first-order energy correction (3.5) with such an operator is fraught with difficulty because of the high degree of singularity of a fourth-order derivative but again, in the spirit of perturbation theory, we rewrite (3.19) in terms of non-relativistic operators as $H' = \left(-\frac{1}{2}\mu c^2\right) (\mathbf{p}^2/2\mu)^2 = -\left(E_n^{(0)} + Ze^2/r\right)^2$. Subsequent evaluation of (3.5) is straightforward through the expectation values listed in (1.10) for hydrogenic states to give

$$E_{n\ell}^{(1)} = -\left(Z^4 e^4 / 2\mu c^2 a_0^2 n^3\right) \left(\frac{1}{\ell + \frac{1}{2}} - \frac{3}{4n}\right). \quad (3.20)$$

The negative sign of the energy correction, as already in the operator in (3.19), and its implication of weakening the binding of all energy levels, is physically plausible because the relativistic effect increases the mass and thereby raises the kinetic energy. The correction depends on both n and ℓ , again as expected, any dependence on other than $1/r$ such as the $1/r^2$ here destroying ℓ -degeneracy. The scaling with Z as the fourth power is shared with other relativistic effects to be studied below and signifies the growing importance of these effects in heavier atoms. Aside from these Z and n dependences, the order of magnitude of the correction is $(e^2/2a_0) [(e^2/2a_0) / \mu c^2] \approx 6 \times 10^{-4}$ eV.

3.2 Spin-orbit coupling

The coupling between the magnetic moments arising from the spin and the orbital motions of the electron also gets naturally incorporated into the Dirac equation and can then be exhibited by a non-relativistic expansion but we consider here a simpler argument from non-relativistic physics that suffices. As in Section 3.2.4, the spin magnetic moment has energy $-(e/\mu c) \mathbf{s} \cdot \mathbf{B}$ (note the Dirac g -factor of 2) but the magnetic field now is not external but that due to the orbital motion of the bound electron itself. This is given by a standard expression of classical electrodynamics

$$\mathbf{B} = -\mathbf{v} \times \mathcal{E}/c = (1/ec) \mathbf{v} \times \nabla V = (-1/e\mu c) \frac{1}{r} \frac{dV}{dr} \boldsymbol{\ell}. \quad (3.21)$$

The spin-orbit perturbation is thereby (the so-called Thomas factor provides an additional factor of $\frac{1}{2}$),

$$\begin{aligned} H' &= \frac{1}{2\mu^2 c^2} \frac{1}{r} \frac{dV}{dr} \mathbf{s} \cdot \boldsymbol{\ell} \\ &= \frac{Ze^2}{2\mu^2 c^2} \frac{1}{r^3} \mathbf{s} \cdot \boldsymbol{\ell}. \end{aligned} \quad (3.22)$$

With $\mathbf{s} \cdot \boldsymbol{\ell}$ evaluated from $\mathbf{j}^2 = (\mathbf{s} + \boldsymbol{\ell})^2 = \mathbf{s}^2 + \boldsymbol{\ell}^2 + 2\mathbf{s} \cdot \boldsymbol{\ell}$ as $\frac{1}{2} [j(j+1) - \ell(\ell+1) - \frac{3}{4}]$ and the expectation value of $1/r^3$ from (1.10), we obtain $E_{n\ell}^{(1)}$ for the spin-orbit correction. There is, of course, no contribution for s states which have no orbital angular momentum but another relativistic correction, called the Darwin term, affects only the s states by precisely the same amount as given formally by the above. In all, upon adding to the mass correction in (3.20), we have the relativistic contribution

$$E_{n\ell}^{(1)} = -\frac{Z^4(e^2/\hbar c)^2}{n^2} \left(\frac{e^2}{a_0}\right) \left[\frac{1}{j+1/2} - \frac{3}{4n}\right]. \quad (3.23)$$

Note that this correction depends only on n and j , so that the energy levels still retain some degeneracy (for example, $2s$ and $2p$ states with $j = \frac{1}{2}$), a result also true for exact solutions of the relativistic Dirac equation. Only field theoretic (QED) terms such as the Lamb shift remove this degeneracy finally.

The occurrence of highly stripped ions of elements such as iron in a variety of astrophysical objects makes relativistic calculations important in precision work. As examples, Ne-like Fe^{16+} (Fe XVII) produces the brightest x-rays from the solar corona and chromosphere and the 530.3 nm green coronal line from Fe^{12+} (Fe XIII) is one of the most intense seen. Oscillator strengths for E1 transitions in Ar^{14+} (Ar XV) and Fe^{22+} (Fe XXIII) are enhanced by 6 and 18% respectively, as a result of the mass and Darwin relativistic perturbations. The $2s2p\ ^3P_1 \rightarrow 2s^2\ ^1S_0$ in Be-like ions has a rapid increase in rate from 86 in C^{2+} to 2000 in O^{4+} , 7×10^6 in Ca^{16+} , and 5×10^7 in Fe^{22+} , the scaling with a power Z^8 characteristic of relativistic effects. M1 decays provide another instance of relativistic effects, the $2\ ^3S_1$ state's decay in He-like ions from C^{4+} (C V) through O^{7+} (O VIII), Ne^{8+} (Ne IX), Mg^{10+} (Mg XI) to Fe^{24+} (Fe XXV) seen in the solar spectrum providing an example, the last mentioned with a 5 ns lifetime.

3.3 Other corrections

The two sub-sections above have considered the dominant relativistic corrections to atomic energy levels and, as noted, are included exactly at the level of the Dirac equation. Corrections that arise beyond this level, from field theoretic effects of quantum electrodynamics, such as the Lamb shift and vacuum polarization, are of little relevance to astronomy. In today's high precision laboratory spectroscopy, however, they have been of considerable interest, much effort being expended on both experimental and theoretical studies in one- and two-electron atoms of high Z [22]. Apart from taking this note of them because of their importance, particularly for verifying quantum electrodynamics to increasingly high accuracy, they lie beyond the scope of this book.

We end this section and chapter with one more correction which, while not relativistic in origin, shares some of the same features and enters at the same numerical level and therefore goes hand-in-hand with the study of relativistic perturbations. This is the effect of the finite size of the nucleus, that it is not a point charge but rather an extended distribution, whether in a proton or a heavier nucleus. Details of how the positive

charge Ze is distributed over the radius $R = R_0 A^{1/3}$ of a nucleus (Z, A) continue to be explored in nuclear physics but, as an illustration of perturbative effects on atomic energies, we consider two simple models, one in which all the charge resides on the shell at radius R and another in which it is uniformly distributed over the volume contained within R . In either case, it is only for $r > R$ that the Coulomb potential energy of the electron is the $-Ze^2/r$ that we have considered in the non-relativistic Hamiltonian. For $r \leq R$, however, the potential is $-Ze^2/R$ in the first model and $-(Ze^2/R) \left(\frac{3}{2} - \frac{1}{2} \frac{r^2}{R^2} \right)$ in the second model. Therefore, the perturbation Hamiltonian H' , which is confined to $r \leq R$, is the difference of these values from $-Ze^2/r$. The nuclear radius R being very small ($R_0 \approx 1.2 \times 10^{-13}$ cm) on the atomic scale, only $\ell = 0$ or s states are affected by these perturbations since, according to (1.9), only their wave functions are finite near the nucleus. Further, over the range $r \leq R$, (1.9) reduces essentially to the normalization factor $N_{n\ell}$ so that the matrix element in (3.5) is easily evaluated. We have finally

$$E_{n0}^{(1)} = k \left(Z^4/n^3 \right) \left(e^2/2a_0 \right) (R/a_0)^2, \quad (3.24)$$

the constant k taking on values $4/3$ and $4/5$ for the first and second models, respectively. For hydrogen in the ground state, the correction (3.24) is, approximately, 5×10^{-9} eV. Note the scaling with Z as the fourth power as in previous sub-sections considered above, the $(Z^3/n^3 a_0^3)$ reflecting the squared normalization N_{n0}^2 of s -states that was noted in Section 1.2.1.

Problems

- 3.1 Evaluate the ground state energy shift in the hydrogen atom due to the second term in (3.3) for a 100 T field.
Which $|n\ell m\rangle$ states are mixed into the ground state $|100\rangle$ in first order due to this diamagnetic perturbation?
- 3.2 Derive (3.5) – (3.7) including the value for $c_{nn}^{(1)}$.
- 3.3 Starting with $E_n^{(3)}$, write down the diagrams describing the fourth-order perturbation $E_n^{(4)}$, and translate them into algebraic expressions.
- 3.4 Calculate the $n = 2$ contribution to α_D in (3.13) for the hydrogen atom.

- 3.5** Establish as stated in Section 3.2.3 that the exact α_D for hydrogen can be calculated by solving an inhomogeneous Schrödinger equation, $(H_0 - E_0)|\phi\rangle = ez|\psi_0^{(0)}\rangle$ and then computing the matrix element $\langle\psi_0^{(0)}|ez|\phi\rangle$.
- 3.6** Calculate the linear Zeeman splittings of the ${}^2P_{\frac{3}{2}, \frac{1}{2}}$ states of the first excited state of the sodium atom in a 0.1 T magnetic field.
- 3.7** Establish (3.20) as per the procedure sketched in the text.
- 3.8** Estimate the spin-orbit splitting of the $2p$ state of the hydrogen atom. In a 0.1 T magnetic field, what are the Zeeman splittings of these states?
- 3.9** Derive the form of the perturbing potential due to the finite size of the nucleus, assuming a uniform distribution of charge over the spherical volume. Calculate the resulting energy correction to the ground state of the hydrogen atom.
- 3.10** A beam of nitrogen atoms in the ground state splits into four components in a Stern-Gerlach magnetic field, and the magnetic moment is measured to be 2.8×10^{-10} erg/Gauss. Calculate the gyromagnetic ratio. Is the magnetic moment due to orbital or spin currents?

Chapter 4

ATOMS IN STRONG MAGNETIC FIELDS

1. Introduction

In Chapter 3, we considered the effect of weak fields, internal or external, on atomic structure. The zero field structure served as the starting point for a perturbation analysis, guiding our intuition regarding the effect of the added fields. In recent decades, strong and ultrastrong magnetic fields have been observed on astronomical objects, and strong field effects seen also with laboratory magnetic fields imposed on highly excited states. We turn to their study in this chapter, dealing with situations wherein the forces due to the external magnetic field are at least equivalent to, if not dominant over, the internal Coulomb forces in the atom. Qualitatively new phenomena and structures have been observed, calling for a change in our intuition based on laboratory atoms. Such a change of ground is provided by considering in place of motion around a nucleus the motion of a free electron in a magnetic field. This is where we will begin. Note first, as has already been discussed in Chapter 1, that the situation with electric fields is different because no matter what the field strength, the combined Coulomb and linear electric potential separates in parabolic coordinates, permitting at least in principle a complete solution. It is because the Coulomb plus diamagnetic potential does not so separate in any system of coordinates that strong magnetic fields pose a greater challenge. Just as perturbation theory discussed in the previous chapter proved relevant beyond atomic physics in all of physics, so too are the strong field phenomena discussed in this chapter likely to have broader and general applicability.

1.1 Free electrons in a magnetic field

The motion of a free charged particle in a uniform magnetic field is well-known classically and quantum mechanically. In the former, the charges may be regarded as “beads on a wire”, free to slide along the field lines (there being no force in this direction) but confined to “cyclotron orbits” in their transverse motion by the $(e/c)\mathbf{v} \times \mathbf{B}$ forces. In the quantum treatment, we introduce, as in Section 3.2.1, the magnetic field through the vector potential \mathbf{A} and minimal coupling to get the kinetic energy

$$T = (1/2\mu) (\mathbf{p} + e\mathbf{A}/c)^2 . \quad (4.1)$$

For a given field, say \mathbf{B} along the z -direction, different choices of \mathbf{A} are possible, subject only to $\mathbf{B} = \nabla \times \mathbf{A}$. Thus, one choice is

$$\mathbf{A} = (-By, 0, 0), \quad (4.2)$$

leading to the Schrödinger equation

$$H\psi = \left[(p_x - eBy/c)^2 / 2\mu + (p_y^2 + p_z^2) / 2\mu \right] \psi = E\psi . \quad (4.3)$$

With no explicit dependence of H on x and z , p_x and p_z are constants of the motion and the solution is of the form

$$\psi(x, y, z) = \exp[i(p_x x + p_z z) / \hbar] \chi(y) , \quad (4.4)$$

with

$$-\left(\hbar^2/2\mu\right) \chi'' + \left(\mu\omega_c^2/2\right) (y - y_0)^2 \chi = \left[E - p_z^2/2\mu\right] \chi, \quad (4.5)$$

where primes denote derivatives with respect to y and we have defined the cyclotron frequency

$$\omega_c \equiv (eB/\mu c) , \quad (4.6)$$

and

$$y_0 \equiv (cp_x/eB) . \quad (4.7)$$

The one-dimensional motion in y in (4.5), the only non-trivial part of the solution, is of a simple harmonic oscillator centered at y_0 and with frequency ω_c . The motion is quantized, so that the energy eigenvalues are

$$E_n = \left(n + \frac{1}{2} \right) \hbar \omega_c + \left(p_z^2 / 2\mu \right) , \quad (4.8)$$

with wave functions

$$\chi_n(y) = \left(\frac{2^n n! \hbar \sqrt{\pi}}{\mu \omega_c} \right)^{-\frac{1}{2}} \exp \left[-\frac{\mu \omega_c}{2\hbar} (y - y_0)^2 \right] H_n \left[\left(\frac{\mu \omega_c}{\hbar} \right)^{\frac{1}{2}} (y - y_0) \right], \quad (4.9)$$

where H_n are the Hermite Polynomials.

Note that p_x enters into (4.4) and (4.7) but not into the eigenvalues in (4.8). Therefore, each level with fixed n and p_z is infinitely degenerate. An understanding of this degeneracy is provided by looking at the classical picture of electrons circling around a field line. The center of this circle has coordinates $(x = 0, y = y_0)$. With the field \mathbf{B} pervading all space, field lines thread through the entire xy -plane and the electron's motion can be slid from one line to another without energy cost, accounting for the infinite degeneracy. For any finite region of space, however, the degeneracy is limited and we will return to this in Section 4.3.4.

An alternative, more symmetric choice for \mathbf{A} is

$$\mathbf{A} = (-By/2, Bx/2, 0), \quad (4.10)$$

which leads to

$$H\psi = (1/2\mu) \left[(p_x - eBy/2c)^2 + (p_y + eBx/2c)^2 + p_z^2 \right] \psi = E\psi. \quad (4.11)$$

Harmonic oscillator potentials now arise in both x and y ,

$$(e^2 B^2 / 8\mu c^2)(x^2 + y^2), \quad (4.12)$$

while the linear terms involve $(eB/2\mu)(p_x y - p_y x) = -(eB/2\mu c)\ell_z$. These coincide with (3.3) for the choice $\mathbf{A} = \frac{1}{2} \mathbf{B} \times \mathbf{r}$ to which this symmetric gauge is equivalent.

This symmetric, “cylindrical” gauge, with (4.11) separating in cylindrical coordinates, is the one of choice in most studies of atoms in magnetic fields. In these coordinates (ρ, z, φ) , we have as solutions of (4.11),

$$\psi = \left(e^{im\varphi} / (2\pi)^{1/2} \right) \exp(ip_z z / \hbar) L(\rho) \quad , \quad (4.13)$$

with

$$-\left(\frac{\hbar^2}{2\mu} \right) \left[L'' + (L'/\rho) - \left(m^2 L / \rho^2 \right) \right] + \left[\left(\frac{1}{8} \mu \omega_c^2 \rho \right) + \left(\frac{1}{2} \hbar \omega_c m \right) \right] L = \left(E - p_z^2 / 2\mu \right) L. \quad (4.14)$$

The resulting eigenvalues are

$$E = \left(n_\rho + \frac{m + |m|}{2} + \frac{1}{2} \right) \hbar \omega_c + \left(p_z^2 / 2\mu \right) \quad , \quad (4.15)$$

with normalized eigenfunctions

$$L(\rho) = \left[\hat{\rho}^{|m|+1} |m|! \right]^{-1} \left[2 \frac{(|m| + n_\rho)!}{n_\rho!} \right]^{1/2} e^{-\frac{\rho^2}{2\hat{\rho}^2}} \times \rho^{|m|} {}_1F_1 \left(-n_\rho, |m| + 1, \rho^2 / \hat{\rho}^2 \right) \quad , \quad (4.16)$$

where

$$\hat{\rho} \equiv (2\hbar / \mu \omega_c)^{1/2} = (2c\hbar / eB)^{1/2} \quad (4.17)$$

is the cyclotron radius and ${}_1F_1$ a confluent hypergeometric function. For a 1 T field, $\hat{\rho} \approx 1.2 \times 10^{-12}$ cm and $\omega_c = 1.8 \times 10^{11}$ s⁻¹.

Although differing in the quantum labels, $|n p_x p_z\rangle$ and $|n_\rho, m, p_z\rangle$ respectively, and seemingly different in appearance, the eigenvalues in (4.8) and (4.15) coincide as they should. The counterpart of the “hidden” infinite degeneracy in p_x in (4.8) is realized in (4.15) as an infinite degeneracy of $m = 0, -1, -2, \dots$. Such an equivalence of the final results is a manifestation of the gauge invariance of quantum mechanics with electromagnetic potentials. The two vector potentials differ by $\nabla \left(\frac{1}{2} B x y \right)$ and a corresponding unitary transformation, $\exp(-ieBxy/2\hbar)$, connects the alternative wave functions in (4.4) and (4.13).

The set of equally spaced levels in (4.8) or (4.15), with spacing $\hbar\omega_c$, constitutes the “Landau spectrum” for an electron in a uniform magnetic field. We have ignored spin so far but, as in Section 3.2.4, its main contribution through the magnetic moment’s coupling to \mathbf{B} is easily incorporated by adding $(eB/\mu c)s_z$ to (4.3) or (4.11), and a corresponding $\pm(\hbar\omega_c/2)$ to the energy in (4.8) or (4.15). For spin antiparallel to \mathbf{B} , this contribution exactly cancels the zero-point energy in (4.8) and (4.15), making the ground state energy exactly zero. Every other energy level has a degenerate pair with spin quantum numbers opposite. Such a spectrum is said to be “supersymmetric”, the result here hinging on the g -factor being exactly 2. Indeed, solutions of the Dirac equation for an electron in a magnetic field, which provide the fully relativistic quantum-mechanical treatment, also give the same energy spectrum [23].

Given the Landau level structure, free electrons in a magnetic field can absorb or emit radiation of frequency ω_c or its harmonics in making transitions between different Landau levels. This is cyclotron radiation, one of the probes for strong magnetic fields in astrophysics [24]. Detection of 53 keV x-ray lines from HZ Her, corresponding to a field of 5×10^8 T, was a pointer to the strongest magnetic fields ever observed, this one on a pulsar. If the electrons become relativistic, as in some astrophysical sources or in our accelerators, this radiation of frequency ω_c in their rest frame appears as high frequency “synchrotron light” to an outside observer.

2. Excited States in a Magnetic Field

2.1 Basic Hamiltonian and spectrum

We turn now to the hydrogen atom in a magnetic field in a regime where perturbation theory fails. First, Section 4.2 will consider the situation when neither Coulomb nor magnetic field dominates but both are on par, leading to novel structures and dynamics. Such a situation obtains for highly-excited Rydberg states in a magnetic field of laboratory strength, typically a few Tesla in most experiments to date. The Coulomb-Rydberg structure of the atom is subverted, replaced by a spectrum characteristic of the “strong mixing” of both fields. Section 4.3 will deal with extremely strong magnetic fields which modify atomic structure down to the very low and ground states, such fields only obtained in some astrophysical contexts (magnetic white dwarfs and neutron stars) or in some solid state analogs of the hydrogen atom (excitons and inversion layers). The regime when both fields are of equal importance is the most difficult and interesting one, calling for non-standard techniques for its analysis. Although the motion of an electron in either field alone

is well understood (Sections 1.2 and 4.1), their simultaneous presence leads to a non-separable problem of great complexity.

Even the separation of the center of mass motion for the nucleus and electrons is not as straightforward as in the case of $B = 0$. With 1 denoting the electron and 2 the proton, the equations of motion are

$$m_1 \ddot{\mathbf{r}}_1 = -e \dot{\mathbf{r}}_1 \times \mathbf{B}/c + \mathbf{F}_{12}, \quad m_2 \ddot{\mathbf{r}}_2 = e \dot{\mathbf{r}}_2 \times \mathbf{B}/c - \mathbf{F}_{12}, \quad (4.18)$$

where over-dots represent d/dt , and the particular form of the force between 1 and 2 is not of interest for this argument. Adding the two equations above, and defining as usual $\mathbf{R} = (m_1 \mathbf{r}_1 + m_2 \mathbf{r}_2)/(m_1 + m_2)$ and $\mathbf{r} = \mathbf{r}_1 - \mathbf{r}_2$, we have

$$(m_1 + m_2) \ddot{\mathbf{R}} = -(e/c) \dot{\mathbf{r}} \times \mathbf{B},$$

so that

$$(m_1 + m_2) \dot{\mathbf{R}} + (e/c) \mathbf{r} \times \mathbf{B} \quad (4.19)$$

is a conserved quantity. Note already that this conclusion rests on equal and opposite charges for 1 and 2, as in a neutral atom. Quantum mechanically, the corresponding operator,

$$\mathbf{P} = (\hbar/i) (\nabla_1 + \nabla_2) + (e/c) (\mathbf{A}(\mathbf{r}_1) - \mathbf{A}(\mathbf{r}_2)) + (e/c) \mathbf{r} \times \mathbf{B}, \quad (4.20)$$

commutes with the Hamiltonian of the hydrogen atom in a magnetic field:

$$H_{\text{tot}} = (\mathbf{p}_1 + e\mathbf{A}(\mathbf{r}_1)/c)^2/2m_1 + (\mathbf{p}_2 + e\mathbf{A}(\mathbf{r}_2)/c)^2/2m_2 - e^2/|\mathbf{r}_1 - \mathbf{r}_2|, \quad (4.21)$$

where, as before, we choose $\mathbf{A}(\mathbf{r}_i) = \frac{1}{2} \mathbf{B} \times \mathbf{r}_i$. The two-particle Schrödinger equation, $H_{\text{tot}} \psi(\mathbf{R}, \mathbf{r}) = E_{\text{tot}} \psi(\mathbf{R}, \mathbf{r})$, has a solution of the form

$$\psi(\mathbf{R}, \mathbf{r}) = \exp [(i/\hbar) (\mathbf{P} - e\mathbf{r} \times \mathbf{B}/2c) \cdot \mathbf{R}] \psi(\mathbf{r}), \quad (4.22)$$

with

$$\begin{aligned}
 H_{\text{tot}} = & \frac{\mathbf{P}^2}{2(m_1 + m_2)} + \frac{e}{2(m_1 + m_2)} (\mathbf{P} \times \mathbf{B}) \cdot \mathbf{r} + \frac{\mathbf{p}^2}{2\mu} \\
 & + \frac{e}{2c} \left(\frac{1}{m_1} - \frac{1}{m_2} \right) \mathbf{B} \cdot \boldsymbol{\ell} + \frac{e^2}{8\mu c^2} (\mathbf{r} \times \mathbf{B})^2 - \frac{e^2}{r}. \quad (4.23)
 \end{aligned}$$

As usual, \mathbf{p} and $\boldsymbol{\ell}$ are the linear and angular momentum, respectively, of a particle of reduced mass $\mu = m_1 m_2 / (m_1 + m_2)$.

The first term in (4.23) is the center of mass kinetic energy. The second term represents a residual coupling between the motions in \mathbf{R} and \mathbf{r} , interpreted as a motional Stark (electric) field seen in the reduced particle's motion by virtue of the velocity $\mathbf{P}/(m_1 + m_2)$ of the center of mass in the \mathbf{B} field. Only by neglecting this term can the motion in \mathbf{r} be considered separate, the justification resting on m_2 being large. We will indeed do so, although this additional electric field may sometimes be large (as on pulsars where B is large) and have conspicuous effects, making every problem of an atom in \mathbf{B} also one with a simultaneous perpendicular electric field. The fourth term in (4.23) indicates yet another subtlety in the separation of the center of mass, the $1/m_2$ causing a small correction to the linear Zeeman term. Once again, it is only upon dropping it that we have the linear and quadratic Zeeman terms as considered in Chapter 3 for the motion in \mathbf{r} [25]. With these approximations, we have finally

$$H\psi(\mathbf{r}) = \left[\mathbf{p}^2/2\mu + (e/2\mu c)\mathbf{B} \cdot \boldsymbol{\ell} + (e^2/8\mu c^2)(\mathbf{r} \times \mathbf{B})^2 - e^2/r \right] \psi = E\psi(\mathbf{r}). \quad (4.24)$$

The superposition of the B -independent terms, which are cylindrically symmetric, with the Coulomb term, which has spherical symmetry, renders (4.24) non-separable in any coordinate system. We will consider in Section 4.2.2 a partial separability upon restricting to a manifold of fixed n but it is the non-separability that makes for the complexity of the problem of an atom in a magnetic field and for some of the fascinating phenomena exhibited by this otherwise seemingly simple system. The linear Zeeman term is easily treated, being diagonal in m . Indeed, the entire Hamiltonian in (4.24) being azimuthally symmetric, the motion in φ can be trivially separated. Parity is also a good quantum number of this Hamiltonian. The non-trivial part, therefore, lies in the last two terms in H which entangle two coordinates and may be viewed in the alternative forms:

$$\begin{aligned} V(r, \theta) &= (e^2 B^2 / 8\mu c^2) r^2 \sin^2 \theta - e^2 / r, \\ V(\rho, z) &= (e^2 B^2 / 8\mu c^2) \rho^2 - e^2 / (\rho^2 + z^2)^{1/2}. \end{aligned} \quad (4.25)$$

When the diamagnetic and Coulomb terms are comparable, perturbation theory as in Chapter 3 fails and we face the full complexity of a non-separable quantum mechanical problem. They have comparable influence when

$$r \approx (8\mu c^2 / B^2)^{1/3} = 2a_0 (B_c / B)^{2/3}, \quad (4.26)$$

where $B_c = (\mu^2 e^3 c / \hbar^3) = 2.35 \times 10^5$ T is the unit of magnetic field defined previously. With $r \approx n^2 a_0$ in Coulomb systems, we have equivalently

$$n \approx \beta (B_c / B)^{1/3}, \quad (4.27)$$

with β a numerical constant of the order of unity, as an index of where strong mixing effects set in. For a reasonable laboratory field strength of 4.7 T, this n is, approximately, 45. It is only for quantum numbers around this value or larger that we can expect to see very non-perturbative effects on a Rydberg spectrum. The high resolutions and low pressures required to access such a spectral region kept such phenomena from being observed until recent decades.

Fig. 4.1 shows the spectrum of hydrogen in two-photon absorption from the ground state in a magnetic field of 6 T [26]. The experiment used two photons because lasers are not easily available to go directly from the ground state to such a region of the spectrum with a single photon. Beyond the energy corresponding to (4.27) and extending past the zero-field ionization energy of 13.6 eV, the spectrum is clearly dominated by equally-spaced, broad resonances. The spacing depends on the m value of the final state, $m = 0$ and 2 being dominated by a spacing of $\frac{3}{2}\hbar\omega_c$, while $m = 1$ by $(0.64)\hbar\omega_c$. Fig. 4.2(a) is an analogous spectrum, this time in ordinary single-photon spectroscopy of Sr [27], again showing a pattern of equally-spaced resonances with a spacing of $\frac{3}{2}\hbar\omega_c$. Historically, the Sr spectrum and similar spectra in other atoms were observed almost fifteen years before Fig. 4.1 in hydrogen because of experimental difficulties in working with atomic hydrogen. However, that all atoms display the same phenomenon of equally-spaced resonances in a magnetic field in the vicinity of the ionization threshold indicates involvement of electronic motion at large distances, the potential in such a

region being the same in all atoms as given in (4.25). The presence of a core region in non-hydrogenic atoms where the Rydberg electron experiences short-range interactions does not disrupt the basic phenomenon. The influence of the core can be taken into account through standard zero-field quantum defects (Section 4.2.5), these being unaffected by the diamagnetic potential which is entirely negligible at such small r .

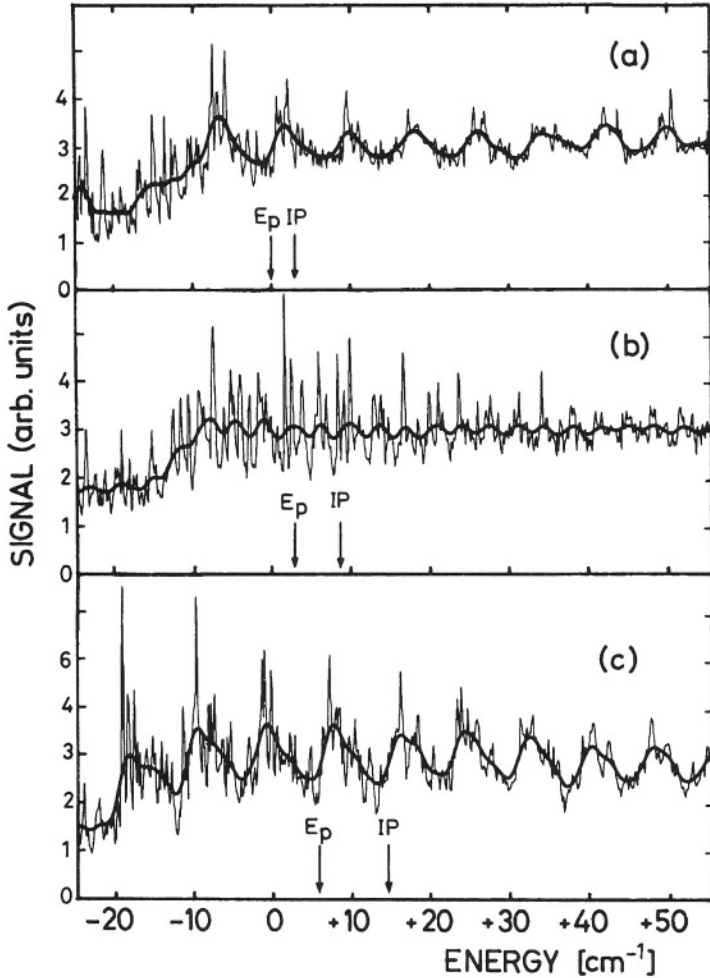


Figure 4.1. Two-photon excitation of even parity states of hydrogen around the ionization limit in a magnetic field of 6 T. (a) $m = 0$, (b) $m = 1$, (c) $m = 2$. Resolution $\approx 0.3 \text{ cm}^{-1}$. The heavy line is a Gaussian average with 2 cm^{-1} full-width at half-maximum. Note $1.5 \hbar \omega_c$ (a and c) and $0.64 \hbar \omega_c$ (b) modulations. From [26].

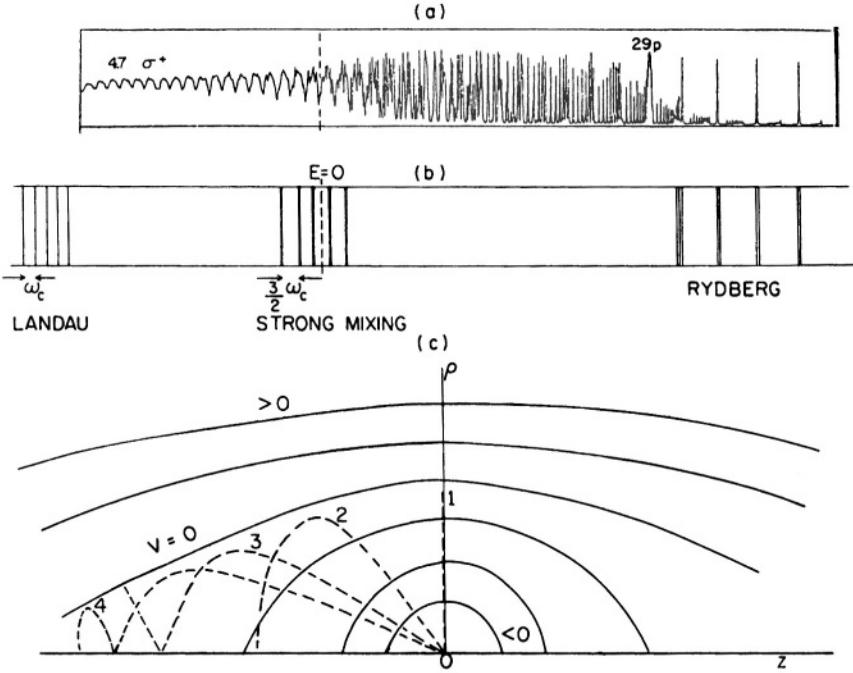


Figure 4.2. (a) Absorption spectrum of strontium with $m = 1$ polarization in a magnetic field of 4.7 T (from [27]). (b) Schematic drawing of (a) to emphasize three characteristic spectral regimes. (c) Equipotentials of the Coulomb plus diamagnetic potential in (4.25). Numbered paths correspond to different modes of quantization around $E = 0$.

Although at first sight reminiscent of the equally-spaced Landau levels in (4.8) and (4.15), that the resonance spacing depends on m and differs from $\hbar\omega_c$ indicates that the magnetic field does not dominate this phenomenon. Indeed, the primary spacing of $\frac{3}{2}\hbar\omega_c$ points to an interplay between the Coulomb and diamagnetic potentials as per the following simple scaling argument. The total energy E of, approximately, zero may be considered as the sum of Coulomb and diamagnetic energies:

$$0 \approx E = E_c + E_m. \quad (4.28)$$

The Coulomb energy E_c is, of course, the Bohr $-e^2/2a_0n^2$ whereas the diamagnetic energy, depending on r^2 , is proportional to n^4 . That the two are equal and opposite in (4.28) leads to the condition (4.27), and

to conform with it, we write $E_m = (e^2/2a_0)(B/\beta^3 B_c)^2 n^4$. The spacing between successive states can then be written as

$$\frac{\delta E}{\delta n} = \frac{\delta E_c}{\delta n} + \frac{\delta E_m}{\delta n} = \frac{e^2}{a_0 n^3} + \frac{2e^2}{a_0 \beta^6} \left(\frac{B}{B_c}\right)^2 n^3. \quad (4.29)$$

Using (4.27) to eliminate n^3 , we get

$$\frac{\delta E}{\delta n} = \frac{3e^2}{2a_0} \frac{B}{B_c} \beta^{-3} = \frac{3}{2} \hbar \omega_c \beta^{-3}, \quad (4.30)$$

the $\frac{3}{2}$ arising from Coulomb and diamagnetic contributions in the ratio 1:2.

The above argument does not fix the value of β although one can plausibly argue for $\beta = 1$ so that with magnetic field alone, (4.29) and (4.30) would give the expected Landau spacing, $\delta E/\delta n = \hbar \omega_c$, but it suffices to show that the $(3/2) \hbar \omega_c$ resonances near the ionization limit are associated with strong mixing of both Coulomb and diamagnetic fields on a roughly equal footing. Neither field may itself be strong and, indeed, for any value of B , however small, there will always be a region around $E = 0$ with an n given by (4.27) where such an equally-spaced resonance spectrum will be seen. Ordinary perturbation theory fails, neither field being weaker than the other but, remarkably, the experimental evidence as in Figs. 4.1 and 4.2 is that this region also has a characteristic spectrum of its own, different from either the Rydberg or the Landau spectrum, when one or the other field dominates. Other examples are now known, including that of a strong mixing of Coulomb and electric fields, showing that such strong-mixing phenomena are quite general in physics.

2.2 Degenerate perturbation theory in an n -manifold

The basic problem is that for the Hamiltonian in (4.24), the only conserved quantum numbers are m and parity, and the Schrödinger equation is non-separable in the two coordinates in (4.25). Were we to start with the hydrogenic states as a basis, the diamagnetic $r^2 \sin^2 \theta$ interaction mixes all states of n and ℓ with the same m and parity. For values of n smaller than that given by (4.27), when the diamagnetic energy is smaller than the spacing between successive Rydberg levels, the problem is at least immediately tractable as a mixing of all the degenerate (in ℓ) states of a given n by the diamagnetic interaction. We consider this “ ℓ -mixing” region first as an application of degenerate perturbation

theory with a finite number of states. Since ℓ is restricted to the values $|m| \leq \ell = n - 1$, that is, at most to $\frac{1}{2}(n - |m|)$ states of the same parity (either all ℓ odd or even), one needs to diagonalize $(e^2 B^2 / 8\mu c^2) r^2 \sin^2 \theta$ among this set.

The $\sin^2 \theta$ structure causes non-zero matrix elements between hydrogenic states of just two types, ones diagonal in ℓ and the others connecting states with $\Delta \ell = \pm 2$. Together with the radial matrix elements of r^2 from (1.10) between the hydrogenic wave functions (1.9), we have

$$\begin{aligned}
 V_\ell &= \langle n\ell m | \frac{1}{2} r^2 \sin^2 \theta | n\ell m \rangle \\
 &= \frac{n^4}{2} a_0^2 \left[1 + \frac{1}{2n^2} + \frac{3}{2} \left\{ 1 - \frac{\ell(\ell+1)}{n^2} \right\} \right] \frac{1}{2} \left[\frac{m^2 - \frac{1}{4}}{\ell(\ell+1) - \frac{3}{4}} \right], \\
 W_\ell &= \langle n, \ell - 1, m | \frac{1}{2} r^2 \sin^2 \theta | n, \ell + 1, m \rangle \\
 &= \frac{5n^4}{2} a_0^2 \left[\left(1 - \frac{\ell^2}{n^2} \right) \left(1 - \frac{(\ell+1)^2}{n^2} \right) \right]^{1/2} \left(-\frac{1}{4} \right) \left[1 - \frac{1}{(2\ell+1)^2} \right] \\
 &\times \left[1 - \frac{1}{(\ell + \frac{1}{2})^2} \right]^{-1/2} \left(1 - \frac{m^2}{\ell^2} \right)^{1/2} \left(1 - \frac{m^2}{(\ell+1)^2} \right)^{1/2}. \quad (4.31)
 \end{aligned}$$

The resulting finite, tri-diagonal matrix can be diagonalized for any n to yield eigenvalues and eigenvectors, displayed in Figs. 4.3 and 4.4. In units of $n^4 a_0^2$, the eigenvalues range from 0 to 5/4, these being the limiting values as $n \rightarrow \infty$. In between, the value 1/4 marks a point of inflection which separates two classes of eigenstates. The eigenvalues between 0 to 1/4 rise linearly with an index N that labels the states, whereas the 1/4 to 5/4 region shows a $N(N+1)$ dependence. As a result, they are dubbed vibrator and rotor states, respectively. The former occur mostly for small values of $|m|$, and are absent for large $|m|$.

Plots of eigenvectors in Fig. 4.4 also point to differences between the two classes of states, the vibrators having dominant concentration of probability at $\theta \approx 0$ and 180° , that is, longitudinal to the magnetic field direction, whereas the rotors concentrate at $\theta \approx 90^\circ$ or perpendicular to \mathbf{B} . Each eigenvector acquires a certain amount of $\ell = 1$ character. Therefore, in photoexcitation from a ground state with $\ell = 0$ as shown in Fig. 4.2, each of these eigenvectors is seen as a spectral line, with intensity proportional to the squared amplitude of $\ell = 1$, in the ℓ -mixing region of such a figure.

An analytical treatment of the diagonalization casts further light on the nature of diamagnetic interaction in an n -manifold. The matrix

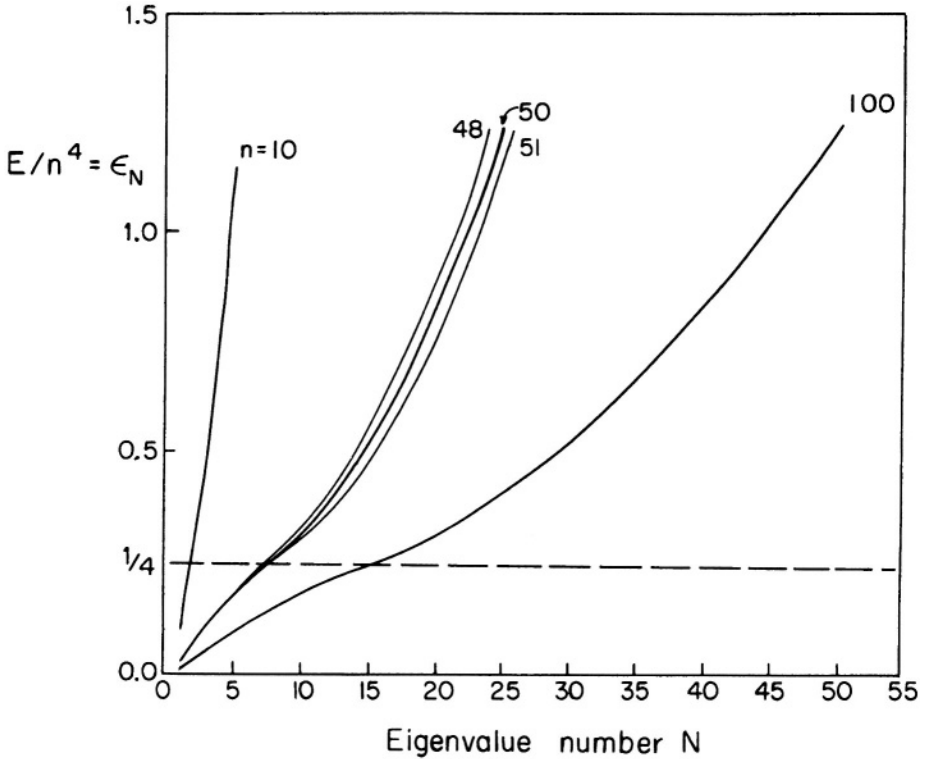


Figure 4.3. Eigenvalues of the diamagnetic energy matrix in (4.31) for $m = 0$ and even parity. The index N takes integer values but the eigenvalues are shown as continuous functions. Note the span $(0, 5/4)$, with a separatrix value at $1/4$ marking the transition from linear to quadratic dependence on N . From U. Fano, F. Robicheaux, and A. R. P. Rau, *Phys. Rev. A* **37**, 3655 (1988).

elements in (4.31) display the radial and angular contributions explicitly. The latter, given by factors on the right, converge rapidly to their limiting values of $\frac{1}{2}$ and $-\frac{1}{4}$ for $\ell = n - 1$, particularly for small m . Replacement of the angular factors by these values for all ℓ is, therefore, a good approximation. The radial factors, on the other hand, reduce to $(5n^4/4)$ in both V_ℓ and W_ℓ for $\ell \ll n$, whereas $V_\ell \approx \frac{1}{2}n^4$ for $\ell \rightarrow n - 1$ while W_ℓ is smaller by one power of n . With these reductions, eigenvalues $E_N = \varepsilon n^4$ and eigenvalues $a_\ell^{(N)}$ of the tri-diagonal matrix, which are determined by the linear algebraic system

$$W_{\ell-1} a_{\ell-2} + V_\ell a_\ell + W_{\ell+1} a_{\ell+2} = \varepsilon a_\ell, \quad (4.32)$$

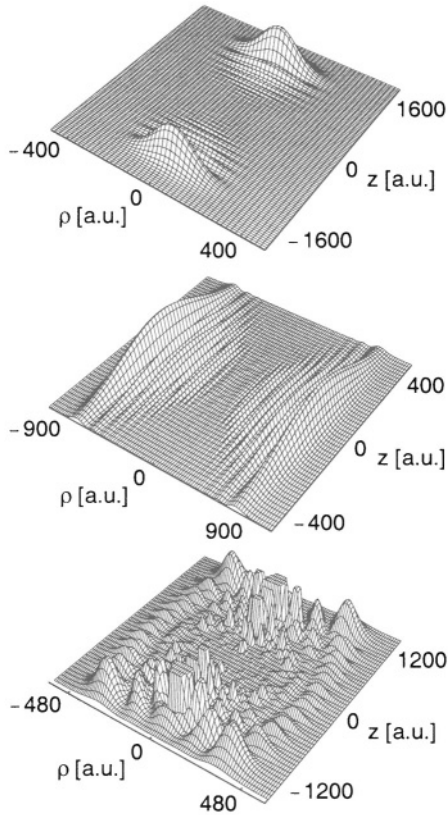


Figure 4.4. Probability distribution of $n = 20$ diamagnetic states of hydrogen with $m = 0$ and even parity in a 6 T magnetic field. The lowest state (top) is localized along the field direction and the highest state (middle) perpendicular to it. A non-localized state in the separatrix region is shown at the bottom. From C. Rangan, K. J. Schafer, and A. R. P. Rau, *Phys. Rev. A* **61**, 053410 (2001).

can be transformed [28] into an equivalent differential equation in $x \equiv (\ell + \frac{1}{2})/n$ regarded as a continuous variable with range $(0, 1)$:

$$(1 - x^2) a''(x) - 2x a'(x) + \left[\frac{4}{5} \varepsilon n^2 - \frac{1}{5} x^2 n^2 \right] a(x) = 0. \quad (4.33)$$

This is the equation for prolate spheroidal functions, with features combining those of both Legendre and Hermite differential equations. For large n , the eigenvalues are given by

$$\varepsilon_N = (\sqrt{5}/n)(N + \frac{1}{2}) , \quad N = 0, 1, 2, \dots \quad (4.34)$$

that is, equally spaced with spacing $(\sqrt{5}/n)$, just as observed for the vibrator states in Fig. 4.3. The lowest eigenvector is given by

$$a_\ell^{(N=0)} = (4/5n^2)^{1/4} (2\ell + 1)^{1/2} \exp \left[-\ell(\ell + 1)/2\sqrt{5}n \right] . \quad (4.35)$$

Note a characteristic shape of an initial rise at small ℓ due to the statistical weight factor $(2\ell + 1)^{1/2}$ but a Gaussian fall-off at large ℓ due to the second factor which reflects the oscillator-like potential in x^2 in (4.33). Such a mix of ℓ values due to the diamagnetic term implies a corresponding distribution of the wave function in the conjugate θ space,

$$\sum a_\ell P_\ell(\cos \theta) \propto \left\{ \exp \left(-\sqrt{5}n\theta^2/2 \right) + \exp \left[-\sqrt{5}n(\pi - \theta)^2/2 \right] \right\} , \quad (4.36)$$

a Gaussian distribution peaked at $\theta = 0$ and 180° as in Fig. 4.4 (top).

The highest eigenvalues and eigenvectors follow from a closely related analysis of a “conjugate” equation to (4.32) obtained by

$$a_\ell \rightarrow (-1)^{\ell/2} b_\ell . \quad (4.37)$$

This conjugation transformation (a local gauge transformation in which every alternate coefficient is multiplied by minus one) has the effect of switching the signs of $W_{\ell\pm 1}$ relative to V_ℓ and ε and gives instead of (4.33),

$$(1 - x^2) b''(x) - 2x b'(x) + \left[n^2 - \frac{4}{5} \varepsilon n^2 - \frac{4}{5} x^2 n^2 \right] b(x) = 0, \quad (4.38)$$

again a prolate spheroidal equation, differing from (4.33) only in some of the coefficients. The values of ε now descend from $\frac{5}{4}$ in equal oscillator-like steps:

$$\varepsilon = \frac{5}{4} - (\sqrt{5}/n)(K + \frac{1}{2}), \quad K = 0, 1, 2, \dots \quad (4.39)$$

The index K is related to N by $K = \frac{1}{2}n - N$. Thus, the rotor states of Fig. 4.3, which are rotor-like when viewed from $\varepsilon = 0$, are also vibrator-like when seen from the opposite limit of $\varepsilon = \frac{5}{4}$, descending in equal steps with twice the spacing of the low states in (4.34). The two classes of states are simply related by the conjugation transformation (4.37).

The highest eigenvector is given by

$$a_\ell = \left(2\pi/\sqrt{5}n^2\right)^{1/4} P_\ell(0) (2\ell + 1)^{1/2} \exp\left[-\ell(\ell + 1)/\sqrt{5}n\right], \quad (4.40)$$

with an obvious resemblance to (4.35), differing from it by alternating minus signs introduced through the $P_\ell(0)$ factor. Once again, the corresponding distribution in θ is

$$\sum a_\ell P_\ell(\cos\theta) \propto \exp\left[-\frac{\sqrt{5}}{4}n\left(\frac{1}{2}\pi - \theta\right)^2\right], \quad (4.41)$$

and coincides with Fig. 4.4 (middle), this time peaked at $\theta \approx 90^\circ$ with a Gaussian width proportional to $n^{-1/2}$. The highest states are seen, therefore, to gain in diamagnetic energy by peaking, or being localized, perpendicular to \mathbf{B} in the region of strongest diamagnetic potential. The lowest states by contrast localize parallel to \mathbf{B} and gain the least diamagnetic energy. The conjugation operation takes $\theta \rightarrow 90^\circ - \theta$, the off-diagonal W_ℓ changing sign whereas the diagonal V_ℓ remain unchanged according to our earlier observation that $\langle \ell | \sin^2\theta | \ell \rangle \approx \frac{1}{2}$ for all ℓ .

Because of the fall-off at high ℓ as shown in (4.35) and (4.40), both the lowest and highest eigenstates show a mix of ℓ values from 0 to a maximum that is proportional to \sqrt{n} . The very high ℓ values in the n -manifold, those between \sqrt{n} and $\ell = n - 1$, are not appreciably present in the vibrator and rotor states. Only a few states around the “separatrix” eigenvalue of $\frac{1}{4}$ contain such high angular momenta. Many of these features of the diamagnetic interaction in a Coulomb n -manifold such as characteristic localized states seem to be generic, common to strong mixing of degenerate manifolds by a second field.

The above analysis of an n -manifold within the basis of spherical $|n\ell\rangle$ states could be carried out alternatively in the parabolic $|n_1 n_2 m\rangle$ basis of Section 1.2.2. With the diamagnetic operator $\frac{1}{2}r^2 \sin^2\theta$ equal to $\frac{1}{2}\xi\eta$ in parabolic coordinates, the only non-zero matrix elements are

$$V_{n_1} = \left\langle n_1 n_2 m \left| \frac{1}{2}\xi\eta \right| n_1 n_2 m \right\rangle = \frac{1}{2}a_0^2(2n_1 + |m| + 1)(2n_2 + |m| + 1)n^2$$

$$\times \left[\frac{n}{4} (2n_1 + |m| + 1) \{n_2(n_2 + |m|) + (n_2 + 1)(n_2 + |m| + 1)\} + n_1 \leftrightarrow n_2 \right],$$

$$W_{n_1 + \frac{1}{2}} = \left\langle n_1 n_2 m \left| \frac{1}{2} \xi \eta \right| n_1 + 1, n_2 - 1, m \right\rangle$$

$$= -n^2 a_0^2 [(n_1 + 1)(n_1 + |m| + 1) n_2 (n_2 + |m| + 1)]^{1/2}, \quad (4.42)$$

where inside the square bracket in the first equation, the second term repeats the first with n_1 and n_2 interchanged. Once again, we have a tridiagonal matrix whose eigenvalues and eigenvectors reduce to the same results as before.

The parabolic analysis has the further advantage of relating to the group-theoretic symmetries discussed in Section 1.2.2. Thus, in addition to the action of the operators already recorded there, that is,

$$j_{1z} |n_1 n_2 m\rangle = \frac{1}{2} \hbar (m + n_1 - n_2) |n_1 n_2 m\rangle,$$

$$j_{2z} |n_1 n_2 m\rangle = \frac{1}{2} \hbar (m - n_1 + n_2) |n_1 n_2 m\rangle, \quad (4.43)$$

we have for $j_{1\pm} \equiv j_{1x} \pm i j_{1y}$,

$$j_{1+} |n_1 n_2 m\rangle = \hbar [n_2 (n_1 + |m| + 1)]^{1/2} |n_1 + 1, n_2, m\rangle,$$

$$j_{1-} |n_1 n_2 m\rangle = \hbar [(n_2 + 1)(n_1 + |m|)]^{1/2} |n_1 - 1, n_2, m\rangle, \quad (4.44)$$

$$j_{2+} |n_1 n_2 m\rangle = \hbar [n_1 (n_2 + |m| + 1)]^{1/2} |n_1, n_2 + 1, m\rangle,$$

$$j_{2-} |n_1 n_2 m\rangle = \hbar [(n_1 + 1)(n_2 + |m|)]^{1/2} |n_1, n_2 - 1, m\rangle.$$

Therefore, from the matrix elements in (4.42), we have a representation of the diamagnetic operator within an n -manifold:

$$\frac{1}{2} \xi \eta = \left(n^2 a_0^2 / 4 \right) \left[3n^2 + 1 - 4m^2 + (20j_{1z} j_{2z} - 8\mathbf{j}_1 \cdot \mathbf{j}_2) / \hbar^2 \right], \quad (4.45)$$

or alternatively, using (1.14),

$$\begin{aligned} \frac{1}{2} \xi \eta &= \left(n^2 a_0^2 / 4 \right) \left[n^2 + 3 + \left(L_z^2 + 4\mathbf{A}^2 - 5A_z^2 \right) / \hbar^2 \right] \\ &= (\hbar^2 / 4\mu) (-2E_n)^{-1} \left[(-2E_n)^{-1} + (3a_0/e^2) + (L_z^2 + \Lambda) / (\mu e^4) \right], \end{aligned} \quad (4.46)$$

where we have defined [29]

$$\Lambda = 4\mathbf{A}^2 - 5A_z^2. \quad (4.47)$$

Therefore, upon restricting to an n -manifold, the combined Coulomb and diamagnetic Hamiltonian permits simultaneous diagonalization of the operators $\{H, L_z, \Lambda\}$. A similar conclusion follows also from averaging the classical equations of motion of \mathbf{L} and \mathbf{A} in the Coulomb + magnetic field over one Kepler period, this averaging being the counterpart of the quantum treatment of a fixed n -manifold. Eigenvalues of Λ label, therefore, the eigenvectors that were denoted above by N and K . Since \mathbf{A}^2 ranges from 0 to $n^2 - m^2 - 1$ according to Section 1.2.2, Λ ranges from $m^2 + 1 - n^2$ when \mathbf{A} is along the z -axis to $4(n^2 - m^2 - 1)$ when \mathbf{A} lies in the xy -plane. Correspondingly, from (4.46), the eigenvalues of $(\rho^2/2n^4 a_0^2)$ range from 0 to 5/4 as discussed, negative values of Λ corresponding to vibrator and positive to rotor states. Fig. 4.5 shows that, geometrically, the tip of \mathbf{A} is confined to move on the hyperboloid defined by (4.47). The two classes of states resulting when \mathbf{A} and, therefore, the Keplerian ellipse (recall that the Laplace-Runge-Lenz vector is along the semimajor axis of this ellipse) lies primarily along or perpendicular to \mathbf{B} . The highest eigenvalues of diamagnetism with the lowest K in (4.39) have the highest Λ and most confinement to the plane perpendicular to \mathbf{B} . The value $\Lambda = 0$, with energy proportional to $\frac{1}{4}n^4$, is a sharp “separatrix” between the two classes of motion. For large $|m|$, the vibrator states with $\Lambda < 0$ are almost absent, \mathbf{L} being more nearly parallel to the z -axis so that the vector \mathbf{A} perpendicular to it is perforce more in the xy -plane.

The set $\{H, L_z, \Lambda\}$ is an alternative to the sets $\{H, L_z, L^2\}$ and $\{H, L_z, A_z\}$ of Section 1.2.2 for the field-free hydrogen atom. While those represented exact symmetries of the Coulomb problem, the spherical and parabolic, respectively, the triad $\{H, L_z, \Lambda\}$ is not an exact symmetry of the Coulomb + diamagnetic Hamiltonian, only approximate so long as one restricts to ℓ -mixing at a fixed n . An equivalent statement is that this symmetry pertains only for degenerate perturbation to order B^2 but not to higher order in powers of B^2 which would

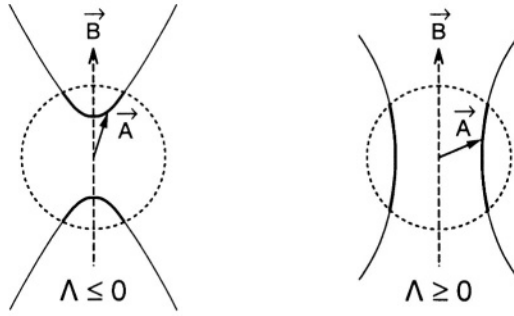


Figure 4.5. Alternative ranges of precession of the Laplace-Runge-Lenz vector about the direction of an external magnetic field. Hyperboloids with $\Lambda = \text{constant}$ in (4.47) define the ranges, the unit sphere representing the maximum length of \mathbf{A} for a fixed n . From J. C. Gay, *Comments At. Mol. Phys.* **13**, 275 (1983), with permission from Taylor and Francis Ltd.

introduce other n states as intermediates in expressions such as (3.7). The structure of $\tilde{\Lambda}$ in (4.47) also does not permit as compact a transformation of one basis to another as the field-free Coulomb problem enjoys in (1.15). However, a further approximation of taking instead the triad $\{H, L_z, \Lambda + A_z^2\}$ permits such a transformation. Particularly for the rotor states, where A_z is small, this further approximation has merit. In this picture, the set $\tilde{\Lambda} = \{A_x, A_y, L_z\}$ behaves like an angular momentum, O_3^λ , with invariants L_z and $\lambda(\lambda + 1) = A_x^2 + A_y^2 + m^2$, and the eigenvectors $|n\lambda\rangle$ provides a good description of the rotor states. This λ is essentially $n - 1 - K$, with K in (4.39). Observing that $\tilde{\Lambda}$ is $\{j_{1x} - j_{2x}, j_{1y} - j_{2y}, j_{1z} + j_{2z}\}$, these eigenvectors are related to the parabolic $|n_1 n_2 m\rangle$ states by a Clebsch-Gordan coefficient analogous to (1.15),

$$|n\tilde{\lambda}m\rangle = \sum_{n_1} (-)^{j_{1z} + \frac{1}{2}(n-1)} \langle j_1 j_2 j_{1z} j_{2z} | \lambda m \rangle |n_1 n_2 m\rangle . \quad (4.48)$$

It had been noted at the end of Section 1.2.2 that the Schrödinger equation for the pure Coulomb potential separates also in momentum space in spherical coordinates. The λ description of combined Coulomb and diamagnetic potentials corresponds to the momentum space equation separating in elliptic cylindrical coordinates [29]. This is again a

partial separability of the potential in (4.25), to order B^2 . Of course, for the field-free hydrogen atom, it provides yet another system of coordinates in which the Schrödinger equation separates besides the two considered in Chapter 1.

2.3 Large-scale numerical calculations

The previous section considered the diamagnetic mixing of degenerate states in an n -manifold, this ℓ -mixing expected to be the most immediate because of their degeneracy. Since, as usual, selection rules for matrix elements of any operator pertain to angular momentum quantum numbers but not n , there are counterpart matrix elements to those in (4.31) which connect one n in general to any other, including those in the continuum. Since the different n states are not degenerate, these mixings are reduced by the energy denominators in perturbation equations such as (3.7). But, with either increasing B or increasing n , these n -mixings by the diamagnetic interaction are also important. Given the infinite pile-up of Rydberg states at the ionization limit, any practical calculation will involve the truncation of the full set of $|n\ell\rangle$ states but, with today's computers, calculations with very large bases are feasible. At one level, such a calculation is essentially a numerical experiment, constituting the theorists' test of quantum mechanics and their ability to compute energies and oscillator strengths at a level comparable to the precision with which experimental colleagues can measure them.

Although the problem of diagonalizing the Hamiltonian in (4.24) in some basis is straightforward in principle, ingenuity in the choice of basis and the numerical techniques used can maximize the quality of the results. We consider here four procedures that have been used. The first works with the spherical $|n\ell\rangle$ states. The angular matrix elements are exactly as in (4.31) but radial matrix elements of r^2 with $n \neq n'$ are complicated. Analytical expressions and recurrence relations are available but are often more unwieldy than a direct numerical calculation with hydrogenic radial functions. Fig. 4.6 for $m = 0$ and even parity and $n \approx 10$ included 110 states [30]. A second procedure uses a variant spherical basis with a more flexible orthonormal set of radial functions than the hydrogenic (1.9). Basis sets of up to 6400 have been employed, with the radial functions chosen as generalized Laguerre functions with a fixed exponent. Matrix elements can then be expressed in closed, analytical form and the bounded Hamiltonian matrix diagonalized by efficient algorithms. Fig. 4.7 shows hundreds of lines for energies $E < -20 \text{ cm}^{-1}$ (corresponding to large n , $n \approx 70$, close to the ionization limit), comparing energies and intensities with a precision experiment on the spectrum of deuterium [31].

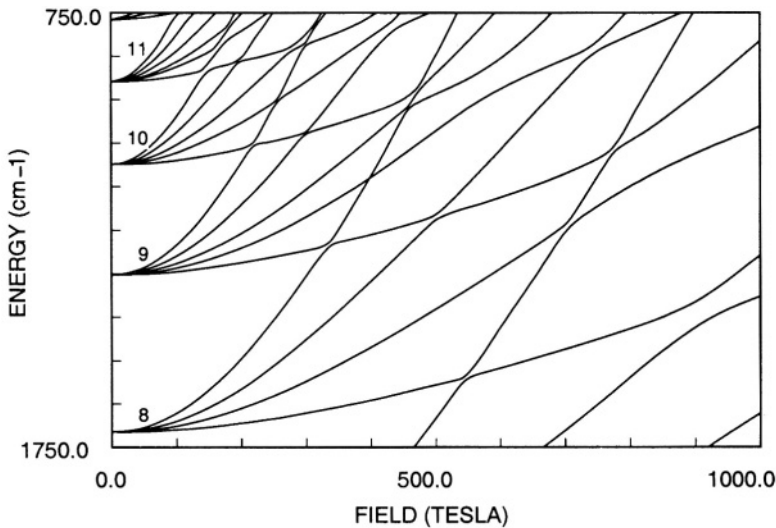


Figure 4.6. Diamagnetic energy of $n = 8 - 11$ states of hydrogen with $m = 0$ and even parity. The basis consisted of all 110 relevant states with $n = 1 - 20$. From M. Zimmerman, M.I.T. Ph. D. thesis, 1970.

The third procedure, closely akin to the second mentioned above, has used a “Sturmian” basis of radial functions as in (1.9) but with r/r_0 in place of Zr/a_0 , with r_0 fixed. For a given ℓ , these form an orthonormal set but with a weight of $1/r$ in the radial integration. Whereas with $r_0 = na_0/Z$ they would coincide with hydrogenic functions, when r_0 is fixed, each Sturmian function is an infinite expansion over the hydrogenic functions, discrete and continuum. The off-diagonal matrix elements of r^2 are confined to $|n - n'| \leq 3$, an enormous simplification. This makes the Hamiltonian matrix tri-diagonal in ℓ and penta-diagonal in n . A price is paid, the additional $1/r$ weight factor in the orthogonality of the Sturmian functions leading to a “generalized eigenvalue” problem, $H\psi = ES\psi$, the matrix S being itself tri-diagonal. Efficient numerical techniques handle such problems [32]. A fourth procedure that also shares a banded Hamiltonian works with “semi-parabolic” coordinates, $u = \sqrt{\xi}$ and $v = \sqrt{\eta}$. In terms of these, the Coulomb Schrödinger equation is converted to harmonic-oscillator form with potentials quadratic in u and v . The diamagnetic potential takes the form $(B/B_c)^2 u^2 v^2 (u^2 + v^2)$. This structure makes immediately clear through oscillator selection rules that any state $|n_1 n_2 m\rangle$ is linked only to others with $\Delta n_1, \Delta n_2 \leq 2$,

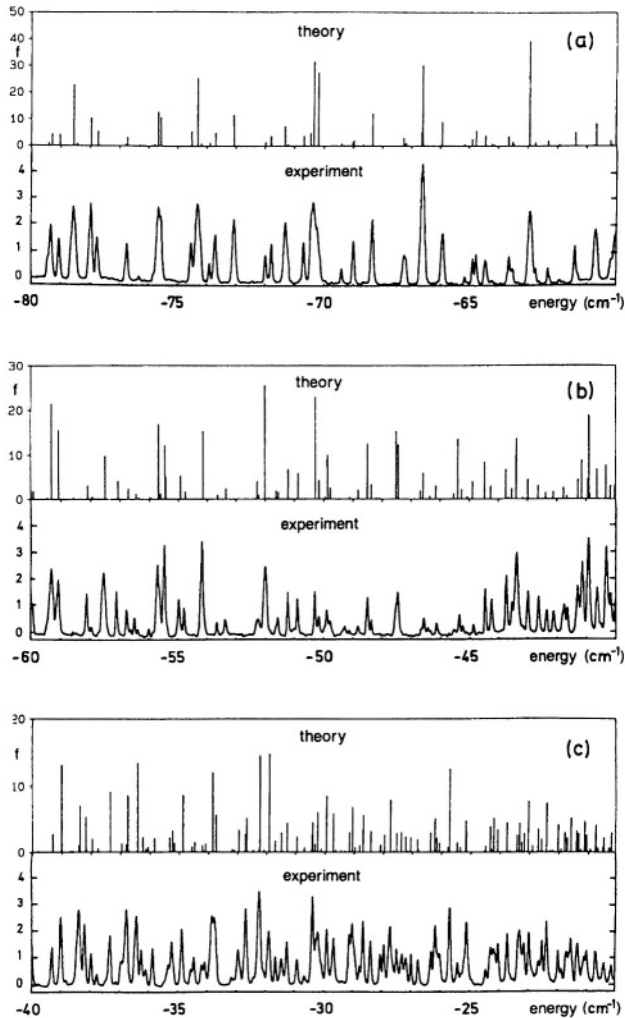


Figure 4.7. Comparison between theoretical oscillator strengths and experimental photoabsorption spectrum to $m = 0$, even parity Rydberg states of deuterium in a magnetic field of 5.96 T. Oscillator strengths are in units of 10^{-6} , experimental data in arbitrary units, and energy is with respect to the ionization threshold. The end of the energy range, above -25 cm^{-1} , corresponds to the chaotic regime for a classical atom in a magnetic field. From [31], with permission from Springer-Verlag.

$\Delta n \leq 3$, thus accounting for a banded Hamiltonian matrix. Very large matrices can then be handled so that calculations can reach E values very close to threshold. The most extensive numerical results and tables on atoms in magnetic fields are to be found in a book [33] and in recent research publications [34] and references therein.

Results obtained by any of the above methods and presented in Figs. 4.6–7 reproduce at low n those of Section 4.2.2 for diagonalization in a fixed n -manifold. The clusters from each n are distinct in this ℓ -mixing region. In the distribution of oscillator strength from the ground state, most is to the highest state of each cluster when $\pi(-1)^{|m|}$ is even. This is the $K = 0$ highest rotor state with wave function concentrated perpendicular to \mathbf{B} . For $\pi(-1)^{|m|}$ odd, however, the oscillator strength is distributed more uniformly over the cluster. Isolating like members of each cluster, one sees a constant spacing of $\frac{3}{2}\hbar\omega_c$ as the ionization potential is approached, corresponding to resonances seen in the experiments of Figs. 4.1 and 4.2.

Another prominent feature are the sharp avoided crossings in Figs. 4.6–7. Even when clusters of eigenvalues from each n interpenetrate, they retain their identity, particularly so when a $K = 0$ state from some n crosses the $K = K_{\max}$ from $n + 1$. This can be attributed to their different localizations, perpendicular and parallel to the field, respectively. While degenerate in energy, the wave functions have negligible overlap as a result of these different localizations. This is again an important generic feature that is encountered in several very non-perturbative problems, including those of electron correlation to be discussed in Chapter 5.

As one penetrates more into the n -mixing regime and approaches $E = 0$, the mixing becomes stronger, even of different K , although the rotor states remain unmixed longer than the vibrators. Electron trajectories calculated for the corresponding classical equations of electronic motion in the combined Coulomb and diamagnetic potential (4.25) display an analogous effect, becoming chaotic a little short of $E = 0$. A rough correspondence between the two results is provided by the distribution of spacing between the quantum eigenvalues: Fig. 4.8. This distribution changes from an initially Poisson distribution to a Wigner one (primarily distinguished by the feature that vanishingly small spacings are absent) as we approach $E = 0$. All this has been of much interest in recent studies of chaos and a general rule that associates Poissonian (Wigner) statistics for the spacing distribution for integrable (non-integrable) systems [35]. As long as quasi-separability holds, vanishing spacings occur and Poisson distributions are seen. However, any experiment with a finite resolution sees a regular pattern of oscillations as in Figs. 4.1 and 4.2. This is borne out in Fig. 4.1 where an averaging over a small energy bin reproduces the experimentally observed regular oscillations, the peaks of these oscillations sometimes embracing a whole set of quantum levels.

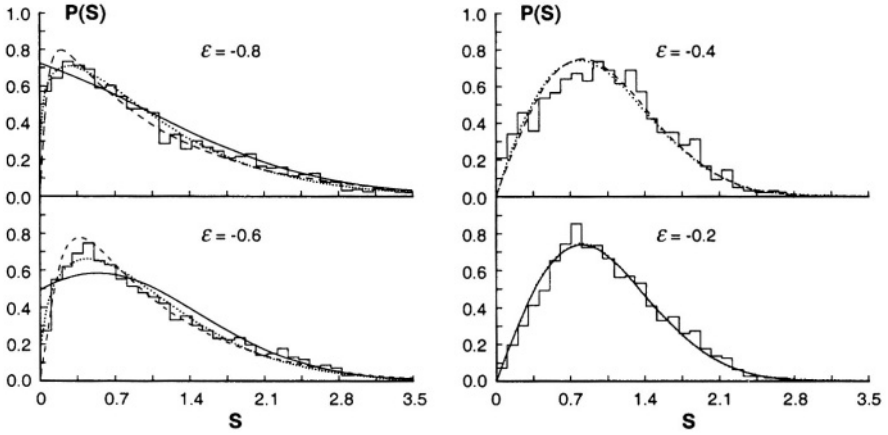


Figure 4.8. Histograms of $P(s)$, the probability distribution of energy-level spacing in hydrogen in a magnetic field at different values of the scaled energy $\epsilon = E(B/B_c)^{-2/3}$. Curves represent various fits that interpolate between the Poisson distribution of the full curve in the first panel to the Wigner distribution in the last panel. From Wintgen and Friedrich [35].

2.4 Quasi-classical JWKB analysis

In recent years, the fascination with chaos in classical mechanics and whether it is realized in a counterpart quantum system has led to many studies of the Coulomb plus diamagnetic problem as a possible example. There has been extensive work on classical trajectory calculations, classical perturbation theory, and various semi-classical quantization procedures applied to such trajectories [36]. This is understandable given that we are dealing with large quantum numbers and, therefore, quasi-classical conditions. Hamilton's equations of motion for the potential in (4.25) are integrated at fixed energy E for trajectories starting at $t = 0$ from near the nucleus with some angle θ to the z -axis. Often the semi-parabolic coordinates mentioned in Section 4.2.3 have proven convenient for these calculations which seek to identify "closed orbits" wherein the trajectory closes back onto the origin after "reflection" from the rising potential encountered at values of ρ and z when $V(\rho, z) = E$. Recurrence times T_ν corresponding to a return after a single or multiple reflection are measured in units of the cyclotron period $T_c = 2\pi\omega_c$ with ω_c given in (4.6).

A prominent recurrence, $\nu = 1$, with $(T_1/T_c) = 2/3$, occurs for a trajectory that propagates along the ρ -axis and is reflected. Clearly, this corresponds to the $\frac{3}{2}\hbar\omega_c$ -spaced resonances of Figs. 4.1 and 4.2 and is associated with motion localized perpendicular to \mathbf{B} . Other recurrences have similarly been associated with other spacings seen in experiments such as Fig. 4.1. Whether through such computations of classical trajectories or equivalent integrations of the time-dependent Schrödinger equation for an initial wave packet, the phenomenon of regularly spaced oscillations may be viewed as constructive interference between the outgoing trajectories or wave fronts from the origin and incoming ones following reflection from $V(\rho, z) = E$.

In this section, we use a JWKB (Jeffreys-Wentzel-Kramers-Brillouin) analysis which has features similar to such classical calculations but is simpler and more straightforward because specific classical trajectories, whether stable or not, need not be computed and we need not deal with the extreme sensitivity to initial conditions that integration of classical equations of motion entail. The two-variable potential in (4.25) is plotted in Fig. 4.2(c), the equipotentials being spherical at small r whereas the rising diamagnetic potential leads to a barrier as ρ increases. For $V \geq 0$, the equipotentials are open along the z -axis (field direction), denoting that at positive energies the electron can escape along (and only along) this axis. The electron has motion simultaneously in ρ and z , the former “transverse” motion always bounded because of the diamagnetic barrier.

At large distances, say when the longitudinal distance z is large, the transverse motion is simply the Landau one of a free electron considered in Section 4.1.1, the Coulomb term being negligible. This motion is quantized with spacing $\hbar\omega_c$. At small- z , however, the potential takes the “wine glass” form (Fig. 4.9) of (4.25) when $z = 0$,

$$V(\rho) = -\left(e^2/\rho\right) + \left(e^2 B^2/8\mu c^2\right) \rho^2. \quad (4.49)$$

Applying the JWKB quantization condition to this motion,

$$2(2\mu)^{1/2} \int_0^{\rho_0} [E - V(\rho)]^{1/2} d\rho = \left(n + \frac{1}{2}\right) h, \quad (4.50)$$

with ρ the turning point: $E = V(\rho)$, gives the bound state eigenvalues for this motion. Note that, as with any such Bohr-Sommerfeld quantization, there is no implication that there is an actual classical motion or trajectory along the ρ -axis at this energy. As sketched in Fig. 4.2(b), the eigenvalues in the $V(\rho)$ of (4.49) evolve from a Rydberg-like spacing at low energies to a final Landau set with equal $\hbar\omega_c$ spacing through

an intermediate set that lies around $E = 0$ and is equally spaced with $\frac{3}{2}\hbar\omega_c$. This is also confirmed by formally differentiating (4.50) to get

$$dE/dn = \left(\hbar^2/2\mu\right)^{1/2} \left[\int_0^{\rho_0} d\rho \{E - V(\rho)\}^{-1/2} \right]^{-1}, \quad (4.51)$$

the integral performed analytically for $E = 0$ to yield $dE/dn = \frac{3}{2}\hbar\omega_c$.

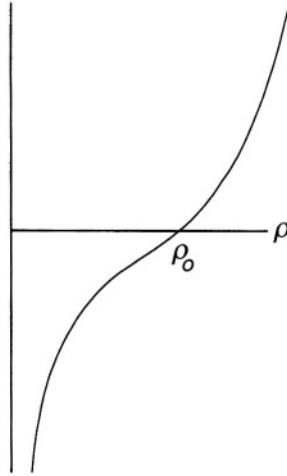


Figure 4.9. “Wine-glass” potential (4.49) perpendicular to the magnetic field direction in combined Coulomb and diamagnetic potentials.

This JWKB picture, while fully quantum-mechanical, has the virtue of providing straightforwardly the three characteristic signatures of the problem of an atom in a magnetic field; see Fig. 4.2(b). The one at small E (and, correspondingly, small distances) of Coulomb Rydberg levels, and the opposite at high E when the electron is essentially free of Coulomb binding and has the Landau level structure of free electrons in a magnetic field, were to be expected. But, perhaps surprisingly, a third region near zero energy, the strong mixing region wherein both fields contribute roughly equally (and opposite in sign), also has a simple structure, namely, equal spacing with $\frac{3}{2}\hbar\omega_c$. Again, this seems a generic result for many instance of superposed fields, equally spaced structures having also been seen for an atom in an electric field near the zero-field ionization limit.

The JWKB picture is, however, not complete, nothing having been said about the electron's longitudinal motion in z . Clearly, for $E > 0$, this motion leads to electron escape so that the states discussed are not strictly bound but resonances, the width reflecting this escape probability. The two motions are, of course, coupled internally by the Hamiltonian itself through the Coulomb term. Thus, in the picture where an electron is somehow initially excited into a rotor state with motion dominantly along the ρ -axis, it will sometimes scatter through the Coulomb potential when near the origin where this potential is strongest, and escape to infinity along the z -axis. The narrowness of the resonances points to the motion along the ρ -axis being quasi-stable and is again clearly because the coupling between ρ and z motions through the Coulomb potential is restricted to a small range of the electron's motion, making it effectively weak. This kind of bounded motion in one coordinate, free motion in another, leading to quasi-band resonances, is a real space counterpart of the more familiar process of autoionization described similarly in terms of state space; see Section 5.3.3.

Local expansion of the potential in (4.25) around the ρ -axis, that is, $\theta = 90^\circ$ gives

$$V(r, 90 \pm \Delta\theta) = -(e^2/r) + (e^2 B^2 / 8\mu c^2) r^2 - (e^2 B^2 / 16\mu c^2) r^2 (\Delta\theta)^2. \quad (4.52)$$

The first two terms give the effects already described, the last is seen to be harmonic in $\Delta\theta$ but with negative sign. This reflects the barrier or a "ridge" along the ρ -axis, motion along it unstable since the potential falls away from it. Nevertheless, that rotor states exist with localization along this region of highest potential, and that quasi-bound states last sufficiently long to appear as observable resonances, is again seen to be a generic feature of such problems. A counterpart involving two electrons will be considered in Section 5.3.4. The quasi-bound states arise from motion mostly at large distances and, therefore, as discussed in Section 4.2.5 below, occur in all atoms, not just hydrogen. The value of m is also largely irrelevant because angular momentum contributions are of short range compared to the Coulomb and diamagnetic terms. How intense a resonance is in photoabsorption can, however, depend on m because of symmetry considerations. Thus, in the two photon absorption experiment of Fig. 4.1, for $|m| = 1$, the symmetry of the final state is $Y_2^1(\theta, \varphi)$ which has a node at $\theta = 90^\circ$ and the $\nu = 1$ or $\frac{3}{2}\hbar\omega_c$ states are absent. (Again, a counterpart two-electron result occurs in Section 5.3.2.) On the other hand, these states are dominantly present for both $m = 0$ and 2.

2.5 Rydberg diamagnetism in other atoms

As already clear from the previous sub-sections of Section 4.2, the equally-spaced resonances seen around the ionization limit and other aspects of the diamagnetic interaction are large- r phenomena, the r^2 dependence in this interaction making for appreciable effects only at large distances. As indeed seen in other atoms as in Fig. 4.2, these phenomena are largely common to all atoms, the potential at large r in any neutral atom given by (4.25). In an atom other than hydrogen, the Rydberg electron does of course see departures from the pure Coulomb field during its excursion into the core region. Here the diamagnetic term is entirely negligible and the departures from the Coulomb potential due to other electrons may be treated as in the field-free atom. Indeed, detailed calculations along these lines are now available, the small- r region treated through quantum defects or one of the other calculational methods for complex atoms discussed in Chapter 1 and then matched to hydrogenic treatment of the large- r region as described in previous sub-sections above. Since the small- r region according to these discussions is the seat of ρ - z coupling, widths and intensities of the resonances vary from atom to atom while energy aspects such as resonance positions are largely independent and as in hydrogen. Fig. 4.10 is an example of the detailed calculations now possible and their precision in comparison with experiment [37].

3. Strong Field Effects on Low-lying States

3.1 Introduction

As per the previous section, laboratory strength magnetic fields significantly influence only the large- n states and, even there, have comparable influence to the atom's internal Coulomb field rather than dominate over it. We now turn to a study when the magnetic field is indeed dominant, distorting even the low- n states down to the ground state. Such a situation occurs only for $B > B_c$ and, therefore, in astrophysical phenomena, although some of these effects may be simulated in condensed matter analogs of atoms even with laboratory fields. The dielectric constant and effective mass in these analogs can effectively weaken the Coulomb binding, enhancing the effect of the magnetic field. Historically, some of these effects were indeed observed first in excitons but we will discuss the hydrogen atom and other neutral atoms in this section. A simple scaling $e^2 \rightarrow e^2/\epsilon$ where ϵ is the dielectric constant, and use of the effective mass for μ will carry over the results to the condensed matter systems (Section 1.2 of [33]).

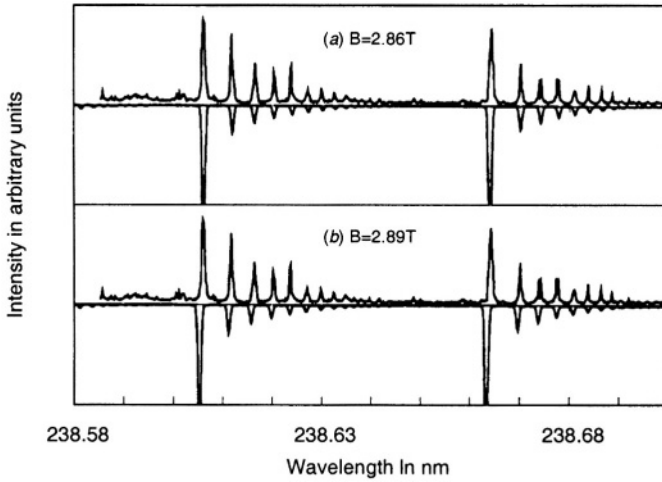


Figure 4.10. Spectrum of barium in a magnetic field. The lower frames of (a) and (b) are theoretical calculations for the values of B indicated, the upper frames (identical) are experimental data. From Rao and Taylor [37].

3.2 Hydrogen in an ultrastrong magnetic field

We will begin with a field $B \gg B_c (= 2.35 \times 10^5 \text{ T})$ which will be termed “ultrastrong” in that the magnetic field is the dominant partner. The discovery of pulsars in the late 1960s and the postulated mechanism for their energy source, of a rapidly rotating neutron star with a magnetic field of about $2 \times 10^8 \text{ T}$, prompted of course the investigation of atomic structure in such magnetic fields [24],[38]. Atoms and ions are clearly present in the plasma surrounding such objects and atomic structure also underlies the material in the crust that such neutron stars are supposed to have (in that respect, resembling more a planet than a gaseous star). Therefore, it is natural to ask what atoms look like in such strong fields. Although atomic transitions have not been observed from neutron stars, perhaps because the limited amount of material involved around such small objects means intensities too feeble for observation at this time, we have noted in Section 4.1.1 that cyclotron emission from the Landau levels of the underlying magnetic field, that is, from free electrons, has given direct evidence of such field strengths.

With one field dominant, we can revert, unlike in Section 4.2, to more standard approximation methods. However, we cannot quite use perturbation theory as in Chapter 3 because no matter how strong the magnetic field, as we have seen in Section 4.1.1, it has no influence

on the electron's z -motion. The Coulomb interaction is alone active in this direction so that we cannot regard it as perturbative compared to the magnetic field. Therefore, the approximation method we employ is not perturbation theory but an adiabatic separation of transverse and longitudinal motions, the magnetic field controlling the former and the Coulomb the latter. For the transverse motion, considered more energetic, the Coulomb field can be neglected to a first approximation. Such adiabatic methods have long been used in quantum physics, particularly for separating nuclear (slow) motion from electronic (fast) motion in molecules as we will see in Chapter 6, and have also figured in electron correlation studies as in Chapter 5.

The extreme adiabatic approximation is to write the wave function for hydrogen in factorized form

$$\psi_{00n}(\rho, z) = L_{00}(\rho) f_n(z), \quad (4.53)$$

where $L_{00}(\rho)$ is the Landau function in (4.16) with $n_\rho = 0, m = 0$. The energy of this lowest Landau state is zero once the spin is included, the spin aligning antiparallel to the field in such a strong \mathbf{B} , and thereby its magnetic-moment coupling to \mathbf{B} canceling exactly the $\frac{1}{2}\hbar\omega_c$ of the Landau state. Since the next Landau state or spin excitation lies $\hbar\omega_c$ above, and this energy dwarfs any longitudinal Coulomb energies (for a pulsar field of 2×10^8 T, $\hbar\omega_c \approx 10^4$ eV), the assumption in (4.53) that we can restrict to the ground state of the transverse motion is an adequate approximation. Effectively, the transverse degrees of freedom of the electron are frozen out and we have a pseudo one-dimensional Coulomb problem for hydrogen in such an ultrastrong field. The picture then, starting with the magnetic field, is that the electron orbits a field line with cyclotron radius $\hat{\rho}$. With a proton placed at some point on the field line, as the electron moves out in $|z|$ it is held back by the Coulomb attraction. The atom is, therefore, a cylindrical object as will be borne out by our analysis, and quite different from the spherically symmetric shape of the field free hydrogen atom in its ground state.

This one-dimensional longitudinal motion, with wave function $f_n(z)$, is in a potential obtained from $-e^2/r$ by integrating over ρ and φ with the $L_{00}(\rho)$ wave function,

$$\begin{aligned} V(z) &= \int_0^\infty \rho d\rho L_{00}^2(\rho) (-e^2/r) \\ &= -(2e^2/\hat{\rho}) \exp(z^2/\hat{\rho}^2) \int_{|z|/\hat{\rho}}^\infty dt \exp(-t^2). \end{aligned} \quad (4.54)$$

One-dimensional motion in this potential results upon substituting (4.53) into (4.24), using (4.14) for the terms in ρ , multiplying by $L_{00}(\rho)$ and integrating over ρ . In this manner, even though (4.24) is non-separable, the form of the solution in (4.53) induces an adiabatic separability of ρ and z as an approximation.

The potential in (4.54) is an even parity, attractive one-dimensional well. We can readily obtain the eigenvalue spectrum numerically in this $V(z)$ but it is instructive to simplify it through standard inequalities to render it as

$$\frac{-e^2(1 + \alpha^2)}{|z| + \alpha\hat{\rho}} \leq V_0(|z|) \leq \frac{-e^2}{|z| + \hat{\rho}/\sqrt{2}} \quad , \quad (4.55)$$

where α is a positive constant.

The spectrum of $V_0(|z|)$ is, therefore, closely approximated by that of the ‘‘cut-off one-dimensional Coulomb’’ potential, $-e^2/|z|$, whose singularity at $z = 0$ is cut-off by a small additive constant involving $\hat{\rho}$. This cut-off is at a value small compared to the Bohr radius a_0 , $\hat{\rho} \approx a_0/20$ for $B = 2 \times 10^8$ T. With $\hat{\rho} \rightarrow 0$ as $B \rightarrow \infty$, the approximation becomes exact in the limit of asymptotically large magnetic field, although admittedly this limit is academic, our non-relativistic treatment breaking down before that. This is an appropriate point to discuss the validity of a non-relativistic treatment of ultra-strong magnetic fields. As long as $\hbar\omega_c$ remains smaller than mc^2 , which is true for the numbers mentioned above (10 keV *vs* 0.5 MeV), relativistic corrections are small and can, if needed, be estimated through perturbation theory as in Section 3.3. It is fortunate that neutron star magnetic fields lie in such a regime, relativity becoming non-perturbative only when $\hbar\omega_c \approx mc^2$ or $B > 4.41 \times 10^9$ T.

The spectrum of the cut-off Coulomb potential, $-e^2/(|z| + \hat{\rho})$, is well-known. The non-degenerate ground state of even parity has a very large binding energy,

$$E_{000} = - \left(e^2/2a_0 \right) \ln^2 \left(\sqrt{2} a_0/\hat{\rho} \right)^2 \quad . \quad (4.56)$$

This expression is readily understood. As in any Coulomb problem, $(e^2/2a_0)$ is the basic dimensional unit of energy. A one-dimensional Coulomb potential has a logarithmic enhancement of this value, $1/|z|$ being logarithmically singular upon integration over dz . The potential in (4.55) is not actually singular because of the cut-off which, therefore, occurs in the argument of the logarithm, the ratio of Bohr radius to cyclotron radius expressing the departure from one-dimensionality of

hydrogen in an ultrastrong field. For $|z| \ll \hat{\rho}$, the system is indeed essentially one-dimensional, the transverse extent of $\hat{\rho}$ small on the scale of a_0 . But, for $|z| < \hat{\rho}$, the three-dimensionality of the Coulomb potential becomes relevant and there is no singularity, $(-e^2/r)$ not being singular upon integration over the three-dimensional volume element $r^2 dr$.

For fields typical of pulsars, $B \approx 2 \times 10^8$ T, the \ln^2 term in (4.56) is, approximately, ten. The ground state of hydrogen in such an ultrastrong field has therefore an energy of -150 eV. The wave function $f_0(z)$ is nodeless, peaked at $z = 0$ and of extent, approximately, $a_0[\ln(a_0/\hat{\rho})]^{-1} \approx (a_0/\sqrt{10})$. The electron orbit can be pictured as roughly cylindrical with transverse cyclotron radius of $(a_0/20)$ and oscillating back and forth in z over an extent of $a_0/3$. It might seem paradoxical that with the magnetic field dominant in the ultrastrong regime, the Coulomb binding energy should actually be larger than the field-free 13.6 eV, or the atom as a whole much smaller than a_0 in size. The explanation lies in the magnetic field's role in converting a three-dimensional Coulomb problem into a pseudo one-dimensional one. The field squeezes the electron's transverse motion to distances of the order of $\hat{\rho}$, thereby making the electron experience more of the proton's Coulomb attraction than it would otherwise when it has an extent of about a_0 . Thereby, the electron gets bound more strongly than in zero field, its z -extent also becoming smaller than a_0 although not as small as its ρ extent. Note an interesting analogy to the similar role played by the outer electron in H^- in forcing the inner electron to be more strongly bound to the proton than it would be on its own in the H atom (Section 2.4.1).

Excited states of the potential in (4.55) come in pairs, of even and odd parity. They have vanishing wave function density at $z = 0$ so that the cut-off is essentially irrelevant, the potential being well approximated by $-e^2/|z|$ for them. The eigenvalues are just the Bohr energies $-e^2/(2a_0n^2)$, $n = 1, 2, \dots$. The full energy spectrum of hydrogen in an ultra-strong magnetic field consists, therefore, of a non-degenerate deeply bound ground state $|000\rangle$ with energy (4.56) and wave function concentrated around $z = 0$, and degenerate pairs of odd and even parity states $|00n\rangle$ with Bohr energies and successively more nodes in z . For realistic values $B \ll B_c$, these are not exactly degenerate but slightly separated in energy.

This entire pattern for $n_\rho = 0$ and $m = 0$ is repeated for other values of $m = -1, -2, \dots$, still with $n_\rho = 0$ because all are degenerate in the Landau spectrum. Upon choosing

$$\psi_{0mn}(\rho, z) = (2\pi)^{-1/2} \exp(im\varphi) L_{0m}(\rho) f_n^{(m)}(z), \quad (4.57)$$

the counterpart one-dimensional potentials to (4.54),

$$V_m(z) = \int_0^\infty \rho d\rho L_{0m}^2(\rho) (-e^2/r),$$

are well approximated by

$$V_m(z) \approx -e^2 / (|z| + \hat{\rho}_m \sqrt{2}) , \quad (4.58)$$

with

$$\hat{\rho}_m = \left(|m| + \frac{1}{2} \right)^{1/2} \hat{\rho} , \quad (4.59)$$

since $\rho L_{0m}^2(\rho)$ is sharply peaked at $\hat{\rho}_m$. Such a potential (4.58) has the same spectrum as discussed in the previous paragraph, with $\hat{\rho}$ replaced by $\hat{\rho}_m$. Fig. 4.11 provides a sketch. Similar Coulomb energy levels are built on other excited Landau levels of non-zero n_ρ and positive m , these themselves $\hbar\omega_c$ apart. All these levels are not strictly bound, since they overlap with continuum states on the lowest Landau level so that they can decay into such states. This is the phenomenon of autoionization (Sections 5.2.2 and 5.3.3).

Quantitative sophistication can be added to the above basic picture of the ultrastrong-field spectrum by using a more general form for $f_0(z)$ in a Rayleigh-Ritz variational calculation. Typical choices involve Gaussian or exponential fall-off in $|z|$, the latter (termed LE) becoming exact for asymptotically large B as already noted. Yet another interesting trial function is a mixed product of spherical and cylindrical dependences,

$$\psi_{0m0} = N \exp(im\varphi) L_{0m}(\rho) \exp(-Z'r/a_0), \quad (4.60)$$

with N a normalization constant and Z' a variational parameter. This set of functions has the interesting structure that with increasing B , as $\rho L_{0m}^2(\rho)$ becomes more sharply peaked at $\hat{\rho}_m$, the function becomes of LE form with results as discussed. In the opposite limit, as $B \rightarrow 0$ and $\hat{\rho}_m \rightarrow \infty$, $L_{0m}(\rho)$ reduces to $r^{|m|} \sin^{|m|} \theta$ so that (4.60) coincides with the exact zero-field hydrogenic states $|n\ell m\rangle$ with $m = -\ell$. Therefore, the form (4.60) gives the exact spectrum in both limits and interpolates smoothly and continuously between them. Remarkably, the Rayleigh-Ritz calculation with (4.60) can be carried out in closed analytical form to give

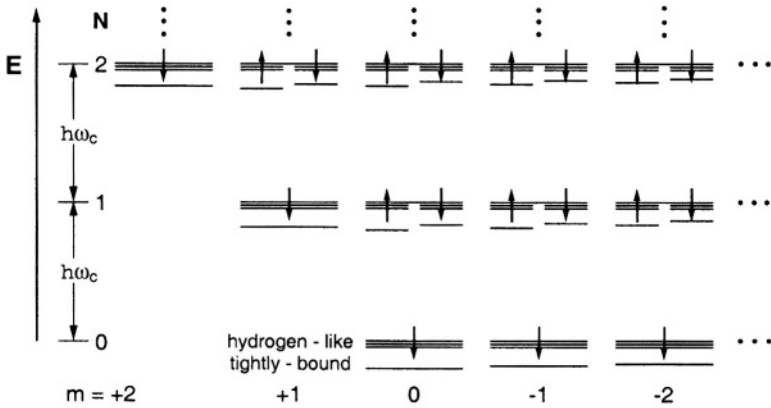


Figure 4.11. Schematic energy spectrum of hydrogen in an ultrastrong magnetic field, showing successive Landau levels (N, m), electronic spin relative to the field direction, and Coulomb levels of (4.55) including a hydrogen-like series and a deep level as in (4.56). From Ruder, Wunner, Herold, and Geyer [33], with permission from Springer-Verlag.

$$E_{0m0} \leq \frac{e^2}{a_0} \left[\frac{1}{2} Z'^2 - \frac{Z'}{|m|+1} \frac{U(|m|+1, 1, \hat{\rho}^2/a_0^2)}{(\hat{\rho}^2/a_0^2) U(|m|+2, 2, \hat{\rho}^2/a_0^2)} \right], \quad (4.61)$$

where U is an irregular confluent hypergeometric function, expressible in terms of exponential integrals.

The ground and low-lying states of hydrogen have also been calculated by even more elaborate numerical calculations. In one, a generalized form of (4.60),

$$\psi_m(\vec{r}) = \sum_{n_\rho} (2\pi)^{-1/2} \exp(im\varphi) L_{n_\rho m}(\rho) f_{n_\rho}(z), \quad (4.62)$$

is substituted into the Schrödinger equation (4.24), multiplied from the left by $(2\pi)^{-1/2} \exp(im\varphi) L_{n_\rho m}$ and integrated over ρ and φ . In the coupled linear differential equations that follow for $f_{n_\rho}(z)$, diagonal matrix elements $\langle n_\rho m | (-e^2/r) | n_\rho m \rangle$ occur as adiabatic potential wells which converge to Landau levels. Eigenvalues and wave functions in these wells reproduce the results of an adiabatic approximation, but retaining off-diagonal matrix elements that couple the various $f(z)$ gives more

accurate results while being more complicated. On the other hand, for $B \approx B_c$ or $B < B_c$, an expansion in spherical functions,

$$\psi_m(\mathbf{r}) = \sum_{\ell} f_{\ell}(r) Y_{\ell}^m(\theta, \varphi), \quad (4.63)$$

is more suitable. Now, substitution in (4.24), multiplication by Y_{ℓ}^{m*} and integrating over θ and φ gives coupled equations for $f_{\ell}(r)$. The matrix elements involved of the diamagnetic interaction are as in (4.31). Results of elaborate numerical calculations of such coupled equations are given in [33], an example being given in Fig. 4.12.

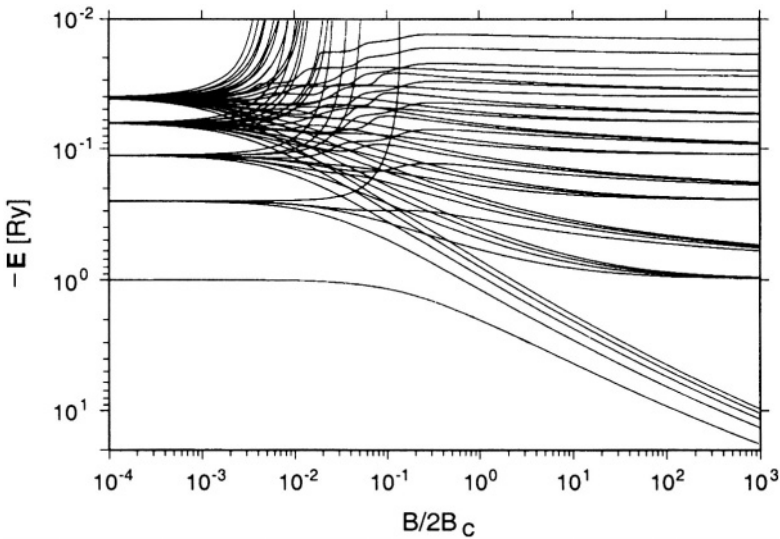


Figure 4.12. Energy values of all $n \leq 5$ states of hydrogen in a magnetic field. The Rydberg series with splittings due to linear and quadratic Zeeman effects at low B evolve to the complete rearrangement of the ultrastrong field domain, the nodeless state with $m \leq 0$ from each n diverging logarithmically as in (4.56) and its counterpart for other values of m from (4.59). From Ruder, Wunner, Herold, and Geyer [33], with permission from Springer-Verlag.

Yet another method has been to apply perturbation theory as in Section 3.2.2 to very high order with the diamagnetic interaction. The ground state energy is thus expanded in powers of B^2 ,

$$E_{000} = \sum_k (B/B_c)^{2k}, \quad (4.64)$$

the coefficients E_k having been computed up to $k = 62$ with over 20-digit accuracy [39]. The perturbation series is divergent, not surprisingly given the logarithmic dependence we have already seen in (4.56) for B very large. There are, however, resummation techniques for such divergent series which then lead to accurate values of E_{000} for all values of B . The leading term at asymptotically large B coincides with (4.56).

With energy levels and wave functions for low-lying states $|n_\rho mn\rangle$ in hand, radiative transitions between them can be computed as in Section 2.2.1. The dipole matrix elements

$$d^{(q)} = \langle n'_\rho m' n' | r^{[q]} | n_\rho mn \rangle, \quad (4.65)$$

with $q = 0, \pm 1$ representing linear and circular polarization, and $r^{[q]} = (4\pi/3)^{1/2} r Y_1^q(\theta, \varphi)$, lead to oscillator strengths

$$f^{(q)} = (\hbar\omega/Ry) |d^{(q)}/a_0|^2 \quad (4.66)$$

and transition probabilities

$$\omega^{(q)} = (2.67 \times 10^9 \text{s}^{-1}) (\hbar\omega/Ry)^3 |d^{(q)}/a_0|^2 \quad (4.67)$$

in the spectrum of hydrogen in ultrastrong magnetic fields. Extensive tables have been presented. Fig. 4.13 gives an example for transitions involving the lowest levels with $n_\rho = 0$. A switch in oscillator strengths from low to high fields occurs in a rather narrow range of magnetic field strength, $B/B_c \approx 0.1$. At very high values of B , the dominant transitions with almost unit oscillator strength are diagonal in n_ρ and m . Such a dominance of $q = \Delta m = 0$ transitions, that is, of linear polarization, is a consequence of the elongated probability distributions along z . Radiative transitions in an ultrastrong field are very anisotropic and polarized. Rydberg series of sharp resonances are seen below the $n_\rho = 1$ and 2 thresholds for photoionization of the ground state of hydrogen.

3.3 Complex atoms in ultrastrong fields

Just as the Bohr energy levels serve as the basis for atomic structure of heavier atoms in The Periodic Table at zero magnetic field, the hydrogenic states discussed in the previous section serve for an understanding of complex atoms in an ultrastrong magnetic field. First, for hydrogenic ions of nuclear charge Z , the energy obeys the scaling relation

$$E(Z, B) = Z^2 E(1, B/Z^2), \quad (4.68)$$

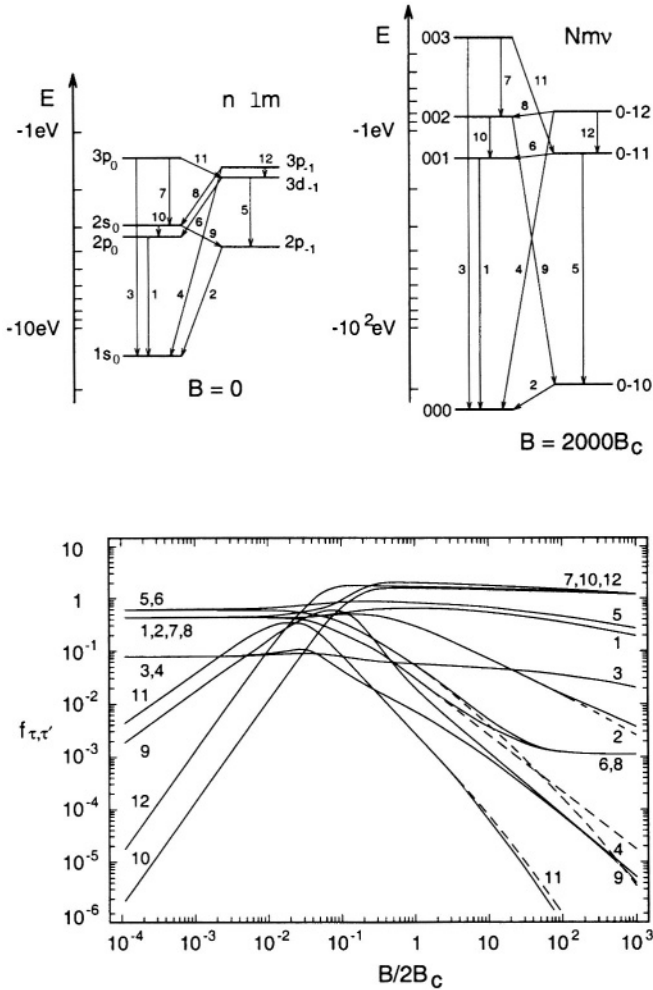


Figure 4.13. Oscillator strengths for transitions between low-lying states of hydrogen in a magnetic field. Full curves take into account the finite mass of the proton, broken curves assume infinite mass. The ultrastrong field energy levels for $m = -1$ do not include an upward shift of 29.6 eV due to the proton cyclotron energy. Note the complete rearrangement of oscillator strengths in the range $10^{-2} \leq (B/2B_c) \leq 10^{-1}$. From Ruder, Wunner, Herold, and Geyer [33], with permission from Springer-Verlag.

as follows from inspection of the Hamiltonian in (4.24). The Z^2 scaling of Bohr energy values is a special case of this more general relationship.

The deeply bound ground state energy for a hydrogenic ion follows from (4.56) and (4.68) as

$$E_{0m0} = -Z^2 \left(e^2/2a_0 \right) \ln^2 (a_0/Z\hat{\rho}_m)^2 . \quad (4.69)$$

The effective critical field for ultrastrong effects also scales as Z^2 , so that $Z^2 B_c$ marks the field strength at which the magnetic field dominates the ion's Coulomb potential.

Considering next a two-electron atom such as He, each electron is confined to the lowest Landau state with $n_\rho = 0, m = 0$ and -1 . The resulting Coulomb binding, which is the sum of (4.69) with $m = 0$ and $m = -1$, may be expected to lie lower than the alternative of placing both electrons into $m = 0$ at the expense of putting one in the first excited state of z -motion to satisfy the Pauli principle. The ground state of He is expected, therefore, to have $M = -1$ (and also $M_S = -1$, both electron spins aligned antiparallel to the magnetic field).

A detailed calculation bears out the expectation of the previous paragraph. The lowest singlet state with $M = 0$ and even parity, and the lowest triplet and singlet states with $M = -1$ and odd parity, are described by wavefunctions $\psi(M, S, M_s, \pi)$ constructed to satisfy the Pauli principle

$$\begin{aligned} \psi(0, 0, 0, +) &= \psi_{000}(\rho_1, z_1)\psi_{000}(\rho_2, z_2), \\ \psi(-1, S, M_S, -) &= \left(1/\sqrt{2}\right) [\psi_{000}(\rho_1, z_1)\psi_{0,-1,0}(\rho_2, z_2) \\ &+ (-)^S \psi_{000}(\rho_2, z_2)\psi_{0,-1,0}(\rho_1, z_1)]. \end{aligned} \quad (4.70)$$

With Gaussian forms for the longitudinal wave functions $f_n^{(m)}(z)$ in (4.70), $f^{(m)}(z) = (\alpha_m/\pi)^{1/4} \exp(-\alpha_m z^2)$, and treating the α as variational parameters, a Rayleigh-Ritz variational calculation gives the energies for low-lying states of H^- , together with the energies of H plus electron at infinity (but with the same spin orientation). The binding energy is the difference between the two corresponding curves. As anticipated, H^- has a triplet ground state in an ultrastrong field unlike the singlet at $B = 0$.

Alternatively, by substituting (4.70) into the Schrödinger equation and solving Hartree-Fock equations for $f(z)$, numerical calculations give the results in Fig. 4.14. Even more elaborate calculations with more general basis functions and states up to $n = 10$ have been carried out for the He spectrum in fields of 10^2 – 10^4 T that are relevant to white dwarfs [33], [40].

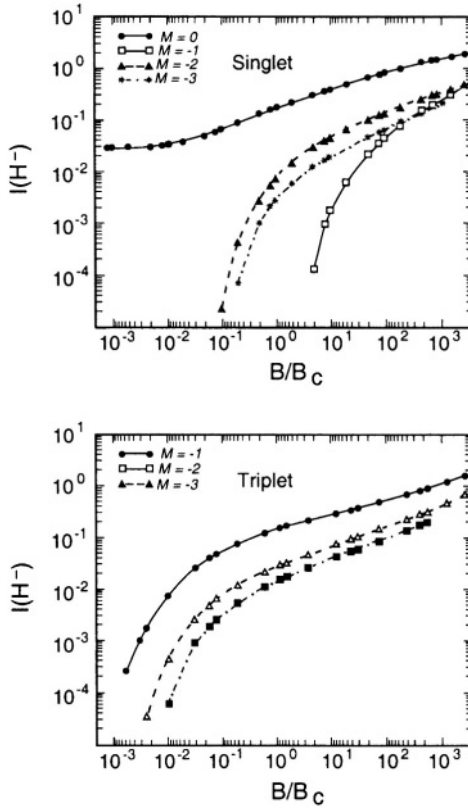


Figure 4.14. Electron detachment energies in a.u. of singlet and triplet states of H^- . From Al-Hujaj and Schmelcher [40].

Variational calculations have been extended to even larger Z -electron atoms [41]. To gain the maximum binding energy, all Z electrons are placed in the deep levels (4.69), the Pauli principle satisfied by distinguishing each in the m quantum number: $0, -1, -2, \dots, -(Z-1)$. In order for the Z -th electron to experience also an ultrastrong field, $\hat{\rho}_{(-Z+1)}$ in (4.59) must also be small compared to (a_0/Z) , so that

$$B > 2 Z^3 B_c \approx 4.7 \times 10^5 Z^3 \text{ T.} \quad (4.71)$$

Pulsar fields, while larger than B_c , fail to satisfy the above for atoms such as iron with $Z > 20$. We will return to this in Section 4.3.4 but for smaller Z values, Hartree calculations with $\psi = \prod_{m=0}^{Z-1} \psi_{0m0}$, using

functions in (4.57) and the choice of exponential functions for $f(z)$ have been carried out.

The binding energy of the last electron, always of interest and particularly so for the ionic composition of the magnetosphere and radiation absorption/emission in the vicinity of neutron stars, turns out to be roughly constant in Z , after an initial drop at low Z : 185 eV for He and 161 eV for Li and thereafter constant at 160 eV for $B = 2.21 \times 10^8$ T. An estimate that includes the effects of antisymmetrization gives the ionization potential as $(160 + 140 \ln \sqrt{Z})$ eV. These values are larger than for laboratory atoms and also show no non-monotonic dependences so that shell structure and The Periodic Table are absent for atoms in ultrastrong magnetic fields.

3.4 Complex atoms in very strong, but not ultrastrong, fields

As noted above in (4.71), the condition that all electrons occupy the nodeless, deeply bound state with logarithmically enhanced binding energy (4.69), is not met for most atoms even in a pulsar's magnetic field. In such a situation, the choice of satisfying the Pauli principle with $n_\rho = 0$ and $n = 0$ for all electrons, with only m different, $(0, -1, -2, \dots)$, is ruled out and some electrons have to be accommodated into $n \neq 0$ while sharing the same lower values of m . Note that higher values of n_ρ and positive m 's are still excluded in determining the ground states of atoms because of the attendant large cost in magnetic energy, such higher quantum numbers lying multiples of $\hbar\omega_c$ above the lowest Landau energy. By the same taken, all electron spins are still aligned antiparallel to the magnetic field, the parallel $m_s = \frac{1}{2}$ requiring an additional energy of $2\hbar\omega_c$.

Under these conditions, which may be dubbed "very strong" but not "ultrastrong", atomic structure is again different from either the laboratory situation or the one discussed in Section 4.3.3. The occurrence of higher n values means the presence of nodes in the longitudinal z -motion and thereby a meaningful momentum p_z . This suggests as an immediate, even if simplified, model for complex atoms in very strong magnetic fields a statistical or Thomas-Fermi model (Section 1.4.3) adapted for this situation. For free electrons in a magnetic field, the energy in (4.8) is independent of p_x . In a volume whose transverse dimensions are L_x and L_y , the number of possible values of p_x in an interval $(p_x, p_x + \Delta p_x)$ is $L_x \Delta p_x / \hbar$. All such values have to be retained for which the orbit center y_0 in (4.7) lies within L_y , that is $\Delta p_x = eBL_y/c$. Hence, the number of states in such a volume of size L_x, L_y , and L_z is

$$(L_x \Delta p_x / h)(L_z \Delta p_z / h) = (eB / h^2 c) V \Delta p_z. \quad (4.72)$$

Given a number density $\rho(\mathbf{r})$, we have then an occupancy of p_z values up to some maximum Fermi momentum p_F according to the relation

$$\rho(\mathbf{r}) = (eB / h^2 c) \int_{-p_F}^{p_F} dp_z = (2eB / h^2 c) p_F. \quad (4.73)$$

With all transverse motion confined to the lowest Landau level and thereby contributing zero energy (recall again that $m_s = -\frac{1}{2}$), the longitudinal kinetic energy density is similarly

$$T_z = (2eB / h^2 c) \int_{-p_F}^{p_F} (p_z / 2\mu) dp_z = e^2 L^5 \rho^3(\mathbf{r}), \quad (4.74)$$

where

$$L \equiv (\pi^4 a_0 \hat{\rho}^4 / 6)^{1/5} \quad (4.75)$$

is a characteristic length made up out of the Bohr radius and the cyclotron radius. This kinetic energy density is drastically different from that in (1.35) for the Thomas-Fermi model for atoms in zero magnetic field. The exponent 3, in particular, in (4.74), which is the adiabatic index, is characteristic of the pseudo one-dimensional electron gas as per the remark following (1.36).

The total energy of the atom, the counterpart of (1.36) which is valid for $B = 0$, now takes the form

$$E = e^2 L^5 \int \rho^3(\mathbf{r}) d\mathbf{r} - Ze^2 \int \rho(\mathbf{r}) r^{-1} d\mathbf{r} + \frac{e^2}{2} \iint \rho(\mathbf{r}_1) \rho(\mathbf{r}_2) d\mathbf{r}_1 d\mathbf{r}_2 / r_{12}. \quad (4.76)$$

Minimization with respect to $\rho(\mathbf{r})$ gives

$$3e^2 L^5 \rho^2(\mathbf{r}) + e[\phi(\mathbf{r}) - \phi_0] = 0, \quad (4.77)$$

where

$$\phi(\mathbf{r}) = -(Ze/r) + e \int d\mathbf{r}' \rho(\mathbf{r}') / |\mathbf{r} - \mathbf{r}'|, \quad (4.78)$$

and ϕ a Lagrange multiplier arising from the condition $\int \rho(\mathbf{r}) d\mathbf{r} = N$, the number of electrons. For neutral atoms, $N = Z$, again $\phi_0 = 0$.

Any anisotropic parts of $\rho(\mathbf{r})$ in (4.76) only serve to increase the energy, so that the ground state must have a spherically symmetric electron number density. This may, at first sight, be surprising given the presence of the strong magnetic field but can be understood on the basis of the picture in Fig. 4.15. Even though individual electrons are in cylindrical volumes of transverse dimension $\hat{\rho}$ as discussed earlier, they arrange themselves as shown into a sphere of radius R so as to minimize the electron-electron repulsion while maximizing the attraction due to the nucleus.

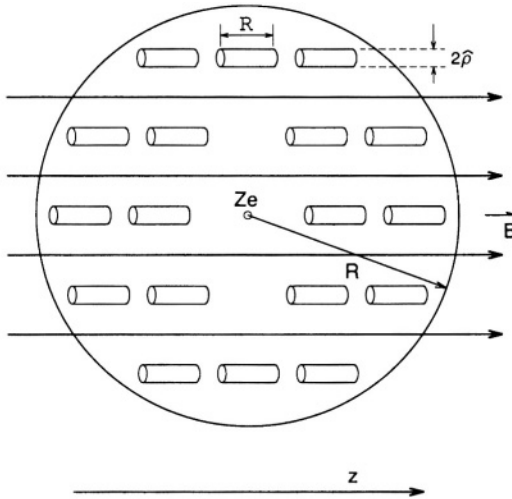


Figure 4.15. Schematic of an atom in a strong magnetic field. Individual electrons distributed over N non-overlapping cylinders form an overall sphere of radius R . From Spruch [6].

Recognizing (4.78) as the Coulomb potential due to the nucleus and electronic charge distribution, Poisson's equation $\nabla^2 \phi = -4\pi e \rho(\mathbf{r})$ gives the Thomas-Fermi differential equation

$$\phi''(x) = [x\phi(x)]^{1/2}, \quad \phi(0) = 1, \quad (4.79)$$

where x is a scaled distance

$$x = (16\pi^2/3Z)^{1/5}(r/L), \quad (4.80)$$

and $\phi(x) = -(r/Ze)[\phi(r) - \phi_0]$. Numerical solution of the above differential equation or, alternatively, variational estimates from (4.76) give for the ground state energy of an N -electron atom with nuclear charge Z under such very strong field conditions,

$$E \approx -150(N^3 Z^6 B^2)^{1/5} \tau \text{ eV}, \quad (4.81)$$

and for its radius

$$R \approx 7 \times 10^{10} (N^2/ZB)^{1/5} \tau^{-1} \text{ cm}, \quad (4.82)$$

where B is in units of 10^8 T and $\tau \equiv (3 - N/Z)^{1/5} 2^{-1/5}$. The atoms are smaller and more tightly bound than their laboratory counterparts and the scaling of E and R with Z also different from the results in Section 1.4.3.

The above results may be expected to be valid when (4.81) lies lower than the corresponding (1.36). Combining also with (4.71), we have

$$\begin{aligned} (Z^{4/3}/5)B_c &\leq B \leq Z^3 B_c, \\ 10^5 Z^{4/3} &\leq B/(1\text{T}) \leq 5 \times 10^5 Z^3, \end{aligned} \quad (4.83)$$

as the value of B for which such a Thomas-Fermi model applies. As before, a simplified treatment of exchange can also be made to extend to a Thomas-Fermi-Dirac model for very strong magnetic fields, the exchange energy taking the form

$$E_{\text{exch}} = 2\pi \hat{\rho}^2 e^2 \int d\mathbf{r} \rho^2(r) \ln[\pi \hat{\rho}^3 \rho(r)]. \quad (4.84)$$

Proceeding beyond the statistical Thomas-Fermi model to incorporate shell structure, much as in Section 1.4.3, the key result is the one given in (4.59) for the radius of each of the Landau levels with $m = 0, -1, -2, \dots$. The electrons in an atom may be considered to fill these values of $|m|$ up to a maximum $|m|_{\text{max}}$ such that its $\hat{\rho}_m$ equals $n^2 a_0/Z'$, that is,

$$|m|_{\text{max}} = n^4 (a_0/Z' \hat{\rho})^2 = (B/2B_c) n^4 / Z'^2. \quad (4.85)$$

It is useful to have an effective charge Z' at this stage which can serve as a variational parameter for the energy expression which will be developed. Once the electrons have filled the values $|m| = 0, 1, \dots, |m|_{\text{max}}$, a new shell n with the next Coulomb energy, $-(Z'e)^2/n^2 a_0$, has to be opened.

For simplicity, considering the total number N of electrons to be so large that shells $n = 1, 2, \dots, n_{\max}$ are completely filled, we have

$$N = (a_0/Z'\hat{\rho})^2 \sum_{n=1}^{n_{\max}} n^4. \quad (4.86)$$

Expressions for the energy also parallel those for laboratory atoms (Section 1.4.3). The virial theorem for this pseudo one-dimensional problem of strong magnetic fields is $\langle T_z \rangle = \langle -V/6 \rangle$, so that we have for such an atom,

$$T_z = (Z'^2/6)(e^2/a_0)(a_0/Z'\hat{\rho})^2 \sum_{n=1}^{n_{\max}} n^2. \quad (4.87)$$

The electron-nuclear potential energy is

$$V_{\text{en}} = -ZZ'(e^2/a_0)(a_0/Z'\hat{\rho})^2 \sum_{n=1}^{n_{\max}} n^2, \quad (4.88)$$

and the electron-electron (direct) energy

$$V_{\text{ee}} = (e^2/2)(a_0/Z'\hat{\rho})^4 \sum_n \sum_{n'} n^4 n'^4 \left(n_{>}^2 a_0/Z' \right)^{-1}, \quad (4.89)$$

where $n_{>}$ is the larger of (n, n') . Ignoring the exchange contribution for simplicity and as having a lower Z -dependence (although it could be incorporated through (4.84)), the total energy is the sum of (4.87) – (4.89). Upon minimization with respect to Z' , the results in (4.81) are again recovered. In addition, however, (4.85) and (4.86) provide a shell structure, with the former providing a characteristic filling factor, the counterpart of $2n^2$ for field-free laboratory atoms. The more rapid increase in n accounts for the smaller size of atoms in very strong fields. Thus, for $B = 10^8$ T, when $(a_0/\hat{\rho}) \approx 20$, all electrons can be accommodated into $n < 5$ even for $N \approx Z \approx 100$. The shell structure, The Periodic Table, and chemistry are very different, therefore, for atoms in very strong fields from that in the laboratory.

The discussion in this and the previous subsection of complex atoms in very strong or ultrastrong magnetic fields represents two limiting cases. For any set of values of Z , N , and $B \ll B_c$, some of the electrons (the inner ones) will be in the very strong field regime while others (the outer ones) are in the ultrastrong domain. Both cases are, therefore, involved. Yet another complication is that once a few electrons are in elongated, cylindrical orbits, their resulting large quadrupole moments become important, leading to strong attraction between neighbouring atoms. This

can result in long-chain molecules becoming the dominant entity, rather than individual atoms. Detailed quantitative calculations become difficult and, notwithstanding much effort, the situation remains unclear [41]. There is some interest in the question because of the nature of the outer crust of neutron stars and whether the presence of such material will permit the stripping of ions and atoms into the magnetosphere by the strong electric fields present on such objects. There are, however, many detailed numerical calculations of small molecules such as H_2^+ and H_2 in strong magnetic fields [42].

4. Strong Magnetic Fields in Astronomy

Magnetic white dwarfs have surface fields of 10^{3-4} T [24]. For example, the spectrum of the hot white dwarf Feige 7 (L795-7) shows well-resolved narrow Zeeman lines corresponding to a magnetic field of 1,800 T. The narrowness of these lines indicates a fairly uniform field strength over the entire surface. In GD90, which has a hydrogen atmosphere, the $H\beta$ line appears as a classic triplet at 479.3, 485.7, and 491.8 nm corresponding to a 500 T field. The $H\gamma$ is seen as a broad absorption centered at 433 nm, the triplet obscured by the quadratic Zeeman effect's many components. Another star, BPM 25114, is seen in the southern skies and its spectrum fitted to model atmosphere calculations and a magnetic field of 3.6×10^3 T.

The origin of such fields on white dwarfs may lie in flux conservation in the core during the collapse of a star, the high conductivity of a carbon-burning core preserving the value of $R^2 B$. These simple scalings when a star collapses suggest fields up to 10^5 T for white dwarfs and 10^9 T for collapse to the smaller radius of a neutron star. An alternative is that they have originated from Ap stars known to have fields of 0.03–3 T, with similar flux conservation during their collapse. Magnetic stars are modeled as oblique rotators, with the dipolar magnetic field inclined to the rotation axis.

Rotating magnetic white dwarfs which are accreting matter from a companion have proved particularly interesting. DQ Her has a 71 s rotation period and is the remnant of a 1934 nova. It is part of an eclipsing binary system with orbital period 4.6 hours. Matter being accreted onto the white dwarf is speeding up the rotation and a field of 100 T has been deduced, strong enough to channel the accretion flow onto the poles. Direct spectral evidence has not been seen from this object, possibly swamped by emission from the surrounding accretion disk, but in AM Her, polarized cyclotron and x-ray emission from such accreted material has been seen. The very strong polarization, both circular and linear, argues for a field strength above 10^3 T, the channeling

of the accretion flow by such a field accounting for the x-ray emission at 5 nm. Grw + 70° 247 is the brightest and one of the most strongly polarized of the magnetic white dwarfs, peaks in the circular polarization at 1.3 and 0.45 μm attributed to first and third cyclotron harmonics of a field in excess of 10^4 T. The strongest field known is about 10^5 T on PG1031 + 234, deduced from its spectrum and polarization.

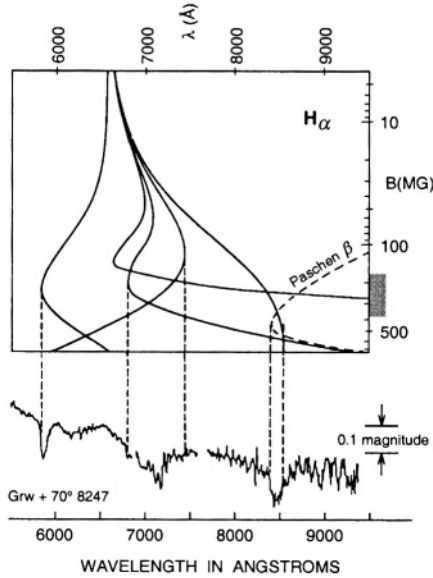


Figure 4.16. Stationary H_α Balmer transitions of hydrogen compared with the optical spectrum of Grw + 70° 8247. A sharp blue edge at 5850 \AA corresponds to the wavelength minimum of a single transition, serving to identify a 320 MG (1 MG=100 T) field on this object. Other transitions, including of the Paschen lines, also correlate with observed features. From Ruder, Wunner, Herold, and Geyer [33], with permission of Springer-Verlag.

Fields of 10^4 T which are far from being perturbative pose the problems discussed earlier in Section 4.2.3 but elaborate numerical calculations now provide reliable energies for low-lying states. Interestingly, the Ly_α $1s, m = 0 \rightarrow p, m = -1$ transition wavelength as a function of field strength reaches a stationary value around 5×10^4 T, the zero field value of 121.6 nm reaching a maximum of 134.3 nm before decreasing again. This stationarity, so that the wavelength is relatively insensitive to variations in B about that value, made possible the identification of a line at 134.7 nm observed by the International Ultraviolet Explorer (IUE) satellite from Grw + 70° 247. This was a happy coincidence because variations in B across the surface tend otherwise to smear out the

transition. Other stationary transitions have since been used to identify the magnetic fields of various white dwarfs, an example shown in Fig. 4.16 [43].

Neutron stars have even stronger magnetic fields, of the order of 10^8 T in radio pulsars and somewhat smaller (10^{5-7} T) in binary pulsars [24], [38]. X-ray binaries also contain neutron stars and are divided into low and high mass types, depending on the mass of the non-degenerate companion star. Most high mass binaries have magnetic fields larger than 10^4 T and accrete from an O or B type star. Their ages are less than 10^7 years whereas low mass binaries are much older, $> 10^9$ years. Their fields range up to 10^6 T. Gamma ray burst sources show lines in the 20 to 70 keV range, again indicators of cyclotron emission between Landau levels in fields of 10^8 T. These objects are presumed to be neutron stars with rotation periods larger than a few seconds.

Problems

- 4.1** Solve the problem of an electron in a constant magnetic field $\mathbf{B} = (0, 0, B)$ in the gauge $\mathbf{A} = (0, Bx, 0)$.
Identify the gauge transformation connecting these solutions to the two considered in the text.
- 4.2** What gauge transformation links the solutions (4.4) and (4.13)?
- 4.3** What is the cyclotron radius and Landau level spacing for electrons in a magnetic field of (a) 10^3 T, (b) 10^8 T?
- 4.4** Estimate the motional Stark field in (4.23) on a neutron star with magnetic field 2×10^8 T if the hydrogen atoms have translational velocities of 100 km/s.
- 4.5** Sketch equipotential contours of the combined Coulomb and diamagnetic fields in (4.25).
Determine the classical turning points for $B = 6$ T, and $\theta = 45^\circ$ and 90° for electrons of energy 0.01 eV.
- 4.6** In analogy with (4.28–30), determine the energy level spacing around zero energy for combined Coulomb and electric (linear Stark) fields.
- 4.7** a) Convert the difference equation (4.32) to the differential equation (4.33) according to the procedure sketched in the text.
Show that the local gauge transformation (4.37) leads to the differential equation (4.38).

- 4.8** Expand the Gaussian distribution, $\exp(-\theta^2/\theta_0^2)$, in terms of Legendre polynomials as $\sum_{\ell} a_{\ell} P_{\ell}(\cos \theta)$ and determine the coefficients a_{ℓ} of the expansion.
- 4.9** From (4.42–44), verify that (4.45) and (4.46) reproduce the desired matrix elements.
- 4.10** Recast the $m = 0$ Schrödinger equation in (4.24) in terms of the semi-parabolic coordinates u and v .
- 4.11** Show that (4.51) gives the spacing $\frac{3}{2}\hbar\omega_c$ around zero energy.
- 4.12** Set up the JWKB formulae analogous to (4.50) and (4.51) for the Coulomb + linear Stark potential and determine dE/dn near zero energy. Use the parabolic coordinates ξ and η , motion in the former being bounded.
- 4.13** For applications in solids with dielectric constant ε and an effective mass m^* for the electrons, obtain an expression for B_c .
- 4.14** Combining (4.84) with (4.76), derive the Thomas-Fermi-Dirac equation for atoms in strong magnetic fields.
- 4.15** With the energy given by (4.87–89), and approximating sums by integrals, minimize to find Z' and the ground state energy of atoms.

Chapter 5

ELECTRON CORRELATIONS

1. Introduction

In this chapter, we will study significant effects and phenomena arising from the interactions among electrons in a many-electron atom. Previous chapters have considered the electron-electron interaction only in its average influence through the mutual screening and the subsequent average self-consistent field experienced by any one of the electrons. Such a description is generally adequate for most phenomena involving only one active electron at a time although we saw in Chapter 2 that for negative ions, a more careful investigation is necessary even in describing their ground state binding energy. However, the correlations between electrons play a more important role once we deal with dynamics that involve more than one electron at a time. Thus, when two electrons are excited simultaneously from the ground state into “doubly-excited states”, these correlations are central to the basic structure and decay (through a process called “autoionization”) of these states. These same states also play a dominant role in the capture of electrons by atoms and positive ions through a process called “dielectronic recombination” which is important in both laboratory and astrophysical plasmas. After a discussion in Section 5.2 of the structure and properties of doubly excited states, Section 5.3 deals with some of the pictures that have been developed to understand them. The process of dielectronic recombination and its applications in astrophysics, together with the effects of external electric and magnetic fields, will be the subject of Section 5.4.

2. Electron Correlations

2.1 Qualitative picture

The potential in an N -electron atom consists of the pairwise Coulomb interactions between all the $(N + 1)$ particles, the N electrons and the nucleus. Self-consistent field methods, such as the Thomas-Fermi or Hartree and Hartree-Fock models discussed in Sections 1.4.3 and 1.4.4, average the electron-electron interaction terms so that each electron can then be regarded as experiencing a potential due to the nucleus and its $(N-1)$ other electron partners. All residual effects due to the electron-electron repulsion terms are then termed the effects of correlation. The configuration interaction calculations discussed in Sections 1.3.3 and 1.4.4, where several alternative independent-electron configurations are superposed in describing the atomic state, embrace these correlations through the matrix elements of the potential between these configurations. Generally, these effects are small, amounting only to a small “correlation energy” as compared to the dominant energy contribution of the principal configuration. Similarly, effects on the wave function also tend to be small so long as one is considering matrix elements of one-electron operators such as those governing photoabsorption. Sometimes, however, particularly with increasing excitation or even in the low-lying states of atoms with several open shells, many configurations are significantly mixed, reflecting stronger electron correlation effects. This is especially so when one turns to multiple excitation when several electrons are simultaneously excited from the ground state.

The N -electron system has many $(3N)$ degrees of freedom but, in the ground state, most of these degrees of freedom may be considered as locked together and effectively frozen. Exciting one electron unfreezes some degrees of freedom but so long as there is only one excited electron, the number of these active degrees of freedom remains limited, no matter how high the excitation, whether to the bound or continuous part of the spectrum. On the other hand, the simultaneous excitation of two electrons unfreezes more, and qualitatively new, degrees of freedom. This is what lends interest to the study of such doubly-excited states, illuminating atomic dynamics not otherwise accessible under single excitation. Of course, exciting more than two electrons brings into play even more degrees of freedom so that the study of triply- or higher multiply-excited states is also of interest. Detailed studies of triply-excited states are only now becoming feasible but in the last three decades, doubly-excited states have been extensively studied and have provided many insights into electron correlation effects. The enormous complexity of the problem and the richness of the phenomena resulting from the ad-

dition of one electron to the exactly-solved hydrogen atom parallels the similar complexity and richness studied in Chapter 4 resulting from the addition of a constant magnetic field.

2.2 The spectrum of He and H^-

Essential aspects of doubly-excited states are conveniently studied in the simplest two-electron systems, namely the helium atom and the negative ion of hydrogen. Consider, for simplicity, the states ${}^1S_0^e$ with total spin, total orbital angular momentum and total angular momentum zero, and even parity, although an exactly similar description applies to any other ${}^{2S+1}L_J^\pi$ state. Fig. 5.1 is a schematic of the ${}^1S_0^e$ spectrum of He and H^- , the individual levels being labeled with independent electron configuration labels (N, ℓ_1, n, ℓ_2) . For the $L = 0$ states under current discussion, ℓ_1 and ℓ_2 are equal, $\ell_1 = \ell_2 = \ell$. Whereas (S, L, J, π) of the combined two electrons are good quantum numbers, their corresponding operators commuting with the two-electron Hamiltonian $H(1,2)$, this is not true of (N, ℓ_1, n, ℓ_2) because their corresponding operators do not commute with the electron-electron interaction $1/r_{12}$ contained in $H(1,2)$. The independent electron labels are, therefore, only partially meaningful, any physical eigenstate involving superpositions of different (N, ℓ_1, n, ℓ_2) configurations. This is a reflection of electron correlations. This is especially so for the states shown in Fig. 5.1 around the excited state thresholds of $He^+(N)$ and $H(N)$ with $N \geq 2$. Thus, even the lowest of these, labeled $2s^2$, being very close in energy to $2p^2$ (the two would be exactly degenerate in a hydrogenic picture with the electron-electron interaction switched off), can be expected to be strongly admixed with it. This situation gets even more extreme with increasing N when more and more states of different (N, ℓ_1, n, ℓ_2) lie close together and get strongly admixed. For all these doubly-excited states, so termed because both N and n are larger than unity, configuration interaction and electron correlation effects are important right from the start.

Another perspective on the spectrum in Fig. 5.1 is provided by viewing the lowest singly-excited states of He shown in Fig. 5.1, $1sn_s$, as a single family of ${}^1S_0^e$ states built on $He^+(1s)$. This includes also the continuum states $1s\epsilon s$ above that threshold at 24.6 eV (all energies measured from the ground state of He). As shown in Fig. 5.1, He and H^- differ substantially in this part of the spectrum, the latter having no singly-excited states at all. Turning next to $N = 2$, a similar family of states $2sn_s$ can be envisaged as built on He^+ or H with $N = 2$. For this family, one electron stays always as $2s$ while its partner ranges from $2s$ through ns to ϵs . The $N = 2$ level of the one-electron atoms He^+ and H is doubly degenerate, so that there exists also a second family of

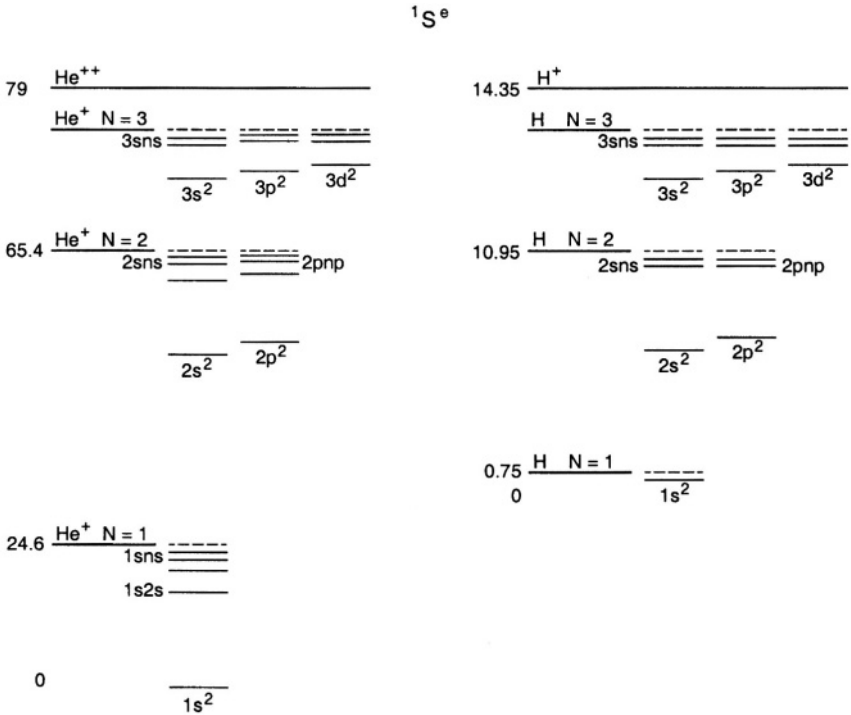


Figure 5.1. Full spectrum of $1S^e$ states of He and H^- , energies in eV above the ground state. Not displayed are the single-electron continuum states above each $\text{H}(N)$ and $\text{He}^+(N)$, and the double-electron continuum above the H^+ and He^{++} levels. Labels correspond to the independent electron picture.

$2pnp$ states of the same $1S_0^e$ symmetry. At the same time, for any energy domain in this region, there is also a singly-excited $1s\epsilon s 1S_0^e$ continuum state that is degenerate with $2sns$ and $2pnp$. Physical eigenstates of the complete $H(1,2)$ are therefore superpositions of the doubly-excited configurations and the underlying singly-excited continuum, the two mixed by the electron-electron interaction. Therefore, they are neither purely bound nor pure continuum states, as are the states of the hydrogen atom or the singly-excited states of He below 24.6 eV. Instead, they are quasi-bound “resonance” states. Were He or H^- to be placed in $2sns$ or $2pnp$, in time the atom would fall apart, one electron dropping down to $1s$ and the other picking up (via the $1/r_{12}$ interaction) the energy released to be ionized as an ϵs electron. Since this happens through a piece of the internal Hamiltonian itself, the phenomenon is called “autoionization”. It is very similar to the phenomenon called the Auger effect wherein a vacancy in an inner shell of an atom is filled by one of the outer elec-

trons, the energy liberated again begin taken up in the ejection of one of the other outer electrons.

Singly-excited states also decay to lower-lying states through radiation emission and thus have finite (radiative) lifetimes. However, at least in principle, upon ignoring the coupling to the radiation field, they can be regarded as bound, just as is the ground state. But doubly-excited states are different in that even with the coupling to the electromagnetic field switched off, they are not strictly bound by virtue of terms contained in $H(1,2)$ itself. This is true for all the doubly-excited states of He and H^- shown in Fig. 5.1, including the sets built on higher states of $He^+(N)$ and $H(N)$ with $N > 2$. In every case, there is always at least one underlying continuum in which they are embedded. However, in some heavy atoms, the energy of the doubly-excited state may lie below the first ionization threshold and such states do not autoionize. That is, in such atoms it takes less energy to excite simultaneously two electrons than to ionize the atom. Notable examples occur in the alkaline earths, beginning with calcium where $3d4p$ states lie below the Ca^+4s continuum at 6.1 eV.

Fig. 5.1 also makes clear the close similarity between He and H^- as regards the doubly-excited part of the spectrum. The two systems differ drastically with respect to singly-excited states, H^- having none at all while He has multiply infinite series of Rydberg states for an electron in the Coulomb field of $He^+(1s)$. But, as regards doubly-excited states, both involve two electrons in the field of a positive charge, the two ions H^+ and He^{++} differing only in the value of that charge (and, in the slightly different effective masses). Multiple series of doubly-excited states occur, therefore, in both systems. The states can be grouped broadly into two classes, depending on whether the two electrons are on par in their excitation or are very different. For the former, which are called “ridge” states, the term to be discussed in Section 5.3.4, He and H^- are completely analogous as isoelectronic partners, a pair of electrons quasi-bound to a positive charge Z (equal to 2 and 1, respectively). When the electrons are disparate in their excitation, one closer to the nucleus than the other, the states are named “valley” states and here the two systems are somewhat different. Such states can be pictured as in Fig. 5.1, grouped into families associated with single-electron energy levels of the inner electron. In He, these are the $He^+(N \geq 2)$ thresholds and the second, “outer”, electron is then bound by the Coulomb potential into states $n \geq N$. In H^- , on the other hand, each $H(N \geq 2)$ level attracts the outer electron not with a Coulomb but rather the dipole $1/r^2$ potential discussed in Section 3.2.3. Such an attractive dipole potential also supports an infinite sequence of states for the outer electron

but with a characteristic spacing different from a Coulomb field, the spacing between successive levels diminishing exponentially in n .

Just as with radiative decay (Section 2.2.3), selection rules govern the process of autoionization decay of doubly-excited states. These follow from the nature of the interaction governing this decay, namely, the electron-electron interaction $1/r_{12}$. This operator is of even parity and commutes with S^2 , L^2 , and J^2 so that the selection rules that follow are that none of these quantum numbers changes in an autoionization. In particular, that the parity and J of initial and final states are equal is an absolute selection rule. The values of S and L may, however, change, particularly in heavier atoms where spin-orbit and spin-spin interactions may combine with $1/r_{12}$ to cause the decay. In He and H^- , the $2sns$ and $2pnp$ states shown in Fig. 5.1 can decay only to the $1s\epsilon s\ ^1S_0^o$ continuum. On the other hand, $^1P_1^o$ or $^3P_1^o$ states such as $2snp$, $2pns$ or $2pnd$ (usually admixed together), decay to the $1s\epsilon p$ continuum which has the same symmetries. These “allowed” autoionization decays have lifetimes typically 10^{-12} – 10^{-13} s, that is, the rates are much larger than typical allowed radiative decays. In general, all $^{1,3}L^\pi$ states with $\pi = (-1)^L$ have allowed autoionization to the $1s\epsilon L$ continua. On the other hand, a doubly-excited state with parity $(-1)^{L+1}$ such as $^3D_2^o$ is forbidden by parity conservation to decay into $1s\epsilon d$. In this case, decay is possible into the $1s\epsilon p\ ^3P_2^o$ continuum but requires the mediation of spin-orbit or other interactions which are weak in He and H^- (but not in isoelectronic analogs of higher Z). The $2p^2\ ^3P_j^e$ state is an example, similar J and parity available only in the $1s\epsilon s$ and $1s\epsilon d$ continua, so that a change in L is necessary. In such situations, autoionization can become so unfavorable that radiative decay will dominate, as for instance in He, $2p^2\ ^3P^e \rightarrow 1snp\ ^3P^o$. In H^- , since there are no singly-excited bound states available, the decay has to be into $1s\epsilon p\ ^3P^o$, which means that both a photon and an electron are simultaneously ejected. The rate of this process is $5.8 \times 10^8\ s^{-1}$, close to the $4.7 \times 10^8\ s^{-1}$ value for the $Ly_\alpha\ 2p \rightarrow 1s$ transition in hydrogen. This suggests a mainly spectator role for the second electron which is “shaken-off” into the ϵp continuum. With the $^3P^e$ state in H^- lying 0.01 eV below the $n = 2$ state of H, it may contribute significantly to the solar continuum as a broad peak on the long wavelength side of the Ly_α transition.

Doubly-excited states in other, heavier atoms afford similar examples. A very interesting one is in He^- . In the ground state of He, unlike in hydrogen, there is no binding for an extra electron so that He^- does not exist as a stable species with possible configuration $1s^2 2s$. However, a doubly-excited state $1s2s2p^4\ P_j^o$ forms a long-lived species, lying $631\ cm^{-1}$ below He $1s2s\ ^3S$. (One could regard this equally as an inner-shell

excitation of one $1s$ electron to $2p$ or as a double excitation, with $2s$ excited to $2p$ and one $1s$ to $2s$. The choice between them is a matter of terminology, these single electron descriptions not rigorously valid anyway). The underlying continuum is perforce a doublet: $1s^2\epsilon p^2P^o$. A spin-flip is involved in the autoionization decay which makes it weak already for $J = \frac{1}{2}$ and $\frac{3}{2}$ but the $J = \frac{5}{2}$ does not have even that option. It has to decay to the $1s^2\epsilon f^2F_{5/2}^o$ continuum. The high orbital angular momentum value of 3 for the ejected electron further disfavors such a decay; recall that the wave function for $\ell = 3$ is suppressed at small r by the centrifugal barrier. In all, the $1s2s2p^4P_{5/2}^o$ state of He^- has an autoionization lifetime of 3.5×10^{-4} s. Thus beams of such states that live long enough to traverse several meters in the laboratory can be, and are, made and studied, even though He^- is not a stable species.

2.3 Experimental observation

As with singly-excited states in atoms, doubly-excited states can be formed under various impact: photon, electron, and heavy charged particles. The first laboratory experiments were of electron collisions with He in the energy range close to the 20.4 eV for the first excitation threshold of He $1s2s^1S$. Electrons of kinetic energy just below this threshold formed temporary negative ion states $1s2s^2$ of He^- which, under autoionization, decayed back to the ground state of He. They, therefore, appeared as resonances in the elastic cross-section of electrons from He. Higher states decay into both the elastic and excited continuum channels and may be observed thus, an example given in Fig. 5.2 [44], and even triply-excited states have been observed [45] (Fig. 5.3). In photoabsorption from the ground state of He, selection rules restrict the excitation to $^1P^o$ symmetry so that, in the first experiments of this kind, doubly-excited states of this symmetry just below the $\text{He}^+(N = 2)$ threshold at 65.4 eV (see Fig. 5.1) were seen. Photons of such energy first became available in the 1960s with synchrotrons and Fig. 5.4 presents the photoabsorption spectrum from the first such observation. Today, as shown in Fig. 5.5, current generation synchrotrons provide an even richer spectrum of such doubly-excited states in He and in other atoms [46]. Triply-excited states have also been seen in synchrotron excitation [47] (Fig. 5.6).

Instead of single-photon excitation with synchrotron light, multiple photon absorption from visible lasers can also be used for double excitation [48]. An example is provided in Fig. 5.7. Doubly-excited states of H^- , seen in photodetachment of this negative ion by laser photons that

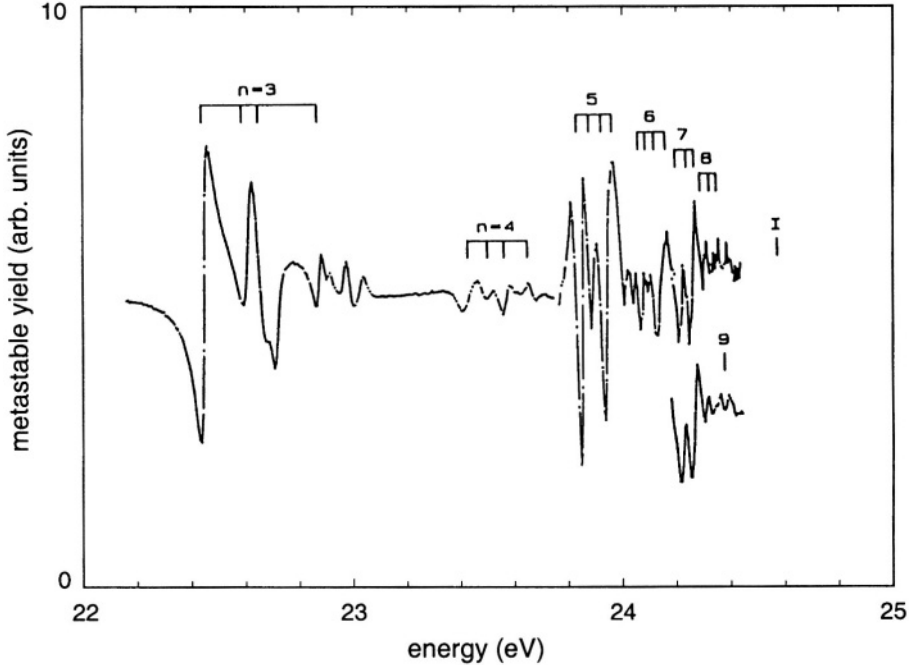


Figure 5.2. Yield of metastable He upon collision of helium in the ground state with electrons of kinetic energy shown. Note series of doubly-excited state He^- resonances with quantum numbers of the outer two electrons both exceeding values up to $n = 9$. From [44].

were Doppler shifted into the 10–14 eV energy range, are shown in Fig. 5.8 [49].

Doubly-excited states are also formed in the collision of protons, or heavier positively-charged particles, with atoms (Fig. 2.4). And, their formation as intermediates in the process of electron-ion recombination through the process called dielectronic recombination is important in planetary and stellar atmospheres. This will be discussed in Section 5.4.

3. Hyperspherical Coordinates

There is a variety of methods for viewing electron correlations, that in terms of configuration interaction between configurations built up of single electron orbitals being one of them. As in Section 5.2 above or earlier in Section 1.3.3, stronger correlations are manifest in the superposition of a larger number of such configurations. As an example, a tight angular correlation between two electrons in a $^1S_0^e$ state is only realized by superposing a large number of ℓ values from zero to some

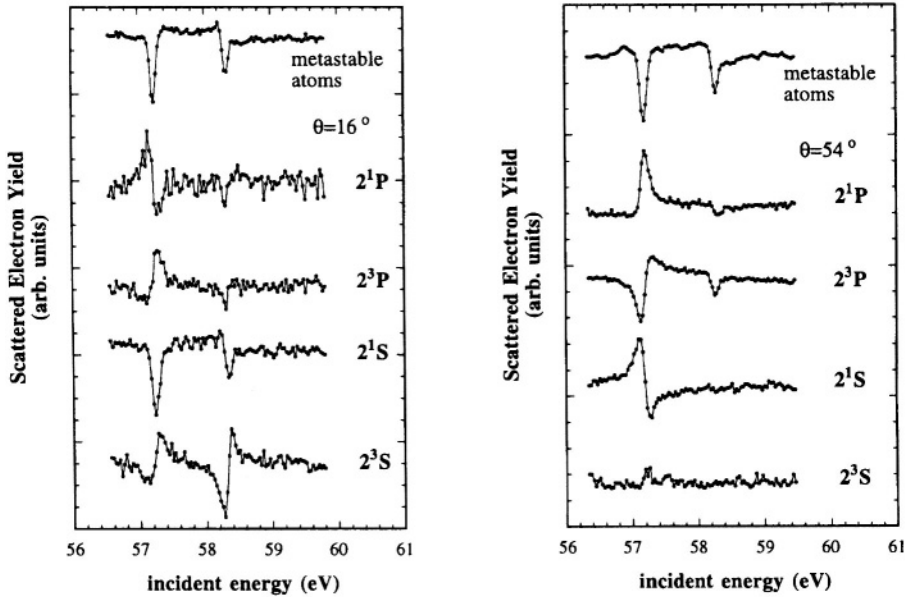


Figure 5.3. Excitation functions for four $n = 2$ states of helium upon electron impact near the 60 eV energy region at two different scattering angles. The top spectrum is the metastable atom excitation function recorded simultaneously with the electron spectra. Angular distribution and energy values serve to identify the resonance structures as $2s^2p^2P$ and $2sp^2^2D$ triply-excited states of He^- . From Trantham *et al* [45].

large number. The uncertainty relation between the ℓ value and the conjugate angle, in this case the angle θ_{12} between the two electronic radii vectors \mathbf{r}_1 and \mathbf{r}_2 , requires such a large superposition in order that the wave function be confined to a narrow range of θ_{12} . As can be seen from Fig. 5.1, high doubly-excited states, with large N and lying close to the double ionization threshold where states with such large values of ℓ are available and lie close together (even degenerate), can be expected to display such tight correlations. Similar remarks apply to radial correlations between the two electrons to be discussed further below, involving mixing of large numbers of (N, n) configurations.

An alternative to the description in terms of independent electrons is to develop a basis which has inherently a two-electron description from the start, such as functions sharply confined in θ_{12} . With the two-electron Schrödinger equation non-separable in any coordinate system, there is no single, natural or unique basis, or set of quantum labels. The choice between different bases is dictated by ease of handling for compu-

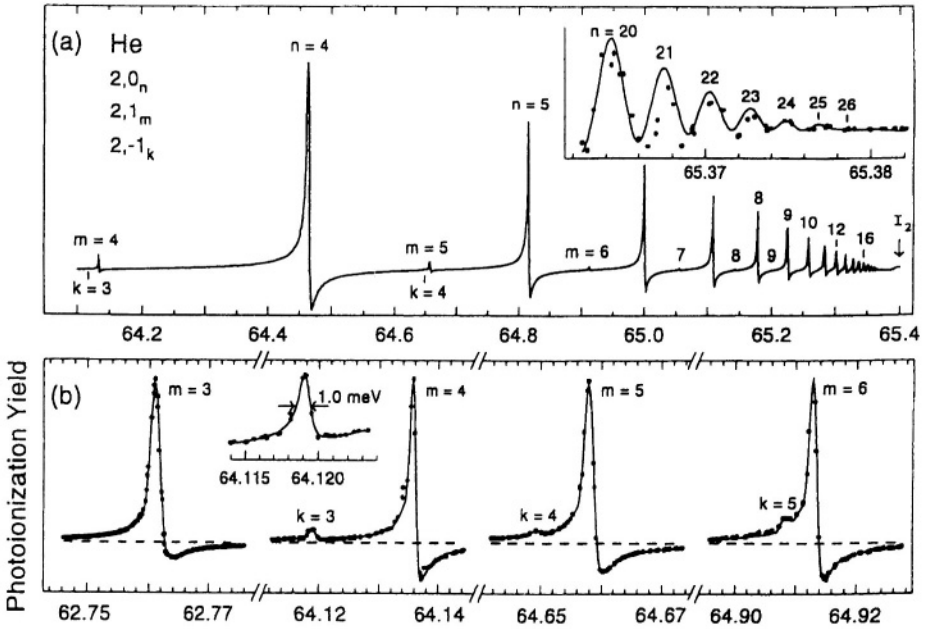


Figure 5.5. Recent observations of $1P^o$ doubly-excited states of He below $\text{He}^+(N=2)$. (a) Resonances of all three series, (b) resonances of the secondary ("minus") and weak ("2pnd") series at higher magnification. From [46].

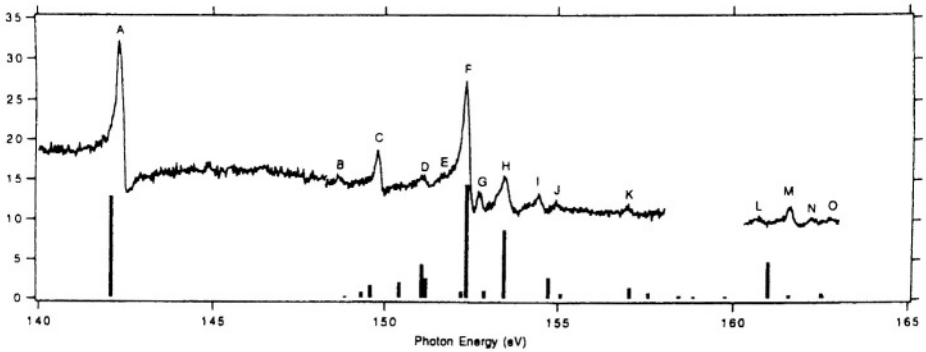


Figure 5.6. Triply-excited "hollow" lithium states as a function of synchrotron photon energy observed by detection of Li^+ ion yield. The bar overlay shows theoretically calculated level positions. From Azuma *et al* [47].

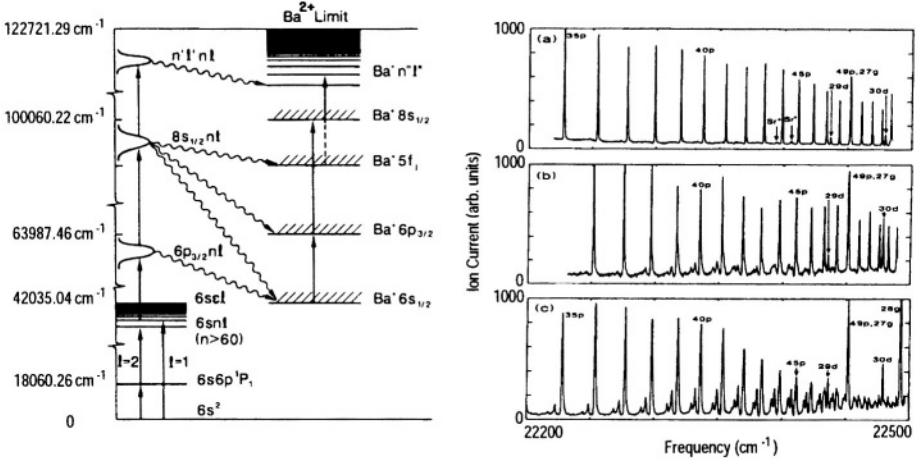


Figure 5.7. Schematic of multiple laser excitation scheme and observed doubly-excited states of barium $n'pnd$ with (a) $n = 54$, (b) $n = 66$, and (c) $n = 72$. One or two pulsed dye lasers first excite $6snp$ or $6snd$, $n > 60$, followed by excitation to a $6pnl$ autoionizing state which is then raised to $8snl$ by another dye laser. A final laser drives the $8snl \rightarrow n'pnd$ state that is observed. From Jones and Gallagher [48].

$$R = \left(r_1^2 + r_2^2 \right)^{1/2}, \quad \alpha = \arctan (r_2/r_1). \quad (5.2)$$

R is a radial distance of the six-dimensional hypersphere, and α , with range $(0, \frac{1}{2}\pi)$, relates to radial correlations just as θ_{12} does to angles. Thus, restriction to small relative ratio of electronic distances from the nucleus corresponds to restriction to $\alpha \approx 0$ or $\frac{1}{2}\pi$, whereas a function restricted to both electrons essentially on par in their radial distances is constrained to $\alpha \approx \frac{1}{4}\pi$. Besides these three “pair” coordinates (R, α, θ_{12}) , three others called Euler angles provide the orientation in space of the plane containing the nucleus and the two electrons. These pair hyperspherical coordinates provide an alternative to the independent electron set $(\mathbf{r}_1, \mathbf{r}_2)$ with the advantage that a description in terms of them focuses on the full three-body system of He or H^- down even to the very coordinates used. In particular, R is an index of the overall size of the system, playing a role analogous to r for the hydrogen atom, while α and θ_{12} are convenient tracers of radial and angular correlation, respectively.

The potential in the system is a function of (R, α, θ_{12}) , independent of the Euler angles:

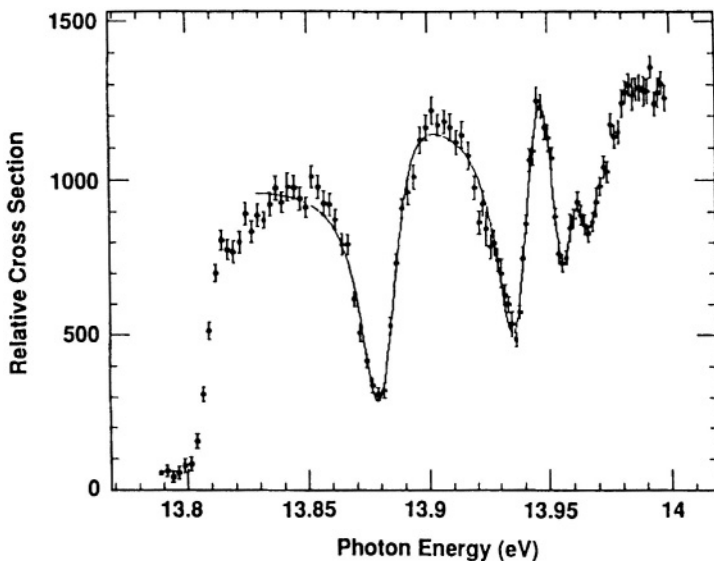


Figure 5.8. $\text{H}^-(N=6, n)$ doubly-excited states seen in photodetachment of H^- to $\text{H}(N=5) + e$. From [51].

$$\begin{aligned}
 V(\mathbf{r}_1, \mathbf{r}_2) &= -Ze^2 \left(\frac{1}{r_1} + \frac{1}{r_2} \right) + \frac{e^2}{r_{12}} \\
 &= C(\alpha, \theta_{12}) e^2 / R, \quad (5.3)
 \end{aligned}$$

where

$$C(\alpha, \theta_{12}) = -Z \left(\frac{1}{\sin \alpha} + \frac{1}{\cos \alpha} \right) + \frac{1}{(1 - \sin 2\alpha \cos \theta_{12})^{1/2}} \quad (5.4)$$

represents an effective Coulomb charge in the six-dimensional hyperspace with anisotropic dependence on the angles α and θ_{12} . Fig. 5.9 provides a sketch for $Z = 2$. At every R , this two-dimensional potential surface is the backdrop for the motion of the configuration point of the He/H^- system.

Writing also the kinetic energy operator, $-\frac{1}{2} (\nabla_1^2 + \nabla_2^2)$, in hyperspherical coordinates, one has

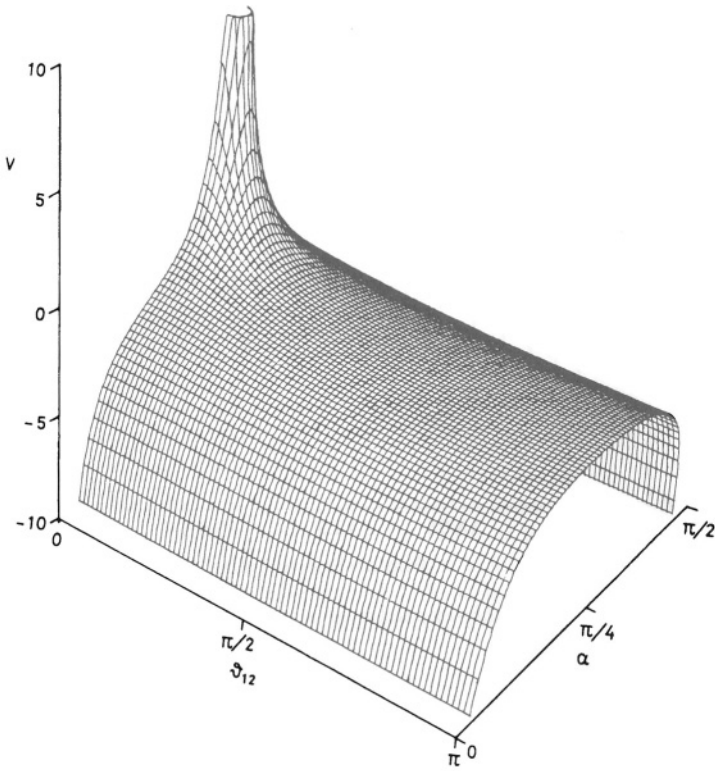


Figure 5.9. Two-electron potential surface in (5.4). Half the range $(0, 2\pi)$ of θ_{12} is shown, the other half obtained symmetrically by reflection. Note the saddle point at $\alpha = \pi/4, \theta_{12} = \pi$. From [51], courtesy of J. Knudson.

$$T(\mathbf{r}_1, \mathbf{r}_2) = -\frac{\hbar^2}{2\mu} \left\{ \frac{1}{R^{5/2}} \frac{\partial}{\partial R} R^{5/2} \frac{\partial}{\partial R} - \frac{\Lambda^2(\hat{R}) + 15/4}{R^2} \right\}, \quad (5.5)$$

where

$$\Lambda^2(\hat{R}) \equiv \frac{\ell_1^2}{\cos^2 \alpha} + \frac{\ell_2^2}{\sin^2 \alpha} - \frac{1}{\sin \alpha \cos \alpha} \frac{\partial^2}{\partial \alpha^2} \sin \alpha \cos \alpha - 4 \quad (5.6)$$

is called the “grand angular momentum” because of its obvious similarity to and generalization of the angular momentum \mathbf{L}^2 in the hydrogen atom. The set of five angular coordinates \hat{R} includes α , θ_{12} , and the three Euler angles. Note that besides ℓ_1^2 and ℓ_2^2 which are the usual

angular momentum operators of the two electrons (scaled by trigonometric factors in α), Λ^2 includes second derivatives with respect to the pseudo-angle α .

The two-electron Schrödinger equation thereby takes the following form in hyperspherical coordinates:

$$\left[-\frac{\hbar^2/2\mu}{R^{5/2}} \frac{\partial}{\partial R} R^{5/2} \frac{\partial}{\partial R} + \hbar^2 \frac{\Lambda^2(\hat{R}) + \frac{15}{4}}{2\mu R^2} + \frac{C(\alpha, \theta_{12})e^2}{R} - E \right] \Psi(R, \hat{R}) = 0. \quad (5.7)$$

This is again non-separable because of the different dependences on R of the angular kinetic energy and the Coulomb potential.

3.1 Coulomb potential and hyperspherical harmonics in six dimensions

The two-electron Schrödinger equation is not separable either in the independent-electron coordinates $(\mathbf{r}_1, \mathbf{r}_2)$ or in the hyperspherical coordinates (R, \hat{R}) . Had the α and θ_{12} dependent terms in (5.7) shared the same dependence on R , or had the coefficient $C(\alpha, \theta_{12})$ been independent of angles, then the problem would have separated in hyperspherical coordinates. Indeed, in the latter case, (5.7) would have been a six-dimensional Coulomb problem of fixed nuclear charge C , a higher-dimensional analog of the three-dimensional system of the hydrogen atom. Its eigenvalue spectrum would have bound states with energies

$$-\frac{1}{2} \frac{C^2 e^2}{\left(\nu + \frac{3}{2}\right)^2 a_0}, \quad \nu = 1, 2, 3, \dots \quad (5.8)$$

and a continuum of positive energies. The “principal” quantum number ν , associated with the hyperradius R , is the analog of n for the hydrogen atom in (1.2), and $\frac{3}{2}$ the dimensional element (for the Coulomb potential in any dimension D , this element is $\frac{1}{2}(D - 3)$).

Each state ν is highly degenerate, encompassing the various eigenstates in \hat{R} of the grand angular momentum Λ^2 , whose eigenvalues and eigenfunctions are

$$\Lambda^2 \phi_{n_{rc} \ell_1 \ell_2 LM}(\hat{R}) = \lambda(\lambda + 4) \phi_{n_{rc} \ell_1 \ell_2 LM}(\hat{R}), \quad (5.9)$$

with

$$\lambda = \ell_1 + \ell_2 + 2n_{rc} \quad (5.10)$$

taking values $\lambda = 0, 1, 2, \dots, (\nu - 1)$, and ϕ given by

$$\begin{aligned} \phi_{n_{rc}\ell_1\ell_2LM} &= \cos^{\ell_1+1} \alpha \sin^{\ell_2+1} \alpha {}_2F_1 \left(-n_{rc} + \ell_1 + \ell_2; \ell_2 + \frac{3}{2}; \sin^2 \alpha \right) \\ &\times Y_{\ell_1\ell_2LM}(\hat{r}_1, \hat{r}_2). \end{aligned} \quad (5.11)$$

In the above, n_{rc} is a radial correlation quantum number associated with the coordinate α , the ${}_2F_1$ a hypergeometric function which, for the case of integer n_{rc} of interest, becomes a Gegenbauer polynomial, and Y is a coupled two-particle angular harmonic with $\ell_1 + \ell_2 = L$,

$$Y_{\ell_1\ell_2LM}(\hat{r}_1, \hat{r}_2) = \sum_{m_1 m_2} \langle \ell_1 \ell_2 LM | \ell_1 m_1 \ell_2 m_2 \rangle Y_{\ell_1}^{m_1}(\hat{r}_1) Y_{\ell_2}^{m_2}(\hat{r}_2). \quad (5.12)$$

The Y 's here are standard spherical harmonics and the coupling introduces the standard Clebsch-Gordan coefficients, the summation running over all m_1 values compatible with $m_1 + m_2 = M$. The 4 in the eigenvalue in (5.9) is again the six-dimensional value of the general dimensional element (D-2) for hyperspherical harmonics.

With the coordinate R symmetric under interchange of the electronic labels 1 and 2, the antisymmetrization required by the Pauli principle is entirely in terms of the angular and spin variables. Since this interchange takes α to $\frac{1}{2}\pi - \alpha$, the required functions are

$$\phi_{n_{rc}\ell_1\ell_2LM}(\alpha, \hat{r}_1, \hat{r}_2) + (-)^S \phi_{n_{rc}\ell_1\ell_2LM} \left(\frac{1}{2}\pi - \alpha, \hat{r}_2, \hat{r}_1 \right), \quad (5.13)$$

with $S = 0, 1$ the total spin of the two electrons.

With Λ^2 in (5.7) replaced by $\lambda(\lambda+4)$, the radial Coulomb equation that remains is exactly analogous to that of the hydrogen atom in (1.8). Its eigenvalues have already been noted in (5.8) and the eigenfunctions are Laguerre polynomials in R , just as in (1.9). The full wave functions of such a six-dimensional Coulomb potential are then products of these radial functions and the angular functions (5.13). They provide a complete basis set for the two-electron problem (continuum functions have to be included as well) which has an effective charge $C(\alpha, \theta_{12})$ that is angular dependent. Such a pair basis set of six-dimensional Coulomb functions

is thereby an alternative to the basis set of products of independent-electron functions used in more conventional configuration interaction methods. Under differing circumstances, one or the other alternative may be preferred, the test being whether convergence and accuracy is achieved with fewer terms in the expansion.

3.2 Adiabatic hyperspherical method

We consider next yet another alternative approximation method for solving the non-separable equation when written in the form (5.7). This method has antecedents elsewhere in physics, an example to be considered later in Section 6.2.3 for molecular systems. The term adiabatic is applied to them generically, this word having the meaning of “slow” and applied whenever dependence on one physical parameter is slow compared to the rest. In such a situation, the slow variable is considered frozen while the motion of the faster variables is first solved. These solutions then determine the motion in the slow coordinate. This provides a natural, hierarchical way to proceed whenever an adiabatic variable is identified.

In the present context, the variable R has been identified as measuring the overall size of the two-electron system, while the angles α and θ_{12} contained in \hat{R} are measures of correlation between the electrons in energy and angle. Arguing, therefore, for the greater importance of these correlations in doubly-excited states, one can consider an adiabatic separation between R and \hat{R} . First freezing R as a fixed parameter, the angular part of the Schrödinger equation (5.7) is solved, that is, eigenvalues and eigenfunctions obtained of the operator $(\Lambda^2/2R^2 + C/R)$:

$$\left[\hbar^2 \frac{\Lambda^2(\alpha, \theta_{12}) + \frac{15}{4}}{2\mu R^2} + \frac{C(\alpha, \theta_{12})e^2}{R} \right] \Phi_\mu(R; \hat{R}) = U_\mu(R) \Phi_\mu(R; \hat{R}), \quad (5.14)$$

the eigenvalues U_μ and eigenfunctions Φ_μ at this stage depending parametrically on R . The index μ includes definitely the conserved quantum numbers L and M but also any other labels that arise at this stage. Expansion in suitable basis functions or direct numerical solution in several variables may be used for this solution, one natural choice being to use the hyperspherical harmonics in (5.9). Eigenfunctions of (5.14) will involve superpositions of several (ℓ_1, ℓ_2) pairs, this being a reflection of angular correlation. These eigenfunctions $\Phi_\mu(R; \hat{R})$ provide a basis for expansion of the full two-electron wave function $\Psi(R, \hat{R})$ in (5.7),

$$\Psi(R, \hat{R}) = \sum_{\mu} F_{\mu}(R) \Phi_{\mu}(R; \hat{R}). \quad (5.15)$$

Inserting (5.15) into (5.7) and using (5.14) leads to coupled differential equations for the radial functions,

$$\left[-\frac{\hbar^2}{2\mu} R^{-5/2} \frac{d}{dR} R^{5/2} \frac{d}{dR} + U_{\mu}(R) - E \right] F_{\mu}(R) = \sum_{\nu} V_{\mu\nu}(R) F_{\nu}(R), \quad (5.16)$$

where $V_{\mu\nu}(R)$ includes matrix elements of d/dR and d^2/dR^2 between $\Phi_{\nu}(R; \hat{R})$ and $\Phi_{\mu}(R; \hat{R})$. They stem from the dependence on R of the Φ_{μ} , reflecting the non-separability of R from \hat{R} .

The set (5.16) of coupled equations is exact if the infinity of basis states μ and ν is retained but, in practice of course, one has to truncate the set, thereby introducing the approximation called the adiabatic hyperspherical approximation. The extreme consists of dropping all the coupling terms $V_{\mu\nu}$, so that each hyperspherical channel μ stands decoupled as a single radial equation with a potential well $U_{\mu}(R)$. Fig. 5.10 provides a sketch of such potentials for $^1S^e$ states in He and Fig. 5.11 for $^1P^o$ states in H^- below the $N = 2$ single ionization thresholds. The form of these potentials can be understood from (5.14) by inspection. The steep repulsive barrier, $(\lambda + \frac{3}{2})(\lambda + \frac{5}{2})/2R^2$, at small R is followed by an attractive well formed by the superposition of the attractive Coulomb $1/R$ and the repulsive $1/R^2$ potentials. At large R , all the terms in (5.14) vanish so that $U_{\mu}(R)$ goes asymptotically to zero, the double ionization energy. For applications, however, to states lying below successive single ionization thresholds, $He^+ (N \geq 2) + e$ or $H(N \geq 2) + e$, one attaches $U_{\mu}(R)$ at large R to the appropriate behavior in these cases. This can be achieved either by simply connecting to the asymptotic forms beyond a certain value of R or by supplementing the basis so as to include not just hyperspherical harmonics but also some single-electron functions in which one electron is confined to the state N . These asymptotic forms consist of the hydrogenic ionization threshold value plus dominantly the Coulomb potential between He^+ and the electron, that is $-e^2/R$, or the dipole potential between $H(N \geq 2)$ and the outer electron. As seen in Section 3.2.3, this dipole potential has an attractive piece $-\alpha_N/R^2$.

Note that two potential wells converge to $N = 2$ in $^1S^e$ symmetry and three in $^1P^o$ symmetry (Figs. 5.10 and 5.11). In independent electron configurations (see Fig. 5.1), these are, respectively, $2sns$ and $2pn_p$ for 1S and $2snp$, $2pns$, and $2pnd$ for $^1P^o$. The adiabatic potential wells

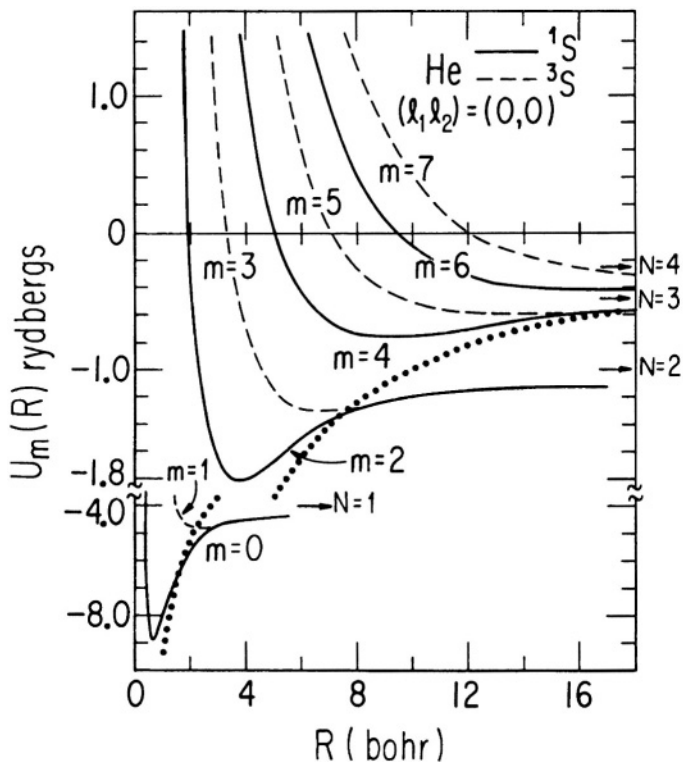


Figure 5.10. Adiabatic hyperspherical potential wells for $1,3S$ states of helium converging to successive $\text{He}^+(N)$ limits. From U. Fano and C. D. Lin, in *Atomic Physics* 4, eds. G. Z. Putlitz, E. W. Weber, and A. Winnaker (Plenum, New York, 1975), with permission.

represent alternative superpositions of these configurations. Thus, each μ represents a particular mix of radial and angular correlation between the two electrons. Correspondingly, in coordinate space, the correlations restrict the electronic distributions in α and θ_{12} to specific values. The deeper wells, for instance, have the electrons further apart, $\theta_{12} \approx \pi$, thereby lowering their mutual repulsion. This trend becomes sharper with increasing N .

The labels + and - on two of the $1P^o$ potential wells in Fig. 5.11 signify that these are constituted mainly of $2snp \pm 2pns$ with a very little admix of $2pnd$, whereas the third and most repulsive well is dominantly of $2pnd$ character. The almost equal mix of $2snp$ and $2pns$ with plus and minus combinations in amplitudes is plausible, these configurations

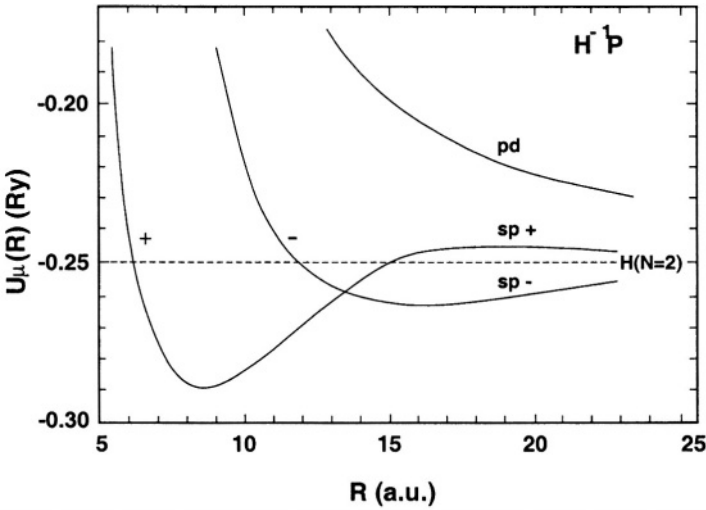


Figure 5.11. Hyperspherical potential wells for $1P^\circ$ states of H^- converging to $H(N=2)$. From C. D. Lin, Phys. Rev. Lett. **35**, 1150 (1975).

being essentially identical and degenerate in the absence of the electron-electron interaction and, therefore, strongly admixed by it. At large R , the degenerate electric dipole of $H(N=2)$ being attractive in one and repulsive in two of the channels, the $-$ well approaches threshold from below (the value of α_N for it is $3.71 ea_0$) whereas the other two wells do so from above. The $+$ and $-$ also have significance for radial correlation between the electrons, these states being, respectively, symmetric and antisymmetric under the purely radial interchange, $r_1 \leftrightarrow r_2$.

Bound and continuum state eigenvalues and eigenfunctions calculated by solving the radial Schrödinger equation in these wells describe two-electron states associated with the $N=2$ threshold. Thus, in $H^- 1P^\circ$, the $-$ well with a sufficiently attractive dipole potential at large R supports an infinite series of bound states below the $H(N=2)$ threshold, two of them having been experimentally observed. Since a dipole potential's eigenvalues are exponentially dependent on ν , higher levels rapidly lie so close to the threshold as to be experimentally unresolvable. Further, the exact degeneracy between $H(2s)$ and $H(2p)$ leading to this dipole being lifted by the Lamb shift, the number of states is limited to a finite value in any case, the dipole model valid only so long as the binding energy of ν is larger than this Lamb shift. As seen from Fig.

5.11, the + well on the other hand, being repulsive at large R , can support only a finite number of states held inside the inner well and indeed only one such is known, lying slightly above the threshold, the electron temporarily held within the outer barrier of the potential but tunneling out through it. The $2pnd$ well in Fig. 5.11 supports no bound states at all.

All the eigenvalues discussed here, whether for + or -, are also, of course, not strictly bound since they can autoionize to the single-electron continuum states $1s\epsilon p$. They are "quasi-bound" states or "resonances". The same considerations apply to higher values of N , the number of potential wells correspondingly larger. In every case, there is one well which has an asymptotic attractive dipole potential, capable of binding a sequence of autoionizing resonances below that threshold with a characteristic exponential dependence on ν of their binding energies. Such states have been observed experimentally and successfully accounted for by adiabatic hyperspherical calculations for $N \leq 7$ (see Fig. 5.8).

The case of He $^1P^\circ$ is different in that in a figure analogous to Fig. 5.11, all three potential wells have asymptotically an attractive Coulomb tail due to the He⁺ + e interaction. The degenerate dipole potential in this case is overshadowed by this Coulomb potential. All three wells support infinite sequences of Rydberg states, labeled by $\nu = 1, 2, \dots \infty$. Because of their very different correlation patterns, excitation mechanisms may be very different for the different μ . Indeed, as shown in Fig. 5.4, only one Rydberg series was seen in the first observations, that marked +. This is because photoabsorption from the ground state is governed by matrix elements of the dipole operator \mathbf{r} (see (2.16)) from the He $1s^2\ ^1S$ state to these $^1P^\circ$ states. This ground state being confined to small radial distances, only those states with significant overlap with them acquire appreciable optical oscillator strength. States in the highest μ channel have little such wave function amplitude at small R because of the large angular momentum barrier (see Fig. 5.11, He being little different from H⁻ in this range of R). The $2snp$ and $2pns$ being very similar in their radial functions, the - combination reduces the small R wave function drastically, so that this state too is unfavored in its excitation oscillator strength. Only the + states, which have significant overlap with the ground state, are thereby seen. This observation of only a single Rydberg series in the first experiments (Fig. 5.4) was, therefore, a dramatic early indicator of the effects of electron correlation. There is a close analogy to other phenomena in physics, such as in the decay of the K°, \bar{K}° system of elementary particles, where mixing of nearly degenerate states in + and - combinations has a dramatic realization in their observed properties. The other two series in He ($N = 2$) were later

seen in synchrotron experiments (Fig. 5.5), weaker by many orders of magnitudes than the + in their oscillator strengths.

For reasons that parallel + states having stronger optical excitation oscillator strength, they have stronger autoionization decays as well. The underlying continuum for this decay is $1s\epsilon p$, with one electron's wave function confined to small distances. Its overlap, therefore, is stronger with the wave function of the + state than the others. Thereby, matrix elements of the operator $1/r_{12}$ which determine the decay amplitude are much larger for the + state than the other two. Correspondingly, the + states have broader decay widths than the - and "2pnd", by many orders of magnitude. The same common physics, stemming from their structure, that makes them easier to excite from the ground state also makes easier their autoionization decay to the ground state continuum.

3.3 Description of resonances

The doubly-excited states in He and H^- , as discussed above in Section 5.3.2, are superpositions of bound and continuum state character and are resonances of these three-body systems. They are conveniently classified into two classes, called "shape" and "Feshbach" resonances, depending on whether their decay with one electron escaping to infinity proceeds primarily through quantum tunneling of that electron through a potential barrier (hence dependent on the shape of that barrier) or because of the aspect of a bound state being embedded in a continuum. The $N = 2$ $^1P^o$ resonances of H^- provide examples of both, the resonance in the + channel being a shape resonance whereas the dipole sequence of - states are Feshbach resonances. As in this example, Feshbach resonances always lie below the continuum threshold with which they are associated ($H(N = 2)$ in this case) and are sharp whereas shape resonances typically lie just above that threshold and are broad [51] (Fig. 5.12).

The circumstance of a discrete state embedded in a continuum is general, existing throughout physics, with important examples in condensed matter, nuclear, and particle physics as well. If the discrete state $|d\rangle$ with energy E_d mixes with a continuum of energy-normalized states $|\epsilon\rangle$ with energies ϵ of a Hamiltonian H , we have

$$\begin{aligned}\langle d|H|d\rangle &= E_d, \\ \langle \epsilon|H|\epsilon'\rangle &= \epsilon \delta(\epsilon - \epsilon'), \\ \langle \epsilon|H|d\rangle &= V_\epsilon.\end{aligned}\tag{5.17}$$

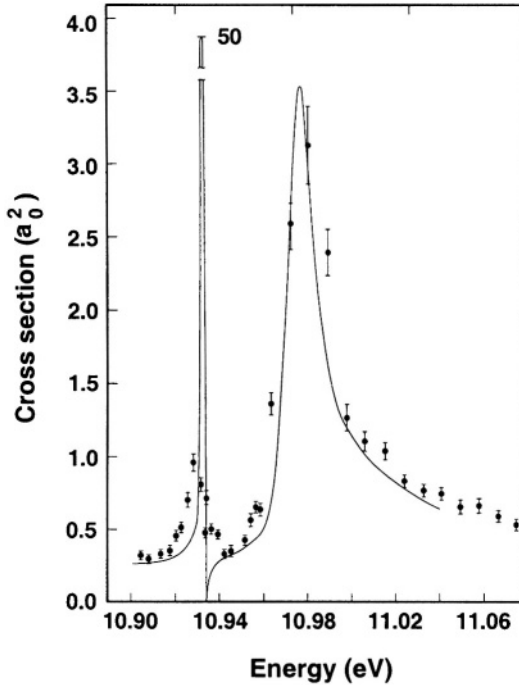


Figure 5.12. A narrow Feshbach and a broad shape resonance of doubly-excited $1P^o$ states of $H^-(N = 2)$ observed in photodetachment. From H. C. Bryant *et al*, Phys. Rev. Lett. **38**, 228 (1977).

With the energy-normalization choice made for continuum wave functions, V_ε has dimensions of $(\text{energy})^{1/2}$.

The physical eigenstate $|E\rangle$ is given by the superposition

$$|E\rangle = a|d\rangle + \int d\varepsilon b_\varepsilon |\varepsilon\rangle, \tag{5.18}$$

where both coefficients a and b_ε will in general depend on E . Applying the Hamiltonian operator to (5.18) and projecting on $\langle d|$ and $\langle \varepsilon'|$, we have, respectively,

$$\begin{aligned} E_d a + \int d\varepsilon V_\varepsilon^* b_\varepsilon &= E a, \\ V_\varepsilon a + \varepsilon' b_{\varepsilon'} &= E b_{\varepsilon'}. \end{aligned} \tag{5.19}$$

In solving (5.19) for $b_{\varepsilon'}$ in terms of a , division by $E - \varepsilon'$ which can become singular requires identification of a principal part and a delta-function contribution from the singularity:

$$b_{\varepsilon'} = \left[\frac{P}{E - \varepsilon'} + \xi(E) \delta(E - \varepsilon') \right] a, \quad (5.20)$$

where $\xi(E)$ is determined through appropriate boundary conditions. Inserting (5.20) into (5.19) gives

$$E = E_d + P \int d\varepsilon' \frac{|V_{\varepsilon'}|^2}{E - \varepsilon'} + \xi(E) |V_E|^2. \quad (5.21)$$

Continuum states $|\varepsilon'\rangle$ have wave functions with the asymptotic form $\psi_{\varepsilon'} \sim \sin(k'r + \delta_b)$, where $\varepsilon' = \frac{1}{2} k'^2$, and δ_b is a background phase shift. With this form, we have from (5.20)

$$\int d\varepsilon' b_{\varepsilon'} \psi_{\varepsilon'} \sim \sin(k'r + \delta_b + \delta_{\text{res}}). \quad (5.22)$$

with

$$\delta_{\text{res}} = -\arctan[\pi/\xi(E)] \quad (5.23)$$

reflecting an additional phase shift because of the configuration interaction with the discrete state $|d\rangle$. From (5.21) and (5.23), as E traverses the value

$$E_{\text{res}} = E_d + P \int d\varepsilon' \frac{|V_{\varepsilon'}|^2}{E - \varepsilon'}, \quad (5.24)$$

$\xi(E)$ changes sign and thereby δ_{res} varies by π . The smaller is the $|V_E|^2$ that multiplies $\xi(E)$ in (5.21), the sharper is this variation for values of E around E_{res} . The discrete state embedded in the continuum, therefore, appears as a resonance, the asymptotic phase shift varying by π in an energy interval $|V_E|^2$ about the energy value E_{res} which is shifted from E_d by the second term in (5.24), again because of the configuration interaction. This variation in the phase shift translates into sharp variations in scattering cross-sections in this energy range.

The coefficients a and b_{ε} can be evaluated as

$$\begin{aligned} a &= (\sin \delta_{\text{res}})/\pi V_E, \\ b_{\varepsilon} &= \frac{V_{\varepsilon}}{\pi V_E} \frac{\sin \delta_{\text{res}}}{E - \varepsilon} - (\cos \delta_{\text{res}}) \delta(E - \varepsilon). \end{aligned} \quad (5.25)$$

If such an embedded discrete state $|E\rangle$ is excited from say the ground state $|0\rangle$ of the system by photoabsorption, the dipole matrix element

that determines the oscillator strength, $\langle E|z|0\rangle$, similarly varies sharply around E_{res} . Indeed

$$\frac{|\langle E|z|0\rangle|^2}{|\langle \varepsilon|z|0\rangle|^2} = \frac{(q + \tilde{E})^2}{1 + \tilde{E}^2}, \quad (5.26)$$

with

$$\tilde{E} = \frac{E - E_{\text{res}}}{\pi|V_E|^2} = -\cot \delta_{\text{res}}, \quad (5.27)$$

and

$$q = \frac{\langle d|z|0\rangle + \text{P} \int d\varepsilon \frac{\langle d|H|\varepsilon\rangle\langle \varepsilon|z|0\rangle}{E - \varepsilon}}{\pi\langle d|H|\varepsilon = E\rangle\langle \varepsilon = E|z|0\rangle}. \quad (5.28)$$

Eq. (5.26) expresses the modified photoabsorption cross-section relative to that of the pure continuum because of the presence of the embedded discrete state. In terms of the “reduced energy” \tilde{E} , measured from the “resonance position” E_{res} in dimensionless units, $\pi|V_E|^2$ (called the half-width $\frac{1}{2}\Gamma_A$ of the resonance), this modified form has a characteristic shape as shown in Fig. 5.13 for a range of values of the “profile index” q .

The three parameters $\{E_{\text{res}}, \frac{1}{2}\Gamma_A, q\}$ together characterize the general shape of a Feshbach resonance which arises from a discrete state embedded in a continuum. The resonances in He and H^- in Figs. 5.4 and 5.12 are of this form. Note, in particular, from (5.26) that the cross-section has a point of zero at $\tilde{E} = -q$, reflecting a complete destructive interference between the alternative pathways, one through $|d\rangle$ and the other through $|\varepsilon\rangle$. When q is large, (5.26) reduces to a “Lorentzian” shape, $(1 + \tilde{E}^2)^{-1}$. This applies to the situation when the background continuum is itself weakly excited, $\langle \varepsilon = E|z|0\rangle$ in the denominator of (5.28) being small. Such a situation is called a Breit-Wigner resonance. Resonances in nuclear and particle physics are often of this shape but doubly-excited resonances in atoms display a much wider range of q values, including the situation $q = 0$ wherein the cross-section dips at the resonance center $\tilde{E} = 0$. Apart from these extreme values of q , when the resonance profile is a symmetric hump or dip, the profile is generally asymmetric, showing both constructive and destructive interference between the two paths (directly to the continuum and via the embedded discrete state) over the energy span of the resonance.

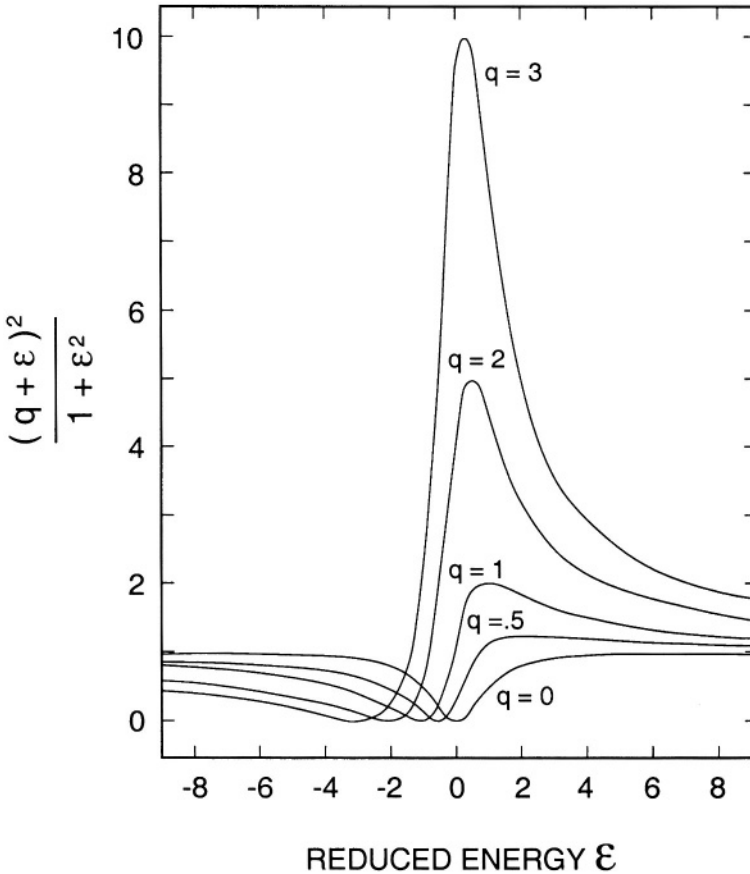


Figure 5.13. Beutler-Fano profiles with different values of the Fano q -parameter. From U. Fano, *Phys. Rev.* **124**, 1866 (1961).

The numerator of (5.28) expresses the dipole excitation to the discrete state, both directly and through the principal part contribution of neighboring continuum states. The denominator, on the other hand, is the excitation amplitude through the degenerate continuum state with energy E . The profile index q , therefore, expresses the ratio of these two contributions. The resonance width $\Gamma_A = 2\pi|V_E|^2$ is given by this degenerate coupling matrix element $V_E = \langle \varepsilon = E | H | d \rangle$. Through the usual energy-time uncertainty relationship, \hbar/Γ_A may be interpreted as the autoionization lifetime of the quasi-bound state.

3.4 High-lying doubly-excited states and double ionization

The adiabatic hyperspherical method has been very successful in describing energies, widths, and profiles of doubly-excited states converging to single ionization thresholds with $N \leq 6$ in He and H^- . It can also be adapted to the study of such two-electron states in more complex atoms, the nucleus and the rest of the electrons in the atom then constituting a more complex structured core than the bare nucleus of He and H^- [4]. But, as is clear from Fig. 5.1, since successive single ionization thresholds N themselves form a Rydberg series that piles up on the double ionization threshold, the potential wells $U_\mu(R)$ as in Figs. 5.10 and 5.11 that converge to these single thresholds overlap as N gets large. Inevitably, the coupling matrix elements $V_{\mu\nu}$ in (5.16) can no longer be ignored and this entire set of coupled equations have to be solved as a single system, a hopeless task particularly close to the double ionization limit, both the number of thresholds N and the number of wells for each N becoming explosively large.

The handling of very high doubly-excited states close to the double ionization limit poses, therefore, the same challenge to the hyperspherical method as it does to conventional configuration interaction with bases formed out of products of independent electron functions. A pointer to how to proceed in the case of a dominant family of high doubly-excited states is provided, however, by the low-lying states. As noted for the $+$ states with $N = 2$, the wave function shows a concentration in the region around $\alpha = \frac{1}{4}\pi$, $\theta_{12} = \pi$ which represents a saddle point of the potential surface in Fig. 5.9. The same feature is seen in similar adiabatic hyperspherical calculations with $N > 2$. Indeed, one explanation for the relatively long lifetime of these states lies in this concentration or “localization” of their wave functions into a sub-region of the full domain of α and θ_{12} whereas singly-excited states, including the continuum states built on single ionization thresholds, have their wave function mostly in the deep valleys of Fig. 5.9 around $\alpha = 0$ and $\frac{1}{2}\pi$. As a result, the overlap between the wave functions is small and along with it the matrix element of $1/r_{12}$ between them which governs the autoionization decay is also small, thus suppressing the decay.

Companion states of double ionization just above threshold, when two slow electrons escape to infinity from a positive charge, also point to the importance of the saddle region of Fig. 5.9. Both theoretical analysis and direct evidence from a variety of experiments show that in all such situations, the double escape conforms to the saddle configuration [4]. Thus, the electrons escape in opposite directions from the nucleus, the

value of θ_{12} confined more and more tightly to π as the energy E above threshold approaches to zero.

The above cues suggest an alternative basis for two-electron states within the hyperspherical approach, which may be termed a “pair basis” and concerns itself throughout with the pair hyperspherical coordinates and corresponding quantum numbers, referring only to the double (again pair) ionization threshold with no involvement of single ionization thresholds and the one-electron quantum number N . With the saddle region singled out for special emphasis, one expands the Schrödinger equation (5.7) around the saddle point, retaining terms up to quadratic powers of $(\frac{1}{4}\pi - \alpha)$ and $(\pi - \theta_{12})$. With such an expansion, the potential in (5.3) and (5.4) is that of a harmonic oscillator in the θ_{12} and an inverted oscillator in the α coordinate, the multiplicative squared frequency in both cases being proportional to $1/R$ and involving the nuclear charge Z . The Schrödinger equation now separates partially to terms of order $1/R^2$ in terms of the variables $\{\sqrt{R}, R^{1/4}(\frac{1}{4}\pi - \alpha), R^{1/4}(\pi - \theta_{12})\}$. Thus, a corresponding basis set of functions can be constructed, with quantum numbers corresponding to these three coordinates: a principal quantum number ν conjugate to R , a quantum number ν conjugate to θ_{12} , and a continuous index for the α motion which has a purely continuous spectrum. In terms of these, the two-electron states of Fig. 5.1 are viewed in an alternative grouping to that set (N, n, ℓ) , as shown in Fig. 5.14. With all reference to independent electrons removed, this is a description consistently throughout of a pair of electrons as an entity attached to the nucleus, quasi-bound states below and double escape states above the double-ionization threshold. Such a correlated pair basis is an extreme alternative to the independent-electron one, particularly well suited to describing two-electron states whose wave functions are concentrated in the saddle region of the potential surface. These have been called “ridge” states.

The two-electron Schrödinger equation illustrates well general features of a genuinely non-separable problem, one in which there is no set of coordinates in terms of which the partial differential equation separates. Unlike in the one-electron hydrogen atom where quantum numbers can be unambiguously assigned to each coordinate, there is no such possibility now, only alternative sets based on various quasi-separabilities, each suited to a specific context. Thus, independent-electron labeling, adiabatic hyperspherical, or the pair description, all provide alternative views of two-electron states. In each case, a complete set of states provides of course a full description, any state of the two-electron atom expressible in terms of an infinite expansion over the basis states. Dif-

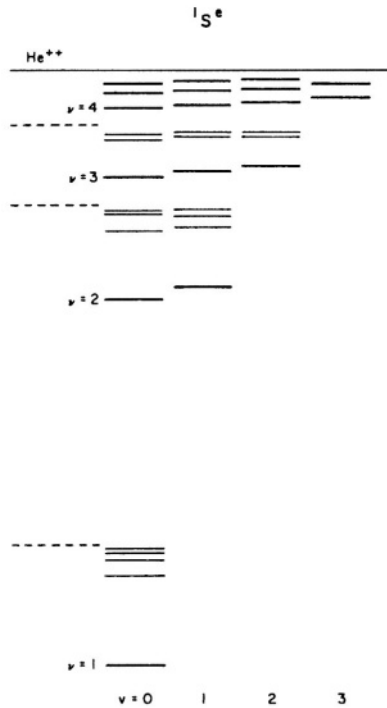


Figure 5.14. Pair description of the $1S^e$ spectrum of He, with pair quantum numbers (ν, v) . Contrast with the independent-electron description in Fig. 5.1. From A. R. P. Rau, in *Atomic Physics 9*, eds. R. S. VanDyck Jr. and E. N. Fortson (World Scientific, Singapore, 1984), with permission of the publisher.

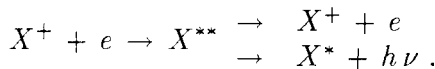
ferent ranges of the spectrum and different types of states (ridge or valley) find one or the other alternatives more economical, requiring fewer terms in the corresponding expansion for an accurate description. Even in the separable hydrogen atom, there is no unique set of quantum numbers or corresponding basis, both the spherical and parabolic descriptions/separations of Sections 1.2.1 and 1.2.2, for instance, being equally valid and complete. Once again, the context decides which one is more suitable. Non-separable problems carry this one step further, an exact description only possible, in principle, as an expansion, and all practical calculations requiring truncation of such an expansion. This truncation is usually done in state space, a finite number of configuration states retained while integrations are carried out over all of geometric coordinate space. The expansion described around the saddle presents an

alternative, the coordinate space truncated to the saddle region but then the Schrödinger equation solved exactly as a quasi-separable problem.

4. Dielectronic Recombination

The integrated oscillator strength for photoabsorption from the ground to doubly-excited states of atoms is never more than about 1% so that their direct role in stellar opacities has not been observed. Instead, one of the important roles for doubly-excited states is as intermediates in the capture of electrons by positive ions in astrophysical and laboratory plasmas. As noted in Section 2.4.3, direct capture accompanied by radiation emission, a process called radiative recombination (RR), is unfavored in many situations. Thus, consider capture of an electron of some low kinetic energy E by Li^+ ($1s^2\ ^1S$) into a Rydberg state $\text{Li}(1s^2n\ell^2\ell)$ with the energy released, $E + |\varepsilon(n\ell)|$, being radiated as a photon. Although energetically possible, such a direct capture is highly suppressed, particularly for high n , the process being akin to a free electron (both the continuum and high Rydberg electron being essentially free) radiating a photon which is forbidden by kinematics (the photon being massless, both energy and momentum cannot be simultaneously conserved in such a process). On the other hand, if the energy E is such that it is close to a doubly-excited state $1s2pn\ell$ of Li, the electron can be captured temporarily into such a state. Subsequently, this state can undergo an autoionization decay back to Li^+ ($1s^2\ ^1S$) + e (E), in which case no capture results, or the $2p$ electron may radiatively decay back to $1s$ so that the system ends up as $\text{Li}(1s^2n\ell)$ plus radiated photon. Fig. 5.15 is a schematic rendering of such a process. Clearly, the relative rates for autoionization and radiative decay play a crucial role. That such a process may be astrophysically important was first suggested by Sayers in 1939 and named “dielectronic recombination” (DR) by Massey and Bates in 1942, the name emphasizing the role played by a pair of electrons, the incident one and an electron in the ion [52]. Starting from the work of Burgess and Seaton, DR has come to be recognized as of major importance in a variety of astrophysical situations.

The formation and alternative decays of the intermediate doubly-excited state can be pictured in general as



With α_c the rate coefficient for capture into X^{**} and α_d the rate for DR, we have as balance equations

$$N_e N(X^+) \alpha_c = N(X^{**}) (\Gamma_A + \Gamma_R),$$

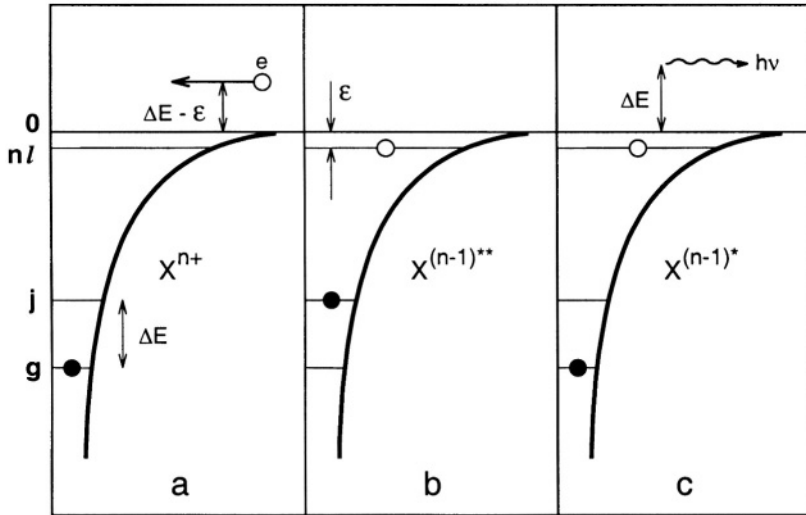


Figure 5.15. Diagram illustrating dielectronic recombination. (a) and (b) Initial capture of electron into nl with excitation of ion $g \rightarrow j$. (c) Stabilization with radiation $j \rightarrow g$. From G. H. Dunn [52], with permission from author and Taylor and Francis Ltd.

$$N_e N(X^*) \alpha_d = N(X^{**}) \Gamma_R, \tag{5.29}$$

where Γ_A and Γ_R are the autoionization and radiative decay widths, so that

$$\alpha_d = \alpha_c \Gamma_R / (\Gamma_A + \Gamma_R), \tag{5.30}$$

or equivalently, in terms of cross-sections for DR and capture,

$$\sigma_d = \sigma_c \Gamma_R / (\Gamma_A + \Gamma_R). \tag{5.31}$$

The initial capture being the inverse process of autoionization, α_c is itself proportional to Γ_A besides temperature-dependent factors of the Boltzmann-Saha formula (1.44) so that

$$\alpha_d = \frac{g^{**}}{2g^+} \left(\frac{h^2}{2\pi m k T} \right)^{3/2} \exp(-E(X^{**})/kT) \frac{\Gamma_A \Gamma_R}{\Gamma_A + \Gamma_R}, \tag{5.32}$$

where the g 's are statistical weights of the X^{**} and X^* states, and $E(X^{**})$ is the energy of the X^{**} state relative to X^+ . With typical autoionization lifetimes much smaller than radiative ones (10^{-13} s vs 10^{-8} s), so that $\Gamma_A \gg \Gamma_R$, the last factor in (5.32) reduces essentially to Γ_R . However, with increasing n , since Γ_A decreases as $1/n^3$ whereas Γ_R remains essentially constant and equal to the decay rate in the ion, the outer $n\ell$ electron playing an inconsequential role as a spectator, α_d becomes proportional to Γ_A and thereby drops off rapidly with n . Similarly, for DR with highly charged ions, where Γ_R increases with Z while Γ_A is essentially independent of the nuclear charge, only a few low values of n contribute appreciably.

Since many n and ℓ values of $1s2pn\ell$ contribute, the total DR rate can be appreciable. The radiated photon frequency $1s2pn\ell \rightarrow 1s^2n\ell$ lies close to the value in the ion, $1s2p \rightarrow 1s^2$, so that these transitions show up as DR "satellites" of that ionic transition. With increasing n , they merge into the ionic value, the screening effect of that outer Rydberg electron becoming negligible. This is why DR is important and must be accounted for if that ionic transition is used as a diagnostic (say for temperature) in a laboratory or astrophysical context.

DR is generally important at higher temperatures, typically dominating over RR for $T > 10^5$ K. It is, therefore, the dominant recombination process in the solar corona (10^6 K, 10^8 cm $^{-3}$) and in solar flares (10^7 K). However, it can contribute even at lower temperatures, only the low-lying X^{**} being relevant because of the exponential factor in (5.32). Thus, in nebulae, the recombination in $C^{3+} + e$ plays a big role, lines at 229.7 nm from C^{2+} ($2p^2^1D \rightarrow 2s2p^1P$) being seen in IUE (International Ultraviolet Explorer) spectra. Typical α_d values for a nebular temperature of 10^4 K are about 10^{-11} cm 3 s $^{-1}$.

The effect of external fields, including even relatively weak electric fields, on DR has only recently been appreciated [52], [53], following dramatic enhancements seen in laboratory experiments involving Mg^+ and Ca^+ . Thus, the DR process, $e + Mg^+(3s) \rightarrow Mg^{**}(3pnf) \rightarrow Mg(3s^2) + h\nu(3p \rightarrow 3s)$, is strongly enhanced by even a few V/cm electric fields. This is again a consequence of the dependence of Γ_A on n and ℓ . Besides the fall-off as $1/n^3$, Γ_A decreases rapidly with ℓ as well. This is because of decreasing overlap of the corresponding wave functions in the matrix element of $1/r_{12}$ that is involved. As a result, in summing over n and ℓ for the total DR rate, ordinarily only a small subset of ℓ , $\ell < 6$, contribute. However, an external electric field, because of the linear Stark mixing in the degenerate ℓ -manifold can access this much larger "reservoir" of ℓ -values at any n . Enhancements of several-fold have been measured. The enhancement is less important for DR in highly-charged

ions because, as noted above, only low values of n contribute in those cases, Γ_A being smaller than Γ_R only for them, and these do not have the reservoir of ℓ values to be exploited.

Magnetic fields seem to have less of an effect but recent studies indicate that “crossed” electric and magnetic fields, with the two fields perpendicular, can lead to substantial enhancements of DR [53]. In such a situation, both m and ℓ cease to be good quantum numbers so that not only the reservoir of ℓ values but also those in m can be accessed. This subject is likely to be very important in the coming years both because of its application to laboratory and astrophysical plasmas and because of fundamental questions posed. As seen in Chapter 4, the study of high Rydberg states in a magnetic field is already non-trivial. It is even more so for crossed fields when even the azimuthal symmetry no longer holds and the Schrödinger equation is non-separable not just in two but in all three dimensions $\{\rho, z, \varphi\}$ or $\{r, \theta, \varphi\}$. Combine this with electron correlations in high doubly-excited states, a problem also of great subtlety as seen in this chapter, and it is clear that the resulting subject of two-electron states in external fields, particularly of perpendicular geometry, will be of great interest and importance in atomic physics in the future.

Problems

- 5.1 Consider the singly-excited states of krypton upon photoabsorption from the ground state. Enumerate the channels and provide the angular momentum quantum numbers that label them.
- 5.2 An intense beam of laser light, tunable around 353 nm, illuminates H^- in the ground state such that three-photon absorption is possible. Which doubly-excited states may be excited in this case?
- 5.3 Expand the sharply-peaked distribution $\delta(1 + \cos \theta_{12})$ of two electrons at a mutual angle $\theta_{12} = \arccos(\hat{r}_1 \cdot \hat{r}_2) = \pi$ in terms of Legendre polynomials $P_\ell(\cos \theta_{12})$ and determine the expansion coefficients.
- 5.4 Consider a Gaussian angular distribution, $\exp\left\{-\frac{(\pi - \theta_{12})^2}{\theta_0^2}\right\}$, with θ_0 a constant, and make an expansion similar to the one in Problem 5.3. Sketch the distribution of the coefficients as a function of ℓ and note the reciprocal relationship to the angular distribution in θ_{12} .
- 5.5 Make the transformation to hyperspherical coordinates to verify explicitly the Schrödinger equation in (5.7).

- 5.6** Following the procedure in the text, derive (5.16).
- 5.7** Enumerate the number of adiabatic potential wells for $^1P^o$ states of He that converge to the $N = 4$ threshold of He.
- 5.8** Carry out the steps indicated in the text to verify Eqs. (5.19)–(5.28).
- 5.9** Fit the H^- Feshbach resonance shown in Fig. 5.12 to the form (5.26) and determine q and Γ .
- 5.10** Expand the Schrödinger equation in (5.7) for 1S states around the saddle point $\alpha = \frac{1}{4}\pi$, $\theta_{12} = \pi$, retaining terms up to quadratic in $(\frac{1}{4}\pi - \alpha)$ and $(\pi - \theta_{12})$. Show that the resulting equation admits a partial separability in the variables $\{R^{1/2}, \xi = (\frac{1}{4}\pi - \alpha) R^{1/4}, \eta = (\pi - \theta_{12}) R^{1/4}\}$, with wave functions of the form $\psi = \exp \left[icR^{1/2} \left\{ 1 + \frac{1}{2}a\xi^2 + ib\eta^2 \right\} \right] \chi(R)$, with a, b , and c constants.

Chapter 6

DIATOMIC MOLECULES

1. Introduction

Just as in terrestrial physics, molecules are abundant in a variety of astronomical contexts. Indeed, since molecular bands are more easily seen than atomic lines at low resolution, they are even used in the gross classification of stars, *e.g.* the intensity of TiO bands defines the subdivisions of M-type stars. Both small, inorganic molecules and large organic ones occur and often have important roles in stellar atmospheres and in large interstellar gas clouds besides in planetary atmospheres as on our Earth. Some of the extremes in density and temperature encountered in astronomical objects compared to those in our laboratories on Earth make some exotic molecules unusually important. The primordial black-body radiation from The Big Bang was first seen in rotational transitions of the CN molecule although not recognized as such at that time. And, as regards the commonest element in the Universe, it is estimated that about half of hydrogen in the interstellar medium is present in the form of molecular H₂. In this and the next chapter, we take up, therefore, the study of molecular physics, first considering diatomic molecules such as H₂, O₂, N₂, NO, CO, etc., and then, in the next chapter, polyatomic molecules. The list of molecules seen in radio and mm wavelengths from the interstellar medium is large and constantly growing. Chemical modeling, therefore, requires reaction rates and cross-sections, sometimes of over a hundred species and a thousand reactions in studying dense interstellar clouds.

We begin in Section 6.2 with a study of the basic quantum physics of molecular binding and of molecular spectroscopy. The role of the nuclear degrees of freedom, which have been unimportant so far in pre-

vious chapters that dealt with single atoms, and of their interplay with the electronic degrees of freedom, is the central object of study. Vibrations and rotations of the inter-nuclear axis, and electronic structure, will be discussed first for the simplest one-electron diatomic molecular ion, H_2^+ , and then extended to neutral species such as H_2 . Section 6.3 will deal with spectroscopic transitions involving these various types of excitations, and Section 6.4 will present a sample of transitions and collisions of interest in astrophysics.

2. Structure of Diatomic Molecules

2.1 Basic mechanism and nomenclature of covalent bonds

Two atoms can bind to form a diatomic molecule both through ionic and non-ionic bonds. The former admits a simple, classical picture wherein one or more electrons from atom A shift to atom B and the resulting positive and negative ions are held together by the electrostatic Coulomb attraction. The classic example is a molecule such as NaCl , where the extra electron outside a closed shell in the alkali atom Na can migrate to fill the hole in the outer shell of the halogen Cl, with Na^+ and Cl^- forming an ionic bond. Most molecules of astrophysical interest involve, however, non-ionic or “covalent” bonding, with the electrons responsible for binding being shared between the two partners A and B. This is a purely quantum-mechanical effect, having its basic origins in the mixing of degenerate states, such a mixing leading to extra binding energy.

The simplest species, H_2^+ , a system consisting of (p + p + e), serves as an illustration. Consider first a situation with all three particles infinitely far apart as defining the zero of the energy. Next, let the electron bind to either of the protons, forming say the hydrogen atom in its ground state. This state, which lies at -13.6 eV, is doubly-degenerate depending on which of the two protons A and B is bound to the electron, the other one at infinite distance away. The degenerate states ϕ_A and ϕ_B can be described as $\text{H}^+ + \text{H}$ and $\text{H} + \text{H}^+$ with wave functions $\exp(-r_A/a_0)$ and $\exp(-r_B/a_0)$, respectively, r_A and r_B the distances to the electron from the nuclei, and the separation between the protons denoted as R_{AB} , with $R_{AB} \rightarrow \infty$. If the protons are now moved closer together to some finite, large value of R_{AB} , the two states are coupled together, the electronic wave function centered on one proton now overlapping the other proton as well. The resulting eigenstates of such degenerate mixing are the symmetric and antisymmetric superpositions of the individual states,

$$\phi_g = \frac{1}{\sqrt{2}} (\phi_A + \phi_B) , \quad \phi_u = \frac{1}{\sqrt{2}} (\phi_A - \phi_B) , \quad (6.1)$$

the labels g and u borrowed from the German gerade and ungerade and denoting even-ness and odd-ness, respectively, with respect to inversion through the center of the molecule (which lies midway between the two protons). In common with any such degenerate mixing of two states in quantum physics, the corresponding eigenvalues lie below and above, respectively, the energy -13.6 eV in the absence of this mixing. There is necessarily a gain in binding, therefore, for the gerade state which persists even upon adding the repulsive Coulomb energy between the two protons. As shown in Fig. 6.1, the two eigenvalues split, the u one always less bound than -13.6 eV as R_{AB} decreases but the g attaining a deeper minimum before it too starts to rise, as the repulsion between the protons overwhelms the gain in binding from the electronic wave function. Note that the latter is limited to -54.4 eV which would be the energy of one electron in the “united atom” limit of both protons coinciding and presenting a nuclear charge of 2 for the atomic electron. As shown, the minimum energy of -16.3 eV is not as small and is attained for $R_{AB} = 1.1\text{\AA}$. The shared electron cloud serves to bind H^+ and H with an additional 2.7 eV of binding energy.

Fig. 6.1 exemplifies the basic analysis of electronic energies in molecular systems, applicable even beyond diatomic species, tracing the electronic binding from the “separated atom” limit of $R_{AB} \rightarrow \infty$ to the united atom limit of $R_{AB} \rightarrow 0$, that is, from $\text{H}^+ + \text{H}$ to He^+ in the current example. The orbital angular momentum of the electron is a good quantum number only in the two limits but not at any finite R_{AB} , the two-center nature of the molecule breaking spherical symmetry. Cylindrical symmetry prevails throughout, however, the molecule being cylindrically symmetric about the inter-nuclear axis. Thus, although the electronic ℓ is not a good quantum number, the curves in Fig. 6.1 can be labeled by its projection (called λ) on the internuclear axis. For the s electron in the H_2^+ example, the projection is, of course, zero and so the two states in (6.1) are labeled σ_g and σ_u^* . An asterisk is attached to non-bonding states. Diatomic molecular nomenclature for λ , the projection of electronic angular momentum on the internuclear axis, uses the Greek letter counterparts $\sigma, \pi, \delta, \dots$, of s, p, d, \dots for $\lambda = 0, 1, 2, \dots$, respectively. The sign being irrelevant, λ equals $|m|$ and each $\lambda \neq 0$ state is always doubly degenerate in energy.

Cylindrical symmetry about the internuclear axis applies to all diatomic molecules (and also linear polyatomic molecules), whether homonuclear (A and B identical) or heteronuclear (A and B different), whereas

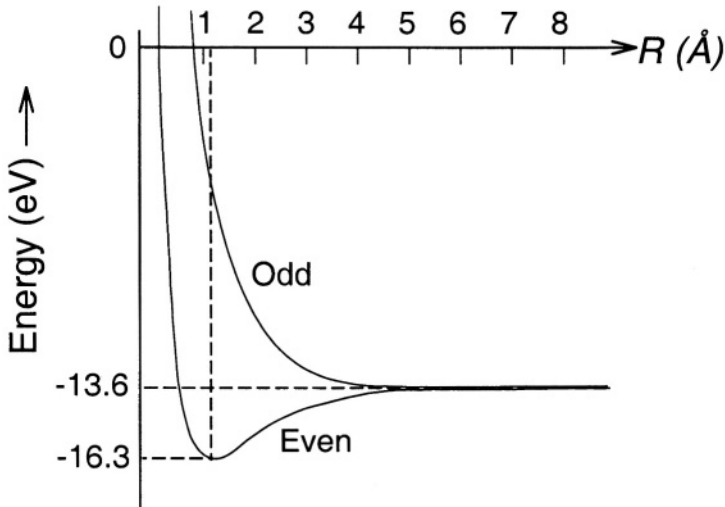


Figure 6.1. Electronic energy in H_2^+ as a function of internuclear separation R . From R. Eisberg and R. Resnick, *Quantum Physics* (John Wiley, New York, 1974), with permission from author and publisher.

the g and u labels of symmetry with respect to inversion are only relevant for the former. When A and B are different, the separated atom limits $A^+ + B$ and $A + B^+$ in the corresponding Fig. 6.1 differ in energy, these asymptotic states no longer degenerate.

The discussion accompanying Fig. 6.1 for the ground state of hydrogen, $\text{H}^+ + \text{H}(1s)$ and $\text{H}(1s) + \text{H}^+$ defining the lowest “molecular orbitals” $\sigma_g 1s$ and $\sigma_u^* 1s$, extends to higher excited states. An exactly similar diagram for $\text{H}^+ + \text{H}(2p_z)$ and $\text{H}(2p_z) + \text{H}^+$ defines the next orbitals $\sigma_g 2p$ and $\sigma_u^* 2p$, the angular momentum projection on the internuclear axis being again zero. On the other hand, the $2p_x$ and $2p_y$ separated atom configurations give rise to $\pi_u 2p$ and $\pi_g^* 2p$, each doubly degenerate. Just as the states of the hydrogen atom provide labels for the many electron configuration of a higher atom, the basic molecular orbitals defined for H_2^+ provide similar labels for more complex molecules. The spin of each electron introduces again another double degeneracy and, with consideration of the Pauli principle that every electron has to have its own distinct labels, the molecular orbitals and overall state labels of total

spin S and total projection on the internuclear axis Λ can be assigned exactly analogously to atoms (Section 1.4.1).

2.2 Molecular orbitals and states of simple diatomic molecules

The next simplest molecule H_2 's ground-state configuration $(\sigma_g 1s)^2$ has both electrons assigned with opposite spin orientation to the lowest, bonding orbital with total spin $S = 0$ to satisfy the Pauli principle. With $\Lambda = 0$, the state is $^1\Sigma_g^+$. Note the use of capital Greek letters for the combined electronic system. The additional label shown as a + arises for Σ terms in diatomic molecules (homonuclear and heteronuclear) because of reflection symmetry in any plane going through the internuclear axis. States even (+) or odd (-) with respect to this reflection have slightly different energy, the former lying lower. Non- Σ terms have a two-fold degeneracy of the two different signs of M_L in the same $\Lambda = |M_L|$. Since linear combinations still have the same energy, the +/- superscripts are usually not shown although, as considered later, the phenomenon of "Lambda-doubling", wherein the interaction of electronic orbital angular momentum with the rotational angular momentum of the nuclei lifts the degeneracy, makes the +/- labels relevant also for $\Lambda \neq 0$.

The ground state of a molecule is designated with a prefix X so that the full description of H_2 in its ground state is $X^1\Sigma_g^+$. With two electrons providing additional binding relative to separated atoms, H_2 is more bound than H_2^+ , having a total binding energy of 4.7 eV (not quite double the 2.7 eV of H_2^+ because of the electron-electron repulsion), and an equilibrium separation R_{HH} of 0.7Å, smaller than in H_2^+ . Fig. 6.2 sketches the potential energy curves for H_2 and its ions [54]. Excited terms are prefixed with A,B,C,... when they have the same multiplicity as the ground term, otherwise a,b,c,... Thus, the first excited state in H_2 , obtained by placing one electron in the bonding and one in the non-bonding orbitals of Fig. 6.1, is $(\sigma_g 1s)(\sigma_u^* 1s) b^3\Sigma_u^+$. This is an unstable state appearing as a continuum above ≈ 12 eV. Within the realm of $1s$ states, four $1s$ electrons completely fill the above two orbitals, $(\sigma_g 1s)^2(\sigma_u^* 1s)^2$, to give a completely-filled state $^1\Sigma_g^+$ with all quantum numbers zero. This is the unstable state of He_2 .

Paralleling the discussion in Section 1.4.1 for two atomic p electrons, consider the 36 states in a molecular description of two such electrons in a heteronuclear diatomic molecule. First, consider the states formed out of $\pi\pi$, that is, when the m values of both electrons are either +1 or -1. The 16 states involved are shown in the top two rows of Table 6.1 in the notation $^{2S+1}\Lambda_\Omega$, where $\Omega = \Lambda + S_z$ is the total projection of electronic angular momentum. Each $\Omega \neq 0$ state is doubly degenerate whereas Ω

Table 6.1. States of $\pi\pi$ in a heteronuclear diatomic molecule [54].

m_A	m_B	M	State
1	1	2	
-1	-1	-2	$^1\Delta_2, ^3\Delta_3, ^3\Delta_2, ^3\Delta_1$
1	-1	0	$^1\Sigma_0^+, ^3\Sigma_0^+, ^1\Sigma_0^-, ^3\Sigma_0^-$,
-1	1	0	$^3\Sigma_1^+, ^3\Sigma_1^-$
1	0	1	$^1\Pi_1, ^3\Pi_2, ^3\Pi_1, ^3\Pi_0$
-1	0	-1	
0	1	1	$^1\Pi_1, ^3\Pi_2, ^3\Pi_1, ^3\Pi_0$
0	-1	-1	
0	0	0	$^1\Sigma_0^+, ^3\Sigma_0^+, ^3\Sigma_1^+$

Since π (and other $\lambda \neq 0$) states are doubly degenerate, together with the spin degeneracy, four electrons form a closed shell such as $(\pi_u 2p)^4$ with total quantum numbers zero: $^1\Sigma_0^+$. Three π electrons, π^3 , are thereby equivalent in their enumeration of states to a π “hole”, exactly analogous to the discussion in atoms. Thus OH with nine electrons has the same $^2\Pi$ ground state as CH discussed above. The molecule O_2 , with sixteen electrons, has orbitals $(\sigma_g 1s)^2 (\sigma_u^* 1s)^2 (\sigma_g 2s)^2 (\sigma_u^* 2s)^2 (\sigma_g 2p)^2 (\pi_u 2p)^4 (\pi_g^* 2p)^2$. The quantum numbers of the state are, therefore, of two equivalent π electrons as in the previous paragraph with the additional g/u labels for this homonuclear case: $X^3\Sigma_g^-$ is the ground state, $a^1\Delta_g$ and $b^1\Sigma_g^+$ excited states lying roughly 1 eV and 1.6 eV respectively, above the ground state. Infrared emission at $1.27 \mu\text{m}$ from this $^1\Delta_g$ state is seen in the airglow of the Earth’s atmosphere and also from Venus. An excited state of O_2 with a rearrangement of the last two molecular orbitals as $(\pi_u 2p)^3 (\pi_g^* 2p)^3$ is also like a $\pi\pi$ -hole. The $B^3\Sigma_u^-$ state of this configuration is responsible for strong ultraviolet absorption (Schumann-Runge bands) to it from the ground state, important in the upper atmosphere and in other contexts. The NO atom with one electron less than in O_2 has a single π electron in the last orbital and a $^2\Pi$ ground state. The same applies to O_2^+ . On the other hand, O_2^- with an extra electron (bound by 0.44 eV) in $\pi_g^* 2p$ is also a $^2\Pi_g$ state. It is an important species in the Earth’s atmosphere.

2.3 The Born-Oppenheimer approximation

Because the quantum mechanics of electronic motion is responsible for binding and, further, from the hierarchy that the internal binding within atoms is larger than the binding between atoms in a molecule, it was natural to begin this chapter as we did. We have viewed molecules and molecular orbitals as built up from atomic states, starting at large R_{AB} and tracing their evolution as the nuclei are moved closer together. But, of course, we could view the whole assembly of nuclei and electrons in a molecule as a single quantum system and solve the Schrödinger equation for the full Hamiltonian to find the eigenvalues and eigenfunctions. For a one-electron diatomic molecule, we have (Fig. 6.3).

$$H = -\frac{\hbar^2}{2M_A}\nabla_A^2 - \frac{\hbar^2}{2M_B}\nabla_B^2 - \frac{\hbar^2}{2m}\nabla^2 - \frac{Z_A e^2}{r_A} - \frac{Z_B e^2}{r_B} + \frac{Z_A Z_B e^2}{R_{AB}}, \quad (6.2)$$

where to keep the discussion general, masses M_A and M_B and charges Z_A and Z_B have been assigned to the nuclei. This two-center Hamiltonian and the resulting Schrödinger equation for stationary states separates in a system of coordinates called elliptic coordinates. However, since there is no simple extension to more electrons or to the case of more than two nuclei, and because there is a natural approximation in terms of the very different motions of the heavy nuclei and the light electrons, the separation of H_2^+ in elliptic coordinates has not generally been exploited.

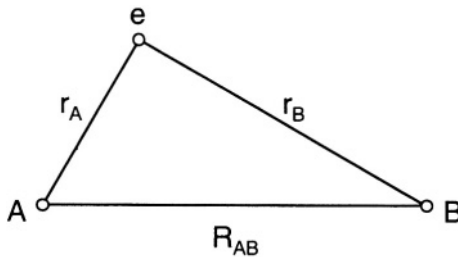


Figure 6.3. Coordinates in a diatomic molecule

Instead, an “adiabatic” approximation is widely used, as has already been implicit in Sections 6.2.1 and 6.2.2. Given the large difference in mass between the electronic m and the nuclear M_A and M_B , the motion of the latter is regarded as slow relative to the electronic motion. Therefore, one solves first the electronic motion in (6.2) (that is, the third, fourth and fifth terms) while regarding the nuclei as held fixed at

A and B. For each position of A and B, in particular their separation R_{AB} , the eigenvalues and eigenfunctions of the electronic motion will depend parametrically on R_{AB} . The total wave function of the system is then approximated as a product of this electronic wave function and a wave function for the nuclear motion involving the coordinate R_{AB} . This point of view applies to the more general situation of several nuclei and several electrons in which case (6.2) is replaced by

$$H = -\sum_A \frac{\hbar^2}{2M_A} \nabla_A^2 - \frac{\hbar^2}{2m} \sum_i \nabla_i^2 - \sum_{A_i} \frac{Z_A e^2}{r_{Ai}} + \sum_{A>B} \sum \frac{Z_A Z_B e^2}{R_{AB}} + \sum_{i>j} \sum \frac{e^2}{r_{ij}}, \quad (6.3)$$

giving a genuinely non-separable (and complicated) Hamiltonian. One writes the full wave function $\Psi(\{\mathbf{R}_A\}, \{\mathbf{r}_i\})$ as

$$\Psi(\{\mathbf{R}_A\}, \{\mathbf{r}_i\}) = \phi_{\text{el}}(\{\mathbf{R}_A\}; \{\mathbf{r}_i\}) \psi_{\text{nucl}}(\{\mathbf{R}_A\}), \quad (6.4)$$

with

$$\begin{aligned} H_{\text{el}} \phi_{\text{el}} &= \left\{ \frac{-\hbar^2}{2m} \sum_i \nabla_i^2 - \sum_{A_i} \frac{Z_A e^2}{|\mathbf{R}_A - \mathbf{r}_i|} + \sum_{i>j} \frac{e^2}{r_{ij}} \right\} \phi_{\text{el}} \\ &= U_{\text{el}}(\{\mathbf{R}_A\}) \phi_{\text{el}}(\{\mathbf{R}_A\}; \{\mathbf{r}_i\}), \end{aligned}$$

and

$$\begin{aligned} H_{\text{nucl}} \psi_{\text{nucl}}(\{\mathbf{R}_A\}) &= \left[\sum_A \frac{-\hbar^2}{2M_A} \nabla_A^2 + U_{\text{el}}(\{\mathbf{R}_A\}) \right. \\ &\quad \left. + \sum_{A>B} \frac{Z_A Z_B e^2}{|\mathbf{R}_A - \mathbf{R}_B|} \right] \psi_{\text{nucl}} = E \psi_{\text{nucl}}, \quad (6.5) \end{aligned}$$

with $\{ \}$ denoting the collective set of coordinates.

The approximation in (6.4) and (6.5) lies in that when (6.4) is substituted into $H\Psi = E\Psi$, the action of the ∇_A^2 terms on $\phi_{\text{el}}(\{\mathbf{R}_A\}; \{\mathbf{r}_i\})$ is neglected. The semi-colon in ϕ_{el} denotes this imbalance in the roles of electronic and nuclear coordinates in ϕ_{el} . Although as clear from (6.4), both are involved, the dependence on the nuclear $\{\mathbf{R}_A\}$ is regarded as "parametric" so that derivatives (both ∇_A and ∇_A^2) are considered small and neglected. The physical justification arises, of course, from the great

disparity between the variation in electronic and nuclear coordinates as a result of the different masses attached to the derivative terms. The ratio m/M_A , which is typically 10^{-4} , represents the relative error in energy so that, with $U_{\text{el}} \approx \text{Ry} \approx 10^5 \text{ cm}^{-1}$, the error involved is a few cm^{-1} . One can, of course, just as in the related discussion of an adiabatic method in Section 5.3.2, go beyond the adiabatic approximation by expanding the full Ψ in (6.4) in terms of a complete set of eigenfunctions ϕ_{el} and thereby obtain coupled equations for a set $\{\psi_{\text{nucl}}\}$ instead of the single (6.4). But, the enormous complexity of the procedure is not justified in most applications to date so that the above scheme due to Born and Oppenheimer is standard throughout molecular physics. For accurate numerical calculations, however, just as in atoms (Section 1.4.4), configuration interaction schemes superpose several molecular orbital configurations in describing ϕ_{el} . A major difference from atoms is that instead of radial functions that decay exponentially in r , molecular calculations employ Gaussian functions centered on each nucleus. Many-center integrals are then more easily carried out, a Gaussian at one R_A easily expressible in terms of a translated function at R_B [55].

The electronic motion provides through (6.4) eigenvalues that depend on the positions of the nuclei. In a diatomic molecule, this dependence is only on the relative separation R_{AB} (Fig. 6.3). Along with the Coulomb repulsion between the nuclei, also dependent only on R_{AB} , the last two terms in (6.4) provide a potential, $U(R_{AB})$, for the motion of the nuclei. With two bodies, A and B, the center of mass motion can be separated, providing the standard translation of this motion with no bearing on the physics internal to the molecule. This leaves behind the motion in the internal, relative coordinate \mathbf{R}_{AB} whose kinetic energy carries a reduced mass

$$\mu_{AB} = \frac{M_A M_B}{M_A + M_B}. \quad (6.6)$$

With \mathbf{R}_{AB} as a three-dimensional coordinate for the motion of the nuclei in a diatomic molecule, we have the Schrödinger equation of motion

$$\left[-\frac{\hbar^2}{2\mu_{AB}} \nabla^2 + U(R) \right] \psi(\mathbf{R}) = E\psi(\mathbf{R}). \quad (6.7)$$

From now on, we will denote \mathbf{R}_{AB} as \mathbf{R} and drop the subscript “nucl” on ψ .

2.4 Rotations and vibrations of the internuclear axis

The Schrödinger equation (6.7) is separable in radial (R) and angular ($\hat{R} = \theta, \varphi$ as in Fig. 6.4), coordinates describing, respectively, “vibrational” and “rotational” motion of the internuclear axis. The shape of the potential wells $U(R)$ as in Figs. 6.1 and 6.2 for most bound molecular states shows that to a good approximation, at least for low-lying states in each well, the rotations and vibrations can be taken as relative to the “equilibrium separation” R_e marking the minimum of the potential. The rotations, therefore, are of a free rigid rotor

$$\left(\frac{-\hbar^2}{2\mu_{AB}} \frac{1}{R_e^2} \nabla_{\hat{R}}^2 \right) \psi_{\text{rot}}(\hat{R}) = E_{\text{rot}}(\hat{R}), \quad (6.8)$$

with

$$\psi_{\text{rot}}(\hat{R}) = Y_j^M(\theta, \varphi),$$

and

$$E_{\text{rot}} = hBJ(J+1), \quad B \equiv h/(\pi^2 \mu_{AB} R_e^2), \quad (6.9)$$

B called the rotational constant, and $J = 0, 1, 2, \dots$ the rotational angular momentum in \hbar units. Each value of E_{rot} is $(2J+1)$ -fold degenerate with $M = -J, -J+1, \dots, J$. A useful conversion is $h/8\pi^2 = 505,379$ MHz amuÅ².

Expanding $U(R)$ about R_e ,

$$U(R) = U(R_e) + \frac{1}{2}k(R - R_e)^2 + \dots, \quad (6.10)$$

with

$$k \equiv (\partial^2 U / \partial R^2)_{R=R_e}, \quad (6.11)$$

we have left in (6.7)

$$\left[\frac{-\hbar^2}{2\mu_{AB}} \left\{ \frac{\partial^2}{\partial R^2} + \frac{2}{R} \frac{\partial}{\partial R} \right\} + \frac{1}{2}k(R - R_e)^2 \right] \psi_{\text{vib}}(R) = E_{\text{vib}} \psi_{\text{vib}}(R), \quad (6.12)$$

with

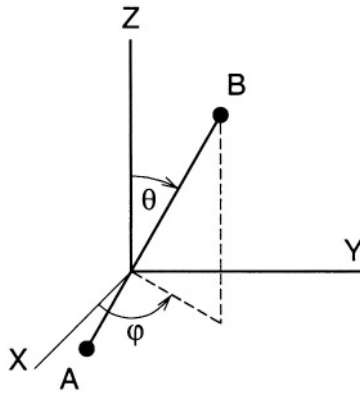


Figure 6.4. Coordinates describing rotations of a diatomic molecule.

$$\psi(\mathbf{R}) = \psi_{\text{rot}}(\hat{R}) \psi_{\text{vib}}(R), \quad (6.13)$$

and

$$E = U(R_e) + E_{\text{vib}} + E_{\text{rot}}. \quad (6.14)$$

With R_e approximately 1\AA , most diatomic molecules have B of the order of a few cm^{-1} (or 10^{11} Hz, $hB_e \approx 10^{-3}$ eV). H_2 as the lightest diatomic molecule has a somewhat larger value, $hB_e \approx 8 \times 10^{-3}$ eV, but even that is very small compared to the other energies in (6.14). In H_2 , $U(R_e)$ equals -31.9 eV, the $2 \times (-13.6)$ eV of each H atom plus the additional 4.7 eV of molecular binding discussed in Section 6.2.1.

The vibrational Schrödinger equation in (6.12) describes the motion of a one-dimensional harmonic oscillator of spring constant k in the variable $x \equiv R - R_e$ once a trivial factor of $1/R$ is removed to eliminate the linear derivative in R :

$$\psi_{\text{vib}}(R) = \psi(x)/R,$$

$$\left(\frac{-\hbar^2}{2\mu_{\text{AB}}} \frac{d^2}{dx^2} + \frac{1}{2} kx^2 \right) \psi(x) = E_{\text{vib}} \psi(x). \quad (6.15)$$

In this picture, vibrations of the molecule about the equilibrium position R_e are described as simple harmonic vibrations, the potential wells being

sensibly approximated by parabolic harmonic oscillator wells according to (6.10). Corrections for larger departures of R from R_e , reflecting that the wells in Figs. 6.1 and 6.2 are no longer parabolic at such larger R , will be considered in Section 6.2.5.

The solutions of (6.15) are well-known,

$$E_{\text{vib}} = \hbar\omega\left(v + \frac{1}{2}\right), \quad v = 0, 1, 2, \dots, \quad (6.16)$$

with $\omega \equiv (k/\mu_{\text{AB}})^{1/2}$, and

$$\psi(x) = \left(\frac{\mu_{\text{AB}}\omega}{\pi\hbar}\right)^{1/4} (2^v v!)^{1/2} H_v(\xi) \exp(-\xi^2/2), \quad (6.17)$$

with $\xi \equiv \left(\frac{\mu_{\text{AB}}\omega}{\hbar}\right)^{1/2} x$, and where H_v are the Hermite Polynomials. In H_2 , $\hbar\omega \approx 0.5$ eV, so that the three terms (electronic, vibrational and rotational) in (6.14) are of decreasing order in energy in steps of roughly two orders of magnitude.

Table 6.2. Rotation and vibration parameters of some diatomic molecules.

Molecule	R_e (Å)	ω/π (cm ⁻¹)	hB (eV)	B (cm ⁻¹)
H ₂	0.741	4395	7.56×10^{-3}	60.9
HD	0.741	3817	5.69×10^{-3}	45.9
D ₂	0.741	3118	3.79×10^{-3}	30.6
N ₂	1.098	2360	2.48×10^{-4}	2
O ₂	1.217	1580	1.78×10^{-4}	1.44
¹² CO	1.128	2170	2.39×10^{-4}	1.93
LiH	1.6	1406	9.27×10^{-4}	7.48

The description developed in this section gives a good first picture of the motion associated with the nuclear degrees of freedom in a diatomic molecule. Rotations in space of the internuclear axis and thereby of the molecule, and vibrations about the equilibrium distance, are described by the discrete spectra of a rotor and a harmonic oscillator, respectively, with their characteristic spacings given in (6.9) and (6.16). Together with potential wells for increasing electronic excitation, the rich spectrum of even the simplest molecule is evident from a figure such as Fig. 6.2. Table 6.2 gives a sample of the parameters defining rotational and vibrational spectra. Note that isotopic partners such as H₂, HD, and D₂, share the same electronic values of R_e and k but differences in μ_{AB}

lead to different rotational and vibrational constants. Of special importance in astronomy is that higher J and v states are easily excited for the temperatures of interest. To a first approximation, the Boltzmann factor and statistical weight of each level gives the relative population of these states as

$$N_J/N_0 = (2J + 1) \exp[-hBJ(J + 1)/kT] \quad (6.18)$$

and

$$N_v/N_0 = \exp(-v\hbar\omega/kT). \quad (6.19)$$

2.5 Anharmonicities and rotation-vibration coupling

It is clear from a glance at any molecular potential well (Fig. 6.2 or see schematic in Fig. 6.5) that the parabolic approximation around R_e becomes increasingly inadequate with increasing vibrational quantum number v . This can be handled at first by retaining higher, “anharmonic”, terms in the expansion (6.10), treating them as perturbations. Thus, perturbation theory (Section 3.2.2) based on taking the harmonic oscillator wave functions (6.17) as the unperturbed functions can estimate energy and other corrections. Qualitatively, the widening of the well from the initial parabola fitted to the minimum is like a lowering of the spring constant k so that higher vibrational levels lie closer than the equal $\hbar\omega$ spacing. Perturbation theory itself fails, however, once the energies approach the region where any electronic potential well flattens as it approaches some constant value of a separated atom limit. Indeed, above this limit the molecule has a vibrational continuum and dissociates into A+B, all of which lies completely out of reach of a harmonic oscillator model with a purely discrete spectrum stretching to infinite energy [56].

One alternative is to use potential functions that can be solved exactly and which approximate well the shapes of molecular potential wells. The Morse function,

$$U(R) = D[1 - \exp\{-a(R - R_e)^2\}], \quad (6.20)$$

is an example, with D and a adjusted to fit a well as in Fig. 6.2 or 6.5. The Schrödinger equation for this potential admits exact solutions with eigenvalues

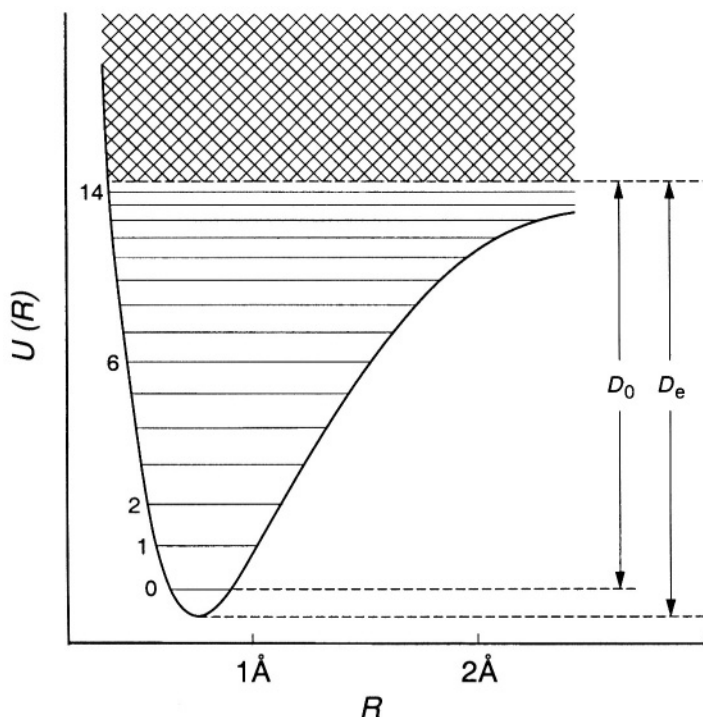


Figure 6.5. Schematic molecular potential well, showing anharmonicities and a dissociation continuum. Vibrational levels and dissociation energies are shown. From [56], with permission of John Wiley and Sons, Inc.

$$E_{\text{vib}} = \hbar\omega\left(v + \frac{1}{2}\right) - \tilde{e}\left(v + \frac{1}{2}\right)^2, \quad (6.21)$$

where ω and \tilde{e} ($= \pi a \hbar^2 \omega / \sqrt{2\mu D}$) are functions of D and a . The above is indeed the form of the first anharmonic correction. Other more complicated models have also been used and also a numerical method called the Rydberg-Klein-Rees (RKR) method. Using the JWKB quantization formula for energy levels in a potential $U(R)$, several empirically known vibrational levels of a molecule are used as input and the formula inverted to get a numerical $U(R)$ which can then be used for generating other vibrational levels and the continuum.

Turning to rotational energies and wave functions, the description in (6.9) is again only a first approximation. The use of R_e in B in (6.9) is reasonable for rotational states of the lowest vibrational levels whose wave functions are more tightly confined around R_e . Otherwise, $1/R^2$

can be expanded beyond the leading term $1/R_e^2$ to take into account this effect of vibrations on rotational levels, again treating the next terms in the expansion as perturbations. A reverse effect, of rotations on vibrations, goes under the name “centrifugal distortion.” Here, with increasing rotational quantum number J , the treatment of the internuclear axis as in rigid rotation has to be modified to account for the centrifugal flying apart of A and B which stretches the axis and increases R_e , thereby altering the vibrational spectrum. Besides centrifugal effects, Coriolis-like effects are also seen. With non-zero J , vibrations of a molecule in the presence of rotation lead to Coriolis coupling between the two motions.

2.6 Parity of molecular states

The parity of a molecular state, that is, its behavior under reflection of all coordinates $\{\mathbf{R}_A\}$ and $\{\mathbf{r}_i\}$, is of interest just as for atomic states, particularly for considering spectroscopic transitions in Section 6.3. With Ψ in (6.4) a product $\phi_{\text{el}} \psi_{\text{vib}} \psi_{\text{rot}}$, the total parity is the product of the parities of each of these three factors. The vibrational ψ_{vib} , depending only on the scalar R , is always even. With reference to Fig. 6.4, the inversion of coordinates amounts to the usual $\theta \rightarrow \pi - \theta$, $\varphi \rightarrow \pi + \varphi$ and the parity of ψ_{rot} is $(-1)^J$ from the standard transformation of spherical harmonics. Even- J rotational states are even and odd ones odd under parity. For the parity of ϕ_{el} , we need to consider space-fixed axes $\{X, Y, Z\}$ and molecular body-fixed axes $\{x, y, z\}$ carefully, the latter defined with z along the axis from A to B. Since the electronic wave function is described with the coordinate \mathbf{r} of the electron measured from the center of mass of A and B, we have to take into account the interchange of A and B and the resulting $z \rightarrow -z$ upon inversion. Thus inversion of all coordinates of electrons and nuclei can be achieved in two steps as follows. See Fig. 6.6. First, a 180° rotation about the y -axis and next a reflection of the electrons in the xz -plane results in all A, B, and electrons inverted as required for the parity transformation. Therefore, the parity of ϕ_{el} is simply the effect of the reflection in the xz -plane which we defined as the $+/-$ label of Section 6.2.2. Thus, in all, Ψ has parity $(-1)^J$ and $(-1)^{J+1}$ for $+$ and $-$ states respectively. Note that the g/u labels defined for homonuclear molecules was the behavior of the electronic wave function under inversion in the molecular center or in body-fixed axes whereas the current consideration is for inversion with respect to the space-fixed axes.

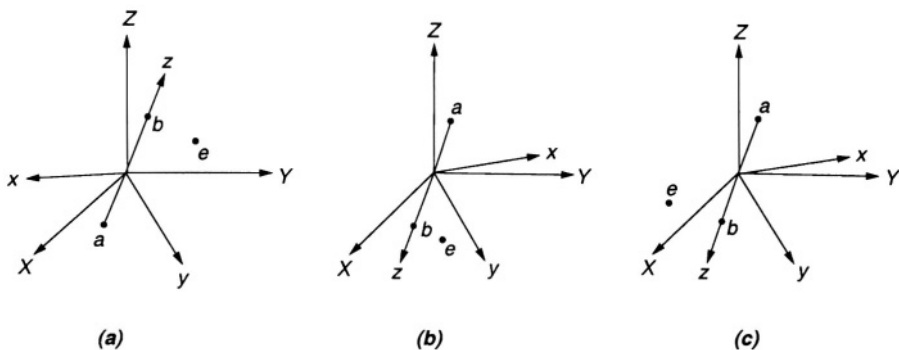


Figure 6.6. Space-fixed $\{X, Y, Z\}$ and body-fixed $\{x, y, z\}$ axes of a diatomic molecule, and successive transformations to define the parity of molecular electronic states. From [56], with permission of John Wiley and Sons, Inc.

2.7 Effect of nuclear spin

The complete wave function of the molecule includes besides Ψ the wave functions of the spins of the electrons and nuclei. For heteronuclear molecules, the Pauli principle applies only to the identical electrons and we have already seen the enumeration of states upon combining ϕ_{el} and electronic spin. For homonuclear diatomic molecules with identical nuclei A and B, identical down to the isotope, the overall wave function has to be symmetric or antisymmetric under A-B interchange as well, depending on whether the nuclei are bosons or fermions, respectively. If the spin is I , the $(2I + 1)^2$ degenerate states of combined spin break into $(2I + 1)(I + 1)$ symmetric and $I(2I + 1)$ antisymmetric states under interchange of the spin coordinates of A and B (for example, for $I = \frac{1}{2}$, three symmetric and one antisymmetric, that is, triplet and singlet, states). For I an integer, the former must have symmetric Ψ and the latter antisymmetric Ψ under interchange of nuclei, whereas for I a half-integer just the opposite, that is, the $(2I + 1)(I + 1)$ are associated with antisymmetric Ψ and $I(2I + 1)$ with symmetric Ψ .

The behavior of Ψ under interchange of nuclei reduces again to that of ϕ_{el} and ψ_{rot} , ψ_{vib} being unaffected because R is left unchanged by this interchange. The interchange of A and B is exactly the same operation as parity for ψ_{rot} , so that as before, we pick up a factor $(-1)^J$ from the rotational wave function under the interchange. For ϕ_{el} , interchange of nuclei affects the electronic coordinates because they are defined with respect to the body-fixed axes. Therefore, interchange of nuclear coordi-

nates can be achieved by inverting all coordinates of nuclei and electrons in space-fixed axes which is the parity transformation and then inverting only the electrons in space-fixed coordinates. The first as we have seen gives \pm for the $+/-$ states. The second, of inversion of electronic coordinates in space-fixed axes, is equal to inversion of them in molecule-fixed axes, the nuclei being unaffected in this step so that the molecule-fixed axes remain unchanged. This inversion gives \pm for g/u as we have seen. Therefore, $\Sigma_g^+, \Sigma_u^-, \Pi_g^+, \Pi_u^-, \dots$ are symmetric and $\Sigma_g^-, \Sigma_u^+, \Pi_g^-, \Pi_u^+, \dots$ antisymmetric under nuclear interchange.

In all, therefore, for homonuclear diatomic molecules with fermionic nuclei, we have $(I + 1)(2I + 1)$ nuclear symmetric states with $J = 0, 2, 4, \dots$ for $\Sigma_g^-, \Sigma_u^+, \dots$ and $J = 1, 3, 5, \dots$ for $\Sigma_g^+, \Sigma_u^-, \dots$ states, and $I(2I + 1)$ nuclear antisymmetric states with $J = 0, 2, 4, \dots$ for $\Sigma_g^-, \Sigma_u^+, \dots$ and $J = 1, 3, 5, \dots$ for $\Sigma_g^+, \Sigma_u^-, \dots$. The J and ϕ_{el} states combine oppositely for bosonic nuclei, that is $(I + 1)(2I + 1)$ nuclear symmetric states with $J = 0, 2, 4, \dots$ for $\Sigma_g^-, \Sigma_u^+, \dots$ and $J = 1, 3, 5, \dots$, for $\Sigma_g^+, \Sigma_u^-, \dots$, and $I(2I + 1)$ nuclear antisymmetric states with $J = 0, 2, 4, \dots$ for $\Sigma_g^-, \Sigma_u^+, \dots$ and $J = 1, 3, 5, \dots$ for $\Sigma_g^+, \Sigma_u^-, \dots$. For any I and any electronic state, one has either the odd or even J values with relative statistical weights $I(I + 1)$. The most dramatic effect of this Pauli principle requirement is for $I = 0$, applicable to diatomic molecules with spinless nuclei such as C_2 . $I = 0$ has only a single symmetric nuclear state (also with total spin 0) and it must have $J = 0, 2, 4, \dots$ for $\Sigma_g^+, \Sigma_u^-, \dots$ and $J = 1, 3, 5, \dots$ for $\Sigma_g^-, \Sigma_u^+, \dots$. Thus, any electronic state of such a molecule has half its rotational levels forbidden. The ground state of C_2 $X^1\Sigma_g^+$ has only even J ! By contrast, O_2 , also with nuclear spin zero but a $^3\Sigma_g^-$ ground state, can only have odd J values. The above argument applies to the isotope ^{12}C but, as soon as we consider $^{12}C-^{13}C$, the nuclei are no longer identical and all J 's occur in the same ground electronic state. The same is true upon replacing $^{16}O_2$ by $^{16}O-^{17}O$. This dramatic effect of the Pauli principle led in fact to the identification of the ^{13}C and the rare ^{17}O isotopes. It was also used in the first determination of the spin of the proton where even and odd rotational levels of H_2 alternate in the intensity ratio $1/3$ arising from $I(I + 1)$ with $I = \frac{1}{2}$.

The example of H_2 with total spin $I = 0$ or 1 , and the attendant effect on molecular states, leads to the two spin states behaving as almost distinct species. The nuclear wave function of states symmetric or antisymmetric under nuclear interchange are mutually orthogonal. Thus, there can be no non-zero matrix elements between them for any operator that depends only on electronic coordinates. Radiative or non-radiative transitions under collisions lead only to changes in J of steps

of 2. Therefore, when H_2 is cooled to very low temperature, all the molecules with odd J will eventually settle down to the $J = 1$ level of the lowest electronic and vibrational state, and all those in even J to the $J = 0$ level. Interactions between nuclei and electrons can couple these states but, being very weak, it can take many months for this to happen. The two behave as two separate species, called ortho and para hydrogen, respectively. The former, with $J = 1 \ ^1\Sigma_g^+$ has triplet ($I = 1$) nuclear spin, the latter with $J = 0 \ ^1\Sigma_g^+$ has singlet ($I = 0$) nuclear spin. A small paramagnetic impurity can catalyse the $J = 1$ molecules to drop down to $J = 0$, leaving behind pure para- H_2 . If it is then warmed, only even J levels will be seen, again for months in the absence of any catalyst that can flip one of the nuclear spins to pass from singlet to triplet. Ordinary H_2 is usually a 3:1 mix of ortho and para forms.

3. Molecular Spectra

As in the case of atoms, interaction of a molecule with the electromagnetic field leads to emission or absorption of radiation as the molecule changes from one state to another. The same considerations of oscillator strengths and selection rules as in Sections 2.2.1 and 2.2.3 apply but now, in addition to transitions involving electronic energy levels, there are also those between rotational or vibrational states and combinations of all three. Given the energies involved, rotational transitions generally lie in far infrared or microwave wavelengths and vibrational ones in the near infrared. Again, as in Section 2.2.3, the dominant transitions are electric dipole (E1) in character and we will focus primarily on them, although higher multipole and magnetic transitions can also be treated in parallel to those in atoms.

3.1 Rotational spectra

The electric dipole coupling to radiation is given by $-\mathbf{d} \cdot \mathcal{E}$, with \mathbf{d} the dipole moment and \mathcal{E} the electric field. The matrix element involved between two rotational levels $\langle J'M' | \mathbf{d} | JM \rangle$. \mathcal{E} vanishes unless selection rules are satisfied. The dipole moment being a vector, we have as before for atomic transitions but now in terms of the nuclear angular momentum that J, J' , and unity form an angular momentum triad, and initial and final states have opposite parity so that

$$J' = J \pm 1, \quad M' = M, M \pm 1. \quad (6.22)$$

Such jumps to the nearest neighboring levels in a rotor spectrum (6.9) involve, therefore, transition frequencies $\nu = 2B(J+1)$. Given the small rotational energy spacings, typically in any electronic and vibrational

state, several rotational levels are thermally populated, with higher J 's having the relative population given in (6.18). Thus a pure rotation spectrum often consists of equally spaced lines, $2B$ apart, with an intensity variation according to (6.18). The relative intensities grow initially because of the statistical factor $(2J + 1)$ but fall at high J due to the Boltzmann term. At an intermediate $J_{\max} \approx (kT/2hB)^{1/2}$, the “rotational band” has peak intensity (Fig. 6.7). With B values $\approx 20 \text{ cm}^{-1}$ for light diatomic and $\approx 1 \text{ cm}^{-1}$ for heavy molecules, the rotational bands lie in the far infrared or microwave range, respectively. In $^{12}\text{C}^{16}\text{O}$, the value of $2B$ is 115 GHz. Equivalently, $h^2/8\pi^2I$ is $3.83 \times 10^{-23} \text{ J} = 2.4 \times 10^{-4} \text{ eV}$. The transition $J = 1 \rightarrow 0$ at 2.6 mm is observed in many directions in the sky.

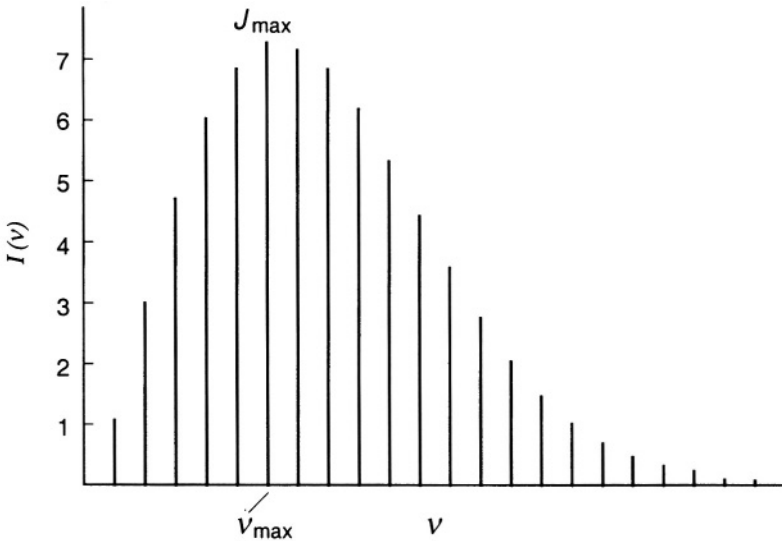


Figure 6.7. A “rotational band” spectrum. From [54], with permission of author and publisher.

The above presumes that the molecule has a permanent electric dipole moment. For homonuclear diatomic molecules in a specific electronic state, there can be no permanent electric dipole moment, the electronic distribution being symmetrical about the center of the molecule. Recall that in such a molecule there is a g/u symmetry with respect to inversion in the center so that $\langle \mathbf{d} \rangle$ vanishes, exactly analogous to atoms having no permanent moment because of parity conservation. In such molecules,

therefore, rotational spectra necessarily involve simultaneous changes in the electronic state.

3.2 Vibrational spectra

Considering next purely vibrational transitions within the same electronic states, the relevant matrix element is $\langle v' | \mathbf{d} | v \rangle \cdot \mathcal{E}$. Again, in a homonuclear molecule, within any single electronic state, the dipole moment vanishes for any internuclear separation R , the electronic distribution always having well-defined symmetry, *g* or *u*, with respect to the center. In a heteronuclear molecule, however, a non-zero moment can arise and, as with any consideration of vibration, we expand d around the equilibrium value

$$d = d(R_e) + (\partial d / \partial R)_{R_e} (R - R_e) + \dots \quad (6.23)$$

The first non-trivial off-diagonal matrix element between states $|v\rangle$ and $|v'\rangle$ is, therefore, $\langle v' | (R - R_e) | v \rangle$. For harmonic-oscillator wave functions (6.17), such a matrix element $\langle v' | x | v \rangle$ is non-zero only when

$$v' = v \pm 1, \quad (6.24)$$

providing the selection rule for vibrational transitions. Higher terms in the expansion (6.23) can give rise to weaker absorptions/emissions with $v' = v \pm 2, v \pm 3$, etc.

A vibrational transition in conformity with (6.24) gives rise to a spectroscopic line of frequency $\omega/2\pi$ with ω given in (6.16). Typical values lie in the 300–3000 cm^{-1} infrared region of the spectrum. The intensity of the line depends on the square of the derivative $(\partial d / \partial R)_{R_e}$ in (6.23) so that what is relevant is not the permanent moment $d(R_e)$ itself but its derivatives. The CO molecule is an example, $d(R_e)$ being only 0.1 D (1 D = 1 debye = 10^{-18} esu cm) but with a large first derivative so that it has a strong infrared absorption around 2150 cm^{-1} . Unlike in the case of rotations, vibrational spacings being large compared to typical thermal energies, the population of higher v levels according to (6.19) is generally small, although at higher temperatures or for molecules with $\omega/2\pi$ in the lower end of the range (about 300 cm^{-1}), absorptions $v = 1 \rightarrow v' = 2$ and higher analogs can be seen alongside the $0 \rightarrow 1$ transition. These higher bands are called “hot bands”.

Typically, one sees combined vibrational and rotational spectra. Fig. 6.8 gives an illustration, transitions $v = 0 \rightarrow v' = 1$ with several simultaneous changes in J grouping as shown, those with $\Delta J = -1$ forming the so-called P branch and the others with $\Delta J = 1$ the R branch. Because of the intensity variation due to rotational level populations according

to (6.18), a characteristic dip in the center, which would correspond to $\omega/2\pi$ of the pure vibrational $v = 0 \rightarrow v' = 1$ with no change in J , is seen. This is the situation for Σ electronic states but in states with $\Lambda \neq 0$, one can also see transitions with $\Delta J = 0$ giving rise to an intermediate “Q branch” in the spectrum. An example occurs in NO whose ground electronic state is ${}^2\Pi$.

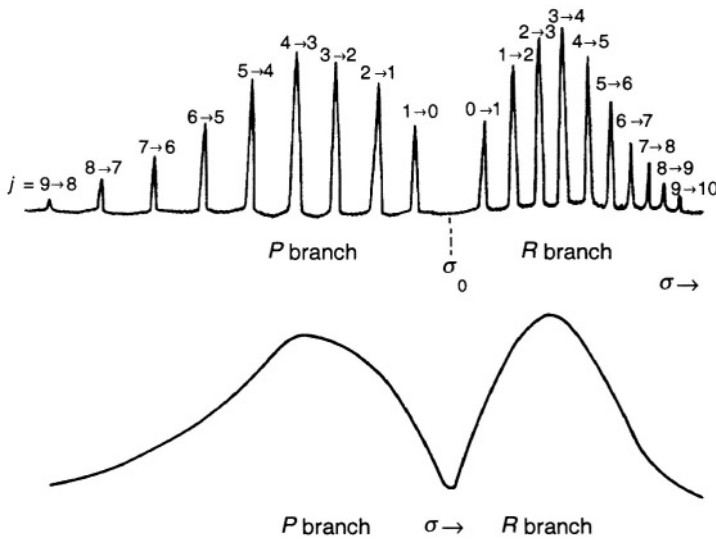


Figure 6.8. Combined vibration-rotation spectra, showing $P(\Delta J = -1)$ and $R(\Delta J = 1)$ branches for a Σ state. From [56], with permission of John Wiley and Sons, Inc.

Vibration-rotation spectra are useful for measuring isotopic composition. As seen in Table 6.2, different isotopes have different values of ω and B so that the spectral lines will be at slightly different frequencies. Fig. 6.9 gives an illustration in HCl , the two Cl isotopes with masses 35 and 37 splitting each line in a spectrum such as in Fig. 6.8. The high resolution attainable in spectroscopy allows observation of such splittings and, from the relative intensities, determines the relative isotopic composition. Related illustration of the role of μ_{AB} in quantities such as ω or the zero-point energy of the resulting vibrational level $v = 0$ was provided by the differences in the dissociation energies of H_2 , HD , and D_2 . The ground electronic state potential well $U(R)$ is the same for each of this isotopic family but the $v = 0$ level in it lies at different positions,

highest in H_2 and lowest in D_2 . Correspondingly, the energy required to dissociate the molecule, that is, the $v = 0$ energy relative to the common energy $U(R \rightarrow \infty)$, is highest for D_2 and lowest for H_2 .

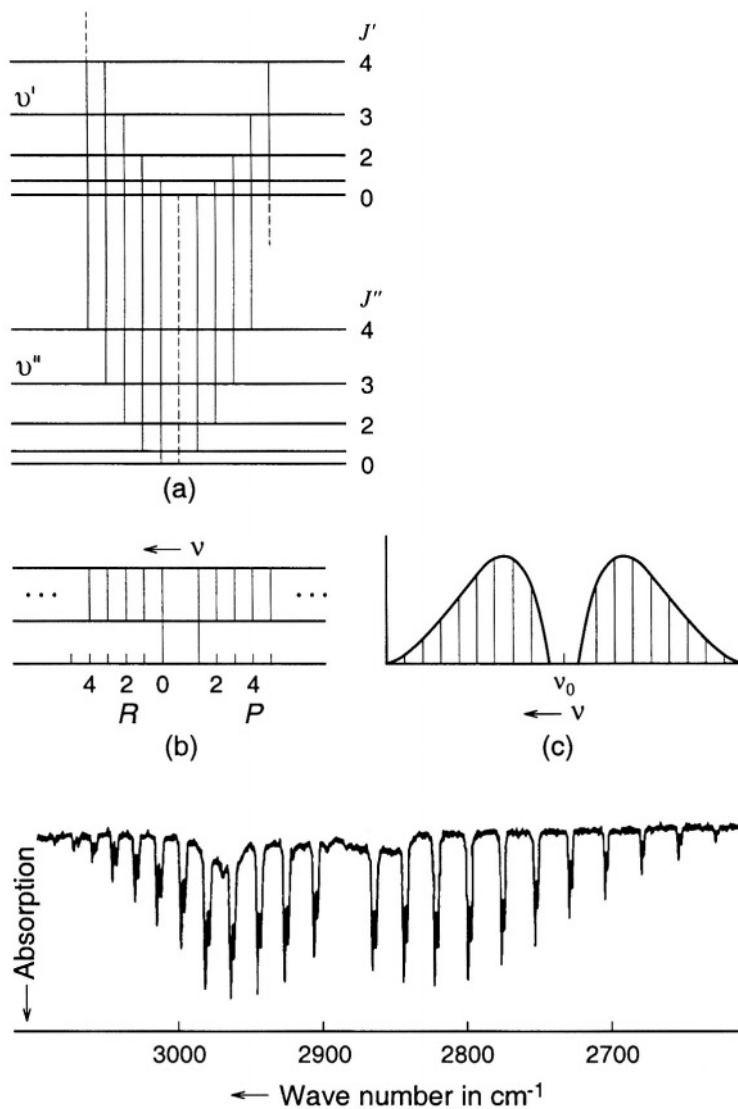


Figure 6.9. Vibration-rotation spectrum of HCl , showing isotopic splittings of ^{35}Cl and ^{37}Cl . From [54], with permission of author and publisher.

3.3 Raman spectra

As discussed in the above subsections, vibration-rotation spectra are available only for heteronuclear diatomic molecules. This leaves out homonuclear molecules, where a simultaneous electronic transition is necessary. Since such transitions often lie in the ultraviolet, superposed vibrational and rotational transitions occur as small shifts that are obscured or buried in the wings, an unsatisfactory state of affairs for their study, particularly given the importance of molecules like H_2 , N_2 , and O_2 . Therefore, the phenomenon of the Raman effect, wherein rotational and vibrational levels can be studied in light scattering even in homonuclear molecules, is of major importance to molecular physics, including applications in astronomy. In the Raman effect, instead of absorption or emission, one looks at the inelastic scattering of light. During the scattering, if the molecule makes a transition between vibrational or rotational levels, this is reflected in the frequency shifts of the scattered light. These shifts can be of either sign. Lines where the scattered photon is of lower frequency than the incident are called Stokes lines, the molecule making an associated transition from a lower to a higher level, while the opposite happens in the anti-Stokes lines with scattered frequency larger than incident. These two sets of lines appear on either side of the elastically scattered light which is referred to as Rayleigh scattering.

A permanent dipole moment is not necessary, an induced moment due to the polarizability of the electron cloud sufficient to cause inelastic scattering. Just as in atoms, all electron distributions, including those in homonuclear molecules, are polarizable by an electric field \mathcal{E} . For vibrational transitions, one can again expand the polarizability $\alpha(R)$ around its value at R_e

$$\alpha(R) = \alpha(R_e) + (\partial\alpha/\partial R)_{R_e}(R - R_e) + \dots \quad (6.25)$$

Just as in the discussion after (6.23), the first term in the expansion leads to $v' = v \pm 1$, the intensity of these scattered components proportional to the square of $(\partial\alpha/\partial R)_{R_e}$. For rotational Raman transitions, the induced effect can be viewed as a change of the molecule's $|J\rangle$ to an intermediate state $|i\rangle$ and then a second scattering in which the intermediate state goes to the final $|J'\rangle$:

$$\sum_i \frac{\langle J' | \mathbf{d} \cdot \mathcal{E} | i \rangle \langle i | \mathbf{d} \cdot \mathcal{E} | J \rangle}{\hbar\nu - (E_i - E_{J'})}. \quad (6.26)$$

Given the selection rules (6.22) for each of these matrix elements, we have $J' = J$ or $J \pm 2$ for the Raman transition. Thus, in the rotational

Raman effect, lines (Stokes and anti-Stokes) appear on either side of the central elastic value (Rayleigh line) with twice the separation of an ordinary rotational absorption/emission spectrum. In place of the P, Q, and R branches of that spectrum, the Raman bands are termed O, Q, and S.

Such rotational and vibrational Raman spectra are exhibited by all molecules, in particular, both homonuclear and heteronuclear diatomic species. For the former, there is the additional effect discussed in Section 6.2.7 that the Pauli principle applied to nuclei leads to alternating weights and, therefore, alternating intensities of odd and even J values. Fig. 6.10 gives an illustrative example in O_2 . The $\Delta J = 2$ rule and the skipping of all even J values (recall from Section 6.2.7 that O_2 $X^3\Sigma_g^-$ has only odd J) makes the separation between successive peaks $8B$. As in the data shown here, modern Raman spectroscopy is carried out with intense lasers to enhance the count rate, although the initial observation by Raman and Krishnan of this phenomenon was done with much weaker conventional light sources requiring long integration times to obtain a spectrum.

3.4 Electronic spectra

Molecular transitions involving changes in the electronic state have most features common with similar ones in atoms, now with the added element of the different dependences on R of the electronic potential wells for the initial and final state. Electric dipole transitions being dominant, they will be our focus, the transition operator involved being

$$\mathbf{d} = \mathbf{d}_e + \mathbf{d}_{\text{nucl}} = -\sum_i e\mathbf{r}_i + \sum_A eZ_A \mathbf{R}_A, \quad (6.27)$$

only the first term contributing between two different electronic states and only when the states conform to E1 selection rules as in Section 2.2.3. That is, parity must change in the transition (therefore, in homonuclear diatomic molecules, only $g \leftrightarrow u$ transitions are allowed) and the angular momentum must change by one unit. For such allowed transitions with non-zero

$$M_e(R) = \langle \mathbf{d}_e \rangle = \int \phi_f^*(R; \mathbf{r}) \mathbf{d}_e \phi_i(R; \mathbf{r}) d\mathbf{r}, \quad (6.28)$$

the matrix element $\langle \Psi | \mathbf{d} | \Psi \rangle$ reduces to

$$\int M_e(R) \psi_{\text{nucl}}^{f*} \psi_{\text{nucl}}^i dR \approx \langle M_e(R) \rangle \int \psi_{\text{nucl}}^{f*} \psi_{\text{nucl}}^i dR. \quad (6.29)$$

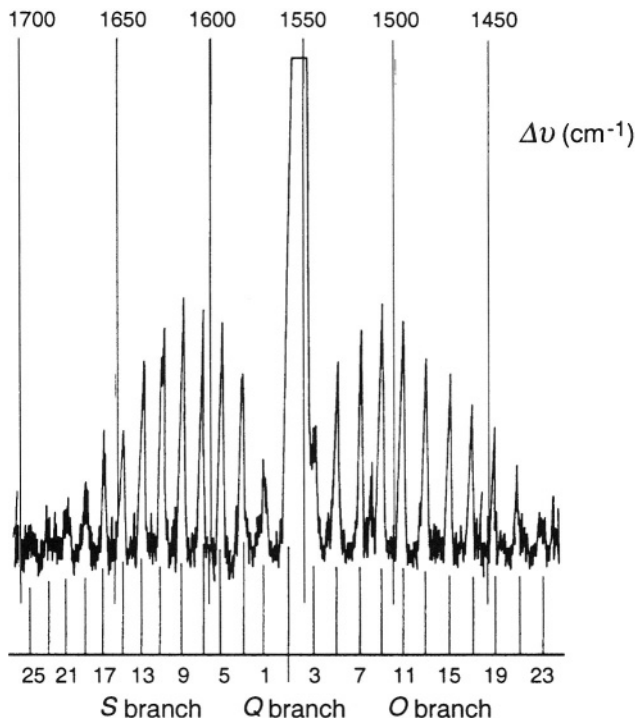


Figure 6.10. Raman spectrum of O₂. Note that all even J values are missing. From [54], with permission of author and publisher.

The parametric dependence on R of the electronic wave functions leads to an R -dependent $M_e(R)$ evaluated between the nuclear wave functions and, to a first approximation, upon taking out of the integral an average value of $M_e(R)$, we are left with an overlap of the initial and final nuclear wave functions.

As shown in Fig. 6.11, between any two electronic states, an overlap between the nuclear wave functions picks out groups of final vibrational states for any given initial one, the vibrational wave functions being non-negligible only over a small range of R (the classically allowed region for the eigenfunctions in the potential well). Thus, an electronic transition is accompanied by several possible vibrational (and rotational) transitions giving rise to a “band spectrum”. With the electric dipole selection rules already accounted for from the electronic wave functions, no other constraints are necessary on changes in v and J apart from

the consideration of overlap, the squared overlap a measure of the corresponding intensities. In particular, $\Delta J = 0$ transitions are allowed, not otherwise seen in pure rotational spectra (Section 6.3.1). The squared overlap, $|\langle v_f | v_i \rangle|^2$, is called the Franck-Condon factor. The approximation involved in (6.29) expresses an attendant “Franck-Condon principle” which, in conformity with the Born-Oppenheimer scheme, rests on the big disparity in the time scales of electronic and nuclear motion. These characteristic times being approximately 10^{-16} and 10^{-13} s, respectively, the nuclei are essentially frozen so that R does not change during an electronic transition. This leads to the “vertical transitions” depicted in Fig. 6.11. Note that, as in the example shown, it can happen that the vibrational $0 \rightarrow 0$ transition is not seen, only transitions involving changes in the vibrational quantum number. One consequence of this is shown in Fig. 6.12. When I_2 is illuminated (“pumped”) with the 514.5 nm line of Ar, a high vibrational level, $v = 43$, is populated. The resulting “population inversion” relative to vibrational levels from 9 to 56 on the ground electronic state can give rise to stimulated laser radiation.

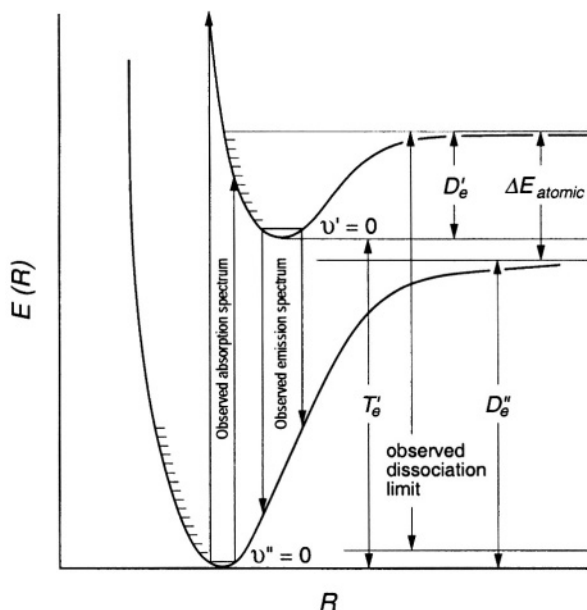


Figure 6.11. Illustration of Franck-Condon transitions between electronic states. From [54], with permission of author and publisher.

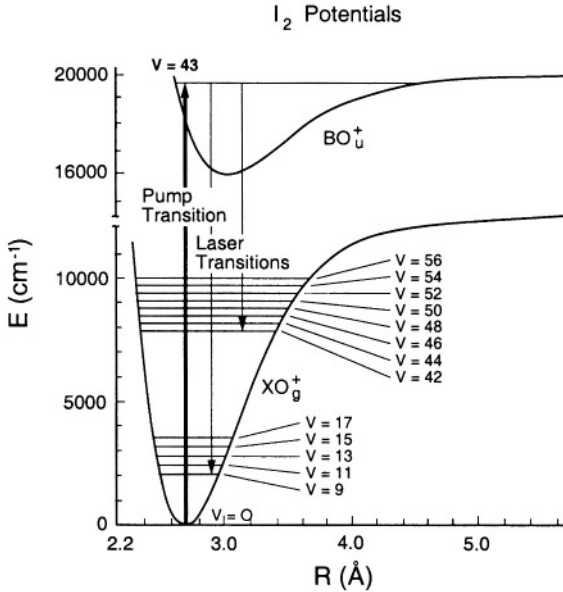


Figure 6.12. As in Fig. 6.11, for the I_2 molecule, showing population inversion of $v = 43$ and subsequent lasing transitions. From [54], with permission of author and publisher.

If the upper states that are reached lie above the dissociation limit (as in the left band of Fig. 6.11), the molecule may dissociate during the photoabsorption. Measuring the translational kinetic energy of the photofragments can provide information on the molecular potentials. “Direct photodissociation” is illustrated in Fig. 6.13(a). Since motion along R is faster than the time for spontaneous radiation back to the lower electronic potential well, such absorptions lead to molecular dissociation. The CH^+ ion, important in interstellar gas clouds, provides an example. At low photon energies around 4 eV (300 nm), absorption from the ground $X^1\Sigma$ to the excited $A^1\Pi$ has Franck-Condon factors favoring bound vibrational levels, and dissociation (to C^+ and H) cross-sections are only about 10^{-20} cm². They have been experimentally measured in the laboratory. The reverse radiative association, $C^+ + H \rightarrow CH^+ + h\nu$ is also important in interstellar clouds. But, at higher energies around 12–13 eV, the purely repulsive $3^1\Sigma^+$ excited state leads to dissociation cross-sections larger by three orders of magnitude. Corresponding rates are $\approx 3 \times 10^{-10}$ s⁻¹ instead of 10^{-13} s⁻¹ for the $^1\Pi$ state. This dissociation leads to H^+ and excited C atoms. Absorption of 127–175 nm ultraviolet radiation by O_2 from the $^3\Sigma_g^-$ ground state to the excited

$B^3\Sigma_u^-$ leads similarly to the Schumann-Runge bands, dissociation to the continuum now leading to excited O^1D which leads to the 630 nm red line of aurorae. Absorption to other excited states such as $A^3\Sigma_u^+$ of 160–240 nm radiation leads on the other hand to $O(^3P)$, important for the subsequent collisional formation of ozone.

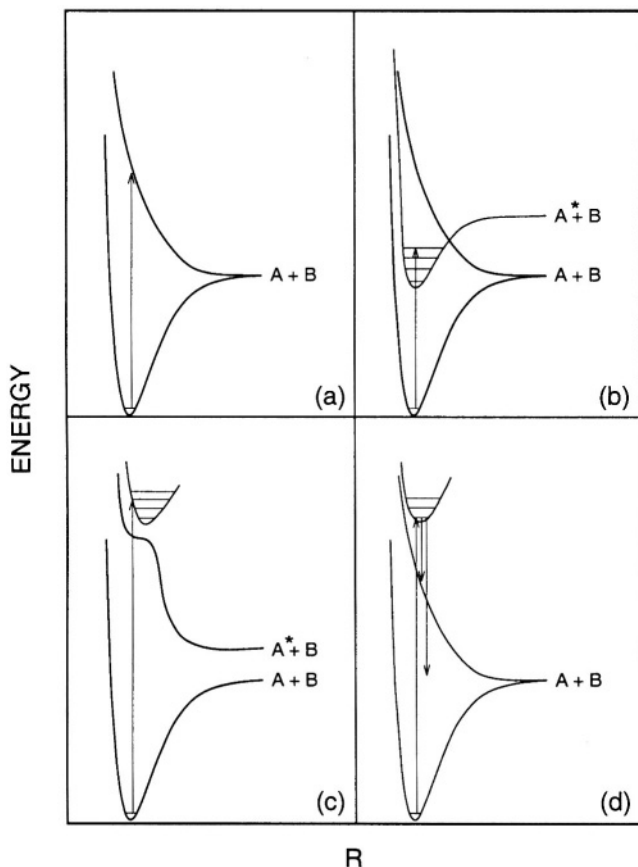


Figure 6.13. Photodissociation of a molecule. (a) Direct. Indirect processes through initial absorption to bound vibrational levels subdivide into (b) predissociation, (c) coupled-states dissociation, and (d) spontaneous radiative dissociation. From K. Kirby and E. F. vanDishoeck, *Adv. At. Mol. Phys.* **25**, 437 (1988), with permission of author and publisher.

“Indirect” photodissociation processes proceed through an initial absorption to bound vibrational levels of an excited electronic state as shown in Fig. 6.13(b)-(d) which are classified, respectively, as predissociation, coupled-states dissociation, and spontaneous radiative dissociation.

tion. In predissociation, a third state of different symmetry crosses the excited electronic state and non-adiabatic couplings lead to its population, and thereby the break-up of the molecule. Examples occur in CO and HCl. Fig. 6.13(c) differs in that the third state is of the same symmetry so that the coupling is stronger. CH and OH provide examples. A series of resonances superposed on a continuum background may be seen. In spontaneous radiative dissociation, shown in Fig. 6.13(d), emission of radiation from bound levels of an excited electronic state into a lower repulsive state, or perhaps the vibrational continuum of the ground state, leads to dissociation. The radiation emitted is seen as a series of peaks. Dissociation of H₂ in the interstellar medium takes place primarily through this process. In laboratory electrical discharges in H₂, the same mechanism operates with electron impact excitation playing the role of photoabsorption. The emitted spectrum extends from the visible to the extreme ultraviolet. Substantial kinetic energies, as much as 1 eV, are also involved in the dissociated H atoms. Solar radiation has its peak intensity at 500 nm, intensity at 150 nm being five orders of magnitude weaker. On the other hand, the interstellar radiation field has substantial intensity throughout the ultraviolet down to 91.2 nm. As a result, while only the lowest-lying channels are effective in dissociation of cometary and planetary molecules, higher channels dominate for the same molecules in interstellar space. All photodissociation calculations are very sensitive to the molecular potentials.

Rotational fine structure can be seen under higher resolution on each vibrational transition. As in pure rotational spectra, the same designation of P, Q, and R branches is used, whether in absorption or emission, according to whether the lines lie lower in frequency, at the frequency, or higher than the pure vibrational transition with $\Delta J = 0$. With non-¹Σ electronic states, the interplay between electronic angular momentum and the angular momentum of the internuclear axis complicates analysis of the rotational structure. Different coupling schemes between the two angular momenta, called Hund's coupling cases, need to be considered. One manifestation of the interaction, that is, of the coupling between the magnetic moments due to the two angular momenta, is to split each $\Lambda \neq 0$ state, giving rise to Λ-doubling and pairs of closely lying lines with separations less than 1 cm⁻¹. In Hund's case (a), the electronic orbital and spin momentum are coupled strongly to the internuclear axis, so that Λ and S_z are good quantum numbers. In Hund's case (b), the spin uncouples from the internuclear axis so that S_z is not defined. All Σ states (Λ = 0) and S = 0 states belong to case (b).

3.5 External field effects on molecular spectra

The Zeeman and Stark effects of static magnetic and electric fields, respectively, in molecules are analogous to those in atoms. In particular, for a $^1\Sigma$ molecule with nuclear spin zero, the only magnetic moment to couple to an external magnetic field \mathbf{B} arises from molecular rotation and leads to changes in energy given by first-order perturbation theory,

$$\Delta E = -(e\hbar/2\mu_{\text{AB}} c) Bg \frac{M_J}{\sqrt{J(J+1)}}, \quad (6.30)$$

where g is the g -factor. Because of the nuclear masses involved, the energy change is generally very small.

The Stark effect can be more important in molecules than in atoms because the former can have permanent electric dipole moments. Thus, polar molecules such as HCl can show the linear Stark effect whereas atoms with the exception of excited states of hydrogen do not (Section 3.2.3). For such a molecule with $\Lambda \neq 0$, we have

$$\Delta E = \mu_e \mathcal{E} M \Lambda / J(J+1). \quad (6.31)$$

States with $\Lambda = 0$ or homonuclear diatomic molecules display only a quadratic Stark effect just as in atoms.

The Zeeman effect also leads to magneto-optic rotation and circular dichroism. In the first, the plane of polarization of light is changed under transmission through a molecular gas whereas in dichroism, the gas exhibits different refractive indices for left and right circularly polarized light. Both arise because the Zeeman effect changes the $\Delta M = +1$ (right circularly polarized) and $\Delta M = -1$ (left circularly polarized) transition frequencies. As a result, because of dispersion, the corresponding refractive indices are slightly different. Magnetic circular dichroism is used in spectroscopy to untangle complex spectra, particularly those of large molecules.

3.6 Collisional processes

Molecules can also be excited or de-excited by collisions with electrons, ions, or neutral species. If n is the number density of such projectiles and v their velocity, then the rate of any transition is given by $nv\sigma(i \rightarrow f)$, where σ is the cross-section for the process. In general, the product is averaged over the distribution (often thermal) of collisional velocities. Such processes are critically important in astrophysical clouds, the most important being rotational excitation through low energy collisions with H_2 and H . Unlike radiative processes, collisions are not subject to strict

selection rules although “propensity rules” govern which transitions are more probable.

For the low kinetic energies that prevail in interstellar clouds, scattering cross-sections can be obtained either through a complete scattering analysis or often through some simpler approximation schemes (Section 2.3). Thus, if the interaction between projectile and molecule is weak, the Born approximation is used. This is an instance of first-order perturbation theory, the transition matrix element evaluated by integrating the interaction multiplied by the initial and final state wave functions of the projectile and target:

$$\langle f|V|i\rangle = \int d\mathbf{r} \int d\tau \exp(-i\mathbf{p}_f \cdot \mathbf{r}/\hbar) \psi_f^*(\tau) V(\mathbf{r}, \tau) \exp(i\mathbf{p}_i \cdot \mathbf{r}/\hbar) \psi_i(\tau), \quad (6.32)$$

where plane waves describe the incident and scattered projectile with coordinate \mathbf{r} , and τ represents collectively all the other coordinates. The cross-section for projectile scattering into a solid angle element $d\Omega_f$ is

$$d\sigma/d\Omega_f = (4\pi^2 M \hbar)^2 |\langle f|V|i\rangle|^2 (p_f/p_i), \quad (6.33)$$

with M the reduced mass of (projectile + target).

The interaction $V(\mathbf{r}, \tau)$ in the case of collisions with electrons and positive ions is the Coulomb potential between the projectile and the electrons and nuclei in the molecule. On the other hand, in the collision between two neutral systems A and B that themselves carry electron clouds, one can trace the interaction from separated to united atom limits much as in Section 6.2.1 and follow along such a potential curve the evolution in R of the system from infinity to the distance of closest approach of A and B. At large R , the most dominant term in the potential is the van der Waals potential proportional to $\alpha_A \alpha_B / R^6$, where α_A and α_B are the electronic polarizabilities of the two molecules. This expresses the interaction between the electric dipole moments induced in each molecule by the other. In the analysis of cold collisions, other terms involving powers R^{-8} and R^{-10} are superposed on the dominant R^{-6} , these often obtained semi-empirically by fitting to experimental data.

4. Astrophysical Applications

Whereas absorption and emission by atoms and positive ions has been studied since the beginnings of astrophysics in the 1860s, the study of molecular species is more recent. Given the dominant abundance of hydrogen in the universe, although it could always have been expected that

its molecular form of H_2 would be a major species, the lack of an electric dipole moment of this symmetric molecule makes its direct observation difficult. The first molecular observations in 1937 were, therefore, of CH and CH^+ , later also CN. The high abundance of CH^+ , sometimes comparable to CH in many molecular clouds, is a puzzle given more loss mechanisms through collisions such as $\text{CH}^+ + \text{H} \rightarrow \text{C}^+ + \text{H}_2$ and $\text{CH}^+ + \text{H}_2 \rightarrow \text{CH}_2^+ + \text{H}$. This suggests additional sources for its formation, possibly from shock-heated or otherwise excited H_2 through $\text{C}^+ + \text{H}_2(v \geq 1) \rightarrow \text{CH}^+ + \text{H}$. Both CH and CH^+ are detected through narrow absorption lines in the spectra of several stars (Fig. 6.14), CH also in the ground state doublet transition of 9 cm in the radio region. For the former lines shown in Fig. 6.14, the Franck-Condon factors are such that only $v = 0 \rightarrow 0$ is observed. These species are widespread in the galaxy and found towards H II regions and in optically dark nebulae. Semiclassical rate coefficients for their formation through radiative association in cold clouds (100 K) are approximately $10^{-18} \text{ cm}^3 \text{ s}^{-1}$ for $\text{C} + \text{H} \rightarrow \text{CH} + h\nu$ and $1.3 \times 10^{-17} \text{ cm}^3 \text{ s}^{-1}$ for $\text{C}^+ + \text{H} \rightarrow \text{CH}^+ + h\nu$. CH is also seen as a weak maser (Section 7.3) in Orion clouds with column densities of $10^{12-15} \text{ cm}^{-2}$. CH and CH^+ are also seen in comets.

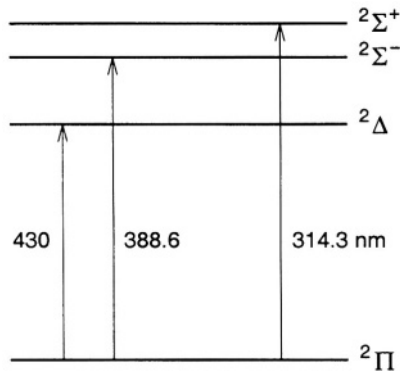


Figure 6.14. Absorption lines of CH seen widely in the galaxy and in dark nebulae.

It is estimated that something like 4% of interstellar hydrogen is in the form of H_2 , the molecular form dominant in the interior of dense clouds where the molecules are shielded from ultraviolet radiation of wavelengths shorter than 91.2 nm. These wavelengths are absorbed by atomic hydrogen, producing H I regions on the outside of such clouds. But wavelengths between 91.2 and 101.7 nm can be absorbed into dis-

crete vibrational levels of excited electronic states of H_2 followed by emission into the vibrational continuum of the ground electronic state. This is the dominant destruction mechanism of H_2 (Section 6.3.4). Rocket flights of the early 1970s were needed to see such absorption bands of H_2 around 100 nm. Up to eight Franck-Condon transitions are seen in the 110 nm absorption $^1\Sigma_g^+ \rightarrow ^1\Sigma_u^+$. The infrared rotational spectrum of H_2 is not seen but weak quadrupole rotation-vibration bands occur. Thus, from the object NGC 7027, the $v = 1 \rightarrow 0$ transitions between 0.9 and 2.7 μm have been observed. Only ortho hydrogen (odd J values) is seen, indicating temperatures greater than several hundred K. A spectacular example from a superluminous galaxy NGC 6240 is shown in Fig. 6.15. Another indirect evidence is the observation of CO in radio wavelengths (the $J = 0 \rightarrow 1$ $^1\Sigma$ transition is at 115 GHz or 2.6 mm), these emissions due to excitation of rotational levels in collisions with H_2 , thereby allowing the H_2 density in such dark clouds to be inferred. Interstellar clouds come in two types, dark and giant, the CO lines more intense in the latter. Typical H_2 densities are 10^3 cm^{-3} in both. A giant cloud of 10 pc diameter, with one CO molecule/ cm^3 would have a total mass of $10^4 M_\odot$, and there are at least a hundred such clouds in our galaxy. Isotopic differences between $^{12}\text{C}^{16}\text{O}$ and $^{13}\text{C}^{16}\text{O}$ are manifest in their spectra. The weakness of the 21 cm radio line of atomic hydrogen in regions of high obscurity is yet another indirect pointer to hydrogen being in molecular form.

Thermal excitation of the lowest five rotational levels of H_2 by the primordial cosmic background radiation has also been noted from the same gas clouds mentioned at the end of Chapter 1 with cosmic redshift $z = 2.337$. This indicates a prevailing temperature of about 9 K at that epoch.

Similar to CO is the molecule CS, its $J = 2 \rightarrow 3$ transition at 147 GHz (≈ 2 mm) also seen in the radio spectrum. The CN molecule with a dipole moment of 1.45 D is another important species, its $J = 0 \rightarrow 1$ 2.65 mm line in the ground electronic and vibrational state having a transition probability of $1.2 \times 10^{-5} \text{ s}^{-1}$. Such millimeter wave transitions are strongly influenced by the 2.8 K cosmic black-body radiation that pervades the Universe. Indeed, that this CN transition was seen in absorption against the general background, or that absorption from $J = 1$ at 387.46 nm relative to that from $J = 0$ at 387.4 had appreciable ratios of nearly $\frac{1}{2}$ (as against an expected 0.03 based on typical interstellar conditions), thereby indicating substantial population of the $J = 1$ state, were early indicators of the presence of this background radiation although not initially recognized as such.

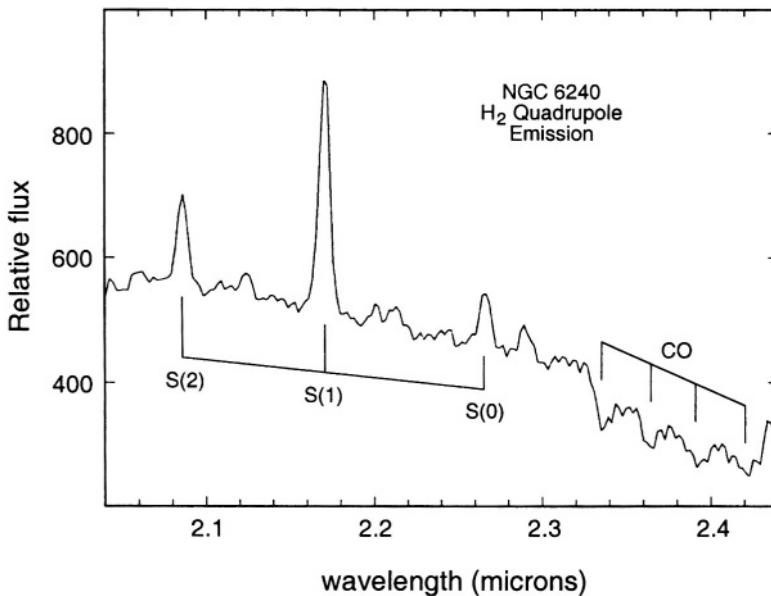


Figure 6.15. Quadrupole emission of H_2 from the galaxy NGC 6240 (red-shift 0.0254). The line $S(1), v = 1 \rightarrow 0, J = 3 \rightarrow 1$ of ortho-hydrogen has the brightness of 10^8 solar luminosities. From T. Oka, *Rev. Mod. Phys.* **64**, 1141 (1992).

Another important diatomic molecule is OH, first seen in its 18 cm radio wavelength transitions in the early 1960s. As shown in Fig. 6.16, each rotational state is split by Λ -doubling and further into pairs of hyperfine levels. All four transitions are seen in dark interstellar clouds, including in maser emission (Section 7.3).

The diatomic molecules O_2 , N_2 , NO, and their ions are important in our atmosphere and in other planetary atmospheres. In the so-called E-layer of the ionosphere (90–130 km), O_2^+ and NO^+ are the main ions (the former during day time and the latter at night), whereas in the higher F-layer it is predominantly O^+ . The formation of atomic O is of interest, either through dissociative recombination, $\text{O}_2^+ + e \rightarrow \text{O} + \text{O}$, or through collisions with any molecule XY whose ionization potential is lower than oxygen's (such as O_2 or NO), $\text{O}^+ + \text{XY} \rightarrow \text{O} + \text{XY}^+$. Since densities of XY decrease with latitude and are low in the F-layer, the effective recombination decreases with latitude in the F-layer while being essentially independent of it in the E-layer. The dissociative recomb-

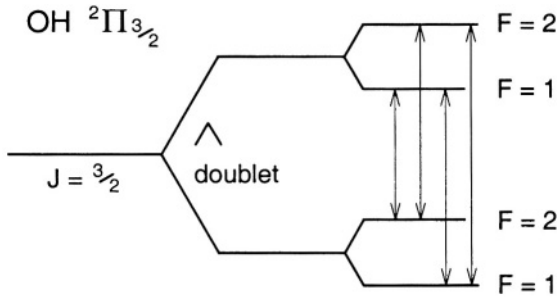


Figure 6.16. Λ -doubling and hyperfine levels in the ground state of OH.

nation coefficients of O_2^+ , N_2^+ , and NO^+ are all of the order of $10^{-7} \text{ cm}^3 \text{ s}^{-1}$ at room temperature. A more important loss mechanism for N_2^+ at altitudes less than 200 km is through $N_2^+ + O \rightarrow NO^+ + N$, this being also the major source of NO^+ . Because NO 's ionization energy of 9.4 eV is lower than that of other atoms and molecules, once NO^+ is formed, it cannot lose its charge through $NO^+ + O \rightarrow NO + O^+$ or $NO^+ + N_2 \rightarrow NO + N_2^+$, and it therefore builds up. Below 100 km, the photoionization of NO is important, Ly_α (10.17 eV) penetrating this far and sufficient to ionize NO but not O_2 . Thus, at 80 km, their density ratio is about 50.

At altitudes above 150 km, about half the O^+ produced by photoionization is in the metastable 2D and 2P states with enough energy to produce N_2^+ through $O^+ + N_2 \rightarrow N_2^+ + O(^3P)$, whereas the other half in the ground 4S state can only produce NO^+ . Subsequent electronic excitation of $O(^3P)$ to $O(^1D)$ followed by the re-radiation $O(^1D) \rightarrow O(^3P)$ is responsible for the 630 nm red line of aurorae. Other transitions arising from $O^+ + e \rightarrow O^* + h\nu$ that are seen in the atmosphere include $4p^3P \rightarrow 3s^3S$ (436.8 nm) and $3s^3S \rightarrow 2p^3P$ (130.4 nm). The 557.7 nm $O^1S \rightarrow ^1D$ produces the green glow at 300 km. It has also been seen recently from the dark side of Venus, attributed to photodissociation of CO_2 on the sunlit side, with the O transported by winds and then collisionally excited by about 4 eV to the 1S state. The 732 and 733 nm decays of $O^+ ^2P_{3/2}$ are also seen in the ionosphere. Photoionization of O^+ and O in the ionosphere also produces O^{++} which is removed by $O^{++} + O \rightarrow O^+ + O^+$. The nearly resonant process (ionization potentials differ by 0.02 eV) $O^+ + H \rightarrow O + H^+$ has a rate

coefficient (product of cross-section and velocity) of $4 \times 10^{-10} \text{ cm}^3 \text{ s}^{-1}$ at 10^3 K in the ionosphere.

Problems

- 6.1 Construct the molecular orbital configuration and the quantum numbers of the ground electronic state of (a) CN, (b) CO.
- 6.2 Using atomic orbitals, $\exp(-r_A/a_0)$ and $\exp(-r_B/a_0)$, evaluate the expectation value of the Hamiltonian for the H_2^+ molecule as a function of the inter-nuclear distance R_{AB} to construct Fig. 6.1. Evaluate explicitly the splitting at large R_{AB} .
- 6.3 Use the entries in Table 6.2 to estimate the temperature at which one can expect 30% of the H_2 molecules in a sample of the gas to be in the first excited vibrational state.
- 6.4 As in Problem 6.3, at what temperature will half of the molecules be in the first excited rotational state?
- 6.5 Inter-relate the entries in the third and fourth columns of Table 6.2 for the isotopic partners H_2 , HD, and D_2 by using the masses of the nuclei involved.
- 6.6 Considering the parameter a in (6.20) to be small, expand to match the quadratic term in (6.10). Evaluate the effect of the next term in the expansion perturbatively.
- 6.7 Use the entries in Table 6.2 to estimate the number of rotational levels of LiH between the ground and first excited vibrational levels of that molecule.
- 6.8 From adjacent vibrational Raman lines at 267 and 343 nm, estimate the fundamental vibrational frequency of the molecule.
- 6.9 Given that the intensities of alternate rotational Raman lines are in the ratio 1:2, identify whether the molecule involved is H_2 or D_2 .
- 6.10 Determine the moment of inertia and the internuclear distance of the $^1\text{H}^{35}\text{Cl}$ molecule, given that the first rotationally excited state lies 21 cm^{-1} above the ground state. Evaluate the corresponding excitation in $^2\text{H}^{35}\text{Cl}$.
- 6.11 The potential energy wells $U(R)$ for different isotopes of the same molecule are the same, while vibrational and rotational energy levels

and dissociation energies vary. Given that H_2 has a dissociation energy of 4.48 eV and a vibrational energy spacing of 0.54 eV (assuming a harmonic oscillator well), calculate the dissociation energies of HD and D_2 .

- 6.12** The band spectrum of $^{35}\text{Cl}_2$ shows an alternating intensity ratio of 3/5. What is the spin of the ^{35}Cl nucleus? Explain.
- 6.13** A diatomic molecule has identical spinless nuclei. Do you expect to see a pure rotational spectrum? Will the molecule exhibit a rotational Raman spectrum? Will your answers differ if the nuclei were not identical?
- 6.14** For ortho and para deuterium ($^2\text{H}_2$), provide the parallel analysis of the rotational spectra to that given for $^1\text{H}_2$ at the end of Section 6.2.7.

Chapter 7

POLYATOMIC MOLECULES

1. Introduction

The diatomic molecules considered in Chapter 6 are the major constituents and have the dominant role in astronomically relevant molecular physics. However, many more complex molecules, starting with the triatomic H_3^+ and H_3 , H_2O , CO_2 , and CS_2 , and continuing to very large organic molecules, also have important roles and will be the object of our study in this chapter. Many of the basic ideas have already been introduced in the previous chapter and we will focus on the additional specific features that are relevant to polyatomic molecules.

2. Structure and Spectra of Polyatomic Molecules

2.1 Born-Oppenheimer approximation and electronic structure

The Born-Oppenheimer adiabatic separation of electronic motion from that of the nuclei (Section 6.2.3) continues to be central to the study of polyatomic species as well, and for the same reasons. The electrons, being much lighter, move faster than the nuclei so that the quantum mechanics of electronic motion can be viewed against the backdrop of a fixed geometrical arrangement of the nuclei which provide the Coulomb attractions to the electrons. Also common to the study of polyatomic and diatomic molecules is the concept of molecular orbitals that the electrons occupy, these playing an analogous role to that of Bohr eigenfunctions for atoms. The major difference between a diatomic molecule and a more complicated polyatomic one is that a single variable \mathbf{R} and cylindrical symmetry about one axis no longer suffices (although cylindrical symmetry still pertains to linear molecules such as O-C-O). The

nuclei are arranged in more complicated geometries and one has to consider the symmetries of these configurations under rotations with respect to various axes and reflections in various planes. This study, also relevant to crystal structure, has a long history and goes under the name of discrete or point group symmetry [50]. It lies outside the scope of this book but we merely note that such systematic classifications and descriptions exist. As a simple example, the fixed linear arrangement of two oxygen atoms symmetrically on either side of the central carbon in the CO_2 molecule makes this molecule invariant with respect to rotations through 180° about a perpendicular axis through the carbon and various reflections through horizontal and vertical planes with respect to the axis of the molecule. The triangular H_3 molecule, on the other hand, has other symmetries such as rotations through 120° .

Since the H_{e1} in (6.5) commutes with the various symmetry operations characterizing the molecule's point group symmetry, the electronic wavefunctions ϕ_{e1} can be labeled by the symmetry of each configuration. They are typically indicated by A_1, A_2, B_1, B_2 , etc, each characterized by the eigenvalues corresponding to the various symmetry operators of rotations and reflections. By their very nature, reflections always have eigenvalues ± 1 . Rotations through 180° also have eigenvalues that take only the two values ± 1 so that in a molecule such as CO_2 , these A_i and B_i are a collection of ± 1 labels. On the other hand, H_3 has some eigenvalues $e^{\pm 2i\pi/3}$. These labels, termed characters, and character tables for each point group symmetry, are available and every molecule can be assigned based on geometry its particular symmetry and corresponding sets of characters. The molecular orbitals are correspondingly built to have the same symmetries and labeled a_1, a_2, b_1, b_2 , etc. For linear molecules, since the projection L_z on the axis remains a good quantum number, the same $\sigma, \pi, \delta, \dots$ labels of diatomic molecules are used, as well as g and u if the molecule (such as CO_2) has a center of symmetry. Each of these molecular orbitals can hold two electrons of opposite spin projection, and orbitals of the same symmetry but increasing energy are denoted $1a_1, 2a_1, 3a_1, \dots$, etc. Thus the ten electrons of H_2O occupy the configuration $(1a_1)^2(2a_1)^2(1b_2)^2(3a_1)^2(1b_1)^2$, where $1a_1$ is mainly the $\text{O}1s$, $2a_1$ a bonding combination of $\text{O}2s, \text{O}2p_z$ and $\text{H}_11s + \text{H}_21s$, $1b_2$ a bonding $\text{O}2p$ and $\text{H}_11s - \text{H}_21s$, $3a_1$ again a combination of $\text{O}2s, \text{O}2p_z$ and $\text{H}_11s + \text{H}_21s$, and $1b_1$ a non-bonding $\text{O}2p_x$. These are the counterparts of the symmetry orbitals $1s_A \pm 1s_B$ discussed in Section 6.2.1 for H_2 .

Starting with atomic orbitals on each nucleus, one constructs linear combinations for the molecular orbitals with the appropriate symmetries. In the case of the H_2O molecule, the construction in the previous paragraph employs, therefore, the seven atomic orbitals: $\text{H}_11s + \text{H}_21s$,

$O1s$, $O2s$, $O2p_z$, $O2p_x$, and $O2p_y$. As in the case of atoms in Section 1.4.4, a Hartree-Fock or self-consistent field (SCF) calculation, possibly with multiple configurations (MCSCF), is carried out by taking these linear combinations of atomic orbitals (LCAO) and diagonalizing H_{el} in that set of basis states. The resulting eigenvalues and eigenfunctions provide the molecular orbitals. Even with a single configuration, such as in the example above with seven basis functions, more molecular orbitals are derived than are occupied in the ground or even low-lying excited states. Thus, of the seven, only the five lowest, $1a_1$, $2a_1$, $3a_1$, $1b_2$, and $1b_1$, are occupied in H_2O and two are unoccupied "virtual orbitals". They may be employed to describe excited states although any change in electronic configuration typically leads to rearrangement of all molecular orbitals. The atomic orbitals in such calculations may be hydrogenic (called "Slater orbitals") or, for ease of multi-center integrals, replaced by Gaussian functions with an $\exp(-cr^2)$ form in place of $\exp(-r/na_0)$.

Such *ab initio* calculations become very cumbersome for medium or large-sized molecules and various semi-empirical methods have been used instead. With the inner electrons and nucleus of each atom described as a simplified "core" and providing a "pseudo-potential" for the other valence electrons (empirical valence ionization potentials used to fit parameters describing the core model Hamiltonian), and further approximations, such methods under the names "complete neglect of differential overlap" (CNDO), etc., are available as complex computer programs for the determination of the electronic states of molecules.

Electronically excited or ionized states of polyatomic molecules are also considered analogously. Photoelectron spectroscopy, which monitors the energies of emitted photoelectrons, is useful for mapping such electronic states. Fig. 7.1 shows the photoelectron spectrum of the water molecule, with three distinct groups of electron kinetic energy, each with additional vibrational structure superposed. From the $(1a_1)^2(2a_1)^2(1b_2)^2(3a_1)^2(1b_1)^2$ 1A_1 ground state of H_2O , ionization out of the $1b_1$ orbital (ionization energy 12.62 eV) to leave behind the $\dots(3a_1)^2(1b_1)$ 2B_1 ground state of H_2O^+ accounts for the extreme right peaks in Fig. 7.1, whereas ionization out of $3a_1$ and $1b_2$ orbitals, respectively (with ionization energies 14.7 and 18.6 eV), accounts for the two higher energy groups of ejected electrons. The last of these states is unstable with respect to the dissociation $H_2O^+ \rightarrow H+OH^+$ so that the vibrational peaks are diffuse and broadened.

An important class of electronic excitations is when an electron in the outermost orbital is excited to a Rydberg orbital, thus the b_1 in H_2O to ns , np , etc., with $n \geq 3$. As in atomic Rydberg states, the outer excited electron moves for the most part in the Coulomb field of the ion, and

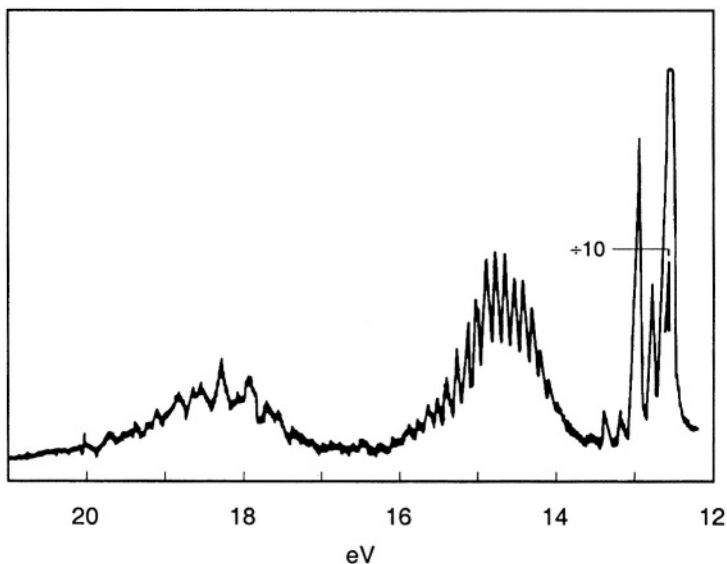


Figure 7.1. Photoelectron spectrum of H_2O . Three groups of vibrationally resolved electron kinetic energies of increasing values correspond to ionization from the $1b_1$, $3a_1$, and $1b_2$ orbitals, respectively, in the 1A_1 ground state. From [54], with permission of author and publisher.

energies are described by the Rydberg formula (1.25) with a quantum defect that depends on the ℓ value of the excited electronic state and its symmetry. Thus, in H_2O , the first ionization energy is 12.62 eV ($101,780 \text{ cm}^{-1}$) and $\delta=1.05$ describes the $4s, 5s, 6s, \dots$ Rydberg states while $\delta=0.7$ provides the energies of the $3p, 4p, 5p, \dots$ series. Rydberg states occur both in diatomic and polyatomic molecules. Indeed, series in H_2 measured to very large n are the basis for determining its ionization potential to great precision.

Other topics that make the study of electronic states in polyatomic molecules more complicated than in atoms or even diatomic molecules include coupling between vibration and electronic wave functions called vibronic coupling. Vibrations can distort even the geometrical structure and, therefore, symmetry of the electronic state. The absorption spectrum of even a simple molecule like NO_2 , the same absorption responsible for the characteristic “smog” of urban atmospheres (NO_2 is a major component of car exhausts), is complex because of such an entanglement of upper electronic states with high vibrational levels of

the ground state. The vibronic coupling and the large density of states in polyatomic molecules also leads to radiationless transitions. Thus, not all the radiation energy absorbed is re-emitted as fluorescence, only about 30% in benzene even at low pressures. At higher pressures and in the condensed phase, some of the energy is trapped (a change from singlet to triplet states often plays a role) to be re-radiated with a time delay, a phenomenon called phosphorescence while some never re-emerges as radiation, the molecule giving up that energy in collision or other radiationless processes.

Yet another phenomenon goes under the name of the Jahn-Teller effect which arises from a nonlinear polyatomic molecule not having an equilibrium nuclear configuration for an orbitally degenerate electronic term. Such an orbital degeneracy can arise from molecular symmetry. Thus, in benzene (C_6H_6), excitation of an electron from the highest occupied molecular orbital is to a π orbital and gives two orbitally degenerate electronic terms. These terms cannot then have the regular hexagonal symmetry of equilibrium C_6H_6 . The lowest energy is achieved for a geometry that departs from the regular hexagon which removes the exact degeneracy of the two molecular orbitals and thus gives an orbitally nondegenerate electronic term.

2.2 Rotation of polyatomic molecules and spectra

As with diatomic molecules, in the Born-Oppenheimer approximation, the total wave function of a polyatomic molecule is a product of the electronic wave function described above and a function describing the rotations and vibrations associated with the degrees of freedom of the nuclei. Again, in a first description, the rotation and vibration wave functions occur separately in product form, the same hierarchy prevailing that makes the associated energies differ by about two orders of magnitude.

We will consider first the rotation. For diatomics, which have only one axis, rotations with respect to the two perpendicular and equivalent directions are described as a single rotor Hamiltonian (6.8) with eigenstates $|JM\rangle$ in (6.9). For a general polyatomic molecule, however, with some fixed equilibrium configuration of the nuclei (obtained by solving the electronic motion as in Section 7.2.1), as with the rotations of any rigid body in three-dimensional space, one has three different moments of inertia I_a , I_b , and I_c (with $I_a \leq I_b \leq I_c$) and corresponding Hamiltonian

$$H_{\text{rot}} = \left(\mathbf{J}_a^2 / 2I_a \right) + \left(\mathbf{J}_b^2 / 2I_b \right) + \left(\mathbf{J}_c^2 / 2I_c \right). \quad (7.1)$$

Molecules in which two of the moments of inertia are equal are called symmetric tops while those with all three moments distinct are asymmetric tops. In the former, if $I_a = I_b < I_c$, as in benzene, we have an “oblate symmetric top”, whereas those with $I_a < I_b = I_c$ are “prolate symmetric tops”. Linear molecules, in common with diatomics, with $I_a = 0$ (all mass concentrated along the axis of the molecule), are trivial examples of prolate tops. Other simple examples are CH_3Br which is also a prolate symmetric top and H_2O which is an asymmetric top. An asymmetry parameter, which vanishes unless all three moments of inertia are distinct, is often defined:

$$\kappa = \frac{(2I_a I_c / I_b) - I_a - I_c}{I_c - I_a}, \quad (7.2)$$

with $-1 \leq \kappa \leq 1$.

The operators $\{J_a, J_b, J_c\}$ are with respect to the three orthogonal axes in the molecular or “body-fixed” frame. They are related to the angular momentum operators in a space-fixed frame, $\{J_X, J_Y, J_Z\}$, through the Euler angles $\{\theta, \phi, \chi\}$ which relate two such frames in three dimensions (Fig. 7.2). The two sets of operators are given in the (Euler) coordinate representation by

$$\begin{aligned} J_a &= i\hbar[\cos \chi \csc \theta \partial / \partial \phi - \cos \chi \cot \theta \partial / \partial \chi - \sin \chi \partial / \partial \theta], \\ J_b &= i\hbar[-\sin \chi \csc \theta \partial / \partial \phi + \sin \chi \cot \theta \partial / \partial \chi - \cos \chi \partial / \partial \theta], \\ J_c &= i\hbar \partial / \partial \chi, \end{aligned} \quad (7.3)$$

and

$$\begin{aligned} J_X &= i\hbar[\cos \varphi \cot \theta \partial / \partial \phi - \cos \phi \csc \theta \partial / \partial \chi + \sin \varphi \partial / \partial \theta], \\ J_Y &= i\hbar[\sin \varphi \cot \theta \partial / \partial \phi - \sin \phi \csc \theta \partial / \partial \chi - \cos \varphi \partial / \partial \theta], \\ J_Z &= -i\hbar \partial / \partial \varphi. \end{aligned} \quad (7.4)$$

The total squared angular momentum $J^2 = J_a^2 + J_b^2 + J_c^2 = J_X^2 + J_Y^2 + J_Z^2$ is conserved because it, commutes with H_{rot} . With no external fields such as electric or magnetic to distinguish any particular direction in the space-fixed axes, J_Z also commutes with the Hamiltonian and, correspondingly, M is a good quantum number.

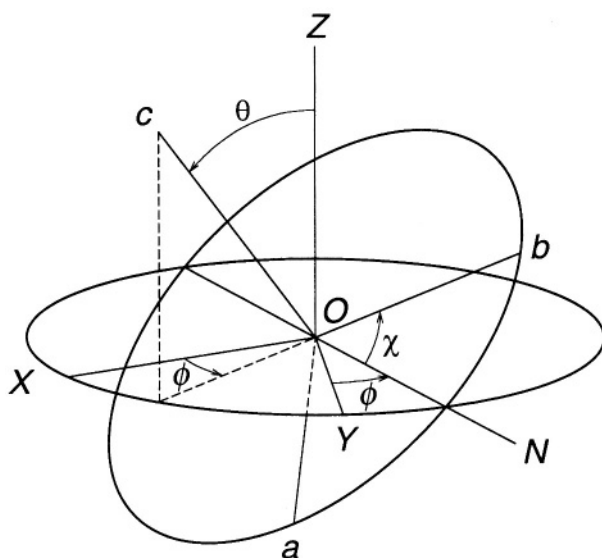


Figure 7.2. Euler angles relating space $\{X, Y, Z\}$ and body $\{a, b, c\}$ frames.

It is convenient also to refer to quantum numbers in the body frame. Consider first a “spherical top” with $I_a = I_b = I_c = I$, although it is not applicable to most molecules. H_{rot} now also commutes with J_c , and a corresponding quantum number $K = 0, \pm 1, \dots, \pm J$ can be assigned. The energy eigenvalues are $E_{\text{rot}} = J(J+1)\hbar^2/2I$ with wave functions

$$\psi_{\text{rot}}(\theta, \varphi, \chi) = P_M^J(\cos \theta) \exp(iM\varphi) \exp(iK\chi), \quad (7.5)$$

and degeneracy $(2J+1)^2$. Next consider a symmetric top in which two moments of inertia, say a and b (oblate), are equal, c being the symmetry axis. The Hamiltonian (7.1) can be written as

$$H_{\text{rot}} = \left(J^2/2I_b \right) + \left(J_c^2/2 \right) (1/I_c - 1/I_b), \quad (7.6)$$

and commutes with J_c so that again K can be defined as its eigenvalue. We have, therefore,

$$E_{\text{rot}} = \frac{J(J+1)\hbar^2}{2I_b} + \frac{K^2\hbar^2}{2} \left(\frac{1}{I_c} - \frac{1}{I_b} \right), \quad (7.7)$$

and eigenfunctions of the same form as in (7.5). For a prolate symmetric top, I_c would be replaced by I_a . Each energy now has the $(2J+1)$ degeneracy in M and an additional doubling of it for $K \neq 0$, states with K and $-K$ being degenerate. The linear molecule, a special case of prolate configurations with $I_a = 0$, has only $K = 0$, that is, no angular momentum about the symmetry axis, and E_{rot} reduces to just the first term in (7.7), in agreement with (6.9).

For an asymmetric top, there is no convenient recasting of (7.1) as in (7.6). Instead, one just has to diagonalize the Hamiltonian in a convenient basis, the symmetric top functions offering one possible choice for such a basis, particularly when the asymmetry parameter κ is small. Thus, for any J , a $(2J+1) \times (2J+1)$ matrix in terms of K has to be diagonalized. Every eigenstate is a superposition of different K values. Numerical programs and tables exist for this purpose and so-called “correlation diagrams” trace the energies from $\kappa = -1$ to $\kappa = 1$. Also, even the energy expressions above for symmetric tops have to be corrected because molecules are not rigid rotors and, as discussed for diatomic molecules (Section 6.2.5), centrifugal distortion and coupling of rotations to vibrations have to be allowed for. The moments of inertia parameters in (7.7) are, therefore, expressed as expansions in powers of $(v + \frac{1}{2})$, and higher order terms involving powers of $J(J+1)$ and K^2 included in (7.7) with coefficients derived semi-empirically by fitting to data.

Pure rotation spectra, arising from radiative transitions between different rotational states require a non-zero electric dipole \mathbf{d} , the transition operator being again $\mathbf{d} \cdot \mathcal{E}$ (Section 6.3.1). Spherical tops and certain symmetric tops such as benzene have no dipole moment and thus no infrared or microwave rotational spectra. When \mathbf{d} is non-vanishing, its vector nature requires for non-zero matrix elements with functions (7.5):

$$\Delta J = 0, \pm 1 \text{ but not } 0 \rightarrow 0, \quad \Delta M = 0, \pm 1, \quad \Delta K = 0, \quad (7.8)$$

the first two constraints as in Section 6.3.1, and the third new one because $\mathbf{d} \cdot \mathcal{E}$ does not depend on χ . If the dipole moment \mathbf{d} is perpendicular to the axis c (see Fig. 7.1), the dot product also involves $\cos \chi$ and then $\Delta K = \pm 1$.

Except that K is not defined for them, polyatomic asymmetric tops also obey the selection rules (7.8). Transitions due to dipole moments along the axes a , b , and c connect states differing in K values in steps

of 2. Microwave spectroscopy spans the frequency range from a few to a few hundred GHz. Microwaves generated by a klystron are sent through a long tube containing the absorbing gas. Since the absorption is generally weak, it is enhanced by applying an electric field which, also acting on the dipole moment \mathbf{d} , shifts the resonant frequency. By modulating this electric field and detecting the absorption in synchrony, very sensitive measurements of even weak absorption are possible. Further, the klystron being a coherent oscillator, extremely accurate frequency determination (down to 0.01 MHz) makes such “Stark-modulation spectroscopy” an effective tool for determining moments of inertia and dipole moments of molecules and thus molecular structure. Even transitions forbidden in electric dipole can be measured, such as magnetic dipole transitions in O_2 . Use of a magnetic field in place of the electric field, which leads to splitting of different M states, gives an analogous Zeeman-modulation spectroscopy.

As in the case of diatomic molecules (Section 6.2.6), the interplay of nuclear spin statistics with rotation causes intensity alternations and anomalies but the analysis is much less straightforward. Hyperfine structure from the coupling of the magnetic (and electric quadrupole) moment of the nuclear spin to the rotational angular momentum is also of interest.

2.3 Vibrations of polyatomic molecules

A molecule with N nuclei has $3N$ degrees of freedom for the motions of the nuclei. With three of these associated with the translation of the center of mass and three with rotations in space (two for a linear molecule with one moment of inertia zero), there remain $(3N - 6)$ or $(3N - 5)$ degrees of freedom which describe various vibrations. Thus, the water molecule with $N = 3$ has three “normal modes” as shown in Fig. 7.3 whereas the linear CO_2 molecule has the four shown in Fig. 7.4. By symmetry, the middle two are degenerate, having identical frequencies. These are bending vibrations while the other two are stretching vibrations, the first a “symmetric stretch” and the last an “asymmetric stretch”. The frequency of the antisymmetric stretch is larger because the central C atom also moves, thereby contributing to the kinetic energy and, through the virial relation, also enhancing the potential energy. Bending motions generally have the smallest frequencies, the frequencies in CO_2 being $\nu_1 = 1388 \text{ cm}^{-1}$, $\nu_2 = 667 \text{ cm}^{-1}$, and $\nu_3 = 2349 \text{ cm}^{-1}$.

The analysis of the normal modes of vibration and their corresponding frequencies can be carried out in terms of a set of suitable $(3N - 6)$ generalized coordinates q_i , the kinetic energy $T = \frac{1}{2} \sum_i m_i \dot{q}_i^2$, and the potential energy U . This last is obtained from solution of the molecular

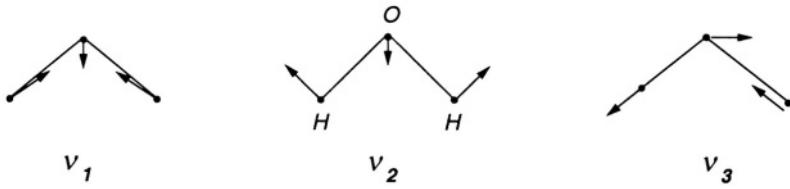


Figure 7.3. Three vibrational modes of H_2O .

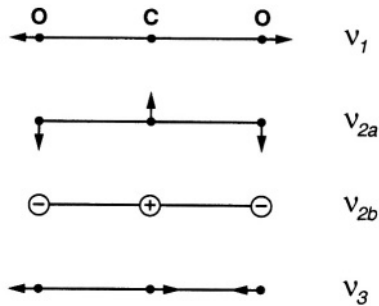


Figure 7.4. Four vibrational modes of CO_2 , middle two degenerate.

electronic Schrödinger equation which provides the equilibrium configuration and energy U_e and also departures from that in the form

$$U = U_e + \frac{1}{2} \sum_{ij} \left(\frac{\partial^2 U}{\partial q_i \partial q_j} \right) (q_i - q_i^e) (q_j - q_j^e) + \dots$$

Often the equilibrium configuration and coordinates q_i can be defined in terms of the bond lengths and bond angles. Thus, for the pyramidal NH_3 molecule with $N = 4$, the six coordinates may be chosen as the three N-H bond lengths $\{R_1, R_2, R_3\}$ and the three HNH bond angles $\{\alpha_1, \alpha_2, \alpha_3\}$ so that

$$U = U_e + \frac{1}{2} k \left[(R_1 - R_1^e)^2 + (R_2 - R_2^e)^2 + (R_3 - R_3^e)^2 \right]$$

$$+ \frac{1}{2} k_{\alpha} \left[(\alpha_1 - \alpha_1^e)^2 + (\alpha_2 - \alpha_2^e)^2 + (\alpha_3 - \alpha_3^e)^2 \right], \quad (7.9)$$

the two force constants k and k_{α} obtained from a quantum chemistry calculation of the electronic motion or often by fitting to vibrational or Raman spectra. It is useful to utilize symmetries as in the above example where the same constant k is expected for each of the NH bonds and the same k_{α} for the three identical angles. A whole elaborate technology of point group symmetries is available for this purpose built on the symmetries of rotations and reflections for molecules having such geometrical symmetries.

Because nuclear masses are large, a classical-mechanical analysis of normal modes often suffices. This involves a Lagrangian constructed from T and the U in (7.9) and a matrix diagonalization to obtain the coordinates of the normal modes in terms of which the Hamiltonian is of one-dimensional harmonic oscillators. The vibrational energies are, therefore,

$$E_{\text{vib}} = \sum_{k=1}^{3N-6} \left(v_k + \frac{1}{2} \right) \hbar \omega_k, \quad (7.10)$$

with wave functions as in (6.17). Thus, in the water molecule, we have $\nu_1 = 3832 \text{ cm}^{-1}$, $\nu_2 = 1648 \text{ cm}^{-1}$, and $\nu_3 = 3942 \text{ cm}^{-1}$, and the zero-point energy is 4636 cm^{-1} . Fig. 7.5 is a sketch of the ground and low-lying excited states labeled as (v_1, v_2, v_3) . As with quantum chemistry calculations for the electronic motion, tables and computer programs are available for carrying out the normal mode analysis of even complex polyatomic molecules. Anharmonic corrections to (7.10) arising from further terms in the expansion (7.9) are also available.

Turning to vibrational spectra, the analysis of the matrix element of the dipole moment \mathbf{d} between an initial and final vibrational state is as in other cases considered earlier. Thus, just as in (6.23) for diatomic molecules, the dipole moment can be expanded around its equilibrium value along any generalized coordinate

$$d = d_e + \sum_k (\partial d / \partial q_k)_e (q_k - q_k^e) + \dots \quad (7.11)$$

Once again, the linear term in the expansion gives the dominant contribution although higher order terms in (7.11) as well as anharmonicities in vibrations also prove important at times. But, within the harmonic approximation of (7.9), with oscillator wave functions independently in each coordinate q_k , the relevant matrix elements of the linear operator

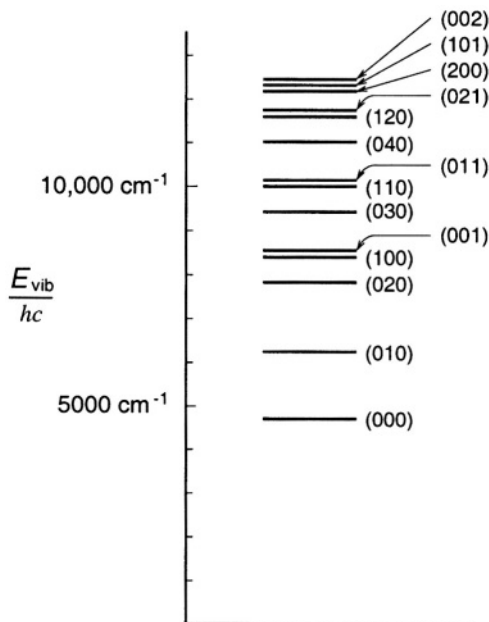


Figure 7.5. Vibrational levels (v_1, v_2, v_3) of H_2O . From [56], with permission of John Wiley and Sons, Inc.

$(q_k - q_k^e)$ are non-zero only for $v_k \rightarrow v_k \pm 1$. An important consideration, however, is that the multiplicative $(\partial d / \partial q_k)_e$ be non-zero for such a vibrational transition to be exhibited. Here again, symmetries of the molecule and the associated group theory prove helpful in determining which transitions take place. As an example, in a linear triatomic molecule like CO_2 (Fig. 7.4), the $k = 1$ symmetric stretch clearly has no dipole moment for any value of q_k and the corresponding vibrational mode is “inactive”. Since vibrational energy spacings fall in the infrared, the usual terminology is that such a mode is “infrared inactive”. The other two modes of bending and asymmetric stretch do have a non-vanishing $(\partial d / \partial q_k)_e$ and are “infrared active”.

Infrared radiation was itself first discovered in an astronomical context, when Sir William Herschel in 1800 saw the response of a thermometer when placed just outside the red region of the solar spectrum. It took over a century before infrared absorption in molecules began to be studied. It is now an active branch of both laboratory and astronom-

ical molecular studies. Intense infrared bands of CH_4 are seen in the atmospheres of the major planets, bands of CO_2 in Venus and H_2O in Mars. One talks of near infrared ($\lambda = 0.8 - 2.5 \mu\text{m}$), mid infrared ($2.5 - 50 \mu\text{m}$) and far infrared ($50 - 1000 \mu\text{m}$) regions. In the CO_2 molecule with states $|v_1 v_2 v_3\rangle$, the $k = 1$ is inactive but transitions $010 \rightarrow 000$ and $001 \rightarrow 000$ have frequencies 667 cm^{-1} and 2349 cm^{-1} , respectively, that is, wavelengths 15 and $4.3 \mu\text{m}$. Generally, with the ground state having the highest occupancy, these $\Delta v = 1$ transitions involving the ground vibrational state and one unit of excitation are the strongest, and are called fundamental frequencies. The 001 (2349 cm^{-1}) and 100 (1388 cm^{-1}) levels are the basis of the CO_2 laser. When mixed with N_2 whose molecules are excited by an electric discharge, collisions between N_2 and CO_2 populate the 001 level, thus creating a population inversion from which stimulated emission at $10.59 \mu\text{m}$ is possible (Fig. 7.6).

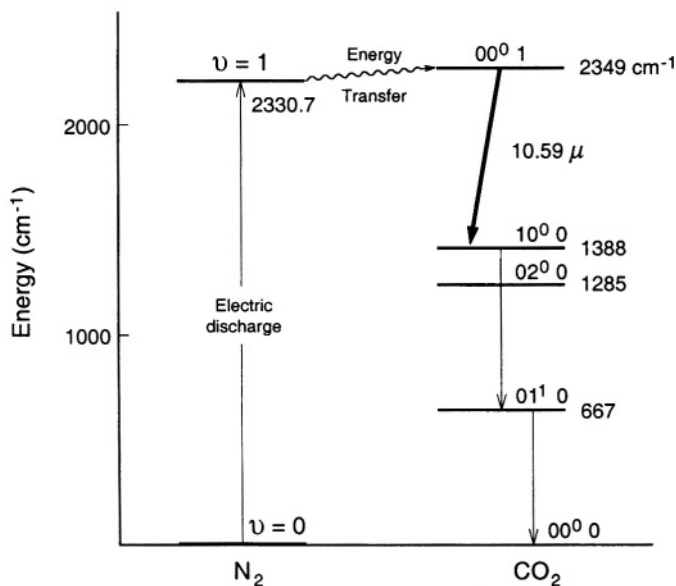


Figure 7.6. Energy levels involved in the $10.59 \mu\text{m}$ lasing transition of the CO_2 laser. From [54], with permission of author and publisher.

Superposed on vibrational transitions is rotational fine structure, which is analyzed as in Section 7.2.2. The resultant close grouping of lines gives rise to “bands” as observed. Thus, for symmetric tops, any allowed vibrational transition changes the dipole moment along the symmetry

axis or in one of the directions perpendicular to it. For the “parallel” vibration-rotation transition, the selection rules on J and K are as in (7.8) for pure rotation spectra:

$$\Delta J = 0, \pm 1, \Delta K = 0, \text{ with } \Delta J = 0 \text{ forbidden for } K = 0. \quad (7.12)$$

For the perpendicular transition, on the other hand,

$$\Delta J = 0, \pm 1, \Delta K = \pm 1. \quad (7.13)$$

For asymmetric tops, the changes in rotational quantum numbers are as before in Section 7.2.2, with K changing in steps of 2 and $\Delta J = 0, \pm 1$. Vibration-rotation absorption between 100 and 750 cm^{-1} in CO_2 , 1000 and 1080 cm^{-1} in O_3 , and 1300 to 1600 cm^{-1} and below 600 cm^{-1} in H_2O , all contribute to the greenhouse effect of the Earth’s atmosphere.

A linear polyatomic molecule has a $^1\Sigma$ ground electronic state and is a symmetric top with $K = 0$. As a result, $\Delta J = \pm 1$ for the parallel vibration-rotation band and $\Delta J = 0, \pm 1$ for the perpendicular band. In CO_2 , ν_3 changes the dipole moment component along the symmetry axis and is hence a parallel band whereas ν_2 changes perpendicular to the symmetry axis, forming a perpendicular band. The latter shows all P, Q, and R branches whereas the Q branch ($\Delta J = 0$) is absent in the ν_3 parallel band. Rotational substructure on the 001→100 CO_2 transition mentioned above gives rise to a group of transitions around 10.59 μm , thus providing partial tunability of the CO_2 laser.

Again, as for diatomic molecules, Raman spectroscopy is an important and useful adjunct to pure vibration-rotation spectra. Since Raman transitions are due to the induced dipole moment by the electric field of the radiation, it is the polarizability rather than the permanent dipole moment, and changes in α that govern the transitions. Complementary information is provided so that, for instance, the ν_1 symmetric stretch in CO_2 which has $d = 0$ and is infrared inactive is Raman active. Similarly, in the tetrahedral CH_4 molecule, which has one nondegenerate vibration ν_1 , one doubly degenerate ν_2 , and two (ν_3 and ν_4) triply degenerate vibrations, only ν_3 and ν_4 are infrared active but all four are Raman active. Molecules with a center of symmetry obey a “rule of mutual exclusion”, infrared active modes being Raman inactive, and vice versa. This is because such molecules have the inversion through the center as a good symmetry so that states are either g or u under it. The electric dipole operator is u (a vector) whereas the polarizability is g so that no pair of states can have simultaneously non-vanishing values for both.

2.4 Degeneracies and rovibronic couplings

Even for the simplest polyatomic molecule, our discussion so far in terms of a product wave function of electronic, vibrational, and rotational motions is only approximate, although it provides the basic understanding of the electronic and nuclear motions. Couplings between these, arising from anharmonicities in the vibrations of the nuclei or centrifugal distortions, as well as the entanglement of electronic with nuclear degrees of freedom as, for instance, when vibrations even change the geometrical arrangement of the molecule, complicate the discussion. In particular, the presence of degeneracies which have already been noted has the implication that the corresponding states may be mixed by any additional coupling no matter how weak. The full wave function is a “rovibronic” function, its factorization as a product of rotational, vibrational and electronic functions only an approximation.

A first example is in linear molecules such as CO_2 where the two bending modes ν_{2a} and ν_{2b} are degenerate (Fig. 7.4). With z the molecular axis, these vibrations in the xz - and yz - planes are like two orthogonal simple harmonic motions of a pendulum in x and in y . Equivalently, such a two-dimensional pendulum can be viewed in circular coordinates (the familiar conical pendulum or Lissajous figures) with an angular momentum ℓ in an angular coordinate $\varphi = \arctan(y/x)$. Although these are the conventionally used symbols, they should not be confused with the electronic angular momentum or the azimuthal coordinate of nuclear rotation in Section 7.2.2. The terms ℓ and φ here refer purely to the vibrational motions orthogonal to the molecular axis. In a state with such a vibrational angular momentum ℓ , interactions of the bending with the rotation of the molecule gives a rotational energy as in (7.7) but with ℓ replacing $|K|$:

$$E = hB[J(J+1) - \ell^2] + hA\ell^2, \quad (7.14)$$

with A the inverse of the moment of inertia of the nuclei about the molecular axis for the degenerate vibration.

Each rotational level undergoes “ ℓ -doubling”, the two states $|+\ell\rangle$ and $|-\ell\rangle$ forming the superpositions $[|+\ell\rangle \pm |-\ell\rangle]/\sqrt{2}$ under the interaction between rotation and vibration, and having slightly different energies. Thus, in HCN, with $B = 1.477 \text{ cm}^{-1}$ and vibration frequency $\nu_2 = 711.7 \text{ cm}^{-1}$, the splitting is $112.2 (v_2 + 1)J(J+1)$ MHz. Transitions between the levels of any doublet are dipole allowed, leading to microwave absorption, the levels themselves indicated by $|v_1 v_2^\ell v_3\rangle$.

Exact degeneracy is not necessary for such mixings by weak coupling terms, and near-degeneracies can suffice. Thus, in CO_2 , $2\nu_2$ is very close to ν_1 with the consequence that states with the same value of $2\nu_1 + \nu_2$ are nearly degenerate and mixed by anharmonicities or other couplings. This is called a Fermi resonance. A similar example obtains in benzene, a stretching C-H vibrational frequency lying close to the sum of two other vibrational frequencies. This gives rise to two strong bands at 3099 and 3045 cm^{-1} . In larger molecules, with more vibrational frequencies, such accidental near degeneracies are more common and this phenomenon, therefore, quite ubiquitous.

Another spectacular example of degenerate configurations, leading to a so-called “inversion doubling”, is provided by molecules such as NH_3 with two equivalent pyramidal configurations, the N atom on one or the other side of the plane formed by the three H atoms. The two configurations are separated by a potential barrier of 2075 cm^{-1} (≈ 5.8 kcal/mole), the maximum energy corresponding to the N lying in the plane of the H atoms. As in other such examples, starting from the initial one (Section 6.2.1) of H_2^+ binding (with two protons separated to infinity and an electron bound to one or the other providing two degenerate configurations), the same basic quantum-mechanical theme of physical eigenstates being the plus/minus superpositions obtains, any vibrational state of NH_3 being split into two states $(|\psi_{I,v}\rangle \pm |\psi_{II,v}\rangle) / \sqrt{2}$. The two levels are split by an energy representing the tunneling of the system between the two configurations I and II. In H_2^+ , it is an electron that tunnels over atomic-scale distances so that the splitting lies correspondingly in the eV range. But in NH_3 , with the entire massive N atom having to tunnel through the intervening barrier, the splittings are considerably smaller, approximately 24 GHz (wavelength = 1.25 cm) for the ground vibrational state. Indeed, in most molecules with two equivalent geometrical configurations of this type, the barrier is so large relative to the vibrational energy that the tunneling probability and, therefore, doublet spacing is quite negligible and the molecule can be considered effectively frozen in one of the configurations, but in NH_3 there is an appreciable effect.

In the JWKB approximation, the splitting of a vibrational level of frequency ν is given by

$$\Delta E = (\nu/\pi) \exp \left\{ -\frac{2\pi}{\hbar} \int [2\mu(V - E_{\text{vib}})]^{1/2} ds \right\}, \quad (7.15)$$

where μ is the reduced mass (of N relative to the three H) and the integral runs between the turning points defining the classically forbidden region

$V \geq E_{\text{vib}}$. Fig. 7.7 gives the doublet structure of the rotational spectrum of NH_3 . With the rotational constant B approximately 298 GHz, the doublet splitting of 24 GHz (0.67 cm^{-1}) is an order of magnitude smaller than the spacing between successive rotational levels. The energy levels are well represented by $\nu = 23787 - 151.3 J(J + 1) + 211 K^2$ MHz.

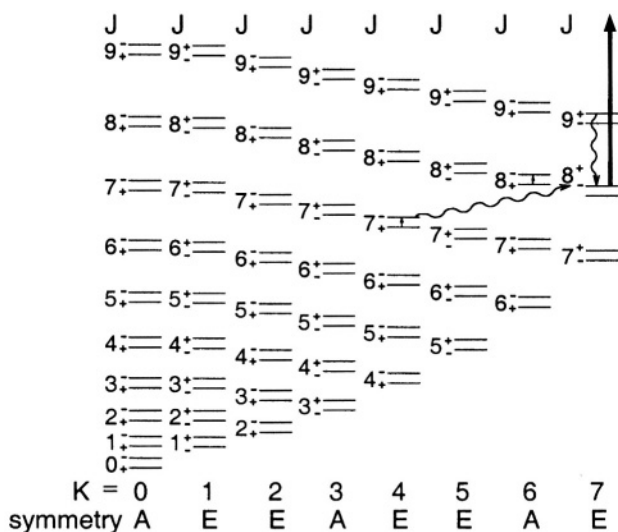


Figure 7.7. Doublet spectrum of the ammonia molecule NH_3 . From [54], with permission of author and publisher.

One important application of the NH_3 doublet spectrum is that it serves as the basis for a maser (microwave amplification by stimulated emission of radiation). Population inversion between any two levels, such that the upper energy state has a higher population, can give rise to amplification of radiation, stimulated emission from the upper level dominating over absorption from the lower. The first maser was demonstrated by Townes and by Basov and Prokhorov in the ammonia molecule, followed soon after by hydrogen masers operating at 1420 MHz between the $F = 1$ and $F = 0$ hyperfine levels.

3. Astrophysical Applications

Besides the various diatomic species considered in Section 6.4, a large number of polyatomic molecules have been seen through their microwave spectral lines in interstellar space. These include H_2O , CO_2 , SO_2 , OCS , NH_3 , HCN , H_2CO , CH_3OH , $\text{C}_2\text{H}_5\text{OH}$, CH_3SH , C_3N , HC_5N , HNCS , $\text{C}_2\text{H}_5\text{CN}$, etc. Indeed HC_nN ($n = 5, 7, 9, 11$) were unfamiliar in the laboratory but seen in radio astronomy. Similarly, ethynyl C_2H has not been studied in its gas phase in the laboratory whereas astronomical data has given its rotational, spin-doubling, and hyperfine constants. The $J = 0 \rightarrow 1$ transition in HCN at 87 GHz and six transitions with $\Delta K = 0$ and $J = 5 \rightarrow 6$ in CH_3CN at 110 GHz, HCO^+ at 89.2 GHz, and N_2H^+ at 93.2 GHz are examples of prominent lines in radio astronomy. Negative ions of interest are O_3^- , NO_2^- , and NO_3^- in the Earth's ionosphere. Even very large molecules such as poly aromatic hydrocarbons (PAH) have been seen as infrared emission bands of planetary nebulae, H II regions, and extragalactic sources, whereas a number of nebulae show broad emissions at $11.2 \mu\text{m}$ attributed to silicon carbide grains.

Among triatomic molecules, CO_2 is important in the Martian atmosphere, being the main component up to 200 km (O after that). Its photoionization $\text{CO}_2 + h\nu \rightarrow \text{CO}_2^+ + e$ and $\rightarrow \text{CO} + \text{O}^+ + e$ are followed rapidly by processes producing O_2^+ : $\text{CO}_2^+ + \text{O} \rightarrow \text{CO} + \text{O}_2^+$ and $\text{O}^+ + \text{CO}_2 \rightarrow \text{O}_2^+ + \text{CO}$.

A particularly interesting molecule is H_3 and its ion H_3^+ , the three protons arranged in the form of an equilateral triangle with internuclear distances of 0.87 \AA , slightly larger than the 0.74 \AA separation in H_2 [57]. H_3^+ is a simple and stable species, the major ion in high pressure electric discharges in H_2 gas through the rapid reaction $\text{H}_2^+ + \text{H}_2 \rightarrow \text{H}_3^+ + \text{H}$. Similarly in astrophysical clouds, with the H_2^+ often due to initial ionization of H_2 by cosmic rays. The reaction has a large rate ($10^{-9} \text{ cm}^3 \text{ s}^{-1}$) and can be viewed as a proton hopping from H with proton affinity 2.7 eV to H_2 with the larger 4.4 eV proton affinity. Although known since its discovery by J. J. Thompson in 1911, the H_3^+ spectrum was first observed only in 1980 and its abundant existence seen first in an astronomical context. Thereby, it joins its fellow two-electron species H^- (Section 2.4) in its importance in astronomy. It is abundant both in dense (10^{3-5} cm^{-3}) and diffuse (10^{1-3} cm^{-3}) clouds. It is present substantially in the ionosphere of Jovian planets and plays a pivotal role in interstellar ion-molecule chemistry, forming column densities of $10^{14-15} \text{ cm}^{-2}$ in these clouds. Both in Jupiter's atmosphere, as well as later in those of Uranus and Saturn, and in interstellar clouds, vibration-rotation emission lines have been seen. Indeed, infrared lines at $3.953 \mu\text{m}$ from H_3^+ gave the first evidence for substantially higher temperatures

($\approx 10^3$ K) near Jupiter's poles than had been expected. Jupiter also shows strong $2 \mu\text{m}$ emission from the upper reaches of its atmosphere. With few other molecular spectral lines in this region, H_3^+ is readily observed with infrared telescopes. H_3^+ has also been observed in the supernova SN1987A, two strong emissions at 3.41 and $3.53 \mu\text{m}$ having been attributed to thermal emission from H_3^+ at 1000 – 2000 K. Lacking an electric dipole moment, its pure rotational spectrum is forbidden, although the isotopic partner H_2D^+ does possess such a spectrum and a line has been reported in the NGC 2264 molecular cloud. Having no bound excited electronic states (again as in H^-), it has no visible or ultraviolet spectrum.

The reaction $\text{H}_3^+ + \text{HD} \rightleftharpoons \text{H}_2\text{D}^+ + \text{H}_2$ is important for the deuterium fraction in interstellar clouds, the ratio D/H being approximately 10^{-5} in the interstellar medium (Fig. 1.7). The primordial deuterium fraction in the early Universe, when the equilibrium ratios of these light nuclei were fixed, is a key parameter for cosmological models, being very sensitive to the baryon density. H_3^+ plays a central role in the chemistry of interstellar clouds. Its low proton affinity means that it readily protonates other atoms and molecules: $\text{H}_3^+ + \text{O} \rightarrow \text{OH}^+ + \text{H}_2$, $\text{H}_3^+ + \text{C} \rightarrow \text{CH}^+ + \text{H}_2$ and $\text{H}_3^+ + \text{CO} \rightarrow \text{HCO}^+ + \text{H}_2$. These ions then initiate a whole sequence of chemical reactions such as $\text{OH}^+ + \text{H}_2 \rightarrow \text{H}_2\text{O}^+ + \text{H}$, $\text{H}_2\text{O}^+ + \text{H}_2 \rightarrow \text{H}_3\text{O}^+ + \text{H}$, $\text{H}_3\text{O}^+ + \text{e} \rightarrow \text{H}_2\text{O} + \text{H}$ and $\rightarrow \text{OH} + \text{H}_2$, $\text{HCO}^+ + \text{e} \rightarrow \text{CO} + \text{H}$, etc. Astrophysical detection of H^{13}CO^+ and laboratory measurement of the $J = 1 \rightarrow 0$ microwave spectrum have given key evidence of the chemistry of ions in clouds. The similar process, $\text{H}_3^+ + \text{N}_2 \rightarrow \text{N}_2\text{H}^+ + \text{H}$ is also important.

Besides the above collisions with CO and N_2 , H_3^+ is also removed by dissociative recombination, $\text{H}_3^+ + \text{e} \rightarrow \text{H}_2 + \text{H}$ or $\rightarrow \text{H} + \text{H} + \text{H}$, with a rate $10^{-7} (300/T)^{1/2} \text{ cm}^3 \text{ s}^{-1}$, the reaction interesting in that the electron is captured into a high Rydberg state, followed by a sequence of transitions into higher lying vibrational levels from which predissociation occurs to a repulsive potential curve of H_3 . Detailed laboratory observations have been made recently.

In recent decades, astronomical masers have been of great interest [58]. A key parameter characterizing radio observations of them is the antenna temperature defined as follows. The power radiated per unit area by a cloud is given by the Planck expression

$$\frac{8\pi h\nu^3 \Delta\nu}{c^2 (e^{h\nu/kT} - 1)}, \quad (7.16)$$

which reduces for $h\nu \ll kT$ to the Rayleigh-Jeans value of $2kT\Delta\nu/\lambda^2$ as the energy radiated per unit solid angle. An ideal antenna of radius a at a distance R from the cloud intercepts $(\lambda/a)^2 R^2$, the solid angle subtended by the antenna at the cloud being $(a/R)^2$. Therefore, the power incident upon the antenna is

$$\frac{1}{2} \frac{2kT\Delta\nu}{\lambda^2} \frac{\lambda^2 R^2}{a^2} \frac{a^2}{R^2} = kT\Delta\nu, \quad (7.17)$$

the $\frac{1}{2}$ factor to express an effective area. The antenna temperature, defined as the power per unit bandwidth divided by the Boltzmann constant k , equals the thermal temperature T only in the Rayleigh-Jeans limit. Otherwise, for an object of angular size θ so that the surface area is $\pi R^2\theta^2$, the antenna temperature T_A and brightness temperature T_B are related by

$$kT_A = \frac{8\pi h\nu^3}{c^2 (e^{h\nu/kT_B} - 1)} \pi R^2\theta^2 \frac{A_{\text{eff}}}{R^2}. \quad (7.18)$$

A 100 m telescope operating at 3 cm wavelength or a 10 m telescope at 3 mm have resolutions of $1'$. The angular size of a cloud of diameter 100 A.U. at 1 kpc is $0.1''$, so that $T_A \approx 3 \times 10^5$ K, and only a maser can account for such a high brightness temperature. This was indeed how the first astronomical masers in OH were identified in 1965 from the direction of several H II regions. VLBI (Very Long Baseline Interferometry) observations two years later established that the emission came from spots only a few milli-arc seconds across, implying brightness temperatures of 10^{12} K. Masing has been seen for all four transitions in Fig. 6.16. Later, H_2O masers were seen, some emitting a solar luminosity in a single spectral line (1.35 cm or 22 GHz of the $6 \rightarrow 5$ rotation transitions), only 50 kHz in width. Both OH and H_2O masers have been seen from other galaxies as well. SiO and CH_3OH (over 20 masing lines) have also been seen as intense masers from Orion (500 pc). HCN and NH_3 are other molecules exhibiting astronomical masing, several inversion doublets of NH_3 (Fig. 7.7) seen as masers.

Strong maser activity seems to be from regions of gas density (10^{5-11} cm^{-3}) higher than normally found in giant molecular clouds, perhaps from condensations in the interstellar medium near very luminous O or B stars which pump the molecules to the upper state. There are also stellar masers associated with M-type red giant or infrared stars, formed in the outer regions of the photosphere. Interstellar masers are taken to be indicators of active star formation. Thus NGC 6334 which is about 20 pc in size has several H_2O and OH masers. The H_2O masers appear first,

persisting for roughly 10^5 years, the OH masers lasting until the ionized region expands beyond 10^{17} cm after which densities and excitation are not sufficient for masing. Observation of masers provides maps of velocity fields across the source, both low ($\approx 20 \text{ km s}^{-1}$) and high ($\approx 100 \text{ km s}^{-1}$) features being seen. Polarization of the masing emission probably arises from the Zeeman effect, indicating fields of 10–100 Gauss. Besides such information on local conditions in the interstellar medium in the masing region, proper motions of the masers can be used to determine distances to these sources both within our galaxy and in others. Such direct measurements of galactic (thus the center of the galaxy has been located at $7.1 \pm 1.5 \text{ kpc}$) and intergalactic distances are of great cosmological interest since they are independent of the complicated hierarchy and standard candles otherwise used for distance indicators on this scale.

Problems

- 7.1** How many rotational and how many vibrational degrees of freedom does the molecule CH_3OH have?
- 7.2** Ignoring nuclear spins, which of the following molecules are polar and which are paramagnetic?
 NO , OH^- , NH_3 , NH_4^+ , CH_3 , CH_3Cl .
- 7.3** What are the eigenvalues and eigenstates of a symmetric-top Hamiltonian, (7.1), with $I_a = I_b$? Sketch the low-lying states of the spectrum for such an oblate symmetric top.
- 7.4** For the asymmetric-top Hamiltonian in (7.1), find the eigenvalues when the angular momentum of the system is (a) 1 (b) 2.

References

- [1] C. Schwob, L. Jozefowski, B. deBeauvoir, L. Hilico, F. Ne, L. Julien, F. Biraben, O. Acef, and A. Clairon, *Phys. Rev. Lett.* **82**, 4960 (1999); M. Niering, R. Holzwarth, J. Reichert, P. Pokasov, Th. Udem, M. Weitz, T. W. Hänsch, P. Lemonde, G. Santarelli, M. Abgrall, P. Laurent, C. Salomon, and A. Clairon, *ibid* **84**, 5496 (2000).
- [2] D. Kleppner, M. G. Littman, and M. L. Zimmerman, *Sci. Am.* **244** (5), 130 (1981).
- [3] V. I. Korbov, *Phys. Rev. A* **61**, 064503 (2000).
- [4] U. Fano and A. R. P. Rau, *Atomic Collisions and Spectra* (Academic Press, Orlando, 1986).
- [5] J. C. Slater, *Phys. Rev.* **36**, 57 (1930); G. Burns, *J. Chem. Phys.* **41**, 1521 (1964); Y. D. Jung and R. J. Gould, *Phys. Rev. A* **44**, 111 (1991); R. H. Garvey, C. H. Jackman, and A. E. S. Green, *ibid* **12**, 1144 (1975).
- [6] Larry Spruch, *Rev. Mod. Phys.* **63**, 151 (1991); N. H. March, *Self-consistent fields in atoms* (Pergamon, Oxford, 1975); L. D. Landau and E. M. Lifshitz, *Quantum Mechanics: Non-relativistic theory* (Pergamon, Oxford, 1977); E. Lieb, *Rev. Mod. Phys.* **48**, 553 (1976).
- [7] W. Kohn, *Rev. Mod. Phys.* **71**, 1253 (1999); R. G. Parr and W. Yang, *Density functional theory of atoms and molecules* (Oxford Univ. Press, Oxford, 1989); R. M. Dreizler and E. K. V. Gross, *Density functional theory* (Springer, Berlin, 1990).
- [8] S. Chandrasekhar, *Rev. Mod. Phys.* **56**, 137 (1984).
- [9] C. F. Fischer, *The Hartree-Fock Method for Atoms* (John Wiley, New York, 1977); J. P. Desclaux, *Comput. Phys. Commun.* **9**, 31 (1975); I. P. Grant, B. J. McKenzie, P. H. Norrington, D. F. Mayers, and N. C. Pyper, *ibid* **21**, 207 (1980); I. P. Grant, *Adv. At. Mol. Opt. Phys.* **32**, 169 (1994).
- [10] F. Herman and S. Skillman, *Atomic Structure Calculations* (Prentice-Hall Inc., Englewood Cliffs, 1963).

- [11] A. R. P. Rau and U. Fano, *Phys. Rev.* **167**, 7 (1968).
- [12] E. Harrison, *Cosmology* (Cambridge Univ. Press, 2000), Second edition, Chapters 14 and 15.
- [13] D. Tytler, J. M. O'Meara, N. Suzuki, and D. Lubin, *Phys. Reports* **333-4**, 409 (2000).
- [14] C. E. Moore, *Atomic Energy Levels* (U. S. Govt. Printing Office, Washington, D. C., 1971).
- [15] M. J. Seaton, *Adv. At. Mol. Opt. Phys.* **32**, 295 (1994).
- [16] M. Inokuti, *Rev. Mod. Phys.* **43**, 297 (1971) and **50**, 23 (1978); *Adv. At. Mol. Opt. Phys.* **33** (1994).
- [17] S. Chandrasekhar, *Radiative Transfer* (Dover, New York, 1960).
- [18] E. P. Wigner, *Phys. Rev.* **73**, 1002 (1948); A. R. P. Rau, *Comments on At. Mol. Phys.* **14**, 285 (1984).
- [19] T. Ohmura and H. Ohmura, *Phys. Rev.* **118**, 154 (1960).
- [20] M. Ya. Amusia and N. A. Cherepkov, *Case Stud. in At. Phys.* **5**, 49 (1975); W. R. Johnson, *Adv. At. Mol. Opt. Phys.* **25**, 375 (1988); M. Ya. Amusia, in *Atomic, Molecular and Optical Physics Handbook*, ed. G. W. F. Drake (Am. Inst. of Phys. Woodbury, 1996), p. 287.
- [21] H. J. Silverstone, *Phys. Rev. A.* **18**, 1853 (1978); V. Franceschini, V. Grecchi, and H. J. Silverstone, *ibid* **32**, 1338 (85).
- [22] P. J. Mohr, in *Atomic, Molecular and Optical Physics Handbook*, ed. G. W. F. Drake (Am. Inst. of Phys., Woodbury, 1996), p. 341; Appendix A of P. J. Mohr and B. N. Taylor, *Rev. Mod. Phys.* **72**, 351 (2000); G. W. F. Drake, *Adv. At. Mol. Opt. Phys.* **31**, 1 (1993).
- [23] R. Haymaker and A. R. P. Rau, *Am. J. Phys.* **54**, 928 (1986).
- [24] G. Chanmugam, *Annu. Rev. Astron. Astrophys.* **36**, 147 (1992).
- [25] L. P. Gorkov and I. E. Dzyaloshinsky, *Sov. Phys. JETP* **26**, 449 (1968); P. Schmelcher and L. S. Cederbaum, *Phys. Rev. A* **43**, 287 (1991).
- [26] A. Holle, G. Wiebusch, J. Main, B. Hager, H. Rottke, and K. H. Welge, *Phys. Rev. Lett.* **56**, 2595 (1986); J. Main, G. Wiebusch, A. Holle, and K. H. Welge, *ibid* **57**, 2789 (1986).
- [27] W. R. S. Garton and F. S. Tomkins, *Astrophys. J.* **158**, 839 (1969).
- [28] A. R. P. Rau and Lijun Zhang, *Phys. Rev. A* **42**, 6342 (1990); P. A. Braun, *Rev. Mod. Phys.* **65**, 115 (1993).
- [29] E. A. Solov'ev, *Sov. Phys. JETP Lett.* **34**, 265 (1981); D. R. Herrick, *Phys. Rev. A* **26**, 323 (1982); J. C. Gay, D. Delande, F. Biraben, and F. Penent, *J. Phys. B* **16**, L693 (1983).

- [30] M. L. Zimmerman, J. C. Castro, and D. Kleppner, *Phys. Rev. Lett.* **40**, 1083 (1978).
- [31] A. Holle, G. Wiebusch, J. Main, K. H. Welge, G. Zeller, G. Wunner, T. Ertl, and H. Ruder, *Zeit. für Physik D* **5**, 279 (1987).
- [32] C. W. Clark and K. T. Taylor, *J. Phys. B* **15**, 1175 (1982); D. Delande and J. C. Gay, *ibid* **17**, L335 (1984).
- [33] H. Ruder, G. Wunner, H. Herold, and F. Geyer, *Atoms in Strong Magnetic Fields* (Springer-Verlag, Berlin, 1994); *Atoms in Strong Fields*, eds. C. A. Nicolaides, C. W. Clark, and M. H. Nayfeh, NATO ASI Services B, Vol. 212 (Plenum, New York, 1990); W. Becken, P. Schmelcher, and F. K. Diakonov, *J. Phys. B* **32**, 1557 (1999).
- [34] P. Falsaperla and G. Fonte, *Phys. Rev. A* **47**, 4143 (1993); Yu. P. Kravchenko, M. A. Libermann, and B. Johansson, *ibid* **54**, 287 (1996).
- [35] D. Wintgen and H. Friedrich, *Phys. Rev. A* **35**, 1464 (1987); G. Wunner, U. Woelk, I. Zech, G. Zeller, T. Ertl, F. Geyer, W. Schweizer, and H. Ruder, *Phys. Rev. Lett.* **57**, 3261 (1986); H. Friedrich and D. Wintgen, *Phys. Reports* **183**, 37 (1989).
- [36] M. L. Du and J. B. Delos, *Phys. Rev. A* **38**, 1896 and 1913 (1988); J. Main, G. Wiebusch, K. Welge, J. Shaw, and J. B. Delos, *ibid* **49**, 847 (1979); *Irregular Atomic Systems and Quantum Chaos*, ed. J. C. Gay (Gordon and Breach, Philadelphia, 1992).
- [37] S. Watanabe and H. Komine, *Phys. Rev. Lett.* **67**, 3227 (1991); P. F. O'Mahony and F. M. Furtado, *ibid* **67**, 2283 (1991); P. Dando, T. S. Monteiro, D. DeLande, and K. T. Taylor, *ibid* **74**, 1099 (1995); D. Delande, K. T. Taylor, M. H. Halley, T. van der Veldt, W. Vassen, and W. Hagervorst, *J. Phys. B* **27**, 2771 (1994); J. Rao and K. T. Taylor, *ibid* **30**, 3627 (1997).
- [38] A. K. Harding, *Science* **251**, 1033 (1991); E. S. Phinney and S. R. Kulkarni, *Annu. Rev. Astron. Astrophys.* **32**, 591 (1994).
- [39] J. Cizek and E. R. Vrscaj, *Int. J. Q. Chem.* **21**, 27 (1982); J. C. LeGuillou and J. Zinn-Justin, *Ann. Phys. (N.Y.)* **147**, 57 (1983); A. V. Turbiner, *J. Phys. A* **17**, 859 (1984).
- [40] M. V. Ivanov, *J. Phys. B* **27**, 4513 (1994); M. D. Jones, G. Ortiz, and D. M. Ceperley, *Phys. Rev. A* **59**, 2875 (1999); O. A. Al-Hujaj and P. Schmelcher, *ibid* **61**, 063413 (2000); M. D. Jones, G. Ortiz, and D. M. Ceperley, *ibid* **54**, 219 (1996).
- [41] Dong Lai and E. E. Salpeter, *Phys. Rev. A* **53**, 152 (1996).
- [42] J. C. Lopez and A. V. Turbiner, *Phys. Rev. A* **62**, 022510 (2000); T. Detmer, P. Schmelcher, and L. S. Cederbaum, *ibid* **57**, 1767 (1998).
- [43] J. R. P. Angel, J. Liebert, and H.S. Stockman, *Astrophys. J.* **292**, 260 (1985); J. L. Greenstein, R. J. W. Henry, and R. F. O'Connell, *ibid* **289**, L25 (1985);

- G. Wunner, W. Rösner, H. Herold, and H. Ruder, *Astron. Astrophys.* **149**, 102 (1985).
- [44] S. J. Buckman and D. S. Newman, *J. Phys. B* **20**, L711 (1987).
- [45] D. Roy, A. Delage, and J. D. Carette, *J. Phys. B* **11**, 895 and 4059 (1978); K. W. Trantham, M. Jacka, A. R. P. Rau, and S. J. Buckman, *ibid* **32**, 815 (1999).
- [46] K. Schulz, G. Kaindl, M. Domke, J. D. Bozek, P. A. Heimann, A. S. Schlachter, and J. M. Rost, *Phys. Rev. Lett.* **77**, 3086 (1996).
- [47] Y. Azuma, S. Hasegawa, F. Koike, G. Kutluk, T. Nagata, E. Shigemasa, A. Yagishita, and I. A. Sellin, *Phys. Rev. Lett.* **74**, 3768 (1995); S. Diehl, D. Cubaynes, H. L. Zhou, L. VoKy, F. J. Wuilleumier, E. T. Kennedy, J. M. Bizau, S. T. Manson, C. Blancard, N. Berrah, and J. Bozek, *J. Phys. B* **33**, L487 (2000).
- [48] P. Camus, T. F. Gallagher, J. M. Lecomte, P. Pillet, L. Pruvost, and J. Boulmer, *Phys. Rev. Lett.* **62**, 2365 (1989); U. Eichmann, V. Lange, and W. Sandner, *ibid* **64**, 274 (1990); R. R. Jones and T. F. Gallagher, *Phys. Rev. A* **42**, 2655 (1990).
- [49] P. G. Harris, H. C. Bryant, A. H. Mohagheghi, R. A. Reeder, H. Sharifian, C. Y. Tang, H. Tootoonchi, J. B. Donahue, C. R. Quick, D. C. Rislove, W. Smith, and J. E. Stewart, *Phys. Rev. Lett.* **65**, 309 (1990); P. G. Harris, H. C. Bryant, A. H. Mohagheghi, R. A. Reeder, C. Y. Tang, J. B. Donahue, and C. R. Quick, *Phys. Rev. A* **42**, 6443 (1990).
- [50] U. Fano and A. R. P. Rau, *Symmetries in Quantum Physics* (Academic, New York, 1996).
- [51] H. C. Bryant, B. D. Dieterle, J. Donahue, H. Sharifian, H. Tootoonchi, D. M. Wolfe, P. A. M. Gram, and M. A. Yates-Williams, *Phys. Rev. Lett.* **38**, 228 (1977).
- [52] *Atomic Excitation and Recombination in External Fields*, eds. M. H. Nayfeh and C. W. Clark (Gordon and Breach, New York, 1985).
- [53] T. Bartsch, A. Müller, W. Spies, J. Linkemann, H. Danared, D. R. DeWitt, H. Gao, W. Zong, R. Schuch, A. Wolf, G. H. Dunn, M. S. Pindzola, and D. C. Griffin, *Phys. Rev. Lett.* **79**, 2233 (1997); T. Bartsch, S. Schippers, A. Müller, C. Brandau, G. Gwinner, A. A. Saghir, M. Beutelspacher, M. Grieser, D. Schwalm, A. Wolf, H. Danared, and G. H. Dunn, *ibid* **82**, 3779 (1999).
- [54] J. I. Steinfeld, *An Introduction to Molecular Spectra* (MIT Press, Cambridge, MA, 1974), Second ed.
- [55] J. A. Pople, *Rev. Mod. Phys.* **71**, 1267 (1999).
- [56] I. N. Levine, *Molecular Spectroscopy* (John Wiley, New York, 1975).
- [57] A. Dalgarno, *Adv. At. Mol. Opt. Phys.* **32**, 57 (1994); T. Oka, *Rev. Mod. Phys.* **64**, 1141 (1992).
- [58] M. Elizur, *Annu. Rev. Astron. Astrophys.* **30**, 75 (1992).

Index

- 21 cm line, 34, 36, 202
- absorption coefficient, 43
- absorptivity, 42
- acceleration form, 48, 64
- accretion disk, 131
- acoustic mode, 34
- adiabatic approximation, 116, 151, 168, 176, 207
- adiabatic index, 24, 39, 127
- Ag, 29
- age of Universe, 33
- airglow, 175
- allowed transition, 49
- ammonia doublet, 222, 223
- ammonia maser, 223, 226
- angular correlation, 12, 16, 62, 142, 146, 151, 153
- angular momentum
 - grand, 148, 149
 - rotational, 179
- anharmonic correction, 183
- anharmonicity, 182, 217, 221, 222
- anomalous Zeeman effect, 81
- antenna temperature, 225, 226
- anti-Stokes line, 193
- antisymmetrization, 12, 18–22, 62, 150,
see also Pauli principle
- asymmetric stretch, 215, 218
- asymmetric top, 212, 214, 220, 227
- asymmetry parameter, 212, 214
- atom, 17–30, *see also* hydrogen atom
 - hollow, 145
 - in ultrastrong field, 122–126
 - in very strong field, 126–131
- atomic orbital, 10, 18, 21, 28, 205, 207–209
- atomic potential, 25, 29, 30
- atomic units, 3, 70, 71
- Au, 29
- Auger effect, 138
- aurora, 35, 52, 197, 204
- autoionization, 113, 119, 135, 138, 156
 - lifetime, 140, 161, 166
 - profile, 159, 160
 - selection rule, 140
 - width, 159, 160, 165
- azimuthal quantum number, 4, 71, 81
- B, 18, 20–22, 33
- Ba, 33, 115, 146
- Balmer, 2
 - continuum, 46
 - formula, 3
 - series, 3, 31
 - spectra, 2, 131, 132
- band edge, 3
- band spectrum, 194, 206
- bands, 189, 219, 224
- baryometer, 36
- Be, 18, 33
- bending, 215, 218
- benzene, 211, 214, 222
- Bethe trial function, 38, 61
- Beutler-Fano profile, *see* resonance
- Big Bang, 30, 169
- black-body, 2, 37, 42, 43, 169, 202, 225
- body-fixed axes, 184, 185
- body-fixed frame, 212, 213
- Bohr-Rydberg formula, 14, 15, 210
- Boltzmann factor, 31, 182, 188
- Boltzmann-Saha equation, 31, 165
- bond angle, 216
- bond length, 216
- bonding, 171
- Born approximation, 56, 67, 200
- Born-Oppenheimer, 176–178, 195, 207, 211
- bosonic nuclei, 185, 186
- Brackett series, 3, 37

- Breit-Wigner, 159
 brightness temperature, 226
 Bunsen burner, 2
- C, 18, 33, 34, 36
 C^- , 61
 C_2 , 186
 C_2H , 224
 Ca, 18, 32, 166
 carbon, 18, 34, 36
 Cass A, 34
 center of mass, 92
 centrifugal distortion, 184, 214, 221
 Cepheids, 35, 43
 CH, 174, 196, 198, 201
 CH_3 , 227
 CH_3Br , 212
 CH_3Cl , 227
 CH_3CN , 224
 CH_3OH , 226, 227
 CH_4 , 219, 220
 Chandrasekhar function, 61, 67
 Chandrasekhar limit, 24
 chaotic, 109
 character table, 208
 characters, 208
 chemical potential, 24
 chromosphere, 32, 42, 84
 circular dichroism, 199
 circular polarization, 50, 80, 131
 classical trajectory, 109–111
 Clebsch-Gordan coefficient, 8, 105, 150
 closed orbit, 110
 clouds, 36, 42, 169, 196, 199, 201–203, 224–226
 CN, 201, 202, 205
 CNDO, 209
 CO, 181, 188, 189, 202, 205, 225
 CO_2 , 204, 207, 215, 216, 218–222, 224
 collisional capture, 66
 collisional cooling, 52
 comet, 198, 201
 complex atom, 17–30
 in ultrastrong field, 122–126
 in very strong field, 126–131
 configuration interaction, 16, 17, 28, 29, 158, 178
 conical pendulum, 221
 conjugation transformation, 101, 102
 continuum absorption, 63
 continuum normalization, 46, 56, 57, 67, 157
 Coriolis effect, 184
 corona, 32, 84, 166
 correlation, 11
 angular, 12, 16, 62, 142, 146, 151
 diagram, 214
 energy, 136
 radial, 17, 62, 143, 146, 153
 cosmic
 background, 37, 202
 red-shift, 36, 202
 cosmochronology, 33
 Coulomb plus diamagnetic, 87, 91–113
 chaos, 109
 equipotentials, 96, 111, 133
 resonances, 113
 strong mixing, 91, 94, 97, 112
 Coulomb plus Stark field, 133
 covalent bond, 170–172
 cross-section, 44, 46, 59, 60
 CS, 202
 Cu, 29
 cut-off Coulomb potential, 117
 cyanogen, 32
 cyclotron
 emission, 91, 115, 131, 133
 frequency, 88
 harmonic, 91, 132
 orbit, 88
 period, 110
 radiation, 91
 radius, 90, 116, 133
 cylindrical gauge, 90
- damping, 45, 66
 dark cloud, 202, 203
 Darwin term, 83
 debye, 189, 202
 degeneracy, 3, 6, 31, 72, 79, 84, 89, 170, 211, 220
 Kramers, 78
 pressure, 9
 degenerate mixing, 155, 171
 degenerate perturbation, 97–105
 dense cloud, 224
 density functional, 22, 27, 28
 detailed balance, 43, 65
 determinantal wave function, 21, 22
 deuterium, 36, 37, 61, 106, 108, 181, 190, 191, 205, 206, 225
 diagram for perturbation
 basic, 72, 73
 fourth-order, 85
 r-th order, 74
 second-order, 74
 third-order, 74, 75
 diamagnetic, 71, 85, 94, 98, 102–104, 106, 107, 114, 121
 diamagnetic susceptibility, 54
 diamagnetic Zeeman effect, 75, *see also* diamagnetic
 dichroism, 199
 dielectric constant, 66, 114, 134

- dielectronic recombination, 66, 135, 142, 164–167
 rate, 164, 166
- dielectronic satellite, 166
- diffuse cloud, 224
- dipole approximation, 44, 49
- dipole matrix element, 45, 122, 158
 alternative forms, 46–48, 64
- dipole moment, 45, 66, 76, 77, 187, 192, 201, 214, 217, 220, 225
- dipole operator, 45, 49, 155, 187, 189, 193, 214
- dipole potential, 76, 139, 152, 154
- dipole state, 76, 139, 154
- Dirac equation, 51, 83, 91
- Dirac-Fock, 29
- direct energy, 13, 28
- dispersion, 199
- dissociation, 190, 196, 206
- dissociative recombination, 203, 225
- Doppler shift, 34–36
- double ionization, 138, 161
- doubly-excited state, 16, 59, 63, 135–147, 153–157, 161–166, *see also* autoionization, resonance
- E-layer, 203
- E1, 50, 53, 187, 193, *see also* electric dipole
- E2, 52, 215
- Earth
 airglow, 175
 atmosphere, 203, 204, 220
 ionosphere, 205, 224
- edge
 band, 3
 photoionization, 46
 Lyman, 46
- effective charge, 10, 11, 21, 38, 119, 129, 130, 138, 147
- effective mass, 114, 134
- effective quantum number, 14, 21
- Einstein coefficient, 43, 49
- electric dipole, 49, 50, 63, 80, 122, 154, 187, 193, 214
- electric field, 44, 45, 66, 70, 76, 83, 187, 192, 214
 atomic unit, 70
- electric quadrupole, 52, 215
- electron affinity, 61, *see also* negative ion
- electron correlation, 62, 135, 136, 142–144, *see also* hyperspherical
- electron degeneracy, 9, 24
- electron gas, 23, 24
 one-dimensional, 127
- electron pair, 144, 146, 162, 163
- electron trajectory, 109–111
- elliptic coordinate, 176
- elliptic cylindrical, 105
- emissivity, 42
- energy normalization, 46, 67, 157
- equilibrium separation, 171, 179
- ethynyl, 224
- Euler angle, 146, 149, 212, 213
- exchange, 13, 47
- exchange energy, 13, 19, 27–29, 129
- exciton, 91, 114
- F-layer, 203
- Fano profile, *see* resonance
- Fano q-parameter, *see* resonance
- Fe, 32, 36, 84
- Fermi hole, 27
- Fermi momentum, 23, 127
- Fermi resonance, 222
- Fermi-Wentzel golden rule, 44
- fermionic nuclei, 185, 186
- ferromagnetism, 13
- Feshbach resonance, 156, 157, *see also* resonance
- fine structure, 19, 36
- finite size correction, 84–86
- fluorescence, 211
- fluorine, 20
- forbidden transition, 49, 52
- form factor, 57, 67
- Franck-Condon, 195, 196, 201, 202
- Fraunhofer lines, 1, 2
- g*-factor, 80, 91, 199
- galactic center, 227
- galactic nuclei, 34
- galaxy, 33, 35, 36, 201, 202, 227
 magnetic field, 69
- gamma ray bursts, 133
- gauge, 70, 88–90, 133
- gauge invariance, 90
- gauge transformation, 90, 101, 133
- Gaussian function, 178, 209
- generalized coordinate, 215–217
- generalized eigenvalue, 107
- generalized oscillator strength, 55–58, 67
- gerade, 171
- giant cloud, 202, 226
- golden rule, 44
- grain, 224
- grand angular momentum, 148, *see also* hyperspherical
 eigenfunction, 149
 eigenvalue, 149
- greenhouse effect, 220
- group theory, 218
- gyromagnetic ratio, 86, *see also g*-factor
- H, *see* hydrogen atom

- H I region, 201
- H II region, 33, 34, 201, 224, 226
- H^- , 11, 38, 49, 60, 61, 137
 - doubly-excited state, 137–141, 147, 151–157, 167
 - ground state, 61–64
 - in ultrastrong field, 124, 125
 - one-electron model, 62
 - photodetachment, 63–66, 147, 157
 - resonance, 156, 157, 168
- H_2 , 169, 173, 180, 181, 186, 187, 190, 198, 201–203, 205, 206, 224, 225
- H_2O , 208–210, 216–219, 226
- H_3 , 208, 224, 225
- H_2^+ , 170–174, 176, 205, 222
- H_3^+ , 35, 224, 225
- Hartree-Fock, 28, 29, 47, 124, 136, 209
- Hartree-Fock-Slater, 29
- HCl , 190, 191, 198, 199, 205
- HCN, 221, 224, 226
- He, *see* helium
- He^-
 - doubly-excited state, 140–142
 - triply-excited state, 143
- He_2 , 173
- Heisenberg exchange, 13
- helioseismology, 34
- helium
 - doubly-excited state, 59, 137–145, 152–156, 161–163
 - exchange energy, 13, 14, 19
 - ground state, 9–11, 38, 48
 - hyperspherical analysis, 147–156, 161–163
 - in ultrastrong field, 124–126
 - metastable, 51
 - photoionization, 48
 - singly-excited state, 12–16, 38, 51, 58
 - Hamiltonian, 10
- Hermite polynomial, 89, 181
- heteronuclear, 171, 185, 189, 192
- hole, 18, 19, 73
 - Fermi, 27
- hollow atom, 145
- homonuclear, 171, 184–186, 188, 189, 192, 193
- hot band, 189
- Hubble flow, 35
- Hund's case, 198
- Hund's coupling, 198
- Hund's rules, 19, 39
- hydrogen
 - maser, 223
 - molecular ion, 35, 170, 224, 225
 - molecule, *see* H_2
- hydrogen atom, 3–8, 201, 204, 225
 - Bohr model, 3
 - eigenstates parabolic coordinates, 6–8, 38, 76, 102, 105
 - eigenstates parity, 4
 - eigenstates spherical representation, 3–5, 38, 102
 - electron affinity, 61
 - excited state, 3–8, 38, 47, 58, 66, 67, 76, 77, 85, 86
 - expectation values, 6
 - ground state, 3, 38, 47, 58, 66, 67, 77, 78, 85, 86
- Hamiltonian, 3, 4
- hyperfine structure, 34, 223
 - in magnetic field, 91–113, 132
 - in ultrastrong field, 115–122
 - metastable, 51
 - momentum space, 8
 - oscillator strength, 47, 58
 - radial functions, 4, 5
 - radial quantum number, 5
 - scaling relations, 5, 6
- hydrogen negative ion, *see* H^-
- hydrogenic orbital, 9, 10, 12, 13, 20
- hydrogenic ordering, 17
- Hylleraas, 17, 61
- hyperfine structure, 34, 215, 223
- hyperspherical
 - adiabatic, 151–155, 168
 - angular momentum, 148
 - channel, 152, 154
 - coordinate, 142–144, 146, 167
 - harmonics, 149–151
 - kinetic energy, 148
 - pair description, 162, 163
 - potential surface, 147, 148
 - potential wells, 152–155, 161
 - principal quantum number, 149
 - quantum numbers, 162
 - Schrödinger equation, 149
- I_2 , 195, 196
 - in-out correlation, 62
 - inactive mode, 218, 220
 - independent electron labels, 137, 138
 - infrared, 3, 175, 188, 202, 214, 218, 219, 224
 - absorption, 189
 - active, 218
 - emission band, 224
 - inactive, 218, 220
 - telescope, 225
 - inner screening, 21
 - integrable system, 109
 - interaction line, 72
 - intercombination, 15
 - interstellar cloud, 203, *see also* clouds
 - interstellar hydrogen, 201

- interstellar medium, 198, 225, 227
- inversion, 184, 186, 220
- inversion doublet, 226
- inversion doubling, 222
- inversion layer, 91
- ionic bond, 170
- ionization potential, 31, 32, 45, 95, 126
- ionosphere, 203–205, 224
- iron, *see* Fe

- Jahn-Teller, 211
- Jovian planets, 224
- Jupiter, 35, 224, 225
- JWKB method, 110–113, 134, 183, 222

- Kepler period, 104
- kinetic energy density, 23, 127
- Kirchhoff, 1, 2, 42
- klystron, 215
- Kohn-Sham, 28
- Kramers degeneracy, 78

- ℓ -doubling, 221
- ℓ -mixing, 97–102, 104, 109
- Lagrange multiplier, 24, 128
- Laguerre function, 106, 150
- Lamb shift, 84, 154
- lambda-doubling, 173, 198, 203, 204
- Landé g -factor, 80, 91, 199
- Landau function, 90, 116–120
- Landau spectrum, 89, 91, 96, 115, 120, 133
- Laplace-Runge-Lenz vector, 6, 104, 105
- laser, 195, 196
 - CO₂, 219, 220
- LCAO, 209
- Legendre polynomial, 102, 134, 167
- length form, 48, 64
- Lenz's law, 77
- Li, 14, 18, 33, 145, 164
- LiH, 189, 205
- linear molecule, 207, 212–216, 218–220
- linear polarization, 50, 131
- linear Stark effect, 76, 166, 199
- linear Zeeman effect, 71, 79–81, 86, 93
- Lissajous figure, 221
- localization, 102, 109, 113, 161
- loops in perturbation diagrams, 73
- Lorentzian, 159
- LS-coupling, 20
- Lyman
 - alpha, 3, 32, 36, 140, 204
 - continuum, 46
 - edge, 46
 - forest, 36, 37
 - limit, 36
 - series, 3, 31, 36

- M1, 51, 52, 84
- Madelung rule, 17, 39
- magnetic dipole, 51, 84, 215
- magnetic field
 - atomic unit, 71, 78, 94
 - Earth's, 69
 - galactic, 69
 - solar, 81
 - very strong, 126–132
 - ultrastrong, 115–126, 133
- magnetic monopole, 70
- magnetic white dwarf, 91, 131, 132
- magneto-optic rotation, 199
- magnetosphere, 126
- many-body perturbation theory, 73
- many-center integral, 178
- Mars, 219, 224
- maser, 201, 203, 223, 225–227
- MCSCF, 209
- mean free path, 42
- meteor, 32
- Mg, 32
- microwave, 214, 221, 225
- microwave spectroscopy, 215
- millimeter wave, 202
- minimal coupling, 49, 70, 88
- missing mass, 35
- molecular
 - bands, 169
 - bonds, 170–175
 - Hamiltonian, 176, 177
 - orbital, 172–175, 205, 207–209
 - parity, 184, 185
 - potential, 182
 - potential curve, 172, 174, 183, 195–197
 - spectra, 187–194
 - spectroscopy, 169
 - structure, 170–173, 207–211
- molecule
 - diatomic, 170–182
 - electronic spectrum, 193–197
 - lambda quantum number, 171, 173
 - linear, 207, 212–216, 218–220
 - paramagnetic, 227
 - polar, 227
 - polyatomic, 171, 207–220
 - pyramidal, 216, 222
 - Raman spectra, 192, 193, 206, 220
 - reflection symmetry, 173, 184, 185
 - rotation, 179–181, 187, 188, 211–214
 - strong magnetic field, 131
 - structure, 170–173, 207–211
 - tetrahedral, 220
 - triangular, 208, 224
 - vibration, 179–183, 189–191, 215–219

- vibration-rotation, 182–184, 190, 191, 220, 221
- water, 208–210, 216–219, 226
- moment of inertia, 212–214
- moments of oscillator strength, 53, 54
- momentum space, 8, 105
- momentum transfer, 56–60, 67
- Morse function, 182
- motional Stark field, 93, 133
- multi-configuration, 29, 209
- multi-center, 209
- multi-electron states, *see also* doubly-excited state
 - notation, 12
- multipole, 53, 67

- N, 19, 32, 86
- N₂, 181, 192, 203, 204, 225
- N₂H, 224
- n*-mixing, 106, 109
- Na, 86
- NaCl ℓ , 170
- nebula, 166, 201, 224
 - diffuse, 33
 - planetary, 33, 34, 42, 52, 224
- negative ion, 11, 61, 125, 140, 141, 175, 224, *see also* H⁻
- neutron star, 91, 115, 117, 126, 131, 133
- NH, 174
- NH₃, 216, 222, 226, 227
- nitrogen, *see* N, N₂
- NO, 203, 204, 227
- NO₂, 210
- non-bonding, 171
- non-integrable, 109
- non-ionic bond, 170
- non-perturbative, *see* strong mixing
- normal mode, 66, 215, 216
- normalization
 - continuum, 46, 56, 67, 157
- nova, 35, 131
- nuclear interchange, 186
- nuclear spin, 34, 185, 186, 215
- nucleosynthesis, 33

- O, 20, 32, 52, 203, 204
- O branch, 193, 194
- O₂, 175, 181, 186, 192–194, 203, 204, 215
- O₃, 197, 220, 224
- O₂⁻, 175
- oblate, 212, 213, 227
- OH, 175, 198, 203, 204, 226, 227
- one-dimensional atom, 39, 116–120
- opacity, 42, 43, 60, 63, 164
- Opacity Project, 43
- optically thick, 42
- optically thin, 42

- orbital, 10, 12, 13, 21, 28, 208, 209
- Orion, 33, 201, 226
- ortho hydrogen, 187, 202, 206
- orthogonal group
 - four dimensions, 8
- orthohelium, 14, 15
- oscillator strength, 43–49, 53, 54, 57, 66, 84, 109, 122, 123, 156, 159, 164
- outer screening, 21
- oxygen, *see* O, O₂
- ozone, 197, 220, 224

- P branch, 189, 190, 193, 198, 220
- PAH, 224
- pair basis, 162, *see also* hyperspherical
- pair coordinate, 144, 146
- para hydrogen, 187, 206
- parabolic, 6–8, 38, 87, 102, 105, 134, 163
- parabolic approximation, 182
- parabolic coordinates, 7, 134
- parahelium, 14, 15
- parallel transition, 220
- paramagnetic, 71, 227
- parametric dependence, 151, 152, 177, 194
- parity, 4, 20, 50–52, 76, 93, 140, 184, 185, 188, 193
 - mixed, 7
- Paschen continuum, 46
- Paschen series, 3, 31, 37, 132
- Paschen-Back, 79
- Pauli principle, 9, 12, 13, 17–19, 22, 26, 27, 39, 62, 124–126, 150, 172–174, 185, 186
- Periodic Table, 22, 29, 30
 - in ultrastrong field, 126
 - in very strong field, 130
- perpendicular transition, 220
- perturbation theory
 - diagram, 72–75
 - first order, 72, 74, 199
 - high order, 74–76, 121
 - time-independent, 71–86
- phase shift, 158, 159
- phase space, 23, 39, 126, 127
- phosphorescence, 211
- photoabsorption, 42–46, 141, 144–146, 159, 196
 - cross-section, 43, 44, 46, 159
- photodetachment, 61, 63, 64, 141, 147, 157
- photodissociation, 196–198, 204
 - coupled-state, 197
 - indirect, 197
 - spontaneous, 198
- photoelectron spectroscopy, 209, 210
- photoionization, 46–48, 64, 204, *see also* oscillator strength

- edge, 46
- photosphere, 32, 226
- Planck, 2, 225, *see also* black-body
- planetary nebula, 33, 34, 42, 52, 224
- Poisson distribution, 109, 110
- polarizability, 45, 54, 66, 77, 192, 200, 220
- polarization, 44, 45, 50, 80, 96, 122, 131, 199, 227
- poly aromatic hydrocarbon, 224
- population inversion, 195, 223
- potential in magnetic field, 94, 96, 111, 112
- potential surface
 - two-electron, 147, 148
- potential well, *see* hyperspherical, molecular
- predissociation, 197, 198, 225
- primordial deuterium, 36, 37, 225
- primordial radiation, 37, 169, 202
- profile index, 159, 160, *see also* autoionization
- prolate, 100, 101, 212, 214
- prolate spheroidal function, 100, 101
- propensity rule, 55, 200
- proton affinity, 224, 225
- pseudo-potential, 209
- pulsar, 91, 93, 115, 116, 118, 125, 133
- pump, 195

- Q branch, 190, 193, 198, 220
- q-parameter, 159, 160, 168
- quadratic Stark effect, 77, 199
- quadratic Zeeman effect, 71, 93, 131, *see also* diamagnetic
- quadrupole, 52, 202, 203, 215
- quantum defect, 14, 38, 95, 114, 210
- quantum defect theory, 15
- quantum electrodynamics, 11, 84
- quasar, 36, 37
- quasi-bound state, 138, 160, *see also* resonance
- quasi-classical, 110–113
- quintessence, 1

- R branch, 189, 190, 193, 198, 220
- r-process, 33
- radial correlation, 17, 62, 143, 146, 153
- radiation transport, 41, 42
- radiationless transition, 211, *see also* autoionization
- radiative capture, 64–66
- radiative recombination, 164
- radiative width, 165
- radio recombination, 33
- Raman, 193
 - active, 220
 - effect, 192
 - inactive, 220
 - spectroscopy, 193, 220
 - spectrum, 192–194, 206
 - transition, 192
- Random Phase Approximation, 76
- rate equation, 42
- Rayleigh scattering, 192
- Rayleigh-Jeans, 2, 226
- Rayleigh-Ritz, 10, 17, 38, 119, 124
- Rayleigh-Schrödinger, 71
- recombination, 142, 164
- recombination era, 30
- recurrence time, 110
- red giant, 52, 226
- red-shift, 36, 39, 202
- reduced energy, 159
- reduced mass, 4, 178, 200
- reflection, 50, 208, *see also* inversion
- refractive index, 199
- relativistic mass, 82
- relativistic perturbation, 82–84
- resonance, 94–97, 113, 138, 141–147, 155–160
 - Breit-Wigner, 159
 - q-parameter, 159, 160
 - Fermi, 222
 - Feshbach, 156, 157, 159, 168
 - phase shift, 158, 159
 - position, 159
 - profile, 159, 160
 - “shape”, 156
 - width, 159, 160
- resonance transition, 50
- ridge state, 139, 162
- rigid rotor, 179, 180
- rotation, *see* molecule, transformation
- rotation-vibration coupling, 182–184, 190, 191, 219–221
- rotational
 - band, 188
 - constant, 179–181, 221, 223
 - degree of freedom, 227
 - energy, 179–181, 221
 - fine structure, 198, 219
 - quantum number, 179, 220
 - Raman, 192, 205, 206
 - spacing, 187
 - spectrum, 188, 193, 202, 206, 214, 225
- rotations
 - four dimensions, 8
- rotor, 98, 102, 104, 105, 109, 113, 179
- rovibronic, 221
- rule of mutual exclusion, 220
- Russell-Saunders coupling, 20
- Rutherford cross-section, 57
- Rydberg constant, 2, 3

- Rydberg orbital, 209
- Rydberg series, 13, 14
- Rydberg-Klein-Rees, 183

- S branch, 193, 194
- s-process, 33
- saddle point, 161, 168
- Saturn, 224
- scaling
 - hydrogen atom, 5, 6
 - Thomas-Fermi model, 26, 27
- Schrödinger equation
 - diatomic molecule, 177–179
 - hydrogen atom, 4
 - in magnetic field, 88, 89, 92, 93
 - two-electron, 143, 149, 151
 - vibrational, 180
- Schumann-Runge, 175, 197
- screening constant, 21
- selection rule, 49–53, 58, 80, 140, 189, 193, 214, 220
- self-consistent field, 22, 29, 135, 209
- semi-classical quantization, 110–112
- semi-parabolic coordinates, 107, 110, 134
- separated atom, 171
- separatrix, 99, 100, 102, 104
- shake-off, 140
- shape resonance, 156, 157
- shell structure, 22
 - in ultrastrong field, 126
 - in very strong field, 130
- silicon carbide, 224
- singlet, 10, 12–15, 18, 21, 187
- SiO, 226
- six-dimensional Coulomb, 149, 150
- Slater determinant, 22, 28
- Slater orbital, 209
- Slater screening, 20
- sodium, 86
- solar
 - chromosphere, 32, 42, 84
 - continuum, 140
 - corona, 32, 84, 166
 - flare, 166
 - magnetic field, 81
 - rotation, 34, 39
 - spectra, 32, 84
- source function, 42
- space-fixed axes, 184–186, 212, 213
- space-fixed frame, 184–186, 212, 213
- spectroscopic notation, 12
- spectroscopic state, 18
- spectrum, *see* Landau, Raman, rotational, vibrational
- spherical harmonics, 4, 150
- spherical tensor, 50
- spherical top, 213
- spin-flip, 51, 58, 141
- spin-orbit, 19, 50, 51, 58, 79, 80, 83, 86, 140
- spin-spin, 140
- spontaneous emission, 42, 49
- Sr, 94, 96
- standard candle, 35
- Stark effect, 6, 70, 71, 75–78, 166, 199
- Stark-modulation, 215
- statistical weight, 65, 166, 182, 186
- stellar classification, 32
- Stern-Gerlach, 86
- stimulated emission, 43, 195, 219, 223
- Stokes line, 192
- strong mixing, 91, 94, 96, 97, 112
- Sturmian basis, 107
- subsurface level, 18
- sum rule, 53, 57, 67
- sunspot, 71, 81
- superluminous galaxy, 202
- supernova, 34, 225
- supersymmetry, 91
- susceptibility, 54
- symmetric stretch, 215, 218
- symmetric top, 212–214, 219, 227
- symmetry
 - inversion, *see* inversion
 - nuclear interchange, 186
 - parity, *see* parity
 - point group, 208, 217
 - radial interchange, 154
- synchrotron, 141
- synchrotron light, 91

- term, 19
- thermodynamic equilibrium, 43
- Thomas factor, 83
- Thomas-Fermi model, 22–25, 39, 126–129
 - one dimension, 126–129
- Thomas-Fermi-Dirac model, 27, 39, 129, 134
- Thomas-Reiche-Kuhn, 53, 67
- thorium, 33
- three-photon, 167
- time reversal, 78
- TiO, 32, 169
- transformation
 - conjugation, 101
 - gauge, 90, 101, 133
 - rotation, 50
 - spherical to parabolic, 8, 38
 - unitary, 7, 38, 90, 105
- triplet, 12–15, 18, 22, 187
- triplely-excited state, 136, 143, 145
- two-electron atom, 8, *see also* doubly-excited state
 - potential surface, 147, 148
- two-photon transition, 52, 94

- ultraviolet, 3, 32, 41, 175, 198, 201
- Undheim, 17
- ungerade, 171
- united atom, 171
- Uranus, 224

- valley state, 139, 163
- van der Waals, 200
- variational principle, 10, 16, 17, 24, 38, 49, 61, 64, 119, 124, 129
- vector potential, 49, 70, 88–90, 92
- velocity form, 48, 49, 64
- Venus, 175, 204, 219
- vertical transition, 195
- vibration, 170, 179–182, 214–216
 - energy, 180–183, 217
 - frequency, 221
- vibration-rotation band, 202
- vibration-rotation spectrum, 190, 191, 198, 220
- vibrational
 - degree of freedom, 227
 - level, 181–183, 218
 - Raman, 193, 205
 - selection rule, 189
 - spectrum, 189, 190, 217
 - transition, 187
 - wave function, 180, 181, 194
 - vibrator, 98, 101, 102, 104
 - vibronic coupling, 210
 - virial theorem, 6, 12, 54, 130
 - virtual orbital, 209
 - VLBI, 36, 226

 - water, 207–210, 215–217, 224–226
 - white dwarf, 24, 52, 124, 131–133
 - Wien, 2
 - Wigner coefficient, 8, *see also* Clebsch-Gordan
 - Wigner distribution, 109, 110
 - Wigner threshold law, 63

 - x-ray, 32, 84, 91, 131
 - x-ray binary, 133

 - z-parameter, 36, 37, 202
 - Zeeman effect, 71, 78–81, 199, 227
 - anomalous, 81
 - linear, 71, 78
 - modulation, 215
 - normal, 81
 - quadratic, 71, 93, 131, *see also* diamagnetic
 - zero-point energy, 190
 - zero range, 62

Previously published in Astrophysics and Space Science Library book series:

- **Volume 267: The Nature of Unidentified Galactic High-Energy Gamma-Ray Sources**
Editors: Alberto Carramiñana, Olaf Reimer, David J. Thompson
Hardbound, ISBN 1-4020-0010-3, October 2001
- **Volume 266: Organizations and Strategies in Astronomy II**
Editor: André Heck
Hardbound, ISBN 0-7923-7172-0, October 2001
- **Volume 265: Post-AGB Objects as a Phase of Stellar Evolution**
Editors: R. Szczerba, S.K. Górný
Hardbound, ISBN 0-7923-7145-3, July 2001
- **Volume 264: The Influence of Binaries on Stellar Population Studies**
Editor: Dany Vanbeveren
Hardbound, ISBN 0-7923-7104-6, July 2001
- **Volume 262: Whistler Phenomena Short Impulse Propagation**
Authors: Csaba Ferencz, Orsolya E. Ferencz, Dániel Hamar, János Lichtenberger
Hardbound, ISBN 0-7923-6995-5, June 2001
- **Volume 261: Collisional Processes in the Solar System**
Editors: Mikhail Ya. Marov, Hans Rickman
Hardbound, ISBN 0-7923-6946-7, May 2001
- **Volume 260: Solar Cosmic Rays**
Author: Leonty I. Miroshnichenko
Hardbound, ISBN 0-7923-6928-9, May 2001
- **Volume 259: The Dynamic Sun**
Editors: Arnold Hanslmeier, Mauro Messerotti, Astrid Veronig
Hardbound, ISBN 0-7923-6915-7, May 2001
- **Volume 258: Electrohydrodynamics in Dusty and Dirty Plasmas Gravito-Electrodynamics and EHD**
Author: Hiroshi Kikuchi
Hardbound. ISBN 0-7923-6822-3, June 2001
- **Volume 257: Stellar Pulsation - Nonlinear Studies**
Editors: Mine Takeuti, Dimitar D. Sasselov
Hardbound, ISBN 0-7923-6818-5, March 2001
- **Volume 256: Organizations and Strategies in Astronomy**
Editor: André Heck
Hardbound, ISBN 0-7923-6671-9, November 2000
- **Volume 255: The Evolution of the Milky Way Stars versus Clusters**
Editors: Francesca Matteucci, Franco Giovannelli
Hardbound, ISBN 0-7923-6679-4, January 2001
- **Volume 254: Stellar Astrophysics**
Editors: K.S. Cheng, Hoi Fung Chau, Kwing Lam Chan, Kam Ching Leung
Hardbound, ISBN 0-7923-6659-X, November 2000
- **Volume 253: The Chemical Evolution of the Galaxy**
Author: Francesca Matteucci
Hardbound, ISBN 0-7923-6552-6, May 2001
- **Volume 252: Optical Detectors for Astronomy II State-of-the-art at the Turn of the Millennium**
Editors: Paola Amico, James W. Beletic
Hardbound, ISBN 0-7923-6536-4, December 2000
- **Volume 251: Cosmic Plasma Physics**
Author: Boris V. Somov
Hardbound, ISBN 0-7923-6512-7, September 2000
- **Volume 250: Information Handling in Astronomy**
Editor: André Heck
Hardbound, ISBN 0-7923-6494-5, October 2000

- **Volume 249: The Neutral Upper Atmosphere**
Author: S.N. Ghosh
Hardbound, ISBN 0-7923-6434-1, (in production)
- **Volume 247: Large Scale Structure Formation**
Editors: Reza Mansouri, Robert Brandenberger
Hardbound, ISBN 0-7923-6411-2, August 2000
- **Volume 246: The Legacy of J.C. Kapteyn**
Studies on Kapteyn and the Development of Modern Astronomy
Editors: Piet C. van der Kruit, Klaas van Berkel
Hardbound, ISBN 0-7923-6393-0, August 2000
- **Volume 245: Waves in Dusty Space Plasmas**
Author: Frank Verheest
Hardbound, ISBN 0-7923-6232-2, April 2000
- **Volume 244: The Universe**
Visions and Perspectives
Editors: Naresh Dadhich, Ajit Kembhavi
Hardbound, ISBN 0-7923-6210-1, August 2000
- **Volume 243: Solar Polarization**
Editors: K.N. Nagendra, Jan Olof Stenflo
Hardbound, ISBN 0-7923-5814-7, July 1999
- **Volume 242: Cosmic Perspectives in Space Physics**
Author: Sukumar Biswas
Hardbound, ISBN 0-7923-5813-9, June 2000
- **Volume 241: Millimeter-Wave Astronomy: Molecular Chemistry & Physics in Space**
Editors: W.F. Wall, Alberto Carramiñana, Luis Carrasco, P.F. Goldsmith
Hardbound, ISBN 0-7923-5581-4, May 1999
- **Volume 240: Numerical Astrophysics**
Editors: Shoken M. Miyama, Kohji Tomisaka, Tomoyuki Hanawa
Hardbound, ISBN 0-7923-5566-0, March 1999
- **Volume 239: Motions in the Solar Atmosphere**
Editors: Arnold Hanslmeier, Mauro Messerotti
Hardbound, ISBN 0-7923-5507-5, February 1999
- **Volume 238: Substorms-4**
Editors: S. Kokubun, Y. Kamide
Hardbound, ISBN 0-7923-5465-6, March 1999
- **Volume 237: Post-Hipparcos Cosmic Candles**
Editors: André Heck, Filippina Caputo
Hardbound, ISBN 0-7923-5348-X, December 1998
- **Volume 236: Laboratory Astrophysics and Space Research**
Editors: P. Ehrenfreund, C. Krafft, H. Kochan, V. Pirronello
Hardbound, ISBN 0-7923-5338-2, December 1998
- **Volume 235: Astrophysical Plasmas and Fluids**
Author: Vinod Krishan
Hardbound, ISBN 0-7923-5312-9, January 1999
Paperback, ISBN 0-7923-5490-7, January 1999
- **Volume 234: Observational Evidence for Black Holes in the Universe**
Editor: Sandip K. Chakrabarti
Hardbound, ISBN 0-7923-5298-X, November 1998
- **Volume 233: B [e] Stars**
Editors: Anne Marie Hubert, Carlos Jaschek
Hardbound, ISBN 0-7923-5208-4, September 1998
- **Volume 232: The Brightest Binaries**
Authors: Dany Vanbeveren, W. van Rensbergen, C.W.H. de Loore
Hardbound, ISBN 0-7923-5155-X, July 1998

Missing volume numbers have not been published yet.

For further information about this book series we refer you to the following web site: www.wkap.nl/series.htm/ASSL